

Winter 2004

# Chemical heterogeneity of glaciofluvial deposits: Outcrop study and implications for reactive transport

Gordon M. Sturgeon  
*University of New Hampshire, Durham*

Follow this and additional works at: <https://scholars.unh.edu/dissertation>

---

## Recommended Citation

Sturgeon, Gordon M., "Chemical heterogeneity of glaciofluvial deposits: Outcrop study and implications for reactive transport" (2004). *Doctoral Dissertations*. 253.  
<https://scholars.unh.edu/dissertation/253>

This Dissertation is brought to you for free and open access by the Student Scholarship at University of New Hampshire Scholars' Repository. It has been accepted for inclusion in Doctoral Dissertations by an authorized administrator of University of New Hampshire Scholars' Repository. For more information, please contact [nicole.hentz@unh.edu](mailto:nicole.hentz@unh.edu).

# NOTE TO USERS

This reproduction is the best copy available.

**UMI**<sup>®</sup>



**CHEMICAL HETEROGENEITY OF GLACIOFLUVIAL DEPOSITS: OUTCROP STUDY  
AND IMPLICATIONS FOR REACTIVE TRANSPORT**

BY

**GORDON M. STURGEON**

B.S. with honor, University of Wyoming, 1987

M.A.Ed., Virginia Tech, 1989

M.S., University of Wyoming, 1994

DISSERTATION

Submitted to the University of New Hampshire

in Partial Fulfillment of

the Requirements for the Degree of

Doctor of Philosophy

In

Earth Sciences

December, 2004



UMI Number: 3158682

### INFORMATION TO USERS

The quality of this reproduction is dependent upon the quality of the copy submitted. Broken or indistinct print, colored or poor quality illustrations and photographs, print bleed-through, substandard margins, and improper alignment can adversely affect reproduction.

In the unlikely event that the author did not send a complete manuscript and there are missing pages, these will be noted. Also, if unauthorized copyright material had to be removed, a note will indicate the deletion.

**UMI**<sup>®</sup>

---


UMI Microform 3158682

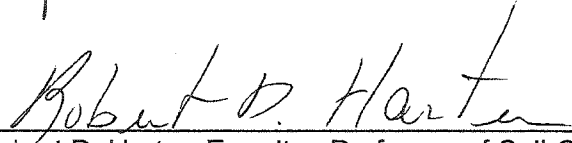
Copyright 2005 by ProQuest Information and Learning Company.

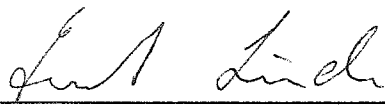
All rights reserved. This microform edition is protected against unauthorized copying under Title 17, United States Code.

ProQuest Information and Learning Company  
300 North Zeeb Road  
P.O. Box 1346  
Ann Arbor, MI 48106-1346

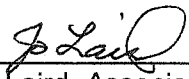
This dissertation has been examined and approved.

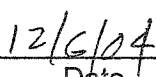
  
\_\_\_\_\_  
Dissertation Director,  
J. Matthew Davis, Associate Professor of Hydrogeology

  
\_\_\_\_\_  
Robert D. Harter, Emeritus Professor of Soil Chemistry

  
\_\_\_\_\_  
Ernst Linder, Professor of Mathematics

  
\_\_\_\_\_  
William C. Clyde, Associate Professor of Paleontology

  
\_\_\_\_\_  
Jo Laird, Associate Professor of Geology

  
\_\_\_\_\_  
Date

**DEDICATION**

To Eilyn and Sarah

## ACKNOWLEDGEMENTS

I would like to express my sincere appreciation to professors Ernst Linder, Bob Harter, Will Clyde, Jo Laird, and especially Matt Davis for their guidance and invaluable assistance throughout this project.

I am also indebted to:

- Phil Lucason, a former master's student in the Department of Natural Resources, for his help clearing the outcrop, collecting sediment samples, surveying sample locations, and recording field data.
- Toti Larson, a former master's student in the Department of Earth Sciences, for his help with sediment color measurements and sample preparation for chemical extraction and batch adsorption experiments.
- Professors Wally Bothner and Karen Von Damm of the Department of Earth Sciences for lending their expertise in support of the petrographic, photographic, and analytical chemistry aspects of the project.
- Richelle Allen-King, Associate Professor in the Department of Geology at the University at Buffalo, and Michael Pickering, a former master's student in the Department of Geology at Washington State University, for analyzing the carbon content of my sediment samples.

Funding for this project was generously provided by the National Science Foundation (Grant # 9526795).

## TABLE OF CONTENTS

|   |      |
|---|------|
| DEDICATION.....   | iii  |
| ACKNOWLEDGEMENTS .....                                    | iv   |
| LIST OF TABLES.....                                       | ix   |
| LIST OF FIGURES .....                                     | ix   |
| ABSTRACT.....   | xi   |
| <br>  |      |
| CHAPTER   | PAGE |
| <br>  |      |
| INTRODUCTION .....  | 1    |
| 1. AQUIFER REACTIVITY AND REACTIVE SOLUTE TRANSPORT ..... | 10   |
| Origins of Reactivity .....                               | 10   |
| Solute-Solid Reactions .....                              | 12   |
| Adsorption.....   | 13   |
| Introduction.....   | 13   |
| Surface Charge.....                                       | 14   |
| Lewis Acidity and Basicity .....                          | 16   |
| Polarity.....   | 16   |
| Adsorption of Cations .....                               | 17   |
| Adsorption of Anions.....                                 | 20   |
| Proton Stoichiometry.....                                 | 21   |
| Adsorption of Nonionic Organic Compounds .....            | 21   |
| Coadsorption of Metal Ions and Organic Ligands .....      | 24   |
| Reaction Rates .....                                      | 24   |
| Modeling Reactive Transport.....                          | 27   |

|   |    |
|---|----|
| The Advection-Dispersion Equation.....                            | 27 |
| Modifying the ADE to Account for Sorption.....                    | 31 |
| Empirical vs. Surface Complexation Models of Solute Sorption..... | 37 |
| Introduction.....   | 37 |
| Empirical Approach.....   | 37 |
| Surface Complexation Approach .....                               | 39 |
| Surface Functional Groups.....                                    | 39 |
| Surface Area and Microporosity .....                              | 42 |
| The Electrical Double Layer .....                                 | 43 |
| Examples of Surface Complexation Models .....                     | 45 |
| Surface Complexation Modeling of Experimental Systems.....        | 46 |
| Surface Complexation Modeling of Natural Systems.....             | 47 |
| <br>  |    |
| 2. LEAD SORPTION VARIABILITY: IMPLICATIONS FOR SOLUTE TRANSPORT   |    |
| MODELING .....  | 57 |
| Abstract.....   | 57 |
| Introduction .....  | 58 |
| Methods .....   | 61 |
| Results.....  | 64 |
| Discussion.....   | 65 |
| Comparison to Cape Cod Site .....                                 | 65 |
| Modeling Pb <sup>2+</sup> Sorption at the Deerfield Site.....     | 67 |
| Estimating Reactive Surface Area .....                            | 71 |
| Conclusions.....  | 71 |
| <br>  |    |
| 3. CHARACTERIZATION AND ORIGIN OF HETEROGENEITIES IN A            |    |
| GLACIOFLUVIAL DEPOSIT.....  | 84 |

|   |     |
|---|-----|
| Abstract.....   | 84  |
| Introduction .....  | 85  |
| Methods .....   | 86  |
| Field Methods .....   | 86  |
| Laboratory Methods.....   | 88  |
| Statistical Methods.....  | 90  |
| Results .....   | 92  |
| Permeability .....  | 93  |
| Porosity .....  | 94  |
| Dithionite-Citrate Extractable Manganese.....                   | 94  |
| Dithionite-Citrate Extractable Iron .....                       | 97  |
| Dithionite-Citrate Extractable Aluminum.....                    | 98  |
| Correlations between Sediment Properties.....                   | 98  |
| Discussion.....   | 99  |
| Origin of Grain Coatings .....                                  | 99  |
| Potential Application to Subsurface Characterization.....       | 101 |
| Conclusions.....  | 102 |
| 4. IMPACT OF CHEMICAL HETEROGENEITY ON REACTIVE TRANSPORT ..... | 117 |
| Abstract.....   | 117 |
| Introduction .....  | 118 |
| Background .....  | 118 |
| Conceptual Model.....   | 119 |
| Methods .....   | 121 |
| Results.....  | 122 |
| Uniform Pattern of Goethite Grain Coatings .....                | 123 |

|   |      |
|---|------|
| Banded Pattern of Goethite Grain Coatings.....            | 124  |
| Random Pattern of Goethite Grain Coatings .....           | 124  |
| Discussion.....   | 125  |
| Conclusions.....  | 126  |
| 5. SUMMARY.....   | 136  |
| Project Conclusions.....                                  | 136  |
| Suggestions for Future Research.....                      | 139  |
| REFERENCES .....  | 143  |
| <br>  |      |
| APPENDICES  | PAGE |
| <br>  |      |
| A. SUPPLEMENTAL INFORMATION ON MATERIALS AND METHODS..... | 155  |
| Scale of Observation.....                                 | 156  |
| Sampling Strategy.....                                    | 157  |
| Grain Coatings .....                                      | 158  |
| Reactivity.....   | 159  |
| Magnetic Susceptibility.....                              | 160  |
| Surface Area .....  | 160  |
| Sediment Color .....                                      | 161  |
| B. MAPPING AQUIFER HETEROGENEITY.....                     | 164  |
| Introduction .....  | 165  |
| Structure-Imitating Approach.....                         | 166  |
| Process-Imitating Approach .....                          | 170  |
| Descriptive Approach .....                                | 171  |
| C. SCANNING ELECTRON MICROSCOPE (SEM-EDS) RESULTS .....   | 175  |
| D. DATA SUMMARY OF MEASURED SEDIMENT PROPERTIES.....      | 181  |



## LIST OF TABLES

|            |  |
|------------|--|
| CHAPTER 2  |  |
| 2.1        | Univariate Statistics for Measured Properties ..... 74                       |
| 2.2        | Correlations between Measured Properties ..... 75                            |
| 2.3        | Summary of Pb <sup>2+</sup> Sorption Models ..... 76                         |
| CHAPTER 3  |  |
| 3.1        | Abundance of Minerals in Selected Samples ..... 104                          |
| 3.2        | Basic Statistical Characteristics of Measured Properties ..... 105           |
| 3.3        | Correlations between Physical Properties and Extractable Metals ..... 106    |
| CHAPTER 4  |  |
| 4.1        | Ground Water from a Glacial Aquifer in South-Central New Hampshire ..... 128 |
| 4.2        | Cobalt Arrival Times for Various Percentages of Goethite ..... 129           |
| APPENDIX D |  |
| D.1        | Analytical Results for Measured Sediment Properties ..... 182                |

## LIST OF FIGURES

|              |  |
|--------------|--|
| INTRODUCTION |  |
| I.1          | Stochastic (Gaussian) model of permeability ..... 8  |
| I.2          | Location of the Deerfield site ..... 9   |
| CHAPTER 1    |  |
| 1.1          | Block model of a heterogeneous mineral surface ..... 49  |
| 1.2          | Dissolved cation and associated water molecules ..... 49   |
| 1.3          | Three mechanisms of cation adsorption ..... 50   |
| 1.4          | Effect of pH on electrostatic attraction of cations ..... 51   |
| 1.5          | Predominant coordination environment of Pb <sup>2+</sup> adions on AlO <sub>6</sub> and FeO <sub>6</sub> ..... 52  |
| 1.6          | Adsorption of a polar organic compound by water-bridging ..... 52  |
| 1.7          | Example of a relatively high-velocity breakthrough curve ..... 53  |
| 1.8          | Adsorption isotherm ..... 54   |
| 1.9          | Ditrigonal cavity on a phyllosilicate clay mineral ..... 54  |
| 1.10         | Gouy-Chapman and Stern-Grahame models of the electrical double layer ..... 55                                      |
| 1.11         | Electrical potential vs. distance relationships for surface complexation models ..... 56                           |
| CHAPTER 2    |  |
| 2.1          | Deerfield outcrop and sample locations ..... 77  |
| 2.2          | Schematic diagram of air permeameter ..... 78  |
| 2.3          | Images of Pb <sup>2+</sup> partition coefficients for the Deerfield outcrop ..... 79                               |
| 2.4          | Relationship between Pb <sup>2+</sup> partition coefficient and permeability ..... 80                              |
| 2.5          | Photomicrographs of (hydr)oxide grain coatings on Deerfield sediments ..... 81                                     |
| 2.6          | Models of reactive surface area for thin continuous grain coatings and thick discontinuous grain coatings ..... 82 |

|     |   |    |
|-----|---|----|
| 2.7 | Relationship between $Pb^{2+}$ partition coefficient and geometric surface area of (hydr)oxide grain coatings ..... | 83 |
|-----|---|----|

### CHAPTER 3

|      |   |     |
|------|---|-----|
| 3.1  | Data locations.....   | 107 |
| 3.2  | Outcrop map showing lithofacies 1 through 8.....  | 108 |
| 3.3  | Permeability: (a) histogram; (b) facies relationships .....   | 109 |
| 3.4  | Variograms of (a) physical and (b) chemical properties .....  | 110 |
| 3.5  | Porosity: (a) histogram; (b) facies relationships .....   | 111 |
| 3.6  | Dithionite-citrate extractable manganese: (a) histogram; (b) facies relationships; (c) color relationships..... | 112 |
| 3.7  | Zone map and cumulative frequency plots for dithionite-citrate extractable manganese .....                      | 113 |
| 3.8  | Dithionite-citrate extractable iron: (a) histogram; (b) facies relationships; (c) color relationships .....     | 114 |
| 3.9  | Zone map and cumulative frequency plots for dithionite-citrate extractable iron .....                           | 115 |
| 3.10 | Dithionite-citrate extractable aluminum: (a) histogram; (b) facies relationships .....                          | 116 |

### CHAPTER 4

|     |   |     |
|-----|---|-----|
| 4.1 | Uniform, banded, and random patterns of goethite coatings .....               | 130 |
| 4.2 | Breakthrough curves and concentration vs. distance plots for uniform case.... | 131 |
| 4.3 | Breakthrough curves and concentration vs. distance plots for banded case....  | 132 |
| 4.4 | Breakthrough curves for random case.....                                      | 133 |
| 4.5 | Concentration vs. distance plots for rows 7 and 8 in random case .....        | 134 |
| 4.6 | Concentration vs. distance plots for rows 2 and 3 in random case .....        | 135 |

### APPENDIX B

|     |  |     |
|-----|--|-----|
| B.1 | Schematic representation of kriging .....    | 173 |
| B.2 | Schematic representation of simulation ..... | 174 |

### APPENDIX C

|     |   |     |
|-----|---|-----|
| C.1 | Photomicrographs of sample 4H .....           | 176 |
| C.2 | SEM-EDS results for area 2 of sample 4H ..... | 177 |
| C.3 | SEM-EDS results for area 3 of sample 4H ..... | 178 |
| C.4 | SEM-EDS results for area 4 of sample 4H ..... | 179 |
| C.5 | SEM-EDS results for area 6 of sample 4H ..... | 180 |

### APPENDIX D

|      |   |     |
|------|---|-----|
| D.1  | Grain size distribution curve for sample 1062 ..... | 204 |
| D.2  | Grain size distribution curve for sample 1112 ..... | 205 |
| D.3  | Grain size distribution curve for sample 2052 ..... | 206 |
| D.4  | Grain size distribution curve for sample 2072 ..... | 207 |
| D.5  | Grain size distribution curve for sample 5052 ..... | 208 |
| D.6  | Grain size distribution curve for sample 6025 ..... | 209 |
| D.7  | Grain size distribution curve for sample 6032 ..... | 210 |
| D.8  | Grain size distribution curve for sample 7073 ..... | 211 |
| D.9  | Grain size distribution curve for sample 7112 ..... | 212 |
| D.10 | Grain size distribution curve for sample 8112 ..... | 213 |

## ABSTRACT

# CHEMICAL HETEROGENEITY OF GLACIOFLUVIAL DEPOSITS: OUTCROP STUDY AND IMPLICATIONS FOR REACTIVE TRANSPORT

by

Gordon M. Sturgeon

University of New Hampshire, December, 2004

Spatial variations in the reactive properties of geologic systems and their influence on contaminant transport are poorly understood. Consequently, an outcrop study was conducted in a glaciofluvial deposit in Deerfield, New Hampshire in order to: 1) identify the sediment properties controlling heavy metal adsorption, 2) evaluate the extent to which geologic information can be used to characterize their spatial variation, and 3) assess the impact of spatial variations on heavy metal transport. Four hundred seventy-six, spatially-located sediment samples were collected from an eight square meter vertical exposure of outwash sands and gravels. Lithologic facies were mapped on outcrop photographs. Sample color, permeability, porosity, grain size, surface area, lead ( $Pb^{2+}$ ) sorption, carbon content, magnetic mineral content, and dithionite citrate-extractable iron, manganese, and aluminum content were measured in the laboratory.

Fifty-seven percent of the variation in  $Pb^{2+}$  sorption can be explained by a linear combination of sediment permeability and extractable iron, manganese, and aluminum, indicating that  $Pb^{2+}$  sorption is controlled by (hydr)oxide grain coatings. Reactive surface area, estimated from sample grain size and (hydr)oxide mass together with observations of grain coating morphology and numerical abundance, accounts for 65 percent of the sorption variation. Three sorption-related properties: permeability, extractable iron, and extractable manganese are strongly related to sediment facies

and/or color and thus can be mapped over a wide range of spatial scales. Differences in the geometries of iron and manganese enrichment, petrographic observations, and SEM-EDS analyses indicate the grain coatings originated from the post-depositional weathering of biotite and garnet, coupled with local, redox-driven redistribution of the liberated iron and manganese.

Numerical simulations show that spatial variations in (hydr)oxide grain coatings increase plume mobility and dispersion when the spatial scale of the heterogeneity is similar to the scale of the problem. Overall, the outcrop study findings suggest that  $Pb^{2+}$  partition coefficients can be estimated from relatively simple and inexpensive measurements of permeability and dithionite-citrate extractable metals. The results further suggest that information regarding sediment facies and color can help produce more efficient and geologically realistic descriptions of chemical heterogeneity.

## INTRODUCTION

Subsurface fluid flow and solute transport can be strongly affected by heterogeneities, or spatial variations, in the properties of the surrounding geologic materials. Heterogeneities in physical properties affect fluid flow by creating preferential flow paths and flow barriers such as gravel layers and clay lenses in sandy sediments. Both permeability and porosity influence fluid flow. However, the effects of permeability variations tend to overshadow the effects of porosity variations, because permeability can vary more than ten orders of magnitude in sedimentary deposits, while porosity typically varies by less than a factor of four (Freeze and Cherry 1979).

Permeability variations not only affect fluid flow; they also affect solute transport by controlling the rate of solute spreading, or dispersion (Gelhar and Axness 1983, Dagan 1988). Solute transport is further influenced by the spatial distribution of reactive geologic materials such as organic or (hydr)oxide grain coatings, because many solute plumes move more slowly than the ground water when they encounter these surfaces.

To date, most heterogeneity research has focused on the spatial variability in the physical properties of the media and how they affect contaminant transport. Relatively little research has addressed chemical heterogeneity – the spatial variability in the reactive properties of the media – even though recent theoretical, laboratory, and field studies have shown it to influence solute movement (Friedly et al. 1995, Tompson et al. 1996, Yang et al. 1997, Szecsody et al. 1998).

The purpose of this research was to investigate the nature of chemical heterogeneity and its geologic controls in a glaciofluvial deposit in Deerfield, New Hampshire. More specifically, the research addressed five fundamental questions.

First, what are the sediment properties controlling heavy metal adsorption? Studies of cation adsorption to glacial outwash in Falmouth, Massachusetts, and to fluvial and eolian sands and silts in Chalk River, Ontario have identified oxide and hydroxide grain coatings as the dominant reactive phases (Jackson and Inch 1989, Friedly et al. 1995, Fuller et al. 1996). However, other studies have found that clay minerals (Inch and Killey 1987) or carbonate minerals (Fuller and Davis 1987) control sorption.

Second, what are the relationships between the sediments' physical and reactive properties? If the relationships are strong, less field and laboratory data may be needed to characterize heterogeneity and simulate the migration of contaminants at a site.

Third, can the spatial patterns of physical and reactive properties be related to mappable geologic properties? Traditional approaches to dealing with aquifer or reservoir heterogeneity have been to ignore it or represent it using stochastic models (Figure I.1). If the hydrogeologic properties needed to model flow and transport can be related to mappable geologic properties, it may be possible to develop more realistic models of heterogeneity by mapping key geologic features at a site.

Fourth, what are the geologic origins of the spatial patterns of reactive properties? The characterization of chemical heterogeneities is constrained by our ability to efficiently gather chemical property data and meaningfully interpret it. These tasks in turn are predicated on our understanding of the geologic processes responsible for the heterogeneities.

Fifth, what is the impact of the spatial pattern of reactivity on solute transport? The influence of physical heterogeneities on solute transport has been studied extensively, but the practical effects of reactive zone geometry and scale are not well known.

A comprehensive study involving field and laboratory research, theoretical analysis, and numerical simulation was developed to answer these five questions. The field research was conducted in the Rollins borrow pit in Deerfield, New Hampshire (Figure 1.2). The field site was selected for its high physical and chemical heterogeneity and its excellent three-dimensional exposures. Four hundred seventy-six, spatially-located, 30 gram sediment samples were collected from an eight square meter outcrop of glaciofluvial sands and gravels. Lithofacies bounding surfaces were mapped on outcrop photographs. Permeability and porosity were measured on 476 samples. Twenty-four hour dithionite citrate (DC)-extractable iron (Fe) and manganese (Mn) were measured on 99 samples. Munsell color was measured on 91 samples. Lead ( $Pb^{2+}$ ) sorption was measured on 72 samples. Magnetic mineral content and twenty-four hour DC-extractable aluminum (Al) were measured on 71 samples. BET surface area was measured on 43 samples. Grain size was measured on 10 samples, and organic and inorganic carbon were measured on 9 samples. Univariate, multivariate, and spatial statistical analyses helped characterize the heterogeneity and identify significant cross-correlations. Thin section and SEM-EDS analyses supported predictive models of chemical heterogeneity and shed light on its geologic origin. And finally, a series of numerical modeling experiments with the reactive transport code OS3D (Steeffel and Yabusaki 1996) tested hypotheses regarding the effects of the spatial pattern of reactivity on heavy metal transport.

A conceptual model of chemical heterogeneity was developed in the early stages of this study. The model provides a useful framework for presenting the information in this dissertation. According to the conceptual model, chemical heterogeneity has three attributes: 1) the relationship between aquifer properties and reactivity at a given point, 2) the spatial distributions of the reactive properties, and 3) the accessibility of the

reactive surface sites. Reactive site accessibility, in turn, has three attributes that influence the rate and extent of solute-solid interactions: the location of reactive sites on individual particles – whether they are exposed on surfaces or “hidden” in secondary pores; the spatial density of reactive particles – whether diffuse or concentrated in zones; and the orientation of reactive zones with respect to ground water flow.

Chapters 1 and 2 address the first attribute of chemical heterogeneity. Chapter 1 reviews the sources and mechanics of aquifer reactivity and presents several approaches for modeling sorption in flowing ground water. The first section in Chapter 1 describes the origin of solid phase reactivity in terms of isomorphous substitutions and surface composition, structure and roughness. The next two sections provide an introduction to absorption and precipitation, along with a detailed discussion of the processes and kinetics of adsorption. The advection-dispersion equation is derived in Section 4, its limitations for modeling solute transport are noted, and supplemental equations for equilibrium and kinetic adsorption are given. The chapter closes with a critical evaluation of the empirical and surface complexation approaches to modeling adsorption under the assumption of local equilibrium.

Chapter 2 presents a site-specific investigation of the relationship between aquifer properties and reactivity that builds on the Chapter 1 overview. It begins with a review of attempts to identify the dominant reactive phase at a variety of sites in Europe and North America; then it focuses on the Deerfield site. Summary statistics for Deerfield sediment properties are provided, along with bivariate and multivariate relationships between reactivity (defined in terms of  $Pb^{2+}$  partition coefficients) and physical and chemical properties. The regression results are used to identify the solid phases controlling  $Pb^{2+}$  sorption, and to develop predictive models of  $Pb^{2+}$  partition



coefficients and reactive surface area that are based on relatively simple and inexpensive measures of sediment characteristics.

Chapter 3 tackles the second attribute of chemical heterogeneity – the spatial distribution of reactive properties. First, it describes the spatial variation of sorption-related properties in the context of stochastic models. In the stochastic approach to modeling heterogeneity, the spatial relationships of aquifer properties are typically described in terms of variogram function models. Variogram models are constructed for permeability, porosity, and DC-extractable metals to quantify and compare their spatial correlation structures.

Since an understanding of the geologic origins of sorption-related properties is needed to interpret their spatial variation, field and petrographic observations are combined with extractable metal data to reveal processes controlling their spatial distributions at the Deerfield site. Heterogeneities in sorption-related properties are also assessed with respect to two mappable geologic features: sediment color and lithofacies bounding surfaces. Lithofacies are bodies of sediment that can be distinguished from one another on the basis of their sedimentary structures and their mineralogic and petrographic characteristics. Analysis of variance (ANOVA) is used to determine whether or not the observed variability in a sorption-related property can be attributed to differences between color groups or lithofacies. If color differences and/or lithofacies explain a significant portion of its variation, then one or both of these sources of geologic information could be used to map the property over a wide range of spatial scales.

The third attribute of chemical heterogeneity – the impact of reactive site accessibility on solute transport – is evaluated in Chapter 4 with the reactive transport code OS3D. Most reactive transport codes rely on empirical partitioning relationships to

describe the removal of solutes from solution. OS3D was selected because it explicitly models the chemical reactions that take place between solutes and reactive surfaces.

In Chapter 4, Cobalt ( $\text{Co}^{2+}$ ) transport is simulated through a hypothetical sandy aquifer, consisting of inert quartz grains that are variably coated with goethite ( $\alpha\text{-FeOOH}$ ). Goethite is a common analog for (hydr)oxide grain coatings in reactive transport models (Davis and Kent 1990, Tompson et al. 1996), and it is the only (hydr)oxide solid in the OS3D database. Although  $\text{Co}^{2+}$  is not an ideal surrogate for  $\text{Pb}^{2+}$ , it is the only divalent heavy metal available in OS3D. Three patterns of goethite grain coatings are examined: uniform, banded, and random. In each case the physically homogeneous modeling domain contains the same total number of reactive sites in order to isolate the effects of the spatial pattern of reactivity on solute migration. The impacts of these different patterns are evaluated, and suggestions are given for improving models of reactive transport through (hydr)oxide-coated media.

Chapter 5 summarizes the findings presented in Chapters 1 through 4. This final chapter also offers suggestions for follow-up studies to corroborate results, refine conclusions, address nano-scale and basin-scale issues, and improve the cost-effectiveness of characterization methods.

Chapters 1 through 4 were written in journal paper format; therefore, some of the background information has been placed in appendices. Appendix A adds to the methods sections in Chapters 2 through 4. It describes in greater detail the reasons for studying heterogeneity at the centimeter- to meter-scale of observation. It elaborates on the sampling strategy and  $\text{Pb}^{2+}$  adsorption experiments presented in Chapters 2 and 3. It offers critical evaluations of selective extraction methods and sediment color measurement methods, and it describes why the magnetic susceptibility and BET surface area measurements were not used in Chapters 2 and 3.

Appendix B provides a detailed description of heterogeneity mapping methods that expands on the information given in Chapter 3. Appendix C displays SEM-EDS maps and photomicrographs of mineral grains in thin section. Appendix D contains a summary data table for all 476 sediment samples. Appendix D also includes a set of grain size distribution curves for ten samples that represent the range of sediment types exposed in the Deerfield outcrop.

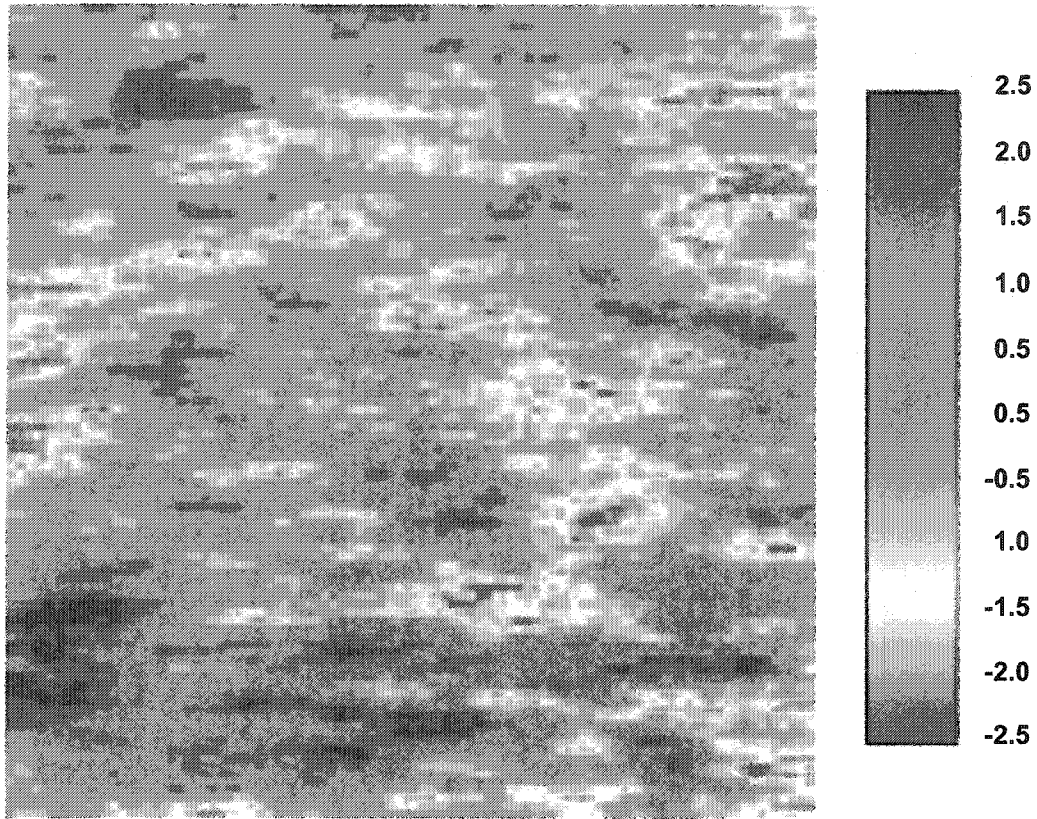


**Figure I.1** Stochastic (Gaussian) model of permeability  $[\ln(k)]$  with a horizontal to vertical anisotropy of 10 to 1. Note the gradual change in permeability across the random field and the lack of connectedness of extreme values. Geostatistical models often lack geologic reality. Although some stochastic methods can simulate discrete geologic features, they still cannot identify their actual locations at a site; they simply indicate their likelihood of occurrence at a given location.

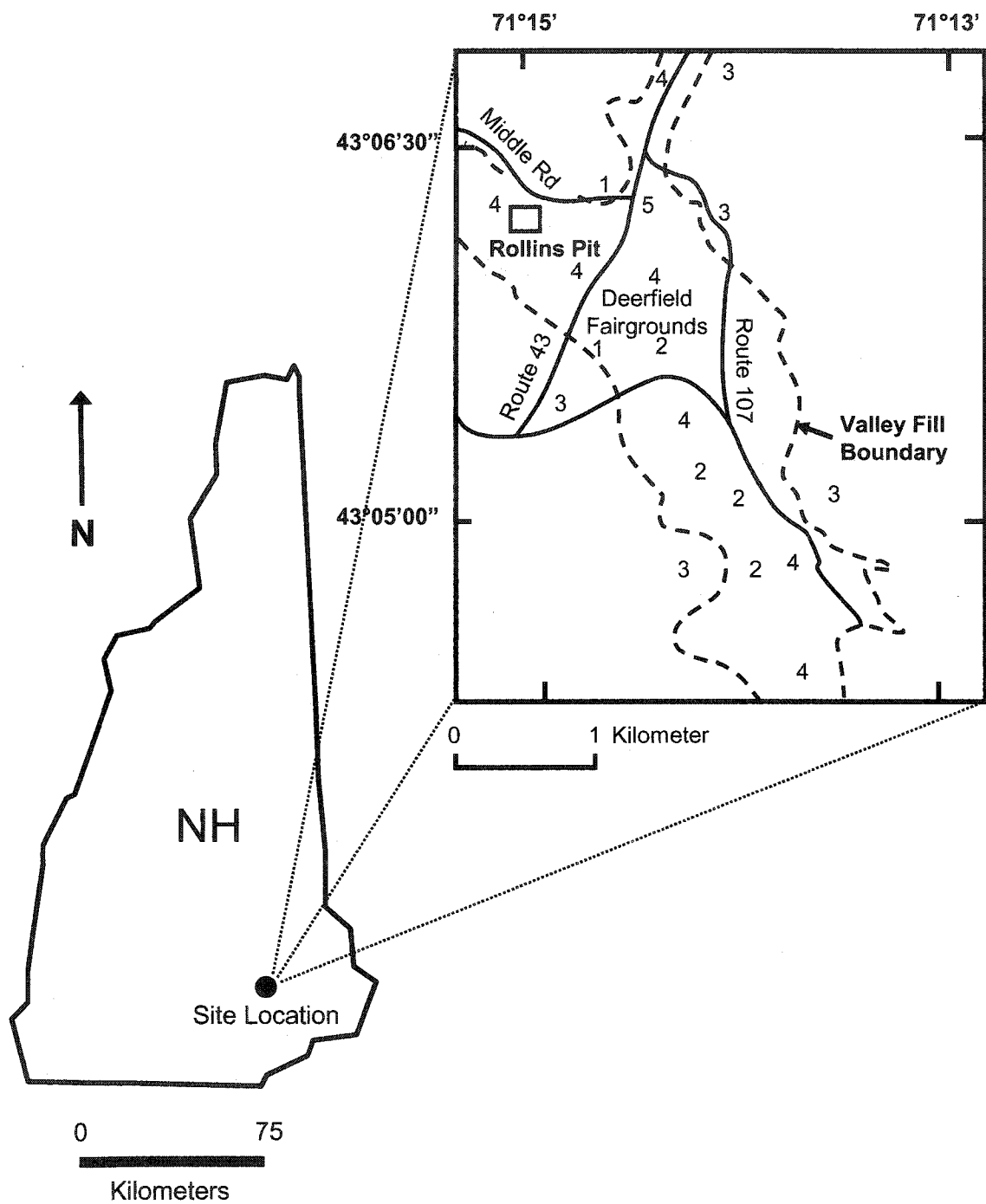


**Figure I.2** Location of the Deerfield site (Rollins Pit). Numbers correspond to surface geologic features: (1) kame terraces, (2) esker ridges, (3) till and bedrock, (4) outwash, (5) moraine. Modified from Moore (1990).

## CHAPTER 1

### AQUIFER REACTIVITY AND REACTIVE SOLUTE TRANSPORT

#### Origins of Reactivity

The reactivity of an aquifer solid depends upon one of its internal characteristics and three of its surface characteristics. The internal property that affects reactivity is the extent of isomorphous substitution (Parks 1990). Isomorphous substitution refers to the substitution of one ion for another of similar size in a crystal without changing the structure of the crystal. When substitutions occur between ions of unequal valence (such as  $\text{Si}^{4+}$  or  $\text{Mg}^{2+}$  for  $\text{Al}^{3+}$ ), excess positive or negative charges may develop within the crystal that attract dissolved anions or cations to its surface. Isomorphous substitutions normally take place during mineral crystallization, and the resulting charge is independent of solution pH; as a result, this source of charge is referred to as permanent charge. Although isomorphous substitutions occur in both primary and secondary minerals, they only produce significant surface charge in phyllosilicate clay minerals.

The three surface features that affect reactivity are: composition, structure, and roughness (Hochella and White 1990). The surface composition of a mineral is almost always different from its bulk composition. Elements are added to and/or lost from all but the most inert surfaces when they are exposed to air or water. The attachment and detachment modifications may be restricted to the top monolayer, or in the case of chemical weathering, they may extend into the mineral thousands of Angstroms or more, depending on the mineral and the weathering conditions. Furthermore, the

attachment and detachment of elements rarely happens uniformly, resulting in surface compositions that are both laterally and vertically heterogeneous (Hochella 1990). Surface compositional heterogeneities create different sites on a surface having different reaction potentials for a given solute (Hochella 1990).

The atomic structures in the top few monolayers of a surface may also be different from those in the bulk. Because the coordination chemistry of surface and near-surface atoms is different from that of like atoms in the bulk, their bond angles and lengths may be modified (Brown 1990). For example, low energy electron diffraction (LEED) images suggest that carbonate groups on calcite surfaces are slightly rotated, and the arrangement of oxygen atoms on (001) hematite surfaces are less distorted, when compared to those in the bulk (Hochella 1990). Structural differences between like atoms may exist not only between the bulk and the surface, but also between individual surfaces. The effect of surface atomic structure on reactivity was demonstrated by Ernsberger (1960) who found that hydrofluoric acid, HF, dissolved quartz 100 times faster on a (001) face than on prism faces perpendicular to it.

The reactivity of a mineral surface generally increases as its atomic and molecular-scale roughness, and therefore its reactive surface area, increases (Hochella 1990). Roughness at this scale is a key factor in surface reactivity because it affects the nature and total number of reactive surface sites. Microtopographic imaging methods generally support the conceptual model for surface roughness shown in Figure 1.1. According to this model surfaces consist of flat areas called terraces, which are separated by steps that may be one or more atomic layers high. Kinks occur where steps change direction. Atomic or molecular size holes in terraces are called vacancies, and individual atoms or molecules positioned on top of terraces are called adatoms or admolecules.

The reactivities of sites on these different surface features vary in part with the number of neighboring atoms or molecules (Hochella 1990). Terrace atoms have the greatest number of neighbors; as a result, they offer the fewest bonding possibilities and tend to be the least reactive sites on a surface. By contrast, adatoms generally have the fewest adjoining atoms or molecules, so they are potentially the most reactive sites.

Perdereau and Rhead (1971) studied the sorption of O<sub>2</sub> and H<sub>2</sub>S gases onto copper surfaces having varying step densities. They concluded that sorption took place preferentially at steps and that the rate of sorption should increase with increased step density. Christmann and Ertl (1976) used several microtopography imaging tools to demonstrate that H<sub>2</sub>(g) was more likely to sorb to Pt (111) surfaces at step or kink sites than terrace sites. Lee and Jackson (1977) also observed preferential sorption of <sup>235</sup>U at step sites vs. terrace sites on biotite and muscovite surfaces.

Unlike bulk properties, mineral surface properties are dynamic. Surface microtopography, composition, and structure change with the attachment and detachment of atoms and molecules (Hochella 1990). Specific attachment/detachment processes are discussed in the following two sections.

### **Solute-Solid Reactions**

The nature and rate of solute-solid interactions are affected by a number of confounding solution-related variables in natural systems including: pH, temperature, redox state, adsorbate character, competitive ion effects, the nature and abundance of soluble organic carbon compounds, and the ratio of total adsorbate present to adsorbent surface area. Nevertheless, the generalizations presented in this section and the next are helpful for understanding aquifer reactivity.



The processes by which a solute may interact with a surface include absorption, adsorption, and precipitation. (If the specific mechanism responsible for uptake is not known, the process is called sorption.) Absorption involves the diffusion of a solute into the interior surfaces of a solid (Fetter 1999). It also refers to the incorporation of a solute into a solid phase by dissolution and subsequent reprecipitation of the solid's surface. Through this process the former solute is included as part of a solid solution or solid inclusion (Brown 1990).

Adsorption is the accumulation of matter at a solid-solution interface without the development of a three-dimensional structure (Sposito 1990). Precipitation is the formation from solution of a solid phase that has a three-dimensional structure. Traditionally, this process was thought to occur only when the ground water was supersaturated with respect to a mineral containing the solute of interest. However, recent studies have shown that solutes can precipitate from apparently undersaturated solutions in the course of adsorption-reduction reactions taking place at sulfide mineral-solution interfaces (Bancroft and Hyland 1990). Furthermore, James and Healy (1972) proposed that the solubility products of precipitates are significantly reduced by the low dielectric constant of water near a surface. If so, precipitation could potentially occur in "unsaturated" solutions containing nonsulfide minerals.

## **Adsorption**

### **Introduction**

According to Schindler (1990) the adsorption of solutes is based on forces acting between the surface, solute, and solvent, and these forces are themselves dependent on four properties of solutes and surfaces: surface charge, Lewis acidity, Lewis basicity, and polarity.

Surface Charge. The coordination environment of atoms at the surface of solids is usually different from that in bulk. In hematite, for example, each  $\text{Fe}^{3+}$  ion in the bulk is in a six-fold coordination with neighboring  $\text{O}^{2-}$  ions. Each of these oxygen ions supplies -0.5 charge to neutralize the +3 charge of the iron, while the remaining -1.5 charge satisfies adjacent  $\text{Fe}^{3+}$  ions. However, crystal bonding terminates at the crystal-liquid interface, so the coordination of surface iron and oxygen atoms is completed by interaction with the solvent (Bohn et al. 1985). In aqueous systems, hydroxide ( $\text{OH}^-$ ) ions in solution bond to coordinatively unsaturated surface cations and hydrogen ( $\text{H}^+$ ) ions bond to unsatisfied surface oxygens, both reactions producing surface hydroxide functional groups. The dissociation constant for water is much lower on a mineral surface than in solution, thereby enhancing this surface hydroxylation process (Parks 1990).

In high pH environments hydrogen ions may be removed from surface hydroxyl groups to produce negative charge sites. The reaction can be described by:



where S represents a surface metal cation. In low pH environments hydrogen ions from solution may be added to the hydroxyl groups, producing positive charge sites:



Although surface ionization is primarily due to the pH-dependent protonation and deprotonation of hydroxyl groups, it may also result from the binding or release of metal cations and anions (Schindler 1990).

The ionization of surface functional groups is the sole mechanism by which oxides, hydroxides, and organic matter develop charge, although the most important functional groups on organic matter surfaces are phenolic ( $-\text{C}_6\text{H}_4\text{OH}$ ) and carboxyl ( $-\text{COOH}$ ) groups (Davis and Kent 1990). Evidence for surface charge and its pH

dependence includes the pH-dependent migration of suspended particles in an imposed electrical field (electrophoresis), and the generation of a pH-dependent electrical potential gradient in the direction of fluid flow (the streaming potential) when fluid flows through a column packed with sediment (Parks 1990).

Phyllosilicate clay minerals develop charge from isomorphous substitution as well as protonation and deprotonation of surface hydroxyl groups. Isomorphous substitutions can lead to a net charge on the structural framework of the mineral, and the net charge is independent of pH. Consequently, clay minerals may simultaneously possess positive and negative charges. For example, in low pH environments a clay mineral may have negatively charged planar surfaces due to isomorphous substitution, and positively charged edges due to protonation of the surface hydroxyl groups that form at broken bonds along phyllosilicate mineral edges.

(Hydr)oxides may also possess positive and negative charge sites at the same time. Although the *net* surface charge may be positive in an acid environment, some of the reactive surface functional groups may be negatively charged, with the proportion of negative charge sites increasing as pH rises. As pH increases, cation retention increases and anion retention decreases (Bohn et al. 1985, Davis et al. 1987). The pH at which the number of positive and negative charges on a surface is equal – the zero point of charge (ZPC) – is unique for each mineral and organic compound.

Ionic solids such as calcite develop surface charge through nonstoichiometric dissolution at the solid-liquid interface (Parks 1990). At constant pH the constituent ions (e.g.,  $\text{Ca}^{2+}$  and  $\text{CO}_3^{2-}$  in calcite) are responsible for surface charge in the same fashion that  $\text{H}^+$  and  $\text{OH}^-$  determine the charge on (hydr)oxide and organic surfaces. Furthermore, some ionic solids such as calcite show pH-dependent charge as well. The pH dependence may be due to changes in the activities of the charge determining ions,

or reactions with water to form ionizable surface functional groups such as CaOH (Parks 1990).

Lewis Acidity and Basicity. The Lewis definitions of acids and bases are more general than those of Bronsted because they are based on the sharing of electron pairs rather than on proton transfers. A Lewis acid is a substance such as a free metal cation or a coordinatively unsaturated surface metal cation that has at least one empty orbital and therefore can accept a pair of electrons to form a new bond. Lewis bases are neutral or anionic substances such as water molecules or deprotonated surface functional groups that can donate an unbonded pair of electrons (a "lone pair") to form a new bond. The bond formed by the donation and acceptance of a lone pair is called a coordinate covalent bond, the structural unit formed by these bonds is termed a metal complex or coordination compound, and the neutral or anionic groups that donate the lone pairs are termed ligands.

An important Lewis acid-base reaction occurs when coordinatively unsaturated surface metal cations coordinate with water molecules:



The positively charged water molecules at these Lewis acid sites are unstable and can either be deprotonated or exchanged for anions in solution (Sposito 1990).

Polarity. Polarity controls the interactions between surfaces, water, and nonionic organic solutes (Schindler 1990). Uncharged organic solutes display varying degrees of polarity. Although polar and amphipatic forms exist (amphipatic organics have both polar and nonpolar entities), most nonionic organic solutes are nonpolar (Bohn et al. 1985). By contrast, water is highly polar; as a result, most uncharged organics are only slightly soluble in aqueous solutions and readily sorb to aquifer solids. Their adsorption

is driven by the incompatibility of nonpolar solutes with water, not by the attraction of these solutes to a surface.

Polarity is also responsible for the hydration of ions in solution. Simple, free ions do not exist in aqueous solutions – they interact with other dissolved ions to varying degrees, and they form coordination compounds with polar water molecules (Figure 1.2). The number of coordinate covalent bonds between the water ligands and the central ion is its hydration number (or coordination number) which is usually between 2 and 6 (Bohn et al. 1985). The ion and its bound water molecules behave as a single large ion. The water ligands are neutral so the hydrated ion has the same charge as that of the central ion. All dissolved ions are surrounded by a shell of water molecules, but ions differ in the strength with which they attract and hold their waters of hydration.

### **Adsorption of Cations**

Cation adsorption occurs by one of three mechanisms: inner-sphere surface complex formation, outer-sphere surface complex formation, or diffuse ion association (Sposito 1989). Surface complexes form when surface functional groups react with dissolved ions to form stable molecular units. The complex is outer-sphere when the ion retains its waters of hydration; it is inner-sphere if it loses one or more of its waters of hydration and bonds directly to one or more surface oxygens. When the dissolved ion remains dissociated from surface functional groups and instead neutralizes charge in a nonlocalized sense by its close proximity to the surface, it is adsorbed by diffuse ion association (Figure 1.3).

In general, diffuse ion association and outer-sphere surface complexation involve only electrostatic interactions – long-range coulombic forces and hydrogen bonding (Brown 1990). Since the identity of the cation is relatively unimportant in these

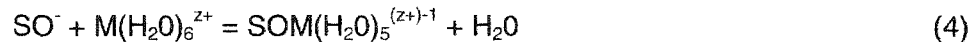
interactions, they are considered nonspecific adsorption processes. On the other hand, inner-sphere surface complexation involves direct, short-range electrostatic (ionic) or covalent bonding. Ionic and covalent bonding depend significantly on the electron configurations of the complexing ion and surface functional group, so inner-sphere surface complexation is considered a specific adsorption process.

Due to the differences in strength between long-range coulombic forces, hydrogen bonding, and short-range ionic or covalent bonding, the relative strength of interaction among the three adsorption mechanisms is: inner-sphere surface complexation > outer-sphere surface complexation > diffuse ion association (Brown 1990). The most important factor determining the relative strength of adsorption for a particular cation is its valence – higher valence ions are typically attracted to and retained by surfaces more strongly than lower valence ions (Bohn et al. 1985, Parks 1990). For ions of equal valence, those with larger dehydrated radii are usually held more strongly. Larger ions have lower surface charge densities so they tend to attract waters of hydration less strongly. As a result, larger dehydrated ions generally have smaller hydrated radii and can approach surfaces more closely, and dehydrate more readily to form inner-sphere complexes.

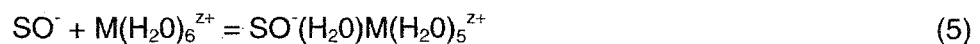
The extent of reversibility in adsorption/desorption studies has often been used to estimate the relative strength of ion adsorption; however, this can be a poor measure of the strength of adsorption, because several factors in addition to adsorptive affinity can affect the ease of reversibility. For example, the slow diffusion of ions out of a microporous medium could be erroneously interpreted as the limited desorption of strongly bound ions.

The adsorption of most metal ions is not constrained by ionic strength or *net* surface charge. These cations apparently lose one or more of their waters of hydration

and bond covalently to one or more deprotonated surface functional groups to form inner-sphere surface complexes (Schindler 1990):



Ionic organic compounds and metal ions with little Lewis acidity such as the alkali metals (e.g.  $\text{Li}^+$  and  $\text{Na}^+$ ) and the alkaline earth metals (e.g.  $\text{Ca}^{2+}$  and  $\text{Sr}^{2+}$ ) generally sorb by electrostatic attraction, because their adsorption is dependent upon the ionic strength of the solution. If the overall charge of the surface also governs their adsorption, the ions do not form complexes with the surface, but rather are located in a detached, diffuse layer about the surface. If the ions can sorb even when the net surface charge is the same as their own, they apparently form outer-sphere complexes with oppositely charged surface functional groups (Figure 1.4). The outer-sphere surface complexation reaction can be described by:



which indicates the metal ion is still coordinated with six water molecules and there is no direct link between the metal ion and the surface functional group (Schindler 1990).

X-ray adsorption spectroscopy (XAS) methods which use a high intensity source such as a synchrotron, can discriminate between inner-sphere and outer-sphere surface complexes. These techniques provide information on: 1) the average interatomic distances between the probed atoms and their first and second nearest neighbors, and 2) the average number and identity of atoms in each of the two shells (Hochella and White 1990). Bargar and colleagues (1997a, 1997b) used XAS to study  $\text{Pb}^{2+}$  adsorption to alumina, hematite, and goethite. They concluded that  $\text{Pb}^{2+}$  bonds predominantly to alumina, and solely to hematite and goethite, as bidentate inner-sphere complexes on the edges of  $\text{AlO}_6$  or  $\text{FeO}_6$  octahedra (Figure 1.5). The average coordination environment for the  $\text{Pb}^{2+}$  adions appears to be a distorted trigonal pyramid with  $\text{Pb}^{2+}$  at

the top and a hydroxide ion or surface oxygen at each corner of the base. On the side of the anion opposite the alumina or iron oxide surface there is a lone pair of electrons and weakly-bonded solvating water molecules. Although aluminum and iron oxides have fundamentally similar crystal chemistries, they exhibited differences in  $Pb^{2+}$  sorption behavior.  $Pb^{2+}$  sorption occurred at lower pH on hematite and goethite than on alumina. Sorption densities were higher on iron oxide edges than on alumina edges, and both mononuclear monodentate and multinuclear Pb complexes were observed on alumina.

### **Adsorption of Anions**

Anion adsorption occurs by the same three mechanisms as for cations. An important inner-sphere surface complexation reaction involving anions is ligand exchange. In ligand exchange dissolved anions displace surface functional groups and bond directly to the solid's peripheral cations. Arsenate ( $AsO_4^{3-}$ ), phosphate ( $PO_4^{3-}$ ), selenite ( $SeO_3^{2-}$ ) and several other oxyanions participate in ligand exchange with the hydroxyl groups on (hydr)oxide surfaces according to the following generalized reaction:



where  $A^{z-}$  is an oxyanion such as  $SeO_3^{2-}$  and S is a surface cation such as ferric iron ( $Fe^{3+}$ ) or  $Al^{3+}$  (Davis and Kent 1990).

Hayes et al. (1987) used XAS to demonstrate that weakly sorbing selenate ions are retained on goethite as outer-sphere surface complexes, whereas strongly sorbing selenite ions are retained as inner-sphere complexes. Their XAS data showed that selenate ions had no detectable iron atoms among their second nearest neighbors, while the distances between selenite ions and neighboring surface irons was too small to accommodate intervening water molecules.



### Proton Stoichiometry

The stoichiometry of H<sup>+</sup> in ion adsorption reactions is poorly understood. Cation adsorption onto a (hydr)oxide, organic matter, or clay mineral surface is generally accompanied by a decrease in solution pH, indicating a release of protons by the surface. However, the net release of protons observed in experiments is due not only to adsorption reactions, but also to solution and surface site adjustments to a new equilibrium condition (Davis and Kent 1990). As a result, it is difficult to infer proton exchange stoichiometry from empirical observations of pH change.

If integer values for the molar ratio of H<sup>+</sup> released to M<sup>z+</sup> adsorbed are observed, a single reaction such as:



or



might be the case. However, noninteger values are the norm and suggest M<sup>z+</sup> hydrolysis during adsorption (Davis and Leckie 1978, Bargar et al. 1997a), exchange in the diffuse layer, or multiple surface reactions involving perhaps, exchange for presorbed cations as well as H<sup>+</sup> (Parks 1990).

### Adsorption of Nonionic Organic Compounds

Adsorption of nonionic organic solutes (NOS) takes place primarily by hydrogen bonding and van der Waals interactions (Sposito 1989). Hydrogen bonding involves strong dipole-dipole interactions between polar molecules. More specifically, a hydrogen bond is an electrostatic bond formed between a hydrogen atom covalently bonded to an electronegative atom such as oxygen (O) or nitrogen (N), and the lone pair

of an electronegative atom on another molecule. The hydrogen atom takes on a partial positive charge because the electron density is shifted toward the electronegative atom to which it is covalently bonded. Similarly, the electronegative atom on the other molecule takes on a partial negative charge. A hydrogen bond, then, is a bridge between two highly electronegative atoms on different molecules. The hydrogen atom is bonded covalently to one of them, and electrostatically to a lone pair on the other. The greater the electronegativity of the atom connected to the hydrogen, the greater the partial positive charge and hence, the stronger the hydrogen bond it can form.

Hydrogen bonding is an important reaction mechanism between polar organic solutes and organic solids, but it does not appear significant in reactions between organic solutes and mineral surfaces because the oxygen atoms on mineral surfaces have low electronegativities. Nonetheless, polar organics may be indirectly adsorbed to mineral surfaces via hydrogen bonding with the waters of hydration on adsorbed cations – a process called water bridging (Figure 1.6). Strongly hydrated cations increase the polarization of their coordinated water molecules relative to water molecules in the bulk solution (Bohn et al. 1985), facilitating the adsorption of polar organics from aqueous solutions.

The dominant mode of adsorption for nonpolar and amphipatic organics is hydrophobic expulsion assisted by van der Waals interactions (Schindler 1990). Hydrophobic expulsion, the expulsion of the solute by the aqueous phase, occurs when both the solute-solute and solvent-solvent interactions are stronger than the solute-solvent interactions (Schindler 1990). Van der Waals interactions involve weak, short-ranged bonds between permanent or induced polar units on a solute and a surface. Polarity is induced in nonpolar units through the fluctuations in their charge distributions that occur over extremely small time scales. On a time scale of  $\leq 10^{-16}$ s electron

movement causes the charge distribution of a nonpolar unit to fluctuate, taking on the character of a flickering dipole. Although the deviations in charge distribution average to zero over longer scales of time, they persist long enough to produce an attractive interaction between nonpolar units when the distance between the units is  $\approx 0.1$  nm or less (Sposito 1989). The van der Waals attraction between two units is very weak, but like hydrogen bonds their effects are additive, so when many units in a polymeric solute interact simultaneously with units on a surface the solute may be strongly retained. Van der Waals attractions operate in all solute-solid interactions, but are only important in the retention of uncharged polymeric molecules because the stronger electrostatic forces involved in the retention of charged species overshadow their effects.

The solubilities of uncharged organic compounds in water decrease with decreasing polar character. The partition coefficient,  $K_d$ , provides a measure of solubility:

$$K_d = \frac{\text{sorbed concentration}}{\text{solution concentration}} \quad (9)$$

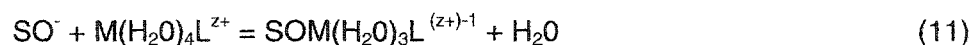
The  $K_d$  for a hydrophobic solute is dependent on one property of the solute (its organic solvent/water partition coefficient) and one property of the adsorbent (the fraction of the surface consisting of organic carbon) such that:

$$\log K_d = \alpha \log K_{ow} + \log f_{oc} + \beta \quad (10)$$

where  $\alpha$  and  $\beta$  are empirical coefficients,  $K_{ow}$  is the concentration in octanol divided by the concentration in water, and  $f_{oc}$  is the solid fraction consisting of organic carbon (Schindler 1990).

## Coadsorption of Metal Ions and Organic Ligands

Metal ions and organic ligands coexist in natural systems. They may sorb independently or they may form aqueous metal-ligand complexes which may or may not sorb to aquifer solids (Schindler 1990). Sorption of these complexes can occur if one or more sites in the coordination shell of the metal ion are still occupied by water molecules:



However, if the organic ligand (L) can simultaneously coordinate with all of the coordination sites on the metal ion, the aqueous complex can not be sorbed by surface complexation (Schindler 1990). EDTA is an example of an organic ligand that can coordinate with all six sites on a metal ion such as  $Pb^{2+}$  and prevent its adsorption.

Inorganic ligands such as  $Cl^-$  and  $CO_3^{2-}$  adsorb weakly or nonspecifically onto most surfaces. These ligands may also inhibit the adsorption of metals with which they form aqueous complexes. Adsorption is inhibited because the complexing ligands reduce the activity of the metal ion, and bind the metal ion in complexes that adsorb less strongly (Parks 1990).

## Reaction Rates

Adsorption and desorption are virtually instantaneous for non-specifically adsorbed ions. Their reaction rates are usually governed only by diffusion to and from the solid surface (Sposito 1989). Specifically adsorbed ions show more complicated behavior, often sorbing and desorbing by multiple mechanisms.

Studies of cadmium (Cd), cobalt (Co), manganese (Mn), and strontium (Sr) sorption on carbonate surfaces (McBride 1979, Lorens 1981, Davis et al. 1987, Fuller and Davis 1987) and arsenate, silver (Ag), Cd, Co, copper (Cu), mercury (Hg), nickel

(Ni), Pb, selenite, and zinc (Zn) retention on oxide surfaces (McKenzie 1972, Anderson et al. 1973, Burns 1976, Kou 1986, Fuller et al. 1993, Ainsworth et al. 1994, Papelis 1995, Papelis et al. 1995, Strawn et al. 1998, Scheinost et al. 2001) demonstrate that the sorption of many anions and heavy metals can occur in two steps: an initial fast process lasting minutes to hours, followed by a slow continuous process requiring several days or even months to reach equilibrium. The initial rapid step is generally thought to be reversible, diffusion-controlled adsorption to readily-available high reactivity surface sites. The slow step has been characterized as 1) surface precipitation, 2) substitution of the sorbed cation for a matrix cation, 3) sorption to surface sites of lower reactivity, or 4) diffusion into micropores followed by sorption to interior sites.

In a study of Cd sorption on calcareous sand, Fuller and Davis (1987) interpreted the first step to be rapid adsorption followed by diffusive transport into micropores, fractures, and disordered surface films of hydrated calcium carbonate. The second step was attributed to the formation of a (Ca,Cd)CO<sub>3</sub> solid solution within the hydrated films found on carbonate grains. The constant rate of sorption in the slow step precluded diffusion as the controlling mechanism, and precipitation of pure cadmium mineral phases was avoided by the use of solutions that were undersaturated with respect to these phases. Information supporting a surface coprecipitation mechanism included the similarity in sorption behavior between the sand and pure calcite (Davis et al. 1987), the similarity in ionic radii between Cd and calcium (Ca), and the low solubility of (Ca,Cd)CO<sub>3</sub>. Xu et al. (1996) used XAS to demonstrate that aqueous Co does in fact sorb to calcite surfaces by forming a solid solution with CaCO<sub>3</sub>.

Ainsworth et al. (1994) examined Co, Cd, and Pb adsorption to ferrihydrite (poorly crystalline Fe<sub>2</sub>O<sub>3</sub>·nH<sub>2</sub>O). They found Pb adsorption was almost completely

reversible, while Co and Cd displayed two-step adsorption behavior with substantial nonreversibility. For Co and Cd the slow step appeared to be incorporation into the iron oxide via isomorphous substitution as the ferrihydrite recrystallized to goethite. Several lines of evidence supported this conclusion: recrystallization of ferrihydrite to goethite was observed during the experiment, Pb adsorption was fully reversible, more Co was irreversibly sorbed than Cd, and the ionic radius of Fe is most similar to Co and most dissimilar to Pb. Furthermore, diffusion could not have been the slow process because Pb adsorption was rapidly reversible. Likewise, slow reversible sorption was ruled out since the Co and Cd that remained sorbed after 16 hours could not be desorbed. Apparently, ionic radius determined whether the metal would be incorporated into the recrystallizing oxide and at what rate. Pb remained nonspecifically sorbed to the oxide surface because its large ionic radius prohibited isomorphous substitution for Fe.

Lehmann and Harter (1984) studied the kinetics of Cu desorption from the surface horizon of a New England soil and found that desorption also occurred in two steps. The initial fast reaction was attributed to the removal of Cu from loosely-binding, low reactivity surface sites; the slow reaction was likely due to release from higher energy sites. An alternative explanation that fast release was from external sites and slow release was from diffusional transfer from internal sites is less likely since: 1) the reaction time was probably too short for the required extent of diffusion, and 2) fast desorption did not occur when the amount of Cu added to the soil was reduced below a threshold concentration.

Researchers are increasingly invoking diffusion to explain the slow adsorption and desorption of anions and cations. In a study of lithium (Li) removal by feldspars and micas, Wood et al. (1990) observed decreasing concentrations in solutions throughout the 28 days of the experiment. In their view Li removal was not due to precipitation or

microbial uptake because Li concentrations did not drop in control solutions containing glass beads; nor was removal due to ion exchange since the Li concentrations did not stabilize after a few hours. Instead they believed Li removal was due to diffusion into secondary pore spaces. Wood (1996) further argued that diffusion through intragranular pores is responsible for the slow rates of desorption observed during the remediation of many contaminated aquifers.

Strawn et al. (1998) applied kinetic and spectroscopic measurements to the study of Pb adsorption and desorption on alumina. In both adsorption and desorption there was a fast reaction followed by a slow reaction. The rate-limiting reaction was neither Pb substitution nor precipitation because Pb sorption was 98 percent reversible within three days, Pb and Al ionic radii are prohibitively dissimilar, and the Pb adion coordination environment, consistent with the formation of bidentate inner-sphere sorption complexes, remained unaltered with time. Strawn and colleagues concluded that the slow reaction was most likely intraparticle diffusion, though they could not rule out the possibility of sorption onto surface sites with large activation energies. In a similar kinetic-spectroscopic study of Cu and Pb sorption onto ferrihydrite, Scheinost et al. (2001) found the adion molecular environment to be stable over time and consistent with bidentate, edge-sharing, inner-sphere sorption. They also attributed the rate-limiting process to intraparticle diffusion.

## **Modeling Reactive Transport**

### **The Advection Dispersion Equation**

Solute transport is most often modeled using the advection dispersion equation, or ADE. The ADE is a statement of the law of the conservation of mass (Freeze and Cherry 1979). In its simplest form this law may be written as:

inputs - outputs = change in storage

When applied to the conservation of a mass flux of solute in one dimension, it may be written as:

$$\frac{\partial}{\partial x} F_x = -n_e \frac{\partial C}{\partial t} \quad (1)$$

where:  $F_x$  = mass flux in x direction

$n_e$  = effective porosity

$C$  = mass of solute per unit volume of solution

$t$  = time

The total mass flux of solute in the x direction (i.e., the total mass of solute transported in the x direction per unit area per unit time) is the sum of the fluxes due to 1) advection – transport by the physical movement of ground water, 2) mechanical dispersion – a mixing process resulting from the differential advection of ground water, and 3) molecular diffusion – movement in response to a gradient in concentration:

$$F_{total} = F_{advective} + F_{dispersive} + F_{diffusive} \quad (2)$$

where:  $F_{advective} = n_e v_x C$

$$F_{dispersive} = -n_e \alpha_x v_x \frac{\partial C}{\partial x}$$

$$F_{diffusive} = -n_e D^* \frac{\partial C}{\partial x}$$

$v_x$  = average ground water velocity in x direction

$\alpha_x$  = dispersivity in x direction

$D^*$  = diffusion coefficient

Diffusion and mechanical dispersion are inseparable in flowing ground water, so their terms are combined and equation (2) becomes:



$$F_{total} = n_e v_x C - n_e D_L \frac{\partial C}{\partial x} \quad (3)$$

where:  $D_L = \alpha_x v_x + D^*$

Substituting equation (3) into equation (1) yields:

$$\frac{\partial}{\partial x} \left[ n_e v_x C - n_e D_L \frac{\partial C}{\partial x} \right] = -n_e \frac{\partial C}{\partial t} \quad (4)$$

Assuming the porosity and ground water velocity in the system are constant, the equation reduces to:

$$\frac{\partial C}{\partial t} = D_L \frac{\partial^2 C}{\partial x^2} - v_x \frac{\partial C}{\partial x} \quad (5)$$

This one-dimensional ADE is a governing equation expressing the relationships between the variables C, x, and t. There are many solution equations that satisfy the relationships expressed by this equation. Unique solutions are found by solving the governing equation for specific initial and boundary conditions.

A weakness of the deterministic ADE is that it assumes mechanical dispersion can be represented by a relationship based on Fick's Law. The Fickian relationship for dispersion was developed using very simple capillary tube and mixing cell models (Bear 1972), and it is not clear how well these simple models apply to complex porous media. In the deterministic ADE all of the dispersive character of the media is embodied in a dispersivity term which has no physical meaning. Its value is simply determined by fitting a solution to the ADE to data from tracer tests or existing contaminant plumes. The value of  $\alpha$  that provides the best fit is taken to be the dispersivity of the media.

Another problem is that the equation is not valid for short travel times and distances (i.e., it is not valid near the upstream boundary). The Fickian expression for dispersion assumes dispersivity is constant. However, field studies have shown that its

value increases as travel time and distance increase, not reaching a constant value until the travel distance is approximately 10 times greater than the dispersivity (Pickens and Grisak 1981, Dagan 1988).

In contrast to the deterministic approach to solving the ADE, the stochastic approach assumes dispersion is caused by the mixing resulting from spatial variations in permeability. It represents the heterogeneity in permeability as a random field – a spatial set of random variables described by the probability distribution of the variables and their spatial correlation. Plus, it gives predictions of solute concentrations in terms of a likely range rather than an absolute answer.

Gelhar and Axness (1983) solved the ADE as a stochastic partial differential equation and found dispersivity was a function of the variance in permeability [ $\ln(k)$ ] and its correlation length ( $\lambda$ ) in the direction of flow. Their model provided a new way to view dispersivity – as a media property related to the characteristics of a permeability random field rather than a fitting parameter with little physical meaning. Since  $\alpha_L = \sigma_{\ln k}^2 \lambda$ , the more heterogeneous the system, the greater the variance in  $\ln(k)$  values, and the greater the dispersion.

Dagan's (1988) stochastic analysis showed  $\alpha_L$  increased rapidly with time, approaching a constant value of  $\sigma_{\ln k}^2 \lambda$  only at large travel times. The travel distance needed to reach a constant value was more than twenty correlation lengths. Thus Dagan's model not only related dispersivity to heterogeneity, it also accounted for the scale dependence of dispersivity observed in field studies.

Neither the deterministic ADE nor its stochastic counterparts is valid for short travel times and distances. This is unfortunate because the behavior of a system near the upstream boundary is often of great interest. Another problem with the stochastic approach is that it requires a great deal of information on the spatial distribution of

permeability in the media. Nonetheless, the stochastic approach gives physical meaning to dispersivity and provides a framework within which the scale dependence of dispersivity can be explained.

The value of dispersivity increases with the scale of observation because ground water encounters greater variations in permeability as travel distance increases. Eventually the flow path becomes long enough that all possible variations in permeability are encountered, so dispersivity reaches a maximum value. It may be difficult to achieve a maximum value of dispersivity in aquifers having substantial variability at large scales. Consequently, the ADE works best when it is applied to relatively uniform media (i.e., media in which mixing takes place at a scale much smaller than the transport distance).

### **Modifying the ADE to Account for Sorption**

The preceding discussion of the ADE applies to nonreactive solute transport; that is, the transport of solutes that do not undergo reactions or transformations as they flow through a system. In order to consider the transport of solutes that sorb to media surfaces, an additional term must be added equation (5):

$$\frac{\partial C}{\partial t} = D_L \frac{\partial^2 C}{\partial x^2} - v_x \frac{\partial C}{\partial x} - \frac{B_d}{n_e} \frac{\partial S}{\partial t} \quad (6)$$

where:  $B_d$  = bulk density of porous media

$S$  = mass of solute sorbed per unit mass of solid

If the rate of sorption is fast compared to the rate of ground water flow, the amount of solute sorbed will not change with time, and an equilibrium model may be used to represent  $S$ . If the rate of sorption is slow compared to the flow velocity,  $S$  will change with time, so a kinetic model is more appropriate.

Under equilibrium conditions, adsorption isotherms are commonly used to describe the adsorption-desorption process. Adsorption isotherms are empirical relationships between the equilibrium concentration of a solute in solution and the amount sorbed. If the relationship is linear, a plot of mass sorbed (S) versus solution concentration (C) will yield a straight line and the isotherm can be described by a linear model of the form:

$$S = K_d C \quad (7)$$

where:  $K_d$  = slope of the linear isotherm

Substituting this expression into equation (6) yields:

$$\frac{\partial C}{\partial t} = \frac{D_L}{R} \frac{\partial^2 C}{\partial x^2} - \frac{v_x}{R} \frac{\partial C}{\partial x} \quad (8)$$

where:  $R$  = retardation factor =  $1 + \frac{B_d}{n_e} K_d$

Since the  $K_d$  of a reactive solute is always greater than 0,  $R$  is always greater than 1. As a result, equation (8) describes two effects of sorption on transport: it reduces dispersion and retards solute movement relative to ground water flow.

The linear adsorption model is appealing because analytical solutions to the ADE for nonreactive solutes can be used with reactive solutes simply by modifying the solution equation coefficients. A drawback of the linear model is that it does not limit the amount of solute that can be sorbed, so it tends to overestimate the adsorption of ionic solutes in all but very dilute solutions. (Although nonionic organic solutes often display linear behavior over a wide range of concentrations, ionic solutes usually display strong nonlinear sorption at high concentrations because the number of charged sites on aquifer surfaces is limited.)

The Freundlich model is more general and has been used to describe the adsorption of a wide variety of metals and organic compounds (Fetter 1999). The Freundlich model is defined by the nonlinear relationship:

$$S = KC^N \quad (9)$$

where:  $K$  and  $N$  are fitting parameters

Substitution of equation (9) into equation (6) provides the retardation factor for the Freundlich model:

$$R = 1 + \frac{B_d}{n_e} KNC^{N-1} \quad (10)$$

The Freundlich model, though more versatile, suffers the same limitation as the linear model, namely there is no upper limit to the amount of solute that can be sorbed.

The Langmuir model is also nonlinear, but it accounts for the finite number of adsorption sites present on a surface:

$$S = \frac{kbC}{1+kC} \quad (11)$$

where:  $k$  = adsorption constant (a measure of the bond strength holding the solute to the surface)

$b$  = maximum amount of solute that can be sorbed

The retardation factor for the Langmuir model is:

$$R = 1 + \frac{B_d}{n_e} \left[ \frac{kb}{(1+kC)^2} \right] \quad (12)$$

Neither the Freundlich nor the Langmuir model can be used in conjunction with analytical solutions to the ADE. However, programs such as MT3D (Zheng 1990) provide numerical solutions to the ADE and can accommodate all three isotherm models.

Kinetic models of sorption are used when the assumption of equilibrium is not valid. The most frequently used kinetic model is the reversible linear model (Travis and Etnier 1981). It assumes the rate of solute sorption is related to the difference between what can be sorbed and what has already been sorbed:

$$\frac{\partial S}{\partial t} = k_1 C - k_2 S \quad (13)$$

where:  $k_1$  = forward rate constant

$k_2$  = backward rate constant

Mass transfer models (Travis and Etnier 1981) of the form:

$$\frac{\partial S}{\partial t} = k_3 (C - C^*) \quad (14)$$

where:  $k_3$  = adsorption rate parameter

$C^*$  = liquid phase concentration of solute in immediate contact with particle surface

describe the situation where the rate of adsorption is limited by diffusion to the adsorption sites. If the adsorption process follows a linear isotherm, the mass transfer model is the same as the reversible linear model.

The reversible nonlinear model is simply a more general version of equation (13) and applies to cases in which the forward adsorption reaction is nonlinear and the backward desorption reaction is linear:

$$\frac{\partial S}{\partial t} = k_1 C^N - k_2 S \quad (15)$$

Success in using equations (13) through (15) has generally been limited to systems with low pore water velocities (Nielsen et al. 1986). For example, van Genuchten et al. (1974) compared predictions of picloram (4-amino-3, 5, 6-trichloropicolinic acid) transport using the reversible linear kinetic, reversible nonlinear

kinetic, and Freundlich equilibrium models, and found that all fit the experimental data at low velocities (14.2 cm d<sup>-1</sup>) while none described the early arrival and extensive tailing observed in breakthrough curves at moderate (45 cm d<sup>-1</sup>) to high (145 cm d<sup>-1</sup>) velocities. They subsequently applied a two-region diffusion-controlled adsorption model (TRM) to the data and found it provided a good fit to the higher velocity breakthrough curves (Figure 1.7).

The two-region conceptualization is an elaboration of the process described by equation (14). It separates the total pore space into two regions – a zone of mobile fluid where advective-dispersive transport occurs, and a zone of stagnant fluid in which only diffusive transport occurs. The immobile region has been visualized as dead end pore spaces, intra-aggregate void spaces, thin films around particles, or zones of low permeability strata (Nielsen et al. 1986, Bajracharya and Barry 1997). Adsorption is viewed as instantaneous, and diffusional transfer is assumed proportional to the difference in concentration between the two regions. Early on, only those sorption sites in direct contact with the mobile phase participate in the sorption process, so breakthrough is earlier than expected. The slow diffusion of solutes through the immobile fluid to the remaining sorption sites and back out again results in the extensive tailing. According to Nielsen et al. (1986) significant preferential transport, reflected in the early arrival and tailing of breakthrough curves, can occur even when there is only a small amount of stagnant water in a system.

Coats and Smith (1964) modified the ADE to represent the diffusional mass transfer of solutes from mobile to immobile regions in porous media:

$$\theta_m \frac{\partial C_m}{\partial t} = \theta_m D \frac{\partial^2 C_m}{\partial z^2} - v_m \theta_m \frac{\partial C_m}{\partial z} - \theta_{im} \frac{\partial C_{im}}{\partial t} \quad (16)$$

$$\theta_{im} \frac{\partial C_{im}}{\partial t} = \alpha(C_m - C_{im}) \quad (17)$$

where:  $\theta_m$  and  $\theta_{im}$  = pore fractions occupied by mobile and immobile phases

$C_m$  and  $C_{im}$  = solute concentrations in mobile and immobile phases

$v_m$  = average pore water velocity in the mobile phase

$\alpha$  = mass transfer coefficient (equation 17 represents the mass transfer between the mobile and immobile zones)

van Genuchten et al. (1974) expanded this model to account for sorption. Their equations are of the form:

$$\theta_m R_m \frac{\partial C_m}{\partial t} = \theta_m D \frac{\partial^2 C_m}{\partial z^2} - v_m \theta_m \frac{\partial C_m}{\partial z} - \theta_{im} R_{im} \frac{\partial C_{im}}{\partial t} \quad (18)$$

$$\theta_{im} R_{im} \frac{\partial C_{im}}{\partial t} = \alpha(C_m - C_{im}) \quad (19)$$

where:  $R_m$  and  $R_{im}$  = adsorption isotherm-based retardation factors in mobile and immobile regions

van Genuchten and Wierenga (1976) provided an analytical solution to equations (18) and (19) for a semi-infinite column and a pulse input of solute that undergoes linear adsorption. They examined the impact of various model parameters on the geometry of breakthrough curves and found that the influence of the dispersion coefficient was relatively small.



## Empirical vs. Surface Complexation Models of Solute Sorption

### Introduction

Approaches to modeling adsorption-desorption equilibria include those based on empirical partitioning relationships and those based on surface complexation theory. Both types of models are equilibrium-based and therefore should only be applied to systems satisfying the assumptions of equilibrium. Empirical models use partition coefficients and adsorption isotherm equations to describe adsorption under a specific set of chemical conditions. This relatively simple approach is appealing, but it is limited to the geochemical conditions under which adsorption was measured. Surface complexation models are more flexible. They describe adsorption in terms of chemical reactions between surface functional groups and solutes, they consider aqueous speciation, and they account for the reactivity of every aqueous species.

### Empirical Approach

Empirical approaches to modeling adsorption have been justified by the difficulties associated with understanding natural systems well enough to use a surface complexation approach. Empirical methods describe adsorption in terms of partition coefficients or equations that relate the concentration of a solute in solution to that adsorbed on a surface at a constant temperature. Most often, sorption is represented by a single-parameter, solute-specific distribution coefficient, or  $K_d$ . The  $K_d$  for a given solute and sediment sample is usually determined by batch experiment. In a batch experiment a sediment sample is split into a series of subsamples, and solutions with different concentrations of the solute of interest are added to each subsample. The sediments and solutions are allowed to react in a temperature- and pH-controlled environment until equilibrium is achieved, and then the solute concentrations in the

equilibrium solutions are measured. A plot of the amount of solute sorbed versus equilibrium solution concentration is the adsorption isotherm for the particular solute and sample. The  $K_d$  is the slope of the line fit to the linear portion of isotherm (Figure 1.8).

The  $K_d$  approach to modeling solute sorption is based on several assumptions: 1) equilibrium between the solute and solid is attained during the batch experiment, 2) the equilibrium conditions in the batch mimic the conditions in the aquifer, 3) the isotherm is linear for the solute concentration range of interest, 4) the removal of the solute from solution is due to a reversible sorption process, 5) surface charge does not change with sorption, 6) the solute of interest is the only adsorbing solute, 7) all aqueous species of the solute have the same affinity for the surface sites, and 8) all exposed surface sites have the same affinity for the solute (Davis and Kent 1990, Christensen et al. 1996).

Bethke and Brady (2000) used both the  $K_d$  approach and the surface complexation approach to simulate the one-dimensional transport of Pb and other heavy metals through an aquifer containing hydrous iron oxide. They compared model predictions with laboratory and field observations of heavy metal behavior and found that the  $K_d$  approach greatly overestimated the rates of contaminant displacement by groundwater flushing and the mobility of contaminant plumes. Furthermore, the  $K_d$ -based models failed to predict the "tailing" of residual contamination commonly observed in the field and laboratory.

Although the  $K_d$  approach works poorly with ionic solutes that sorb strongly to aquifer surfaces and form various species and complexes, it may be adequate for describing the sorptive behavior of hydrophobic organic solutes (McCarthy and Zachara 1989, Stumm and Morgan 1996). The  $K_d$  approach also works well with ionic solutes that sorb weakly, are present in low concentrations, participate in few reactions, and

occur in systems where contaminant concentrations and pH vary little (Brady and Bethke 2000).

### **Surface Complexation Approach**

According to surface complexation theory, surfaces are composed of functional groups that react with solutes to form inner- and outer-sphere complexes that are analogous to complex ions and ion pairs in aqueous chemistry (Davis and Kent 1990). The equilibria of surface complexation reactions are described by mass action expressions having correction factors to account for the distribution of electrostatic energy in the vicinity of a surface. Surface charge is treated as a by-product of the chemical reactions of surface functional groups, and the empirically-derived equilibrium constants, determined for the mass action expressions, are related to thermodynamic constants by the activity coefficients of the surface species.

Surface complexation models differ with respect to the type of surface reactions that take place and the electrostatic correction factors applied. Nevertheless, all reduce to a set of simultaneous equations that can be solved numerically. These equations include: 1) mass action expressions for all reactions, 2) a mole balance equation for surface sites, 3) an equation for the computation of surface charge, and 4) a set of equations for electrostatic corrections (Davis and Kent 1990).

In order to apply the surface complexation modeling approach, information is needed regarding: 1) reactive functional groups on solid surfaces, 2), reactive surface area 3), micro-scale porosity 4), thermodynamic data for applicable reactions, and 5) the electrical character of the mineral-water interface (Davis and Kent 1990).

Surface Functional Groups. Identification of surface functional groups is important because these groups determine which ions are typically exchanged for

adsorbing ions; for example,  $H^+$  for cations on (hydr)oxides,  $Ca^{2+}$  for cations on calcite, and  $Na^+$  and  $H^+$  for cations on montmorillonite. Furthermore, they govern the ways in which adsorption varies as a function of solution composition, and they affect the electrical properties of the solid-solution interface (Davis and Kent 1990).

(Hydr)oxides, organic matter, and aluminosilicate minerals lacking permanent charge have proton-bearing surface functional groups; consequently, adsorption onto these solid phases is pH-dependent. The total densities of surface hydroxyl groups for several oxide minerals range from 1.3-22 sites/nm<sup>2</sup> (Davis and Kent 1990). This range reflects not only the actual differences in the solids arising from variations in microporosity, crystallinity, etc., but also the different techniques used to measure site densities. Total site densities are typically determined from calculations based on crystal structure or by acid-base titration data (Dzombak and Morel 1990). Site densities can also be estimated from constant pH adsorption studies, provided a Langmuir model can be fit to the data (Harter 1984). Consistently lower estimates of hydroxyl site densities on oxide surfaces (0.8-7.3 sites/nm<sup>2</sup>) are obtained from isotherm experiments (Davis and Kent 1990). This observation supports the hypothesis that only a portion of the hydroxyl groups present on a surface participate in adsorption reactions.

Apparently different hydroxyl groups on a surface have different reactivities. The variability in reactivity is considered to be dependent upon: 1) the number of substrate cations with which the hydroxyl's oxygen is coordinated, 2) the identity of the surface metal cation(s) to which the oxygen is bound, and 3) whether the hydroxyl is a terrace, edge, step, kink, or admolecule site (Figure 1.1). The first two characteristics affect the strength of the S-O and O-H bonds in the surface hydroxyl group, while the third affects its flexibility in potential bonding configurations (Brown 1990, Davis and Kent 1990, Hochella 1990).

Indirect evidence for the reactive variability of surface hydroxyl groups includes the aforementioned discrepancy between measures of total site density and measures of maximum adsorption, and the frequent lack of adherence of metal ion adsorption data to the Langmuir isotherm model. Inorganic ions more often display adsorption behavior that fits a multiple site Langmuir model or Freundlich model (Davis and Kent 1990, Parks 1990). Two or more distinct steps in an overall isotherm suggest there are two or more sets of hydroxyl groups with distinctly different binding energies, while Freundlich behavior suggests there may be many different types of functional groups whose binding energies cover a broad spectrum.

Phyllosilicate clay minerals are important adsorbents because they have high specific surface areas and are widespread. These minerals generally consist of stacked sheets of  $M^{z+}O_6$  octahedra and  $SiO_4$  tetrahedra, and are divided into subgroups based on the numbers of each type of sheet in their unit cell structures. Minerals such as kaolinite are designated 1:1 clays because their unit structures consist of one silicon tetrahedral sheet connected to one aluminum octahedral sheet. The smectites, illitic micas, and vermiculites have one aluminum octahedral sheet sandwiched between two silicon tetrahedral sheets in each unit cell, so they are called 2:1 clays.

In addition to edge hydroxyl groups, phyllosilicate clays have a functional group associated with the distorted hexagonal rings of oxygen atoms that occur on the planar surfaces of the tetrahedral sheets. The functional group is a ditrigonal-shaped cavity at the center of each ring (Figure 1.9). The reactivity of the siloxane cavity depends on the nature and extent of isomorphous substitution in the layer silicate structure. If there are no positive charge deficits in the vicinity of a cavity, it will only bind neutral, dipolar molecules, such as water (Sposito 1990). If charge-inducing isomorphous substitutions have taken place, a siloxane cavity can form complexes with cations as well as dipolar

molecules, the strength of the complex depending in part on the size of the cation and the proximity of the substitution(s) to the surface cavity (Sposito 1989). Binding at ditrigonal cavities is predominantly electrostatic, so they are important sites for the adsorption of the major cations in natural waters (i.e.  $\text{Na}^+$ ,  $\text{K}^+$ ,  $\text{Ca}^{2+}$ , and  $\text{Mg}^{2+}$ ).

Kaolinite has very little permanent charge, so the siloxane cavities on its tetrahedral sheets do not bind cations. The principal surface complexation sites on kaolinite are the hydroxyl groups located along the edges of the sheets. On the other hand, smectites, vermiculites and illitic micas have significant permanent charge, so many of their siloxane cavities are reactive.

Hydrous manganese oxides are poorly crystalline minerals with high specific surface areas and an array of adsorption sites. Manganese oxide minerals consist of chains of  $\text{MnO}_6$  octahedra that are linked to form tunnels or sheets. Permanent charge arises from manganese vacancies in the crystal lattice and isomorphous substitutions of  $\text{Mn}^{2+}$  and  $\text{Mn}^{3+}$  for  $\text{Mn}^{4+}$ . Adsorption site densities on these reactive minerals are similar to those reported for goethite (Davis and Kent 1990).

Salt-type minerals include carbonates, sulfates, and halides. The surface functional groups on these minerals consist of the cation or the anion of the salt.

Surface Area and Microporosity. Surface area measurements are needed to estimate the number of surface functional groups per unit mass of solids, provided the density per unit area is known. Reactive surface areas are typically estimated by measuring the adsorption of nitrogen ( $\text{N}_2$ ) or krypton (Kr) gas onto a surface. The most popular method for determining surface area from gas adsorption data is the BET method using  $\text{N}_2$  gas as the adsorptive. In this method, specific surface area is estimated from the volume of gas adsorbed as a function of applied pressure (Brunauer et al. 1938). However, the BET method is not valid for samples containing extensive

microporosity, because the adsorptives tend to clump in the vicinity of micropores. In addition, N<sub>2</sub> gas does not provide accurate measurements for samples having: 1) small surface areas, 2) small masses, and 3) significant amounts of expandable clays (Mackay et al. 1986, Davis and Kent 1990).

Kr can provide more accurate and precise measurements with smaller samples and materials having smaller surface areas; but like N<sub>2</sub>, it does not yield reliable results for soils containing expandable clays. Both N<sub>2</sub> and Kr are nonpolar gases that cannot fully penetrate the interlayer regions that comprise the bulk of the total surface area of expandable clays. If smectite or vermiculite clays are plentiful, better estimates of total surface area are obtained by measuring the retention of a polar solvent such as ethylene glycol monoethyl ether (EGME) which easily penetrates interlayer regions. However, this method is limited to samples having surface areas in excess of about 50 m<sup>2</sup>/g (Davis and Kent 1990).

When expandable clays are abundant and the adsorption of major solution cations or organic solutes needs to be assessed, then a method such as EGME retention should be used to characterize reactive surface area, because these solutes are retained on external and interlayer surfaces. However, if these mineral phases are absent, or anion adsorption or trace cation adsorption is of interest, the N<sub>2</sub> or Kr BET method is more appropriate for measuring *reactive* surface area, because adsorption of anions and trace cations occurs primarily on the external surfaces of clay minerals (Davis and Kent 1990).

The Electrical Double Layer. The net surface charge of a solid is the sum of the charges resulting from isomorphous substitutions and the ionization of surface functional groups. Typically this sum is nonzero. In order to maintain electroneutrality, charge-counteracting ions will be attracted to the surface. The surface charges and

counterions make up an electrical double layer (EDL), and the separation of charges in the EDL creates an electrical potential difference across the solid-solution interface.

Some counterions, particularly multivalent ions, will bond to the ionized surface functional groups while others remain dissociated from the surface, forming a diffuse ion swarm. Evidence for the existence of a diffuse ion swarm includes observations of increased surface charge and electrical potential brought about by fluid movement (Parks 1990). Increases in surface charge and potential with the onset of fluid motion suggests that many charge-neutralizing counterions are not bonded to the surface, because they are easily stripped away by the moving fluid.

Gouy and Chapman developed the basic theory of the EDL in the early 1900's. In their conceptual model of the double layer: 1) all of the counterions were weakly adsorbed to a surface by electrostatic attraction, 2) all counterions resided in a diffuse ion swarm, 3) the electrostatic attraction of ions toward a surface was countered somewhat by their diffusion away from the surface to the more dilute bulk solution, 4) the net result of electrostatic attraction and diffusion was an exponential decrease in counterion concentration with distance from the surface, 5) increasing the ionic strength of the bulk solution reduced diffusion and decreased the thickness of the double layer, and 6) increasing counterion charge also reduced the thickness of the double layer, because fewer counterions were needed to neutralize surface charge (Bohn et al. 1985, Parks 1990).

Their mathematical model assumed: 1) counterions existed as point charges, 2) charged surfaces were planar and infinite in extent, and 3) charges were uniformly distributed across a surface. Counterion attraction was described by Coulomb's law which states that the force of attraction is proportional to both the surface charge and counterion charge, and it is inversely proportional to the distance of charge separation.



Solutions of the Poisson-Boltzmann equation for a planar surface provided the distribution of charge and potential within the EDL (Bohn et al. 1985, Davis and Kent 1990).

The Gouy-Chapman model over-predicts experimental measurements of electrical capacity (Davis and Kent 1990). Stern and Grahame improved the Gouy-Chapman model by accounting for ion volume, and by assuming that some of the counterions are retained on the surface in a specifically adsorbed "Stern" layer (Grahame 1947). The Stern-Grahame model assumes electrical potential decreases linearly across the Stern layer, and then exponentially across the diffuse layer (Figure 1.10).

Examples of Surface Complexation Models. In the constant capacitance model (CCM) surface hydroxyl groups form ionized surface sites according to equations (1) and (2), and only inner-sphere surface complexes are formed. Thus it only considers a single plane of adsorbed ions juxtaposed on the surface. Since the double layer is so thin, the CCM is applicable only to systems of high, constant ionic strength. The EDL structure for the CCM is illustrated in Figure 1.11a.

The diffuse double layer model (DDL) also describes surface reactions in terms of amphoteric hydroxyl groups, and considers only inner-sphere surface complexes. However, in addition to the surface plane of specifically adsorbed ions, it includes a diffuse layer of dissociated counterions. The electrical potential at the beginning of the diffuse layer (i.e., at the diffuse layer plane) is the same as that for the surface, and it decreases with distance from the plane in accordance with the charge-potential relationship of Gouy-Chapman (see Figure 1.11b).

Unlike the original Gouy-Chapman model, the DDL model designates a finite number of sites. Unlike the CCM, it accounts for ionic strength effects on adsorption via

the Poisson-Boltzmann equation, and therefore should be applicable to systems of variable ionic strength.

The triple layer model (TLM) describes the formation of ionized surface functional groups with equations (1) and (2), but it considers three planes in the interfacial region: 1) a surface plane for the adsorption of  $\text{OH}^-$  and  $\text{H}^+$ , and for the formation of inner-sphere surface complexes; 2) a near-surface plane for more weakly sorbed outer-sphere surface complexes; and 3) a diffuse layer plane, representing the closest approach of detached counterions. The electrical potential decreases linearly in the two regions between the three planes according to the charge-potential relationships of the Stern-Grahame model, while the electrical potential decreases exponentially beyond the third plane as in the DDLM (Figure 1.11c).

Four layer models are modified versions of the TLM that contain two planes for outer-sphere surface complexes (Figure 1.11d). The extra plane is included to account for observations that outer-sphere cation complexes appear to approach surfaces more closely than outer-sphere anion complexes (Davis and Kent 1990).

The nonelectrostatic surface complexation model is the most simple approach. It treats all adsorption as inner-sphere surface complexation reactions, and it ignores the electrical double layer entirely by excluding EDL correction terms from mass action expressions. The approach is popular because it is computationally efficient.

Surface Complexation Modeling of Experimental Systems. The five surface complexation models differ primarily in their treatment of the interfacial structure of the EDL and the ionic strength dependence of weakly adsorbed solutes. As a result, differences between model predictions should be most noticeable for aqueous systems in which the concentrations of weakly sorbing ions (e.g.  $\text{Na}^+$ ,  $\text{Ca}^{2+}$ ,  $\text{Mg}^{2+}$ ,  $\text{Cl}^-$ ,  $\text{HCO}_3^-$ , and  $\text{SO}_4^{2-}$ ) vary. For experimental systems in which the adsorbent is a strongly bound ion,

the models often produce comparable results. For example, Hohl and Stumm (1976) measured the adsorption of the strongly binding  $\text{Pb}^{2+}$  cation onto laboratory-synthesized  $\alpha\text{-Al}_2\text{O}_3$ . Their experimental data indicated a non-integer number of protons between 1 and 2 were released during adsorption. They successfully simulated their data using a CCM with two types of adsorption sites: monodentate (SOH) and bidentate (2SOH), while Davis and Leckie (1978) were able to simulate the same experimental data using a TLM that considered only monodentate sites.

Surface Complexation Modeling of Natural Systems. Three problems encountered in the application of surface complexation theory to heterogeneous mixtures of minerals and organic materials are: 1) the identification and quantification of surface functional groups, 2) the characterization of EDL properties, and 3) the determination of equilibrium (binding) constants.

It is generally not possible to determine the number and type of every functional group present in a heterogeneous mixture of particles that may be variably coated with carbonates, (hydr)oxides, or organics. If a single phase controls adsorption and that phase can be identified, then the reactive site density of a sample could be estimated from the abundance of the controlling phase and a site density representative of that phase. Identification of the solid phase(s) dominating adsorption should improve simulations of reactive transport, because the types and numbers of reactive functional groups in a system would be constrained. If the controlling phase(s) cannot be identified, the composite material could be modeled as a whole using the measured surface area and an average site density of average surface functional groups (Davis et al. 1998).

In theory an EDL model should be included in any surface complexation modeling study; however, given the difficulties involved in determining the interactive

effects of overlapping double layers in heterogeneous materials, it could be argued that the non-electrostatic modeling approach is best for natural systems. Another problem that arises from our poor understanding of the interactive effects of mineral phases is the dubious applicability of binding constants derived from simple monomineralic systems to complex natural systems (Davis and Kent, 1990).

Wen et al. (1998) applied the CCM, DDLM, and TLM to model Cu and Cd adsorption onto sediments from the LeAn River in Jiangxi Province, China. In their study, adsorption was described in terms of average surface functional groups represented by monodentate (i.e. SOH) adsorption sites. All three surface complexation models fit the experimental adsorption data over a wide range of solution pH and ionic strength. Apparently, any one of the three models can be used to describe heavy metal adsorption onto these sediments.

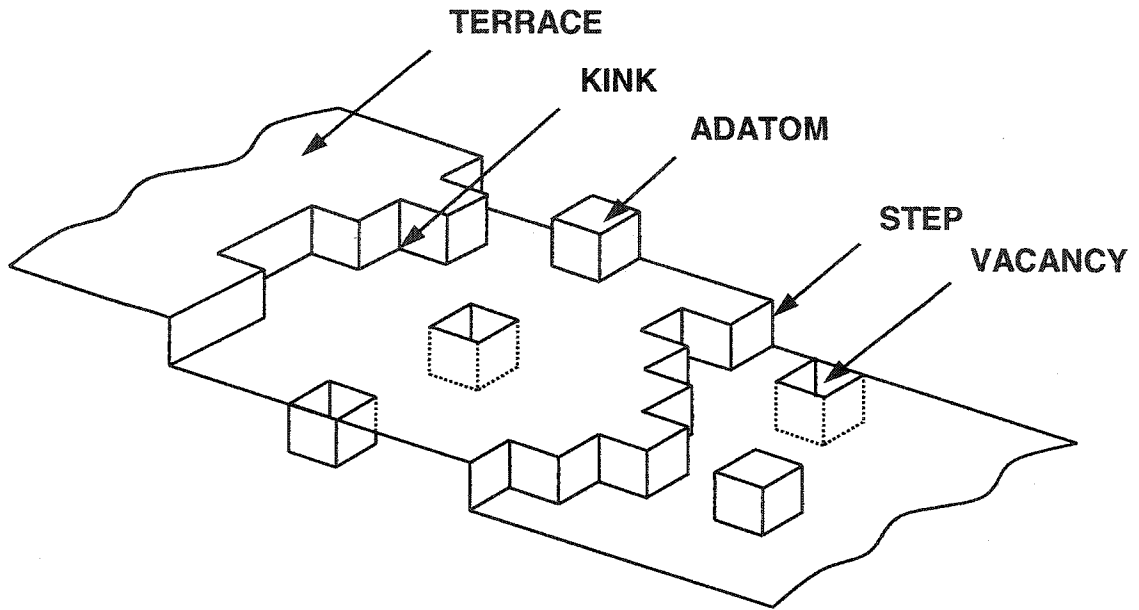


**Figure 1.1** Block model of a heterogeneous mineral surface. In this model each block represents an atom. After Hochella (1990).

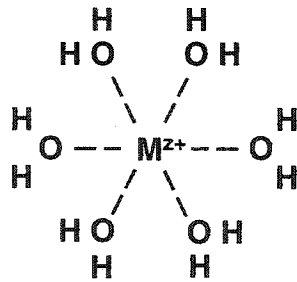


**Figure 1.2** Dissolved cation ( $M^{2+}$ ) and associated water molecules. Dashed lines represent coordinate covalent bonds between the ion and its waters of hydration.

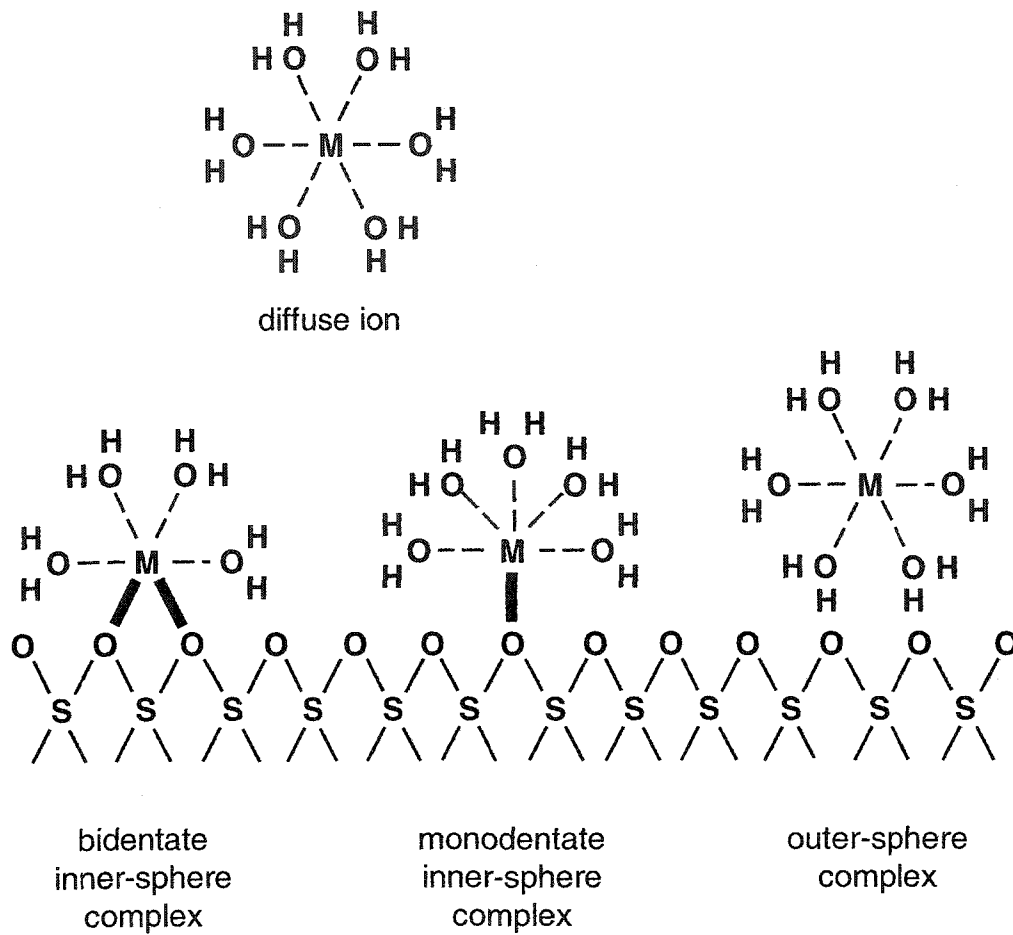


**Figure 1.3** Three mechanisms of cation adsorption. S and M represent solid phase and dissolved cations, respectively. Bold lines represent ionic or covalent bonds.

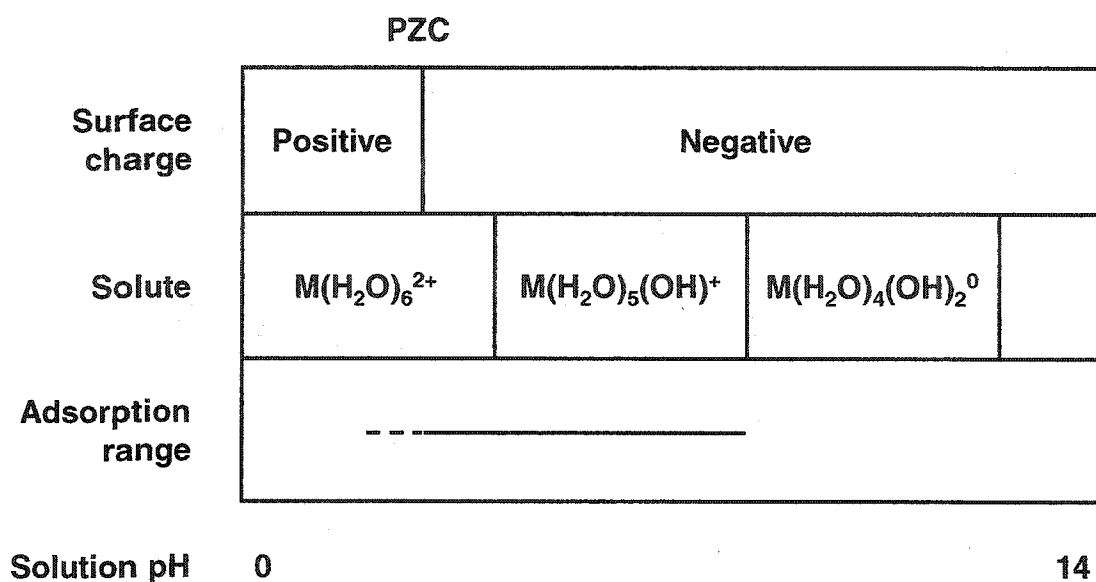


**Figure 1.4** Effect of pH on electrostatic attraction of cations. Electrostatic attraction of hydrolyzable cations is expected when the solution pH is greater than the point of zero charge (PZC) of the adsorbent and less than the pH at which the cation forms a neutral hydro complex. Electrostatic interactions lead to an accumulation of the adsorbed cations in a detached diffuse layer or as outer-sphere surface complexes. In the latter case adsorption can be observed at pH values well below the PZC. Modified from Schindler (1990).

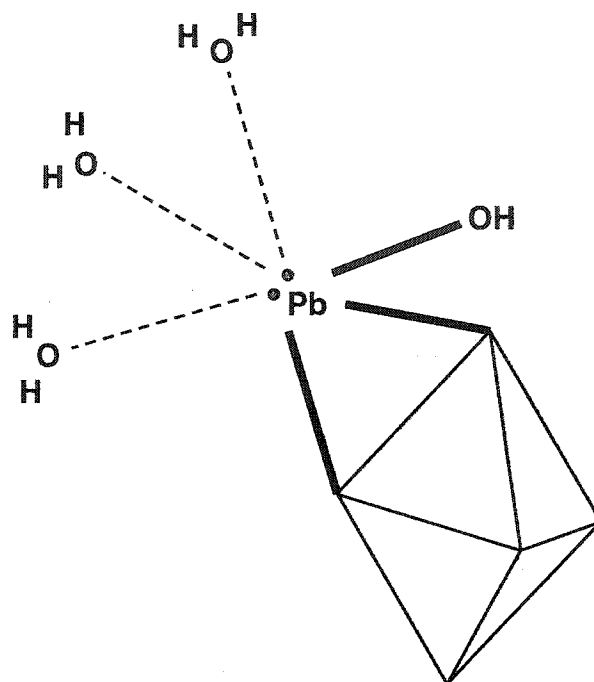


**Figure 1.5** Predominant coordination environment of  $Pb^{2+}$  adions on  $AlO_6$  and  $FeO_6$  octahedra.  $Pb^{2+}$  adions have a trigonal pyramid coordination geometry as shown by the bold lines which represent bonds to two surface oxygen ligands and a hydroxide ion ligand. Modified from Bargar et al. (1997a).

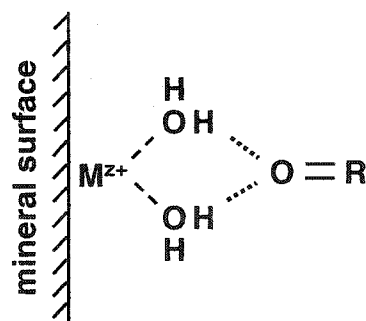


**Figure 1.6** Adsorption of a polar organic compound to a mineral surface by water-bridging.  $M^{z+}$  is an exchangeable cation,  $\cdots$  is a hydrogen bond, and R represents the organic units in the polar compound.



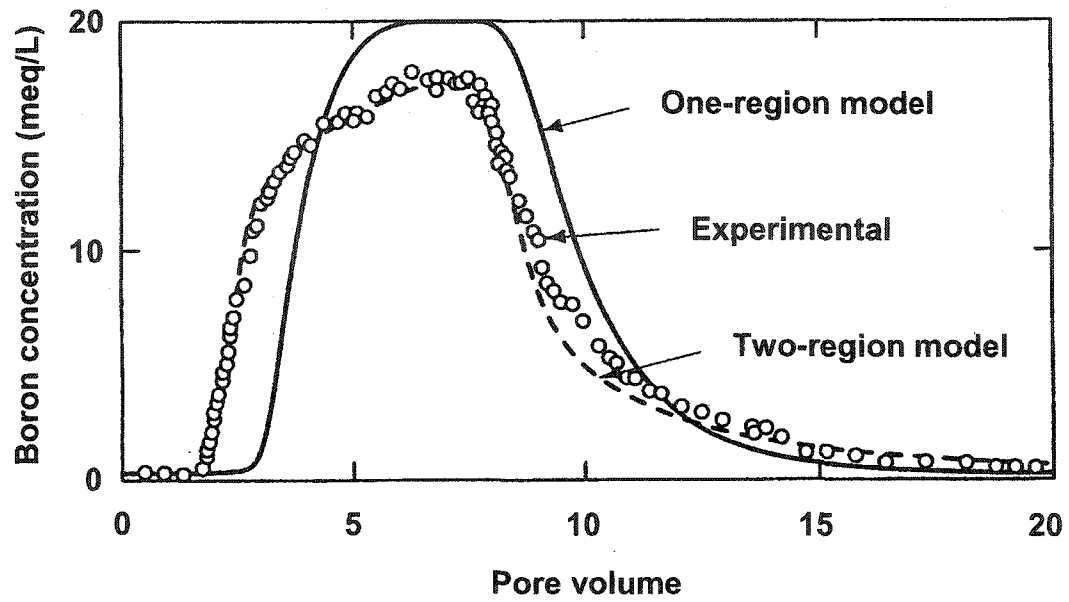


**Figure 1.7** Example of a relatively high-velocity breakthrough curve. Note the superior fit of the two-region model versus the one-region model. *Source:* Nielsen et al. (1986).

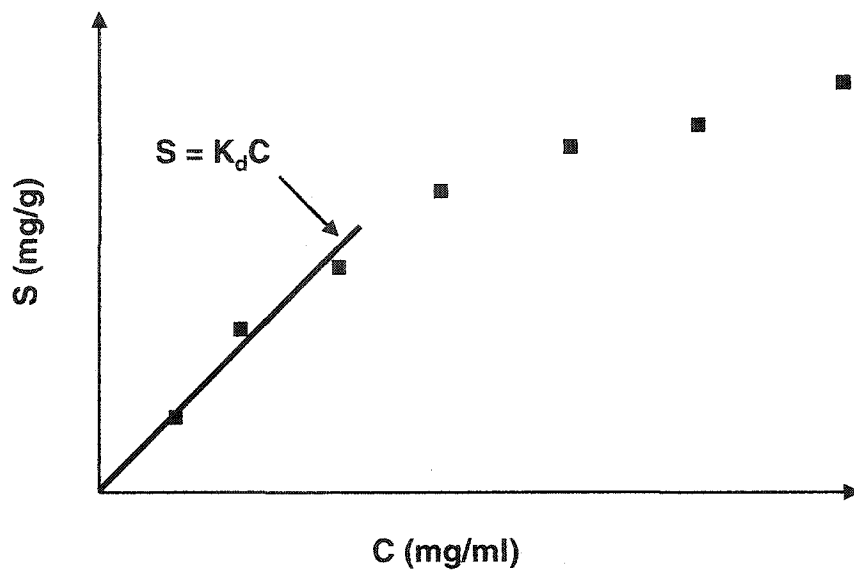


**Figure 1.8** Adsorption isotherm.  $S$  = sorbed concentration,  $C$  = equilibrium solution concentration,  $K_d$  = distribution coefficient (ml/g).  $K_d$  is the slope of the linear portion of the adsorption isotherm.

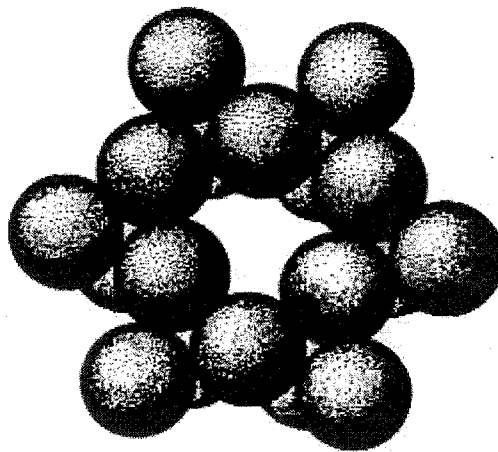


**Figure 1.9** Ditrigonal cavity formed by six corner-sharing silica tetrahedra on the planar surface of a phyllosilicate clay mineral. The cavity has a diameter of approximately 0.26 nm. *Source:* Sposito (1989).

Gouy-Chapman

Stern-Grahame

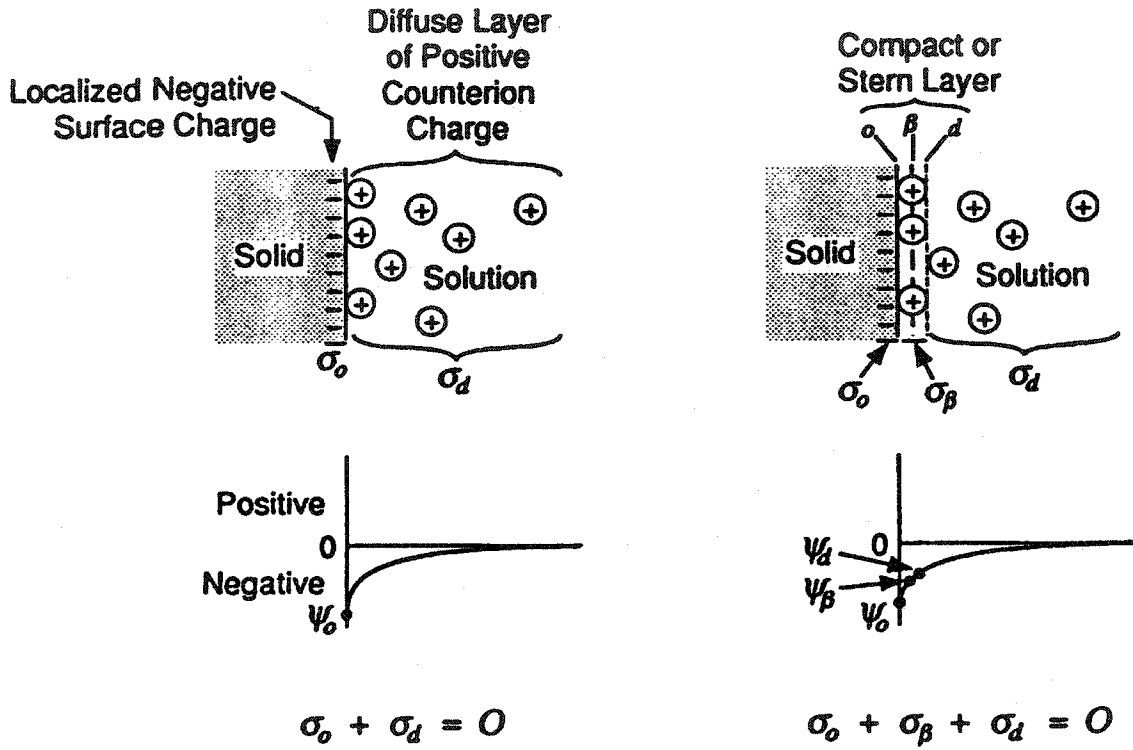
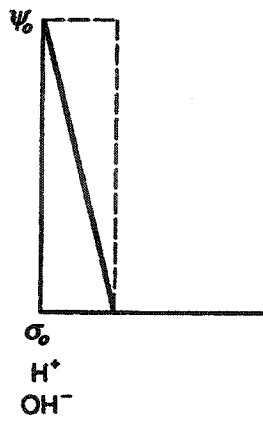
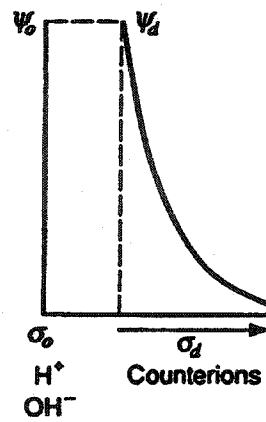


**Figure 1.10** Diagrams showing the distribution of charge ( $\sigma$ ) and the distribution of potential ( $\psi$ ) for the Gouy-Chapman and Stern-Grahame models of the electrical double layer. *Source:* James and Parks (1982).

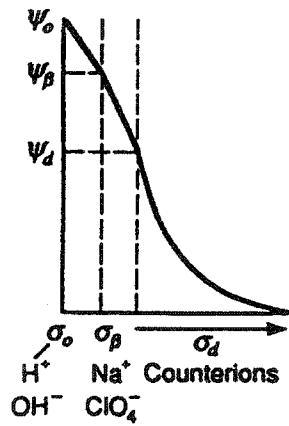
(a) Constant Capacitance



(b) Diffuse Double Layer



(c) Triple Layer



(d) Four Layer

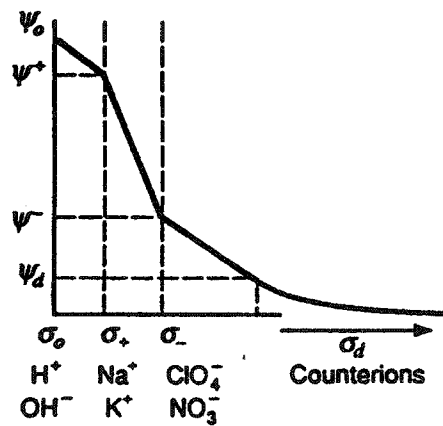


**Figure 1.11** Illustrations of the change in electrical potential with distance from the surface for the: (a) constant capacitance, (b) diffuse double layer, (c) triple layer, and (d) four layer models. *Source:* Davis and Kent (1990).

## CHAPTER 2

### LEAD SORPTION VARIABILITY: IMPLICATIONS FOR SOLUTE TRANSPORT MODELING

#### Abstract

Measures of lead ( $Pb^{2+}$ ) sorption varied three orders of magnitude in an eight square meter outcrop of glaciofluvial sands and gravels in Deerfield, New Hampshire. Fifty-seven percent of the variation in  $Pb^{2+}$  sorption can be explained by a linear combination of sediment permeability and 24-hour dithionite citrate-extractable iron, manganese, and aluminum, indicating that  $Pb^{2+}$  sorption is controlled by iron-, manganese-, and aluminum-rich (hydr)oxide grain coatings. The predominance of extractable iron in the coatings, the relationship between  $Pb^{2+}$  sorption and the extractable iron/aluminum ratio, the color of the sediments, and the appearance of the coatings under cross-polarized light, suggest the grain coatings consist primarily of poorly crystalline goethite with varying amounts of aluminum and manganese substitution.

Two alternative, or perhaps complementary, models explain the quadratic relationship between  $Pb^{2+}$  sorption and permeability. The first is based on sediment texture,  $Pb^{2+}$  sorption, and extractable metal data. It suggests that  $Pb^{2+}$  sorption may be controlled by two reactive phases: clay minerals in the finest sediments and goethite in the coarser sediments. The second model is based on thin section observations of high (hydr)oxide surface areas in the finest and coarsest sediments. (Hydr)oxide surface area is high in several fine-grained, low permeability samples because the (hydr)oxide mass is distributed over a relatively large number of particles. (Hydr)oxide surface area

is high in several coarse-grained, high permeability samples, even though they contain relatively few coated grains and little (hydr)oxide mass, because the coatings have extremely high surface area to mass ratios. A reactive surface area model was developed to quantify the impact of observed differences in grain size, (hydr)oxide mass, grain coating morphology, and the proportion of coated grains on  $\text{Pb}^{2+}$  sorption. The model explains 65 percent of the  $\text{Pb}^{2+}$  sorption variation.

The results indicate that  $\text{Pb}^{2+}$  sorption coefficients can be estimated from relatively simple and inexpensive measurements of sediment permeability and dithionite-citrate extractable metals. Furthermore, the findings suggest it may be helpful to consider grain coating extent and morphology in studies of trace metal sorption. The information can potentially aid the identification of reactive solid phases, improve predictive models of sorption coefficients, and enable differentiation between total surface area and reactive surface area for surface complexation modeling.

### **Introduction**

Reactive transport models contain mathematical expressions to represent the partitioning of solutes between the aqueous and solid phases. Expressions for modeling interphase transfer by sorption are typically based on empirical partitioning relationships or surface complexation theory. Empirical models describe sorption phenomena in terms of simple partition coefficients or equations that relate the equilibrium concentration of a solute in solution to the amount sorbed. Surface complexation (SC) models describe sorption in terms of chemical reactions between surface functional groups and solutes, and are more realistic and robust, particularly for trace metals and other ionic species that sorb strongly to aquifer surfaces (Davis and Kent 1990, Bethke and Brady 2000, Brady and Bethke 2000). SC models require

information regarding reactive functional groups on solid surfaces, reactive surface area, thermodynamic data for applicable reactions, and the electrical character of the mineral-water interface. Although the SC approach has been increasingly applied to natural settings (Fuller et al. 1996, Wang et al. 1997, Davis et al. 1998, Stollenwerk 1998, Wen et al. 1998, Papini et al. 1999, Kent et al. 2000, Barnett et al. 2002, Tonkin et al. 2002), empirical models of sorption remain popular despite their limitations, because the site-specific data needed for SC models are rarely available.

In the SC approach, it is necessary to identify the solid phase or phases controlling sorption in order to identify the surface functional groups to be modeled. These groups determine which ions are exchanged for adsorbing ions; for example,  $H^+$  for cations on oxides and hydroxides, or  $Ca^{2+}$  for cations on calcareous grain coatings. Furthermore, they govern the ways in which adsorption varies as a function of solution composition, and they affect the distribution of charge at the solid-solution interface.

With the empirical approach it is not *essential* to identify the dominant reactive phase(s). Nevertheless, empirical measures of sorption vary within an aquifer due to inconstant geochemical conditions. In order to characterize the spatial variability of sorption in a heterogeneous aquifer, a large number of empirical measurements would be needed. To further complicate matters, reactivity measurement is laborious, and interpretation of measures is problematic because the values do not provide insight into the geochemical processes controlling reactivity. For these reasons, researchers have sought to identify the reactive phases controlling sorption, and relate empirical measures of sorption to geologic properties that are more easily measured and interpreted.

Several studies have examined the relationship between sorption and sediment physical properties such as hydraulic conductivity or grain size. Efforts have focused on

these relationships for several reasons: to shed light on the dominant reactive phase, to evaluate simple physical property measurements as proxies for sorption measurements, and to couple physical and chemical transport processes. Both positive and negative correlations have been found between physical properties and the sorption of organic compounds. Negative relationships were observed in sediments from northern Georgia (Karickhoff et al. 1979), the Glatt Valley in Switzerland (Schwarzenbach and Westall 1981), and Cape Cod, Massachusetts (Barber et al. 1992). Sorption was greatest in the finer fractions of these sediments, because the smaller particles are preferentially coated with naturally-occurring organic carbon. Conversely, positive relationships were found in glacial outwash at the Canadian Forces Base in Borden, Ontario (Mackay et al. 1986, Ball and Roberts 1991, Allen-King et al. 1998) where surface area and organic carbon content are greatest in the larger size fractions (Ball et al. 1990).

A weak negative relationship was reported between hydraulic conductivity and strontium sorption at the Borden site (Robin et al. 1991). Another Borden study did not assess physical properties, but found that carbonate rock fragments and grain coatings controlled the sorption of cadmium (Fuller and Davis 1987). At the Cape Cod site, there was a weak negative relationship between lead sorption and grain size, and no correlation between zinc sorption and grain size (Fuller et al. 1996). However, both lead and zinc sorption were significantly correlated with the abundance of iron and aluminum oxide grain coatings. Oxide grain coatings also controlled the sorption of strontium onto fluvial and eolian sands at the Chalk River Nuclear Laboratories site in Ontario (Jackson and Inch 1989); nevertheless, high surface area ferromagnesian minerals (predominantly biotite and vermiculite) also played a role.

These studies indicate that a variety of solid phases may control aquifer reactivity, and the dominant phase is site and solute specific. Furthermore, they show



that the linear relationship between sorption and physical properties may be positive, negative, or nonexistent. The purposes of this study were to identify the solid phases controlling  $\text{Pb}^{2+}$  sorption in a glaciofluvial sand and gravel deposit, and to develop methods for estimating sorption coefficients and SC model surface properties from relatively simple and inexpensive measures of sediment physical and chemical properties.

### **Methods**

The field research was conducted in a borrow pit in Deerfield, New Hampshire. The site was selected for its high physical and chemical heterogeneity and its excellent three-dimensional exposures. Details of the site geology, mineralogy, and sampling methodology are given in Chapter 3.

Four hundred seventy-six randomly-located sediment samples were collected from an eight square meter vertical exposure of glaciofluvial sands and gravels (Figure 2.1). Each sample was collected with a 30 cm<sup>3</sup> plastic syringe that was modified by sawing off its anterior beveled portion. With the plunger withdrawn to the rear of the syringe barrel, the sawed-off end was pushed into the outcrop face to obtain a minimally disturbed sample. The sediment-laden syringe was then removed from the outcrop face, capped, and stored in ice until oven-dried at 30° C.

Laboratory measurements of physical properties were nondestructive and used entire sediment samples. Measurements of chemical properties consumed sediment and were made on the less than two millimeter size fraction. The gravel fraction (i.e. the greater than two millimeter size fraction) is routinely omitted from chemical property analyses in order to standardize methods and avoid the large labware needed to work with the relatively inert gravel-size particles (Kaplan et al. 2000).

One-dimensional air permeability ( $k_a$ ) was measured on each oven-dried sample prior to its removal from the syringe container in order to obtain measurements on relatively undisturbed samples. A compressed-air permeameter (Figure 2.2) forced a stream of air through the sample at a constant flow rate, and  $k_a$  was calculated from Darcy's law in the form (Katz and Lee 1990)

$$k_a = \frac{2QL\mu P_1}{A(P_1^2 - P_0^2)}$$

where:  $Q$  = flow rate ( $\text{cm}^3/\text{s}$ ),  $L$  = length of sample in syringe (cm),  $\mu$  = viscosity of air (cP),  $A$  = cross-sectional area of syringe ( $\text{cm}^2$ ),  $P_1$  = pressure at the upstream end of the core (atm), and  $P_0$  = pressure at the downstream end of the core (atm). All coarse-grained samples were subjected to permeability measurements at several flow rates to verify Darcy flow conditions, i.e. a linear change in pressure with increasing flow.

After permeability, length, and cross-sectional area measurements were completed, the sample was removed from its syringe container, homogenized, and transferred to a 50 ml centrifuge tube in order to be weighed and stored. Total porosity was calculated from measures of sample mass, length, and cross-sectional area, using an assumed particle density of  $2.65 \text{ g/cm}^3$  (Culley 1993).

$\text{Pb}^{2+}$  sorption was measured on 72 of the 476 sediment samples.  $\text{Pb}^{2+}$  sorption was estimated from batch experiments, and measures of sorption were expressed as single parameter partition coefficients. For the batch experiments, 3 g of sediment were placed in a 50 ml centrifuge tube to which 30 ml of a  $10 \mu\text{M}$   $\text{Pb}^{2+}$  solution were added. The  $\text{Pb}^{2+}$  stock solution was made by dissolving crystalline, reagent grade  $\text{PbCl}_2$  in deionized water. Crystalline  $\text{PbCl}_2$  was used to make the stock solution because at this low concentration the powder readily dissolved in deionized water, and it did not alter the pH of the sediments to which it was added. The tubes were capped and placed on an

orbital shaker set at 80 revolutions per minute for 24 hours at room temperature. After 24 hours the sediment and solution were separated by centrifugation and the supernate was transferred to acid-leached scintillation vials for analysis by flame spectroscopy. The ratio of the sorbed  $\text{Pb}^{2+}$  concentration to the equilibrium solution concentration was the partition coefficient, or  $K_d$ , for each sample.

Deionized water was added to empty centrifuge tubes and sample splits. The blanks tested for the unintentional addition of  $\text{Pb}^{2+}$  to the samples from the containers or the experimental procedures, and the splits checked for the release of  $\text{Pb}^{2+}$  from the sediments themselves. Control samples containing the 10  $\mu\text{M}$   $\text{Pb}^{2+}$  solution and no sediment were also included to account for adsorption to container walls.

The iron, aluminum, and manganese (hydr)oxide grain coating contents of 71 of the 72 sorption samples were determined using a dithionite-citrate (DC) extraction procedure designed to selectively dissolve the coatings and keep the metals in solution (Ross and Wang 1993; Coston et al. 1995). Twenty-one milliliters of 0.2 M ammonium citrate and 0.30 g of sodium dithionite were added to 3 g of sediment, and the mixture was gently shaken at room temperature for 24 hours on an orbital-shaking table. Once the shaking was completed, the samples were centrifuged, and the supernatant analyzed for iron, aluminum, and manganese using flame spectroscopy. Extract solutions were diluted 1:100 for iron and 1:10 for manganese. Standards were prepared with the same concentration of DC solution as the diluted extracts. (Justification for selecting DC as the extractant is provided in Appendix A.)

Total carbon and inorganic carbon were measured on nine of the sorption samples using two separate analyses, and organic carbon was determined by difference (Lee and Macalady 1989). Prior to both analyses approximately five grams of sediment per sample were pulverized in a shatter box with an alumina bowl. The bowl was

cleaned with pre-fired silica sand between samples to avoid cross-contamination. Four grams of the finely-ground sediment were subjected to dry, high temperature combustion in the presence of pre-purified oxygen in order to drive off organic and inorganic carbon as CO<sub>2</sub>. The remaining gram of crushed sediment was acidified with 2N H<sub>2</sub>SO<sub>4</sub> to release the inorganic carbon as CO<sub>2</sub>. The CO<sub>2</sub> evolved from each analysis was measured via titration using a coulometric system. The organic carbon content was calculated by subtracting the weight percent carbon liberated in the acidification process from that obtained by the combustion process.

Bivariate regression quantified relationships between sediment properties. It provided linear correlation information and defined the nature of the bivariate relationship with an equation that could potentially permit predictions and shed light on geologic processes. Multiple regression evaluated relationships involving linear combinations of regressor variables. Scatterplots were inspected for potential collinearity problems among correlated regressors.

## **Results**

Summary statistics for measured sediment properties are presented in Table 2.1. Pb<sup>2+</sup> sorption displays the greatest variability [coefficient of variation (CV) = 124 %], and ranges three orders of magnitude in only eight square meters. Permeability (CV = 89 %) also spans three orders of magnitude. Porosity is the least variable sediment property (CV = 7.3 %) with values ranging from 0.29 to 0.52.

The distributions of all variables, with the exception of porosity, exhibit moderate to strong positive skewness, calling for logarithmic transformations prior to regression. The regression results presented in Table 2.2 show that the relationship between Pb<sup>2+</sup> sorption and organic carbon is not significant ( $\alpha = 0.05$ ). The total carbon content of the

Deerfield sediments is less than 0.07 wt. % (Table 2.1), and in carbon-poor sediments, the sorption of heavy metals is generally thought to be dominated by reactions with iron, aluminum, and manganese (hydr)oxide grain coatings (Jenne 1968, Lion et al. 1982, Tessier et al. 1985, Jackson and Inch 1989, Fuller et al. 1996).

Although bivariate relationships between  $Pb^{2+}$  sorption and DC-extractable metals are weak (Table 2.2), a linear combination of extractable iron and extractable aluminum explains 44 percent of the variability in  $Pb^{2+}$  sorption. Regressing all measured sediment properties onto  $Pb^{2+}$  sorption explains 57 percent of the variability in sorption (Table 2.3). This multiple regression model represents sorption as a linear combination of four sediment properties: permeability, and DC-extractable iron, manganese, and aluminum. The effects of all other measured sediment properties are not significant ( $\alpha = 0.05$ ).

Figure 2.3 presents two images of the spatial distribution of  $Pb^{2+}$  partition coefficients for the Deerfield outcrop. Figure 2.3a was generated from actual measures of  $Pb^{2+}$  sorption, while Figure 2.3b was created from permeability- and DC-extractable metal-based estimates. Despite its smoothed appearance, Figure 2.3b preserves the general features shown in Figure 2.3a. It has a similar, though somewhat narrower range of values, and it shows  $Pb^{2+}$  sorption potential increasing to the right, with the highest potentials near the upper and lower right hand corners of the sampling domain.

## **Discussion**

### **Comparison to Cape Cod Site**

The Deerfield site is similar to the Cape Cod site in terms of depositional environment, permeability, porosity, bulk mineralogy, carbon content, and silt and clay content (Barber et al. 1992, Davis et al. 1993, Chapter 3). However, mean DC-

extractable iron is four times greater than that reported for the Cape Cod site, mean DC-extractable aluminum is five times greater, and mean DC-extractable manganese is 11 times greater (Fuller et al. 1996). The greater mass of (hydr)oxides in the Deerfield sands probably arises from the greater abundance of garnet and biotite source minerals (see Chapter 3).

The Deerfield sands sorbed much less  $\text{Pb}^{2+}$  than those from the Cape, even though the former contained far more DC-extractable iron, aluminum, and manganese. Mean  $\text{Pb}^{2+}$  sorption for the Deerfield samples was  $0.04 \mu\text{mol/g}$  (variance = 0.0003), while mean  $\text{Pb}^{2+}$  sorption for the Cape Cod samples was  $0.22 \mu\text{mol/g}$  (variance = 0.0009). Sediment pH was approximately 5.3 in both studies, so the higher measures of sorption in the Cape Cod samples resulted largely from the use of a more concentrated  $\text{Pb}^{2+}$  solution ( $20 \mu\text{M}$  vs.  $10 \mu\text{M}$ ) and a longer residence time in the batch (48 h vs. 24 h). At these concentrations sorption should be proportional to the amount of  $\text{Pb}^{2+}$  added. Plus, the longer duration of the Cape Cod batch experiments provided more time for the removal of  $\text{Pb}^{2+}$  from solution by diffusion to adsorption sites in intragranular pore spaces (Coston et al. 1995, Strawn et al. 1998, Scheinost et al. 2001).

Fuller et al. (1996) found that correlations between  $\text{Pb}^{2+}$  sorption and extractable metals increased dramatically at the Cape Cod site when sorption and extractable metal values were standardized to sample surface area. Standardizing to sample surface area removes the contribution of variable sample surface area to sample variability, just as standardizing data to sample mass removes the contribution of variable sample mass. In order to remove this source of variability from the Deerfield samples, surface area was estimated using a Kozeny-Carman-type regression equation which relates sample permeability and porosity to BET surface area (Tompson et al. 1996). Then, extractable metal and adsorption data were standardized to sample surface area.

Correlations between our surface area standardized variables are much stronger (Table 2.3). However, the enhanced correlations may be due solely to the presence of a highly variable common denominator.

The problem of spurious correlation between ratio variables has been scrutinized by statisticians and petrologists who often express data in a variety of ratio formulations (Pearson 1896-1897, Chayes 1949, Benson 1965, Chayes 1971). The extent of spurious correlation between ratio variables depends upon the relative values of the coefficients of variation in the parent variables. Deceptively high correlations can arise between ratio variables with a common denominator when the coefficient of variation for the denominator variable is similar to, or greater than, the coefficients of variation for the numerator variables. Since the coefficients of variation for sorption, extractable metals, and surface area are similar for the Deerfield sediments, the impact of common denominator variability on the correlation results was tested by representing surface area as a random variable and recalculating the correlation coefficients. Correlations between the random number standardized variables are roughly the same as those for the surface area standardized variables (Table 2.3), suggesting that the improvement in correlations is spurious. The enhanced correlations reported for the Cape Cod sediments may also be spurious, if the coefficient of variation for sample surface area is similar to, or greater than, the coefficients of variation for  $Pb^{2+}$  sorption and extractable metals.

### **Modeling $Pb^{2+}$ Sorption at the Deerfield Site**

The multiple regression model used to construct Figure 2.3b explains the majority of  $Pb^{2+}$  sorption variation, and it appears to provide reasonable estimates of

$Pb^{2+}$  partition coefficients. The key to explaining much of the remaining variation in sorption may lie in the relationship between sorption and permeability (Figure 2.4).

The quadratic nature of the sorption-permeability relationship may be a consequence of two solid phases controlling  $Pb^{2+}$  sorption: clays in the finest sediments, and poorly crystalline goethite grain coatings in the coarser sediments. Although X-ray diffraction was unable to identify the mineralogy of the coatings, perhaps due to their poor crystallinity, four observations suggest that the coatings consist primarily of poorly crystalline goethite with varying amounts of aluminum and manganese impurities. First, the grain coatings are not visible in thin sections when viewed under cross-polarized light. Second, every sample contains 3 to 1400 times as much iron as aluminum or manganese. Third, the most iron-rich sediment samples are yellow brown – the characteristic color of goethite-rich soils and sediments; and fourth, the regression results show that  $Pb^{2+}$  sorption tends to decrease as the iron in the coatings decreases and the aluminum increases. Decreasing sorption with decreasing iron and increasing aluminum is a sign that the coatings may be made of goethite, because goethite crystals become shorter and thicker, and have less surface area available for sorption, with increasing aluminum substitution for iron (Shwertmann and Cornell 1991).

The relative amount of aluminum in goethite coatings may explain the rising limb of the sorption-permeability model, because the relationship between the extractable iron/aluminum ratio and permeability is positive, and the relationship between the extractable iron/aluminum ratio and sorption is positive. In fact, the ratio of extractable iron to aluminum explains 68 percent of the variation in sorption when the seven low permeability, high sorption samples are excluded. The falling limb of the model is driven by these seven low permeability, high sorption samples. Six of the samples consist of



fine or very fine sand with approximately ten percent silt- and/or clay-size particles, and five contain above average extractable aluminum. The presence of approximately ten percent fines and low extractable iron/aluminum ratios suggests that clay minerals may be controlling sorption in the lowest permeability samples.

The quadratic sorption-permeability relationship may also be due, at least in part, to differences in grain coating morphology and numerical abundance. Ten thin sections were made from representative samples of the lithologies exposed in the outcrop. In three of the ten samples the (hydr)oxide coatings tend to be thin and cover most or all of the edges of the grains that have coatings (Figure 2.5a). Two of these three samples belong to the high permeability, high sorption group; the other belongs to the low permeability, high sorption group. The grain coatings in the seven remaining samples tend to be relatively thick and patchy (Figure 2.5b). Among these seven samples, the frequency and size of the patches generally increase as the concentration of (hydr)oxides increase.

A heuristic model was developed to explain the sorption results in light of these petrographic observations. The model assumes that  $Pb^{2+}$  sorption is a function of reactive surface area, and reactive surface area is a function of total (hydr)oxide mass, median grain size, grain coating morphology, and the proportion of coated grains. Total (hydr)oxide mass was calculated from measures of DC-extractable iron, manganese, and aluminum for the ten thin section samples. Median grain size was determined by sieve analysis (Appendix D). The proportion of coated grains was estimated by visual inspection of thin sections, and grain coating morphology was based on thin section observations of coating shape, using a simple binary classification scheme in which the coatings were categorized as either thin and continuous or thick and patchy.

The relatively thin, continuous coatings were modeled as hollow spheres of (hydr)oxide covering individual spherical grains (Figure 2.6a). The thick, patchy coatings were modeled as simple hemispheres on flat grain surfaces (Figure 2.6b). (Hydr)oxide surface roughness was ignored, and all sediment grains were assumed to be perfect spheres of uniform size. Obviously, actual grain sizes, shapes, and coating morphologies are much more complex, and actual reactive surface areas are much larger than the geometric surface areas predicted by the equations in Figure 2.6. Nonetheless, the reactive surface area model explains 65 percent of the variation in  $\text{Pb}^{2+}$  sorption (see Table 2.3 and Figure 2.7), and it provides an explanation for why the sorption-permeability relationship is quadratic. According to the reactive surface area model, reactivity is high in the lowest permeability samples because they have high (hydr)oxide surface areas by virtue of high total (hydr)oxide concentrations and either thin continuous coatings or patchy coatings that cover a large number of sediment grains. Reactivity is high in the highest permeability samples, even though they contain low concentrations of (hydr)oxides, because the grain coatings are very thin and continuous coatings with much higher (hydr)oxide surface area to mass ratios compared to samples in which the (hydr)oxides are concentrated in patches.

The reactive surface area model has slightly greater predictive ability than the multiple regression model; however, it requires additional information pertaining to grain coating morphology and percent grain coverage, and the methods for quantifying this information need further refinement and testing. Although the multiple regression model has lower resolution, it explains the majority of  $\text{Pb}^{2+}$  sorption variation in terms of four inexpensive and easily measured sediment properties.

### **Estimating Reactive Surface Area**

Surface complexation models require estimates of reactive surface area. The most popular approach for measuring sediment surface area is the nitrogen gas sorption and data analysis method developed by Brunauer, Emmett, and Teller (1938). However, the BET approach provides measures of total sample surface area, while sorption to sediments like those at the Cape Cod site and the Deerfield site appears to be concentrated on specific regions of the sediment surface that are coated with (hydr)oxides. In these and similar settings where sediment surfaces are heterogeneous with respect to sorption, site-specific measures of total surface area overestimate the surface area of the reactive solid phase.

The reactive surface area model could potentially be used to estimate the BET surface area of the grain coatings in a sample. In order to do this, the variation in surface roughness for different grain sizes and coating morphologies would need to be characterized, perhaps by measuring the BET surface areas of samples of fully-coated sediment grains that were grouped according to grain size and coating morphology. The BET surface area of the grain coatings in a field sample could then be determined by multiplying its geometric reactive surface area by a conversion factor. The conversion factor would relate the average measured BET surface area for the relevant group of fabricated samples to their calculated geometric surface area. These estimates of reactive surface area should be an improvement over BET measurements of total surface area typically used in surface complexation models.

### **Conclusions**

1. Measures of  $\text{Pb}^{2+}$  sorption varied three orders of magnitude in the eight square meter study area.

2. Fifty-seven percent of the variability in  $Pb^{2+}$  sorption can be explained by a linear combination of sediment permeability, and DC-extractable iron, aluminum, and manganese, indicating that  $Pb^{2+}$  sorption is controlled by (hydr)oxide grain coatings. Sediment color,  $Pb^{2+}$  sorption, and extractable metal data suggest the coatings consist primarily of poorly crystalline goethite.  $Pb^{2+}$  partition coefficients derived from permeability and extractable metal data have a similar, albeit narrower range of values compared to actual measurements, and a site map of estimated partition coefficients preserves the spatial patterns observed in a site map of actual measurements. The findings demonstrate that reasonable estimates of  $Pb^{2+}$  partition coefficients can be derived for the Deerfield sediments from relatively simple and inexpensive measures of sediment permeability and DC-extractable metals.
3. The relationship between  $Pb^{2+}$  sorption and permeability is quadratic. Sediment texture,  $Pb^{2+}$  sorption, and extractable metal data suggest the quadratic relationship may arise from clay minerals controlling sorption in the finest-textured sediments and goethite controlling sorption in the coarser sediments. Petrographic observations provide an alternative, or perhaps complementary hypothesis. They indicate sorption is high in several low permeability samples because the (hydr)oxides occur on a large number of fine particles. Sorption is high in the highest permeability samples, even though most contain relatively few coated grains and little (hydr)oxide mass, because the coatings tend to be very thin with extremely high (hydr)oxide surface area to mass ratios.
4. A reactive surface area model was developed to quantify the impact of observed differences in grain size, (hydr)oxide mass, grain coating morphology, and grain coating abundance on measures of  $Pb^{2+}$  sorption. The model, which calculates

the geometric surface area of the (hydr)oxide grain coatings, explains 65 percent of the  $\text{Pb}^{2+}$  sorption variation. The model results suggest that consideration of grain coating morphology and numerical abundance can help identify the solid phase(s) controlling reactivity, improve predictive models of  $\text{Pb}^{2+}$  partition coefficients, and estimate reactive surface areas. However, grain coating characterization methods need to be refined, and the usefulness of this coating information needs to be tested in other carbon-poor glaciofluvial environments before it can be considered an effective site-assessment and reactive transport modeling tool.

**Table 2.1**  
**Univariate Statistics for Measured Properties**

| Property                          | <i>n</i> | Minimum | Maximum | Mean    | Variance | CV (%) | Skewness |
|-----------------------------------|----------|---------|---------|---------|----------|--------|----------|
| <b>Permeability</b>               |          |         |         |         |          |        |          |
| (cm <sup>2</sup> )                | 476      | 5.73e-8 | 3.55e-6 | 9.21e-7 | 6.74e-13 | 89.1   | 2.0      |
| [ln(cm <sup>2</sup> )]            | 476      | -16.7   | -12.6   | -14.2   | 0.587    | -5.39  | 0.2      |
| <b>Porosity</b>                   |          |         |         |         |          |        |          |
| (dimensionless)                   | 476      | 0.29    | 0.53    | 0.42    | 0.001    | 7.3    | -1.2     |
| <b>DC-Extractable Mn</b>          |          |         |         |         |          |        |          |
| (μmol/g)                          | 99       | 0.04    | 2.88    | 0.65    | 0.34     | 89.6   | 2.2      |
| [ln(μmol/g)]                      | 99       | -3.12   | 1.06    | -0.87   | 1.00     | -116   | -0.3     |
| <b>DC-Extractable Fe</b>          |          |         |         |         |          |        |          |
| (μmol/g)                          | 99       | 19.2    | 170     | 39.1    | 318      | 45.6   | 4.3      |
| [ln(μmol/g)]                      | 99       | 2.95    | 5.14    | 3.60    | 0.12     | 9.53   | 0.9      |
| <b>DC-Extractable Al</b>          |          |         |         |         |          |        |          |
| (μmol/g)                          | 71       | 2.13    | 22.6    | 8.1     | 14.4     | 46.7   | 1.1      |
| [ln(μmol/g)]                      | 71       | 0.75    | 3.12    | 1.99    | 0.24     | 24.6   | -0.4     |
| <b>Total DC Metals</b>            |          |         |         |         |          |        |          |
| (μmol/g)                          | 71       | 24.1    | 196     | 49.3    | 519      | 46.2   | 3.9      |
| [ln(μmol/g)]                      | 71       | 3.18    | 5.28    | 3.83    | 0.12     | 9.17   | 0.9      |
| <b>Organic Carbon<sup>1</sup></b> |          |         |         |         |          |        |          |
| (weight %)                        | 9        | 0.030   | 0.067   | 0.044   | 1.96e-4  | 32.0   | 0.9      |
| [ln(weight %)]                    | 9        | -3.52   | -2.70   | -3.17   | 0.090    | -9.44  | 0.7      |
| <b>Pb<sup>2+</sup> Sorption</b>   |          |         |         |         |          |        |          |
| (ml/g)                            | 72       | 3.01    | 140     | 21.0    | 675      | 124    | 2.5      |
| [ln(ml/g)]                        | 72       | 1.10    | 4.94    | 2.50    | 1.00     | 40.2   | 0.6      |

<sup>1</sup> Inorganic carbon ranged from < 0.00005 to 0.0013 wt. %.

**Table 2.2**  
**Correlations<sup>1</sup> Between Measured Properties**

|   | (1)             | (2)             | (3)  | (4)  | (5)   | (6) | (7) |
|---|-----------------|-----------------|------|------|-------|-----|-----|
| (1) Permeability<br>[ln(cm <sup>2</sup> )]      | 1.0             |                 |      |      |       |     |     |
| (2) Porosity                                    | -0.29           | 1.0             |      |      |       |     |     |
| (3) DC-Extractable Mn<br>[ln(μmol/g)]           | 0.42            | -0.46           | 1.0  |      |       |     |     |
| (4) DC-Extractable Fe<br>[ln(μmol/g)]           | -0.26           | -0.24           | 0.28 | 1.0  |       |     |     |
| (5) DC-Extractable Al<br>[ln(μmol/g)]           | -0.62           | NS <sup>2</sup> | NS   | 0.68 | 1.0   |     |     |
| (6) Total DC-Extractable<br>Metals [ln(μmol/g)] | -0.39           | NS              | 0.24 | 0.99 | 0.78  | 1.0 |     |
| (7) Organic Carbon<br>[ln(weight%)]             | NS              | NS              | NS   | NS   | NS    | NS  | 1.0 |
| (8) Pb <sup>2+</sup> Sorption<br>[ln(ml/g)]     | NS <sup>3</sup> | NS              | 0.42 | 0.25 | -0.26 | NS  | NS  |

<sup>1</sup> Regression-derived correlation coefficient (r) based on r<sup>2</sup>.

<sup>2</sup> Not significant at the α = 0.05 level.

<sup>3</sup> Significant nonlinear relationship between Pb<sup>2+</sup> sorption and permeability (r<sup>2</sup> = 0.40).

**Table 2.3**  
**Summary of Pb<sup>2+</sup> Sorption Models**

| Model Description   | Model Parameters  | $r^2$ | $r^{2a}$ |
|---|---|-------|----------|
| Linear relationship between sorption (ml/g) and the concentration of individual or total DC-extractable metals ( $\mu\text{mol/g}$ ).   | $\ln K_d$ vs. $\ln \text{Fe}$   | 0.06  |          |
|   | $\ln K_d$ vs. $\ln \text{Mn}$   | 0.17  |          |
|   | $\ln K_d$ vs. $\ln \text{Al}$   | 0.07  |          |
|   | $\ln K_d$ vs. $\ln(\text{Fe}+\text{Mn}+\text{Al})$                          | NS    |          |
| Linear relationship between sorption (ml/g) and individual or total DC-extractable metals ( $\mu\text{mol/g}$ ) standardized to sample surface area, $a_s$ ( $\text{cm}^2/\text{g}$ ).  | $\ln(K_d/a_s)$ vs. $\ln(\text{Fe}/a_s)$                                     | 0.49  | 0.41     |
|   | $\ln(K_d/a_s)$ vs. $\ln(\text{Mn}/a_s)$                                     | 0.55  | 0.43     |
|   | $\ln(K_d/a_s)$ vs. $\ln(\text{Al}/a_s)$                                     | 0.18  | 0.15     |
|   | $\ln(K_d/a_s)$ vs. $\ln((\text{Fe}+\text{Mn}+\text{Al})/a_s)$               | 0.45  | 0.37     |
| Nonlinear relationship between sorption (ml/g) and permeability ( $\text{cm}^2$ ).  | $\ln K_d$ vs. $\ln k$   | 0.40  |          |
| Sorption (ml/g) as a linear combination of DC-extractable Fe and Al ( $\mu\text{mol/g}$ ).  | $\ln K_d$ vs. $\ln \text{Fe}$ , $\ln \text{Al}$                             | 0.44  |          |
| Sorption (ml/g) as a linear combination of permeability ( $\text{cm}^2$ ) and individual DC-extractable metals ( $\mu\text{mol/g}$ ).   | $\ln K_d$ vs. $\ln k$ , $\ln \text{Fe}$ , $\ln \text{Al}$ , $\ln \text{Mn}$ | 0.57  |          |
| Linear relationship between sorption (ml/g) and (hydr)oxide surface area, $a_{rx}$ ( $\text{cm}^2/\text{g}$ ), where $a_{rx}$ is a function of median grain size, total DC-extractable metals, coating morphology, and percent coated grains. | $\ln K_d$ vs. $\ln(a_{rx})$   | 0.65  |          |

<sup>a</sup> Linear relationship between sorption and DC-extractable metals standardized to a set of random numbers having the same coefficient of variation as sample surface area. Similarity between  $r^2$  values for surface area- and random number-standardized variables suggests that the improvement in correlation obtained by standardizing to sample surface area is spurious.



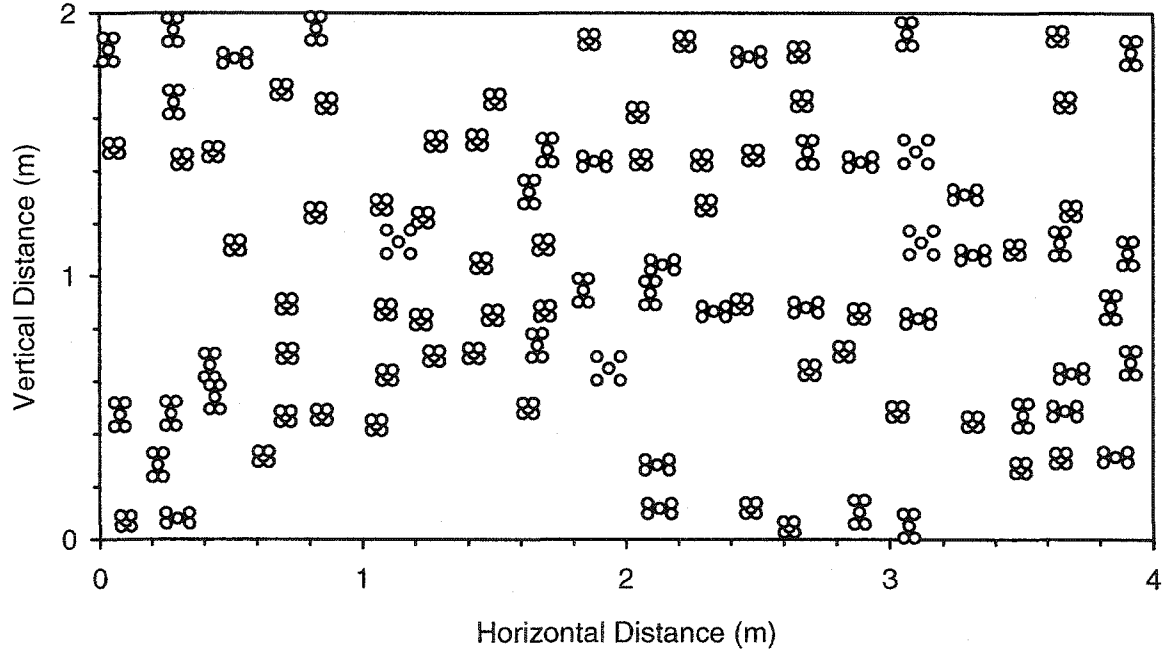
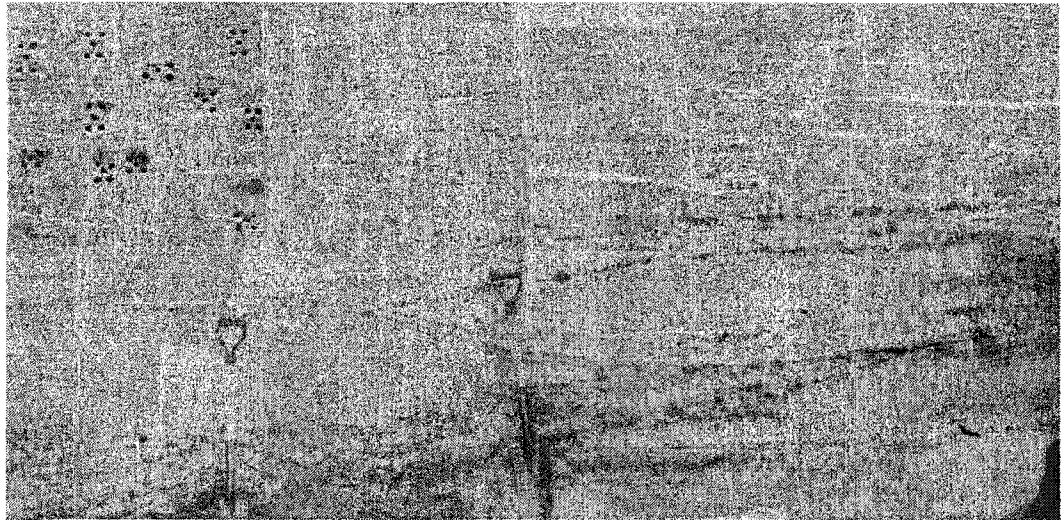


**Figure 2.1** Deerfield outcrop (a) and sample locations (b). The sampling rationale and protocol are described in Chapter 3.

compressed air source  
with pressure regulators

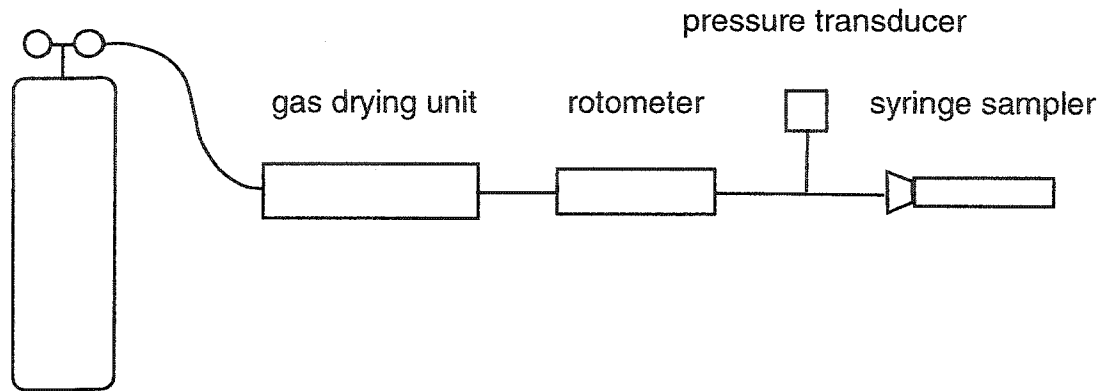


**Figure 2.2** Schematic diagram of air permeameter. The rate of air flow through the sample is controlled by the rotometer. Air pressure at the upstream end of the sample is measured with the pressure transducer. Air pressure at the downstream end is assumed to be atmospheric. Flow rate, pressure, and sample length measurements are used to calculate permeability with a version of Darcy's law that accounts for the compressibility of air.

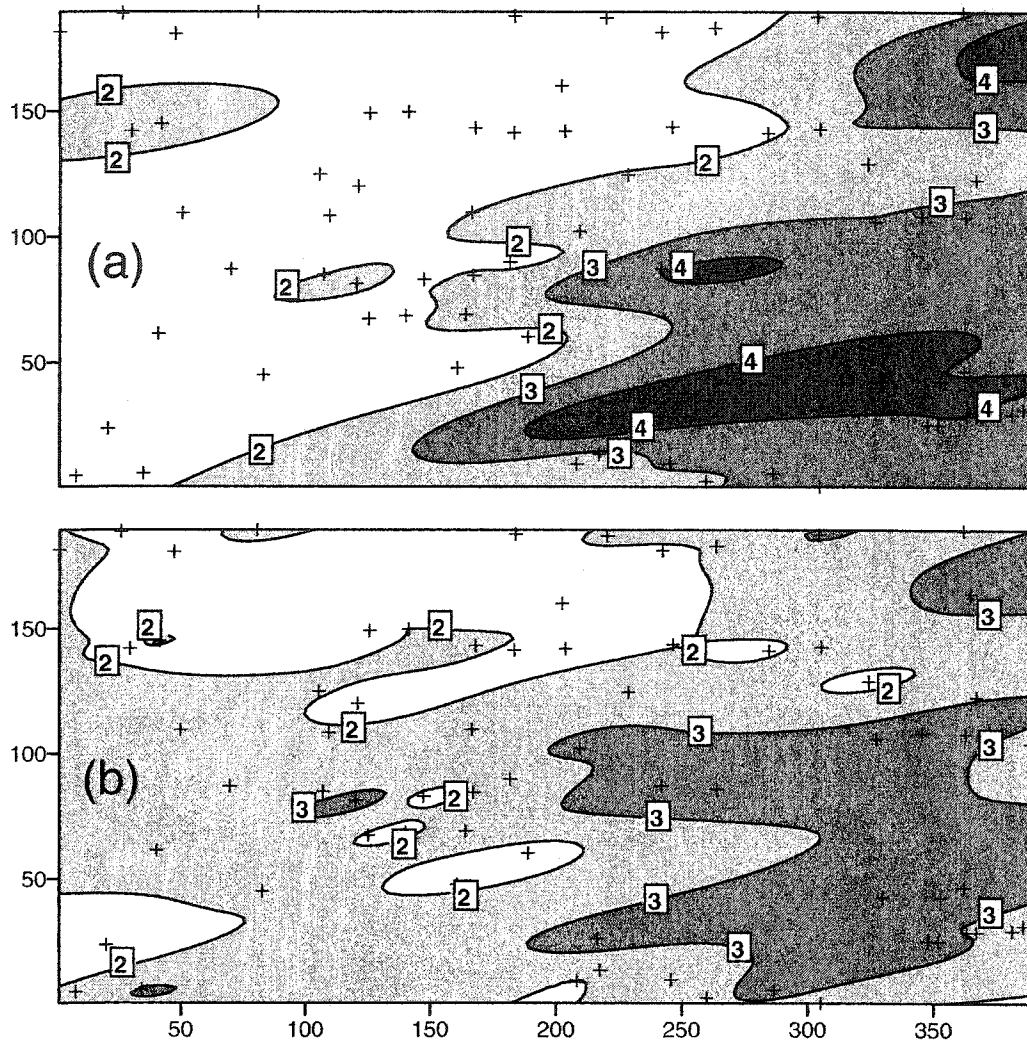


**Figure 2.3** Interpolated images of  $Pb^{2+}$  partition coefficients for the Deerfield outcrop: (a) is based on laboratory measures of  $Pb^{2+}$  sorption; (b) is based on estimated sorption values derived from measures of sediment permeability and DC-extractable metals. Crosses mark the 72 sample locations. Although the estimated sorption field shown in (b) is smoothed, it preserves the general spatial patterns displayed in (a).

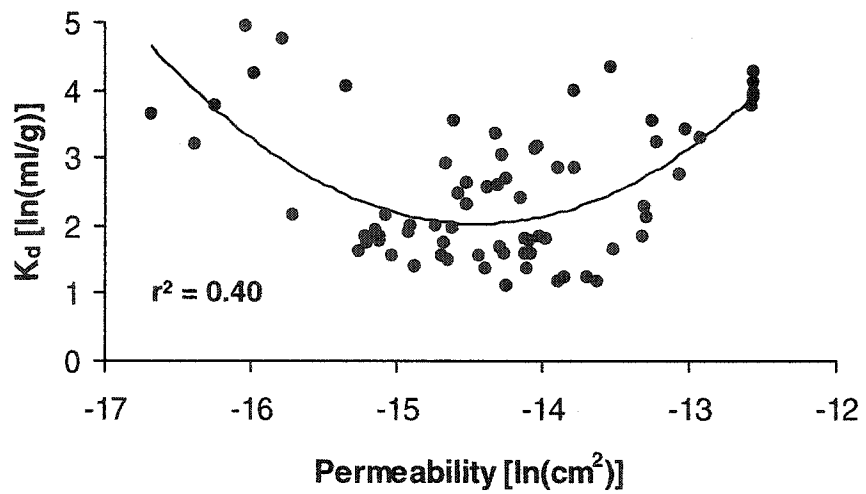


**Figure 2.4** Relationship between  $\text{Pb}^{2+}$  partition coefficient and permeability.

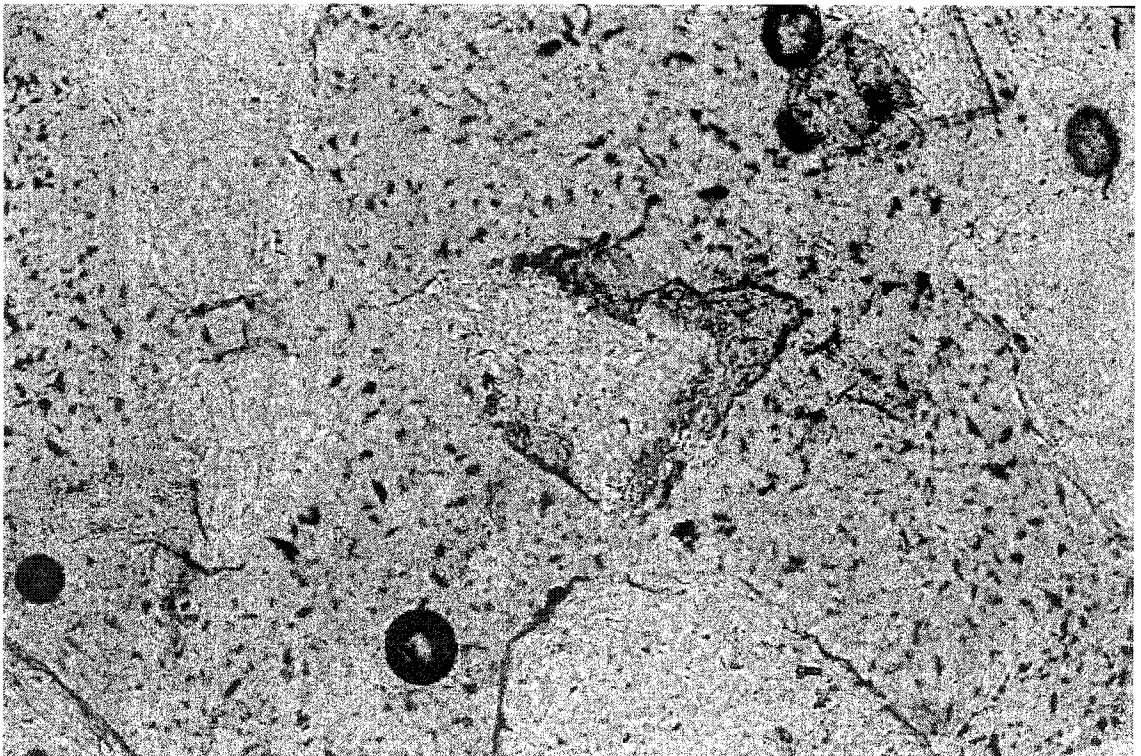
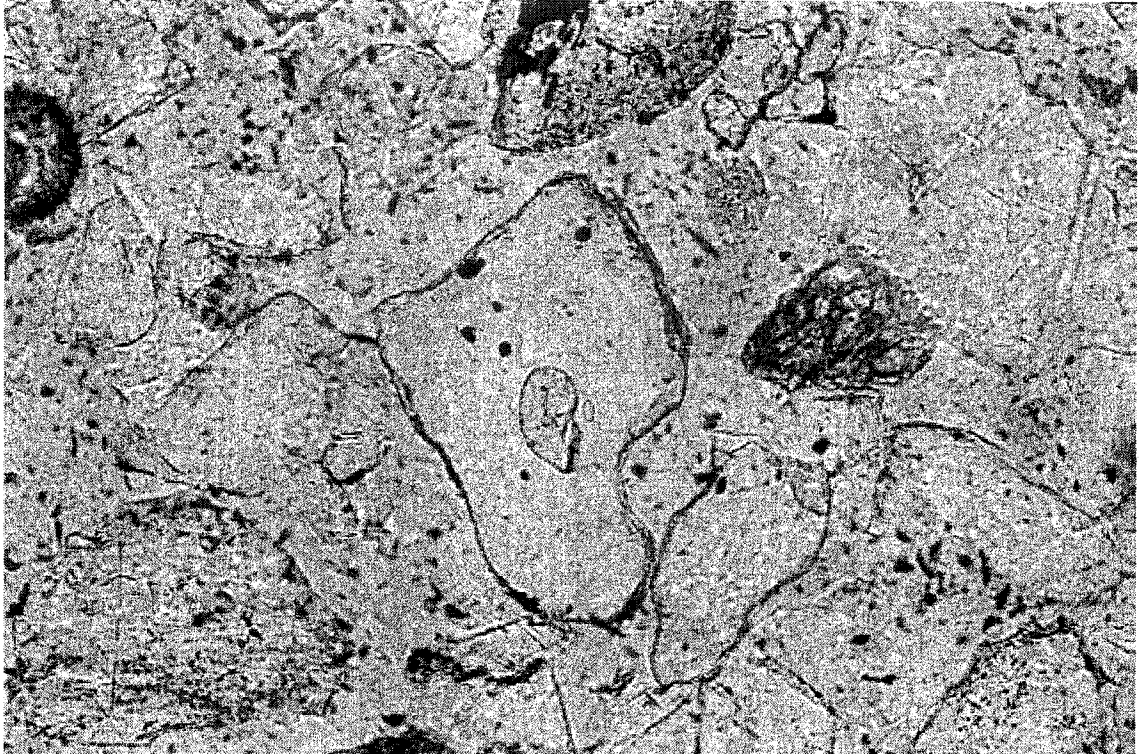
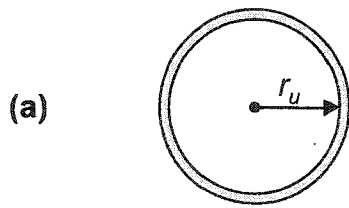
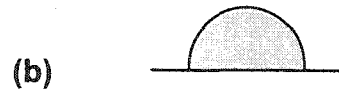


**Figure 2.5** Photomicrographs of (hydr)oxide grain coatings on Deerfield sediments: (a) thin, continuous coatings; (b) thick, patchy coatings. Scale: 1 in = 0.1 mm.



$$a_{rx} = 4\pi(n_s \cdot p) \left[ r_u^3 + \frac{3 v_c}{4 \pi} \right]^{\frac{2}{3}}$$



$$a_{rx} = 2\pi(n_s \cdot p) \left[ \frac{3 v_c}{2 \pi} \right]^{\frac{2}{3}}$$

**Figure 2.6** Models of reactive surface area for sediments with (a) thin, uniform grain coatings and (b) thick, discontinuous coatings. In both models  $a_{rx}$  is reactive surface area ( $\text{cm}^2/\text{g}$ ),  $n_s$  is the number of spheres (spheres/g),  $p$  is the proportion of coated spheres,  $r_u$  is the radius of an uncoated sphere (cm), and  $v_c$  is the volume of coating on a single sphere ( $\text{cm}^3$ ).

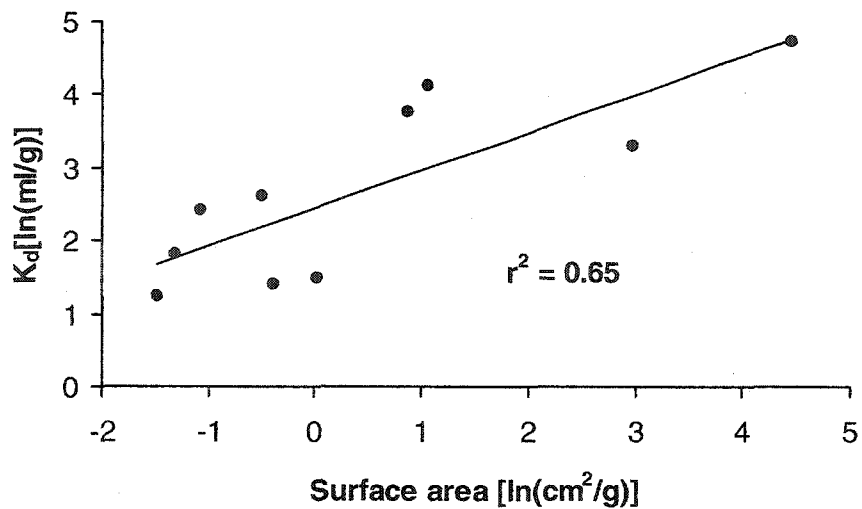


**Figure 2.7** Relationship between Pb<sup>2+</sup> partition coefficient and geometric surface area of (hydr)oxide grain coatings. The (hydr)oxide surface area for each sample was calculated from sample data using one of the two equations in Figure 2.6. The choice of equation depended on whether the grain coatings were predominantly thin and continuous or thick and patchy.

## CHAPTER 3

### CHARACTERIZATION AND ORIGIN OF HETEROGENEITIES IN A GLACIOFLUVIAL DEPOSIT

#### Abstract

The strong influence of subsurface heterogeneity on contaminant migration and in situ remediation calls for an improved understanding of its origins and more efficient methods of characterization. Accordingly, an outcrop study of physical and chemical heterogeneity was conducted in a glaciofluvial deposit in Deerfield, New Hampshire in order to uncover processes controlling the spatial variation of sediment properties, and evaluate the extent to which geologic information can be used to characterize the observed variation. The results indicate that physical and chemical properties at the Deerfield site have distinctly different spatial correlation structures. Lithologic facies explain 30 to 60 percent of the variation in porosity, permeability, dithionite citrate (DC)-extractable manganese, and DC-extractable aluminum. Facies do not separate regions of significantly different DC-extractable iron; instead, 49 percent of its variation is explained by sediment color. Color also accounts for 34 percent of the variation in DC-extractable aluminum and 60 percent of the variation in DC-extractable manganese. Strong relationships with lithofacies and/or color enable detailed mapping of permeability, extractable iron, and extractable manganese. Differences in the geometries of iron and manganese enrichment, petrographic observations, and SEM-EDS analyses indicate that (hydr)oxide grain coatings originated from the post-depositional weathering of biotite and garnet, coupled with local, redox-driven redistribution of the liberated iron and manganese. The findings suggest that facies and



color information can aid the characterization and modeling of heterogeneity at similar glaciofluvial sites.

### **Introduction**

Efforts to forecast solute transport and apply in situ treatment agents are complicated by heterogeneities in geologic materials. To date, most heterogeneity research has focused on the spatial variability in the physical properties of the media and how they affect contaminant migration. Relatively little research has addressed the spatial variability in the sorptive properties of the media. In carbon-poor sedimentary deposits, the sorption of a host of contaminants is believed to be controlled by oxides and hydroxides of iron, aluminum, and manganese that occur as coatings on particle surfaces (Jenne 1968; Lion et al. 1982; Tessier et al. 1985; Jackson and Inch 1989; Fuller et al. 1996). These grain coatings are often concentrated in spatially distinct zones that appear as long narrow bands and/or irregular-shaped patches in outcrops. Field observations, laboratory experiments, and numerical modeling studies indicate heterogeneities in (hydr)oxide grain coatings can strongly influence contaminant fate and transport (Friedly et al. 1995; Tompson et al. 1996; Szecsody et al. 1998). However, grain coating architecture and its geologic origins are poorly understood.

Knowledge of grain coating architecture could improve transport simulations for the many solutes that preferentially sorb to the coatings, but the spatial statistical properties of the coatings are unknown, and methods for mapping coatings are not well developed. Likewise, an understanding of grain coating origins could aid subsurface characterization and refine conceptual transport models, but their genesis in subsoil environments is not well known. Potential diagenetic mechanisms include: direct deposition of detrital (hydr)oxide-coated particles; formation of weathering rinds on iron-,

manganese-, and aluminum-bearing minerals; and precipitation of dissolved iron, manganese, and aluminum along redox fronts.

In this study, permeability, porosity, and (hydr)oxide grain coating heterogeneities are examined in an eight square meter outcrop of glaciofluvial sands and gravels. The observed variation is assessed with respect to two mappable geologic features: sediment color and lithofacies bounding surfaces. Sediment color is evaluated as a proxy for chemical heterogeneity, and lithofacies are evaluated as a framework for explaining both physical and chemical heterogeneities. Facies-based models have proven useful for conceptualizing large-scale physical heterogeneities in glacial and glaciofluvial sediments (Anderson 1989). Davis et al. (1997) found lithofacies bounding surfaces to be important in conceptualizing and modeling permeability heterogeneity in Pliocene-Pleistocene fluvial deposits, and Allen-King et al. (1998) demonstrated the significance of facies in explaining variations in permeability and tetrachloroethene adsorption in glaciolacustrine sands.

Relationships between physical and chemical properties are explored to identify linkages that might simplify the characterization and modeling of chemical heterogeneity. Additionally, field and petrographic observations are used to investigate the diagenetic processes controlling chemical heterogeneity. Chapter 2 describes how the chemical heterogeneity is manifested in terms of lead sorption variability.

## **Methods**

### **Field Methods**

The study site is a sand and gravel pit located in the town of Deerfield, New Hampshire in heterogeneous glacial lake and meltwater stream deposits (Gephart 1985). Sediments exposed in the pit are variably coated with (hydr)oxides, grains are

predominantly sand, and gravelly layers are common. Apart from the fine-grained kettle pond sediments present in a small zone at the center of the pit, silt- and clay-rich strata have not been observed.

Rather than analyzing subsurface cores, heterogeneities were examined on a wall of the borrow pit. The outcrop was treated as an analog for the subsurface environment, and it provided detail in the horizontal direction that would be unavailable in core samples. Heterogeneities were evaluated at the scale of a few centimeters to a few meters, because permeability variation at this scale exerts a strong influence on dispersive transport (Kapoor and Gelhar 1994a, 1994b), and because observations at larger scales would have obscured much of the chemical variation present in the outcrop sediments.

A two-meter by four-meter vertical face was excavated in the north wall of the borrow pit, approximately two meters below the soil surface and three meters above the water table. Polaroid photographs of the outcrop were taken and exposed lithofacies bounding surfaces mapped upon them. Additional photos were taken with a standard 35 mm camera to construct a photomosaic image of the sampling domain, and to document relationships between grain size, sedimentary structures, and (hydr)oxide grain coatings.

Sediment sample points were located in the field using a total station and a sampling grid made from aluminum rods and twine. The sampling protocol was developed with the constraint that variogram estimates in the 0°, 30°, 60°, and 90° directions contained more than 100 pairs of points per lag when the lag increment was no more than 10 cm. First, the sample space was divided into eight, one meter by one meter units. Each unit was further divided into 25, 20 cm by 20 cm subunits. Twelve of these subunits were randomly selected from each of the 8 units for a total of 96

subunits. Five points were sampled from each of the 96 subunits to yield 480 samples (Figure 3.1).

The locations of the five sampling points in a given subunit were determined by generating two random integer numbers between zero and ten — these numbers constituted the local x (cm) and y (cm) coordinates of the lower left point. Two additional random numbers between zero and one were drawn for each subunit to establish the distances between the corner points in the five-spot pattern. If the first random number was less than or equal to 0.7, the spacing between the centers of the corner points in the x direction was 4 cm; otherwise, the spacing was 9 cm. The same rule applied to the second random number which specified the distance between the centers of the corner points in the y direction. The fifth point in each five-spot was placed at the center of the square or rectangle formed by the four corner points.

Each sample was collected with a 30 cm<sup>3</sup> plastic syringe that was modified by sawing off its anterior beveled portion. With the plunger withdrawn to the rear of the syringe barrel, the sawed-off end was pushed into the outcrop face to obtain a minimally disturbed sample. The sediment-laden syringe was then removed from the outcrop face, capped, and stored in ice until oven-dried at 30° C. The 30 cm<sup>3</sup> sample size was the smallest possible volume that provided sufficient sample for the battery of laboratory analyses. Samples were dried at 30° C to inhibit the dehydration of (hydr)oxide grain coatings.

### **Laboratory Methods**

Permeability, length, and cross-sectional area were measured on each oven-dried sample prior to removal from the syringe sampler in order to obtain measures from relatively undisturbed samples. One-dimensional air permeability was measured using

an air permeameter (Figure 2.2). When a sample exceeded the upper limit of the permeameter, it was assigned the maximum measurable value of  $3.55 \times 10^{-6} \text{ cm}^2$ . After permeability, length, and cross-sectional area measurements were completed, the sample was removed from its syringe container, homogenized, and transferred to a 50 ml centrifuge tube in order to be weighed and stored. Dry bulk density was computed from measures of sample mass, length, and cross-sectional area. Total porosity was calculated from the dry bulk density and an assumed particle density of  $2.65 \text{ g/cm}^3$  (Culley 1993).

Thin sections were made from 12 sediment samples. One sample was collected from the center of a large, (hydr)oxide-rich band exposed in the lower central portion of the outcrop; another was taken from a (hydr)oxide-deficient zone adjacent to the band. The remaining ten samples represent the range of sediment types exposed in the outcrop. The 12 thin sections were used to estimate mineral abundances, and to evaluate the character and distribution of (hydr)oxide grain coatings. Thin sections of individual mineral grains were studied by scanning electron microscopy (SEM-EDS) to determine their elemental composition.

The (hydr)oxide grain coating contents of 99 samples were quantified using a dithionite-citrate (DC) extraction procedure designed to selectively dissolve the coatings and keep the metals in solution (Ross and Wang 1993; Coston et al. 1995). Twenty-one milliliters of 0.2M ammonium citrate and 0.30 g of sodium dithionite were added to 3 g of sediment. The mixture was gently shaken at room temperature for 24 h on an orbital-shaking table. Once the shaking was completed, the samples were centrifuged, and the supernatant analyzed for iron, aluminum, and manganese using flame spectroscopy. Extract solutions were diluted 1:100 for iron and 1:10 for manganese.

Standards were prepared with the same concentration of DC solution as the diluted extracts.

The oven-dried color of 91 of the 99 samples was identified by comparing the sample to color chips on Munsell® Soil Color Charts (Munsell Color Co. 1975) under consistent illumination and viewing conditions. According to the Munsell color-order system, every color can be described by three attributes — hue, value, and chroma — and each attribute has its own numerical scale with visually uniform steps. Hue indicates a color's relation to red, yellow, green, blue, and purple. Value indicates a color's whiteness, and chroma its strength, or saturation. Since visual evaluation of color depends highly on the observer (Post et al. 1993), two observers were employed to improve the accuracy of the results.

### **Statistical Methods**

Summary statistics and frequency distributions were generated for permeability, porosity, and DC-extractable metals. Distributions were tested for normality with the Lilliefors test, which is based on the Kolmogorov-Smirnov test, and the Shapiro-Wilk test (Sall and Lehman 1996). If the distribution for a given variable failed these two normality tests, sample values were log-transformed and the transformed distribution was tested for normality. Subsequent parametric statistical analyses were conducted using the distribution that fit or came closest to fitting a normal model.

One-way analysis of variance (ANOVA) tested whether the observed variability in a given sediment property should be attributed to variations within facies or variations between facies. If facies was found to be a significant factor in explaining the variance, ANOVA indicated the proportion of variation that could be explained by the facies model.

One-way ANOVA was also applied to the study of relationships between extractable metals and sediment color.

The Student's t test identified which, if any, facies or color group means were significantly different. The Tukey-Kramer Honestly Significant Difference method (Sall and Lehman 1996) was applied in conjunction with the Student's t test to reduce the likelihood of rejecting the null hypothesis — that the differences between means were due to chance — when in fact it was true.

Bivariate regression quantified relationships between sediment properties when variables were continuous. Bivariate regression provided linear correlation information and defined the nature of the bivariate relationship with an equation that could potentially permit predictions and shed light on geologic processes. Multiple regression evaluated relationships involving linear combinations of regressor variables.

Spatial statistical parameters were estimated using the traditional semivariogram (Isaaks and Srivastava 1989). The semivariogram [ $\gamma(h)$ ] is half the variance of the differences between pairs of measurements whose spatial separation falls within a given interval as a function of  $h$ , the midpoint of that interval:

$$\gamma(h) = \frac{1}{2N(h)} \sum_{i=1}^{N(h)} [Z_i(x+h) - Z_i(x)]^2$$

where  $N(h)$  denotes the number of pairs in the distance class with midpoint distance  $h$ . Plots of  $\gamma(h)$  versus  $h$  contain information about the scale-dependent variability of the data and the distance over which the measures are correlated. When the data values are paired in specified directions, variogram plots also provide information regarding data anisotropy. Variogram plots were constructed for permeability, porosity, and extractable metals using the spatial data analysis code VARIOWIN 2.2 (Pannatier 1996).

## Results

The outcrop consists of a complex of cross-cutting lenticular channel sequences characteristic of braided fluvial systems (Figure 3.2). The channel sands and gravels are cross-bedded and overlain by fairly straight, sheet-like sand bodies. Eight lithofacies were identified in the outcrop. Facies one is a fine to medium sand with trough cross-stratification. Facies two and three are predominantly medium, low-angle cross-laminated sands with thin basal pebble lags. Facies four is a heterogeneous unit consisting of pebbly cross-bedded sands at the base, grading upward to low-angle cross-laminated medium sands. Facies five is a uniform very coarse sand with tabular cross-bedding. Facies six is a medium to coarse, trough cross-stratified sand. Facies seven is a thin lens of uniform very fine sand, and facies eight consists of low-angle cross-bedded sands and gravels.

(Hydr)oxide grain coatings are clearly visible in six of the eight facies. Sediments in facies five and seven do not appear to be coated; nevertheless, thin sections reveal that these facies do contain coated grains. Most of the grain coatings appear to be concentrated in narrow bands (Figure 3.2), and many of the finer bands crosscut lamina boundaries. Naturally-occurring grain coatings do not usually consist of pure iron, aluminum, and manganese (hydr)oxide phases (Coston et al. 1995), and visually separable, yellow brown iron (hydr)oxides, white aluminum (hydr)oxides, and black manganese (hydr)oxides could not be identified in thin sections.

The outcrop sediments are a relatively simple mixture of minerals, dominated by quartz and feldspar plus garnet, muscovite, biotite, and tourmaline (Table 3.1). This mineral assemblage is typical for sediments derived from the weathering of granites and mica schists in temperate climates. The tourmaline-bearing granite and muscovite-



schist rock fragments in the outcrop gravels indicate the source rocks are Devonian binary granites located immediately north and west of the borrow pit, and Silurian pelitic schists that lie just beyond the granites (Kerwin et al. 2004).

### **Permeability**

Permeability ( $n = 476$ ) displays a non-normal, bimodal distribution. Log-transformed permeability is also non-normally distributed (Figure 3.3a); however, it more closely approximates a normal distribution, and it fits a normal model when the samples in the higher mode are excluded. Twenty-five of the 29 samples in the higher mode exceeded the  $3.55 \times 10^{-6} \text{ cm}^2$  detection limit of the air permeameter. Since all 25 samples were assigned the default value of  $3.55 \times 10^{-6} \text{ cm}^2$ , it is possible the true distribution is not bimodal. Nevertheless, the presence of two populations is consistent with observations of discrete zones of very coarse sands and gravelly sands in an otherwise fine to medium sand deposit.

One-way ANOVA tested whether the observed variability in permeability could be attributed to variations within facies or variations between facies. The results suggest that 60 percent of the variation in permeability can be explained by a facies model (Table 3.2). In general, permeability is lower in the three stratigraphically highest facies, and higher in the stratigraphically lower facies (Figure 3.3b). It is highest in the uniform coarse sand (facies five), and lowest in the very fine sand (facies seven).

Permeability exhibits a strong statistical anisotropy. Spatial continuity is greatest in the  $15^\circ$  (subhorizontal) direction and least in the  $105^\circ$  (subvertical) direction. Correlation lengths based on best-fit exponential models are 0.45 m in the subhorizontal direction and 0.10 m in the subvertical direction (Figure 3.4a).

## **Porosity**

The negatively-skewed porosity variable ( $n = 476$ ) does not fit a normal model; instead, it exhibits over-dispersion, suggesting a mixture of several normal distributions (Figure 3.5a). Logarithmic and power transformations did not improve its fit; consequently, ANOVA was performed without prior transformation and resulted in significant differences between facies (Table 3.2). Thirty percent of the variability in porosity can be attributed to facies, and mean porosity in facies three, five, and eight is significantly less than that in facies one, two, and four (Figure 3.5b). Furthermore, mean porosity in facies eight is significantly less than that in any other facies, and it is more than two standard deviations below the overall porosity mean. Facies eight contains a preponderance of pebble-size rock fragments, and its low porosity is probably due, at least in part, to a relatively wide range of grain sizes. Nevertheless, the actual porosity of facies eight may not be as dissimilar as the ANOVA results suggest. Petrographic observations indicate the pebble-size rock fragments often contain ferromagnesian minerals; therefore, the particle densities of the facies eight samples may be higher than assumed, and their actual porosities may be greater than their calculated values.

As shown in Figure 3.4a, the spatial correlation structure for porosity is similar to that for permeability. Directions of maximum and minimum continuity are  $15^\circ$  and  $105^\circ$ , respectively, and correlation scales in these directions are 0.44 m and 0.07 m.

## **Dithionite-Citrate Extractable Manganese**

The distribution of extractable manganese ( $n = 99$ ) exhibits moderate positive skewness (Table 3.2), calling for a logarithmic transformation. Facies differences explain 54 percent of the variability in extractable manganese; they also explain the subtle, bimodal character of its frequency distribution (Figure 3.6a). As with

permeability, manganese contents are relatively low in facies one through three (Figure 3.6b).

Extractable manganese is statistically anisotropic with maximum spatial continuity in the 0° (horizontal) direction. Figure 3.4 shows that measures of extractable manganese are correlated over greater distances than are measures of permeability or porosity. In addition, the variogram plots for extractable manganese increase very slowly at short separation distances. The gradual increase in  $\gamma(h)$  with increasing separation distance is best represented by double exponential functions which model relatively continuous phenomena. The double exponential models shown in Figure 3.4b indicate the correlation lengths for extractable manganese are 1.15 m and 0.22 m in the horizontal and vertical directions, respectively. The vertical variogram reaches a plateau, or sill, at a variance of 0.79 and then increases in an unbounded fashion at large separation distances, reflecting the vertical trend in mean extractable manganese. Fitting the variogram model to the data for relatively small separation distances minimizes the influence of this trend on the model parameters.

There was no statistically significant relationship between extractable manganese and hue, while extractable manganese increased with decreasing value and chroma. Color relationships were more useful for mapping when samples were grouped according to Munsell color names. The Munsell® Soil Color Charts contain two complementary systems of nomenclature: the three part (hue, value, chroma) Munsell notation associated with each color chip, and the descriptive Munsell color name such as brownish gray or pale yellow that corresponds to one or more specific color chips.

Sixty percent of the variability in extractable manganese could be explained by color when samples were lumped into three distinct color groups based on Munsell color names (Figure 3.6c). According to this classification scheme the bright yellow samples

are low in manganese, and the browns and grays are high. Although the groups overlap, the three group means are significantly different ( $P$ -value  $< 0.01$ ). The low manganese group mean is more than one standard deviation below the overall manganese mean. The moderate group mean is slightly less than the overall mean, and the high group mean is about one standard deviation above the overall mean. Alternatively, the low and moderate groups can be combined to form a two-group model that explains 55 percent of the variation in extractable manganese. In the two group scheme the low manganese samples consist of bright yellow, pale yellow, and brownish yellow colors, and the highs consist of browns and grays.

The relationships between extractable manganese and Munsell color names are consistent with the fact that manganese (hydr)oxides and manganese-rich goethite are black-brown (Schwertmann and Cornell 1991, Dixon and Skinner 1992). Since manganese-rich (hydr)oxides are black-brown, the lack of a relationship between manganese and hue was expected. One might expect that the relationship between manganese content and value would be the strongest. Our results confirm that manganese content increases with decreasing value; however, the inverse relationship between manganese content and chroma is strongest. Chroma is the saturation, or departure of a color from the neutral color of the same value (Torrent and Barron 1993), such that low chroma colors are weak and high chroma colors are vivid.

By incorporating sediment color data, zones of significantly different extractable manganese content can be identified in the outcrop (Figure 3.7). Most of the lower portion of the sampling domain comprises a high manganese zone, while the remaining area contains high, medium, and low manganese sediments that cannot be readily differentiated at our scale of observation.

Roughly the same amount of extractable manganese variation can be explained by a facies model or a color-group model. Based on two-way ANOVA, a combined facies and three-group color model can explain 68 percent of the variability in extractable manganese, and the effects of both variables are significant ( $P$ -values  $< 0.01$ ).

### **Dithionite-Citrate Extractable Iron**

The extractable iron variable ( $n = 99$ ) exhibits strong positive skewness (Table 3.2), prompting a logarithmic transformation (Figure 3.8a). The log-transformed values are normally distributed when the one high outlier is suppressed. The extractable iron variogram does not reveal any spatial structure (Figure 3.4b), because the distances between sample points were generally greater than the distance over which extractable iron is correlated. The alternative explanation that there is no spatial structure in this variable is unlikely, because the (hydr)oxide bands at the outcrop exhibit structure (see Figure 3.2).

The ANOVA results indicate there are no statistically significant differences between facies with respect to extractable iron (Figure 3.8b and Table 3.2). Although facies is not a significant factor in explaining extractable iron variation, 49 percent of its variation can be explained by sediment color. Once again, the samples can be lumped into three groups of colors, each having a significantly different mean extractable iron content. However, the three iron groups are not the same as the three manganese groups.

According to this classification scheme, the low iron group consists of grays and non-brown yellows, the high iron group contains yellow brown, and the moderate group includes intermediate colors (Figure 3.8c). These groupings are consistent with the fact

that goethite – the most common iron (hydr)oxide in soils – is yellow brown (Schwertmann 1993). At the outcrop, zones of iron-rich yellow brown sands and iron-poor yellow gray sands can be differentiated from a high frequency zone consisting of fine bands of high, medium, and low iron sediments (Figure 3.9).

### **Dithionite-Citrate Extractable Aluminum**

Extractable aluminum ( $n = 71$ ) is lognormally distributed. The bimodal character of the frequency distribution (Figure 3.10a) cannot be explained by facies differences, because six of the eight facies contribute samples to both modes (Figure 3.10b). Nevertheless, facies explain 31 percent of the variability in extractable aluminum (Table 3.2). Facies five, the highest permeability facies, has a mean extractable aluminum content that is significantly lower than the other facies. By contrast, facies seven, the lowest permeability facies, has the highest mean concentration of extractable aluminum.

Variogram analysis did not reveal spatial structure in extractable aluminum at our scale of observation (Figure 3.4). Sediment color, classified according to Munsell color name, explains only 25 percent of its variability, and mappable color groups cannot be identified. Chroma explains the greatest proportion of extractable aluminum variation (34 percent); apparently, the more vivid sediments contain the most aluminum-rich coatings.

### **Correlations Between Sediment Properties**

As shown in Table 3.3, there is a weak positive relationship between extractable iron and extractable manganese, and a fairly strong positive relationship between extractable iron and extractable aluminum. Porosity is negatively correlated with extractable manganese and extractable iron, whereas permeability is positively

correlated with extractable manganese and negatively correlated with extractable iron and extractable aluminum. Although the physical and reactive properties of the media are correlated, the relationships are moderate to weak – permeability can only explain 7 to 38 percent of the variability in extractable metals, and relationships between porosity and extractable metals are even weaker. A greater percentage of the variation in extractable iron and extractable manganese can be explained by a linear combination of porosity and permeability than by porosity or permeability alone. Nevertheless, more than two-thirds of the variation in these multiple regression models remains unexplained.

## **Discussion**

### **Origin of Grain Coatings**

Based on color-extractable metal relationships, petrographic observations, and laboratory analyses the (hydr)oxide grain coatings at the Deerfield site appear to have originated from local, post-depositional primary mineral weathering, coupled with redox-driven redistribution of the liberated iron and manganese. The spatial distribution of coatings does not appear to have originated from the deposition of detrital (hydr)oxide-coated particles, because the coatings are angular rather than rounded and (hydr)oxide-cemented aggregates were observed in heavily-coated sediment samples. Furthermore, the coatings are not simply weathering rinds on iron- and manganese-bearing minerals, because the (hydr)oxides predominantly coat quartz and feldspar grains. The presence of iron- and manganese-rich coatings on primary minerals that lack iron or manganese indicates these metals have been transported from their original source grains.

If the metals had merely been transported far enough to coat adjacent quartz and feldspar grains, there should be strong correlations between the abundance of

extractable iron or manganese in a sample and the abundance of iron- or manganese-rich minerals. There is a fairly strong positive relationship ( $r_{\text{Spearman-Rho}} = 0.62$ ,  $p = 0.03$ ,  $n = 12$ ) between extractable iron and garnet abundance in the 12 thin section samples. Sediment from the largest (hydr)oxide band in the outcrop contains more than 50 percent garnet by volume (4H in Table 3.1), and SEM-EDS maps (Figures C.2 through C.5 in Appendix C) show the garnets contain iron. These observations suggest garnets are the primary source of iron in the iron-rich coatings, and most of the iron has undergone millimeter-scale transport. Aluminum may also have experienced minimal transport, since the pH of the outcrop sediments is approximately 5.3. Although there is no Spearman-Rho correlation between extractable manganese and garnet abundance, the two most garnet-rich samples (7072 and 4H in Table 3.1) are also the most extractable manganese-rich. Furthermore, the SEM-EDS results shown in Figures C.2 through C.5 confirm the garnets contain manganese as well as iron. The presence of manganese in the garnets, the abundance of extractable manganese in garnet-rich samples, and the absence of other primary mineral sources of manganese suggest that garnets are the source of the manganese in the coatings. The lack of correlation between extractable manganese and garnet indicates that much of the liberated manganese has migrated away from its source grains and precipitated in regions that are garnet-poor.

Figures 3.7 and 3.9 show that manganese-rich zones are diffuse and widespread while iron-rich zones are narrow and isolated. These geometries reflect the tendency for manganese to be more mobile than iron in subsurface environments. Manganese mobility tends to be greater because manganese (hydr)oxides become stable at higher redox potentials than iron (hydr)oxides (Skinner and Fitzpatrick 1992; Dixon and Skinner 1992). Consequently, manganese may remain in solution and migrate under Eh and pH



conditions that promote iron precipitation. In addition, manganese oxides can be reduced by ferrous iron (Postma and Appello 2000). The reductive dissolution of manganese oxides and concomitant precipitation of iron (hydr)oxides further enhances the mobility of manganese relative to iron.

The greater mobility of manganese compared to iron or aluminum explains why extractable manganese is correlated over much longer distances than extractable iron or extractable aluminum. The weathering of biotite in garnet-poor sediments and differences in iron and manganese redox behavior explain why both metals are found in every sample and yet their concentrations are poorly correlated. The weathering of biotite also contributes to the imperfect correlation between extractable iron and garnet abundance. The fairly strong correlation between extractable iron and extractable aluminum most likely arises from the limited mobility of iron and aluminum released from the weathering of biotite and garnet.

### **Potential Application to Subsurface Characterization**

Numerical models of fluid flow and solute transport require digital input maps of the media's physical and reactive properties in order to account for the effects of heterogeneities. (See Appendix B for an overview of heterogeneity mapping methods.) To date, chemical heterogeneity maps have been restricted, almost exclusively, to solute- and solution-specific partition coefficients, due to scant information on the spatial variation of reactive phases.

Results from the Deerfield site suggest that it may be possible to construct more broadly applicable maps of extractable metal variation at carbon-poor glaciofluvial sites by: 1) mapping lithofacies bounding surfaces and sediment color, 2) collecting relatively small numbers of samples to establish relationships between sediment properties and

the mapped features, and 3) assigning sediment property values to the mapped zones using zone-specific frequency distributions. In the absence of lithofacies and color information, more samples would be needed to characterize heterogeneities, and the resultant maps would be less realistic, because they would either lack discrete hydrostratigraphic units, or they would lack a site-specific geologic rationale for grouping the data into units.

Despite its potential advantages, several issues need to be resolved before the approach could be adopted. For example, do the outcrop results hold for larger scales at which subsurface facies mapping is possible? Do the extractable metal results apply to the saturated zone? How would color be mapped between widely-spaced boreholes, and is the Deerfield site representative of other carbon-poor glaciofluvial deposits?

### **Conclusions**

1. The (hydr)oxide grain coatings at the Deerfield site appear to have originated from the post-depositional weathering of biotite and garnet, coupled with millimeter-scale transport of the released iron and aluminum, and centimeter- to meter-scale transport of manganese.
2. Relationships between sediment physical and chemical properties are moderate to weak, and their spatial correlation structures are noticeably different. Therefore, simpler, less expensive physical property measurements cannot serve as surrogates for extractable metal measurements at the Deerfield site.
3. Lithologic facies explain more than half of the variation in permeability and extractable manganese. Although facies is not a significant factor in explaining extractable iron variation, 49 percent of the variability in extractable iron can be explained by sediment color. Color also explains 60 percent of the variability in

extractable manganese. Color zones representing significantly different mean extractable iron and manganese contents can be mapped at the Deerfield site. High extractable iron zones are relatively narrow, distinct features, while elevated extractable manganese values are concentrated in a broad, diffuse zone in the stratigraphically lowermost portion of the outcrop. Differences in scale and geometry between iron-rich zones and manganese-rich zones are consistent with the greater mobility of manganese in groundwater relative to iron.

4. At the Deerfield site, lithofacies and color groups provide a useful framework for conceptualizing and modeling physical and chemical heterogeneities. Nevertheless, there is still a considerable amount of variability within facies and color groups that cannot be explained by the facies and color models. The color group approach to modeling chemical heterogeneity may be limited by the confounding effects of grain size and primary mineral color on sediment color. Intrafacies surfaces may explain most of the remaining variation in the facies models, particularly for extractable iron, since iron-rich grain coatings appear to be concentrated in garnet-rich laminae. However, the facies approach may also have inherent limitations, particularly in sedimentary deposits that have experienced significant diagenetic alteration and/or structural deformation.

**Table 3.1**  
**Abundance (%) of Minerals in Selected Samples<sup>1</sup>**

| Mineral            | Sample Number and Facies |            |            |            |            |            |          |          |            |            |            |            |
|--------------------|--------------------------|------------|------------|------------|------------|------------|----------|----------|------------|------------|------------|------------|
|                    | 1061<br>F1               | 1111<br>F1 | 2051<br>F2 | 2071<br>F2 | 7111<br>F3 | 5051<br>F4 | 4H<br>F4 | 4L<br>F4 | 6022<br>F5 | 6031<br>F6 | 6103<br>F7 | 7072<br>F8 |
| Quartz             | 81.7                     | 77.6       | 80.5       | 77.0       | 77.3       | 80.0       | 30.3     | 82.3     | 80.7       | 82.7       | 70.0       | 67.5       |
| Feldspar           | 13.5                     | 15.3       | 12.6       | 16.6       | 16.4       | 13.4       | 6.6      | 15.9     | 14.6       | 15.1       | 12.8       | 15.8       |
| Garnet             | 2.4                      | 1.6        | 2.5        | 0.0        | 1.6        | 1.2        | 59.0     | 0.4      | 0.0        | 0.0        | 3.3        | 10.0       |
| Muscovite          | 0.6                      | 2.4        | 1.9        | 4.3        | 2.3        | 1.2        | 0.4      | 0.4      | 3.9        | 1.0        | 6.6        | 4.6        |
| Biotite            | 1.5                      | 1.6        | 2.2        | 2.1        | 1.6        | 2.7        | 0.4      | 0.4      | 0.8        | 1.2        | 5.3        | 1.3        |
| Other <sup>2</sup> | 0.3                      | 1.6        | 0.3        | 0.0        | 0.7        | 1.5        | 3.3      | 0.4      | 0.0        | 0.0        | 2.0        | 0.8        |

<sup>1</sup> Based on thin section grain counts.

<sup>2</sup> Predominantly tourmaline.

**Table 3.2**  
**Basic Statistical Characteristics of Measured Properties**

| Property               | Univariate Statistics |           |                       |                 | ANOVA Facies <sup>1</sup> |         | ANOVA Color         |         | Correlation Scales (m) |             |
|------------------------|-----------------------|-----------|-----------------------|-----------------|---------------------------|---------|---------------------|---------|------------------------|-------------|
|                        | <i>n</i>              | $\bar{x}$ | <i>s</i> <sup>2</sup> | <i>Skewness</i> | R <sup>2</sup> adj.       | P-value | R <sup>2</sup> adj. | P-value | $\lambda_h$            | $\lambda_v$ |
| <b>Permeability</b>    |                       |           |                       |                 |                           |         |                     |         |                        |             |
| (cm <sup>2</sup> )     | 476                   | 9.2e-7    | 6.7e-13               | 2.0             | ---                       | ---     | ---                 | ---     | ---                    | ---         |
| [ln(cm <sup>2</sup> )] | 476                   | -14.2     | 0.59                  | 0.2             | 0.60                      | <0.01   | ---                 | ---     | 0.45                   | 0.10        |
| <b>Porosity</b>        | 476                   | 0.42      | 0.001                 | -1.2            | 0.30                      | <0.01   | ---                 | ---     | 0.44                   | 0.07        |
| <b>Extractable Mn</b>  |                       |           |                       |                 |                           |         |                     |         |                        |             |
| (μmol/g)               | 99                    | 0.65      | 0.34                  | 2.2             | ---                       | ---     | ---                 | ---     | ---                    | ---         |
| [ln(μmol/g)]           | 99                    | -0.87     | 1.00                  | -0.3            | 0.54                      | <0.01   | 0.60                | <0.01   | 1.15                   | 0.22        |
| <b>Extractable Fe</b>  |                       |           |                       |                 |                           |         |                     |         |                        |             |
| (μmol/g)               | 99                    | 39.1      | 318                   | 4.3             | ---                       | ---     | ---                 | ---     | ---                    | ---         |
| [ln(μmol/g)]           | 99                    | 3.60      | 0.12                  | 0.9             | 0.05                      | 0.11    | 0.49                | <0.01   | <0.07                  | <0.07       |
| <b>Extractable Al</b>  |                       |           |                       |                 |                           |         |                     |         |                        |             |
| (μmol/g)               | 71                    | 8.1       | 14.4                  | 1.1             | ---                       | ---     | ---                 | ---     | ---                    | ---         |
| [ln(μmol/g)]           | 71                    | 1.99      | 0.24                  | -0.4            | 0.31                      | <0.01   | 0.25                | <0.01   | <0.07                  | <0.07       |

<sup>1</sup> The permeability, porosity, and extractable manganese data violated the "independence between observations" assumption on which ANOVA is based, because several samples were close enough to one another to be spatially correlated. The other two assumptions required for ANOVA, equal variance and normal distributions within facies, were not perfectly met; however, the effects of violating the three assumptions is minimal due to the large sample size.

**Table 3.3**  
**Correlations<sup>1</sup> Between Physical Properties**  
**and Extractable Metals**

|  | (1)   | (2)             | (3)  | (4)  |
|--|-------|-----------------|------|------|
| (1) Permeability<br>[ln(cm <sup>2</sup> )] | 1.0   |                 |      |      |
| (2) Porosity                               | -0.29 | 1.0             |      |      |
| (3) Extractable Mn<br>[ln(μmol/g)]         | 0.42  | -0.46           | 1.0  |      |
| (4) Extractable Fe<br>[ln(μmol/g)]         | -0.26 | -0.24           | 0.28 | 1.0  |
| (5) Extractable Al<br>[ln(μmol/g)]         | -0.62 | NS <sup>2</sup> | NS   | 0.68 |

<sup>1</sup> Regression-derived correlation coefficient (r) based on r<sup>2</sup>.

<sup>2</sup> Not significant at the α = 0.05 level.

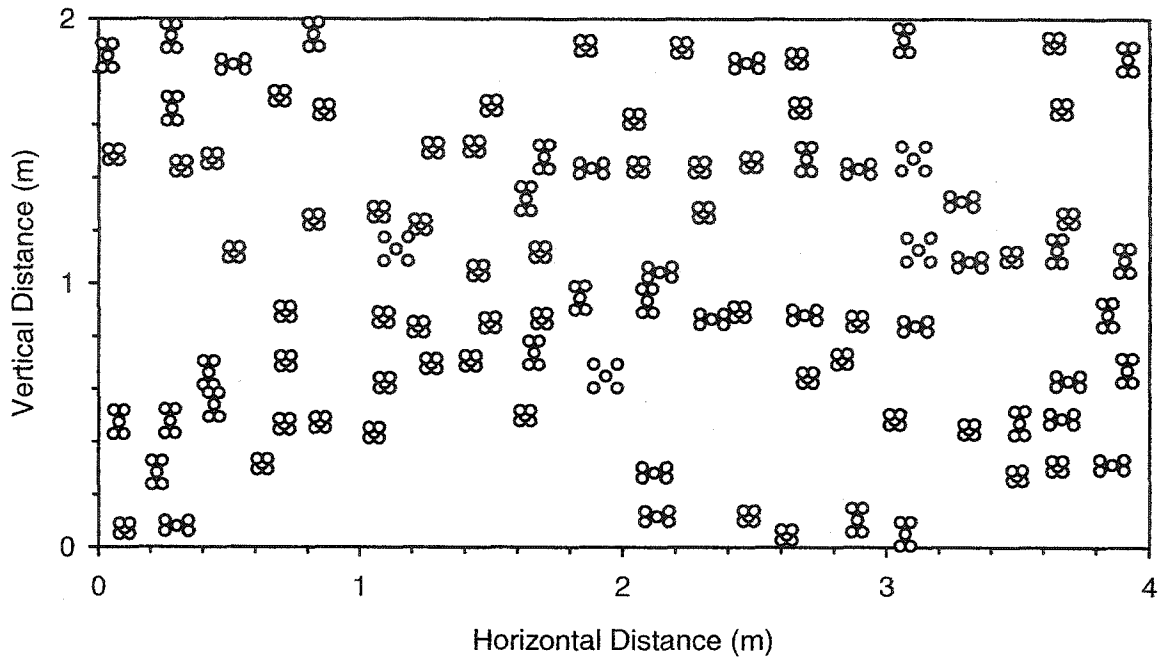


**Figure 3.1** Data locations. This sampling pattern was chosen because the randomly-located, five-spot clusters minimized the number of samples needed to produce high resolution variogram representations of spatial variation.

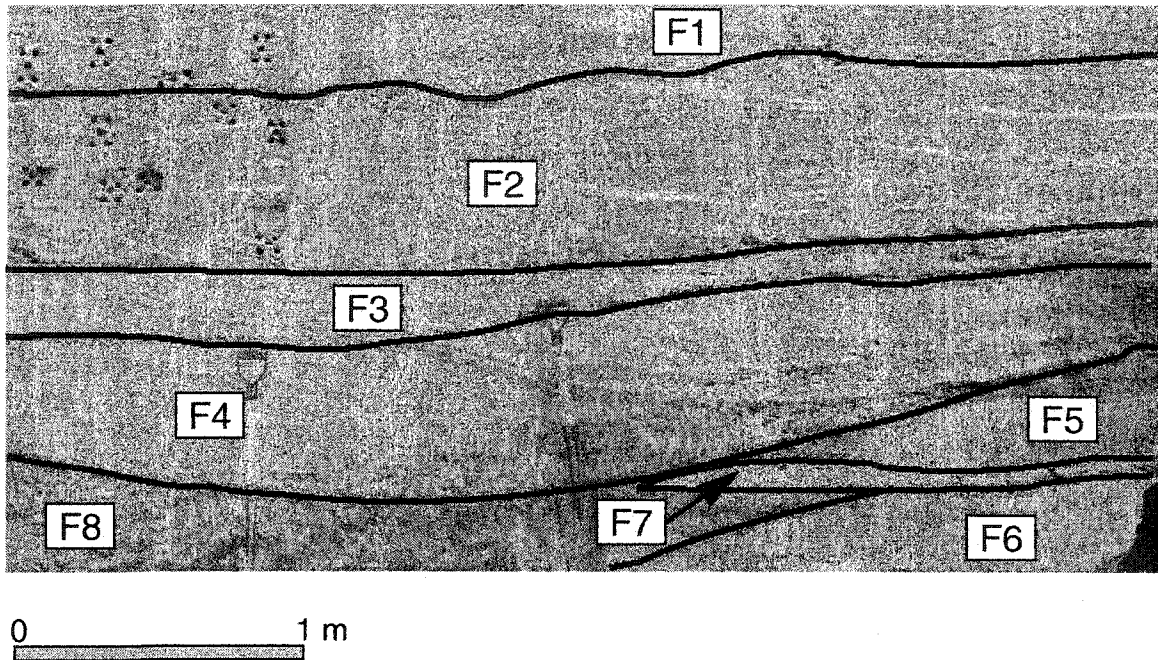


**Figure 3.2** Outcrop map showing lithofacies 1 through 8 (F1 through F8). The upper three facies are fine to medium sands with trough or low-angle cross-laminations. Facies four consists of gravely sands that fine-upward to medium, cross-laminated sands. Facies five and eight are coarse-textured units with tabular cross-bedding. Facies six is a medium to coarse, trough cross-stratified sand, and facies seven is a thin lens of very fine sand.



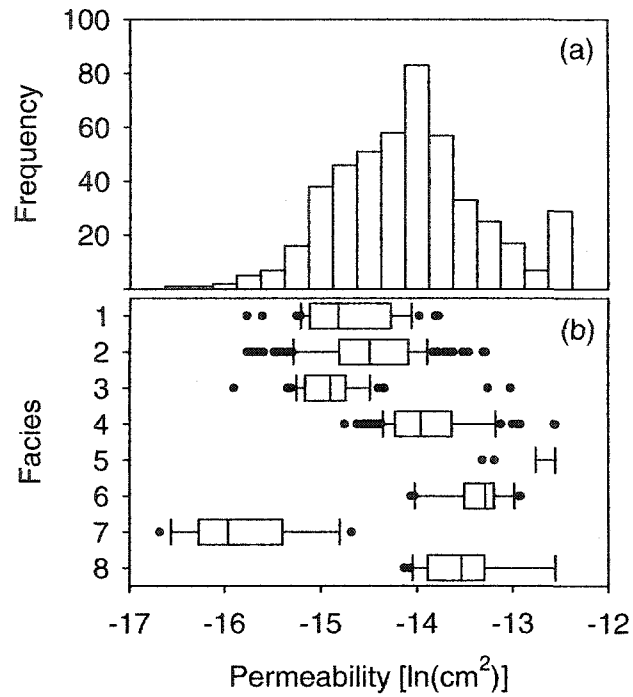


**Figure 3.3** Permeability: (a) histogram; (b) facies relationships. The permeability distribution has an extended left tail as a result of very fine sands in facies seven. Its bimodal character is due to very coarse sands and gravelly sands in facies four, five, and eight.

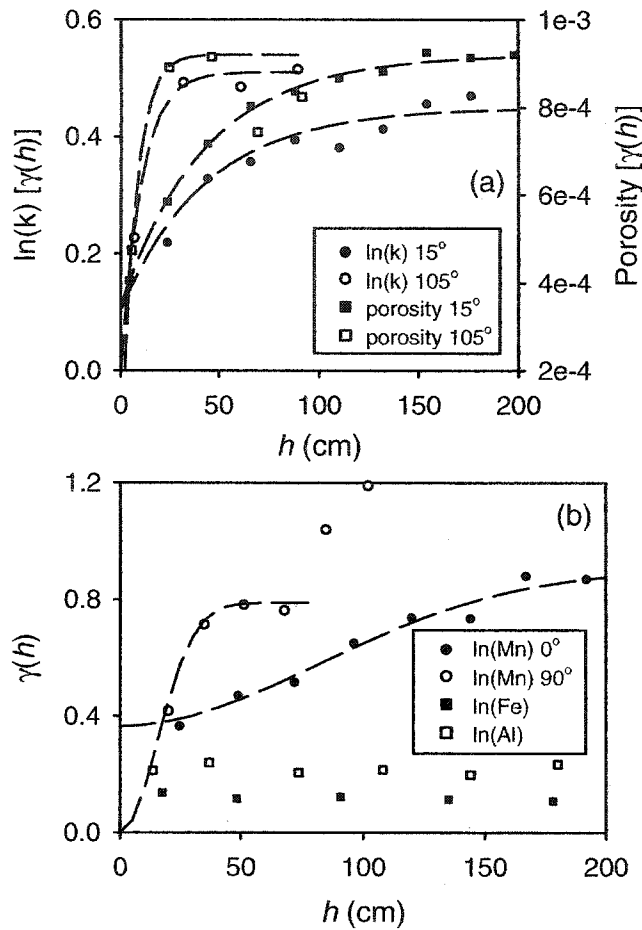


**Figure 3.4** Variograms of (a) physical and (b) chemical properties. Exponential models of the form  $\gamma(h) = \gamma_0 + (\sigma^2 - \gamma_0)[1 - \exp(-h/\lambda)]$  where  $\gamma_0$  is the y-intercept,  $\sigma^2$  is the sill, and  $\lambda$  is the correlation length are fit to the permeability and porosity variograms. Double exponential models of the form  $\gamma(h) = \gamma_0 + (\sigma^2 - \gamma_0)[1 - \exp(-h^2/\lambda^2)]$  are fit to the extractable manganese variograms. Note the similar patterns of spatial variation between physical properties and the dissimilar patterns between physical and chemical properties.

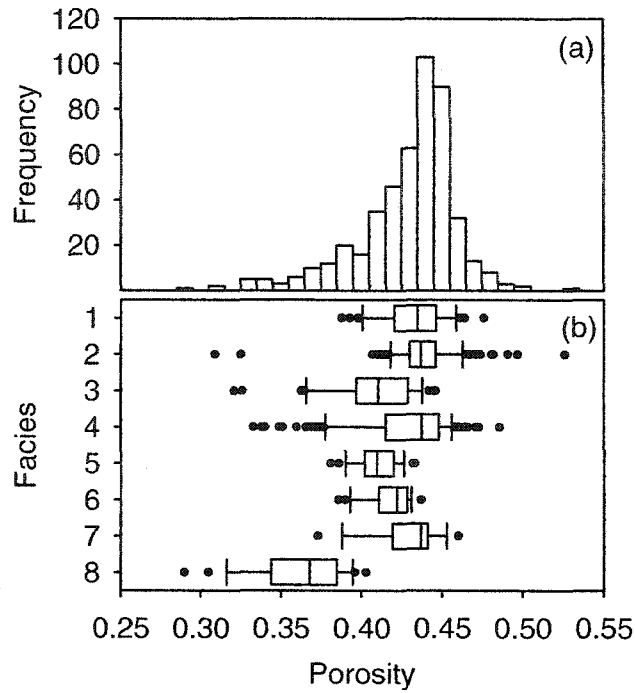


**Figure 3.5** Porosity: (a) histogram; (b) facies relationships. Frequency distributions for hydrogeologic properties often show strong positive skewness, or right-tailing. The atypical left-tailing evident in the porosity distribution is due in part to the gravelly sands in facies four and eight, and the pebbly basal lags in facies two and three.

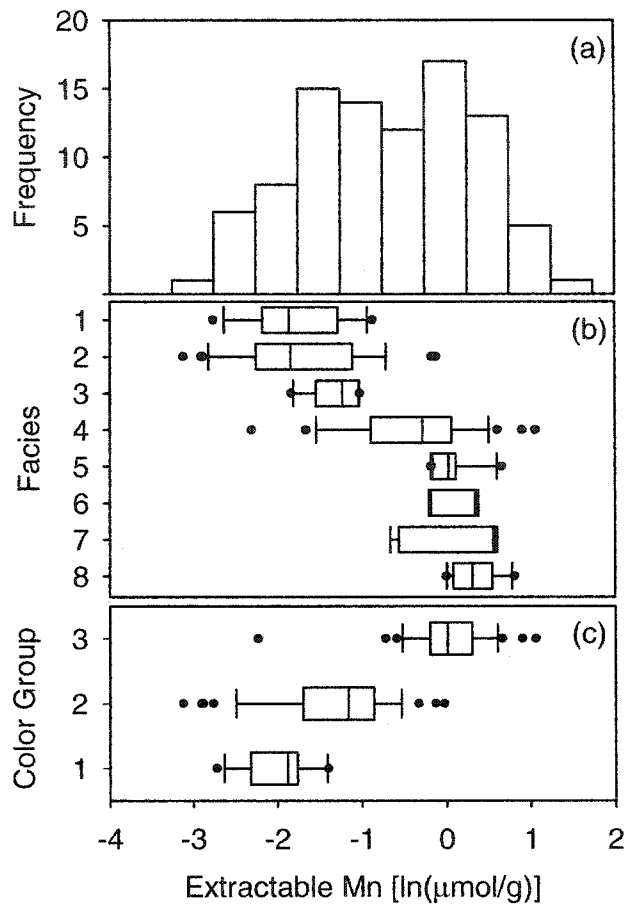


**Figure 3.6** Dithionite-citrate extractable manganese: (a) histogram; (b) facies relationships; (c) color relationships. Color group 1 contains olive yellow and yellow. Color group 2 contains pale yellow and brownish yellow. Color group 3 contains very pale brown, pale brown, light olive brown, light yellow brown, yellow brown, grayish brown, light gray, and light brown gray. A comparison of (a) and (b) reveals the impact of facies on the bimodal character of the extractable manganese distribution.

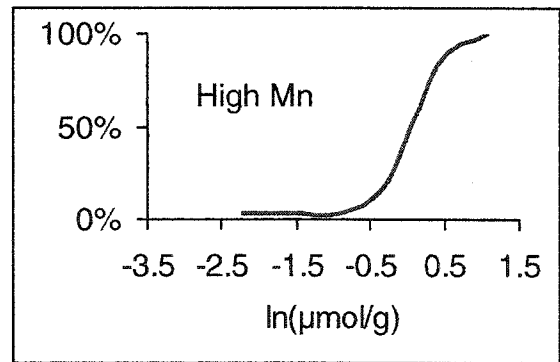
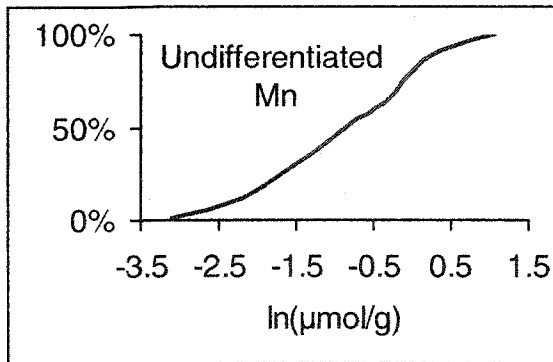
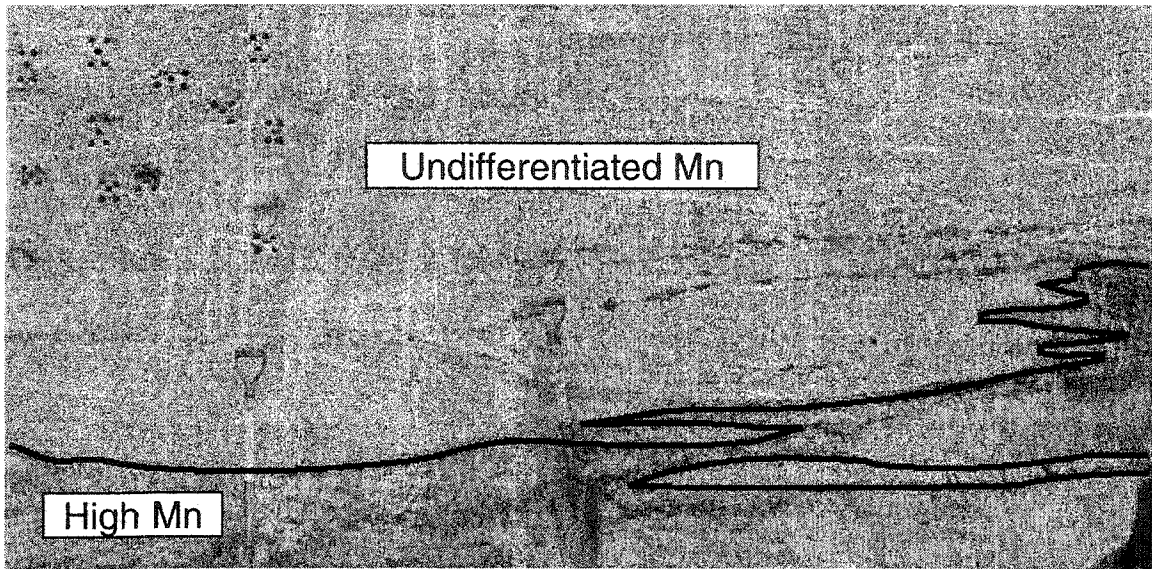


**Figure 3.7** Zone map and cumulative frequency plots for dithionite-citrate extractable manganese. Mapping zones of significantly different dithionite-citrate extractable manganese is possible due to a strong relationship between extractable manganese and sediment color. Furthermore, by defining regions with markedly different cumulative frequency distributions, more realistic stochastic models of extractable manganese heterogeneity can be developed than would be possible in the absence of zonation.

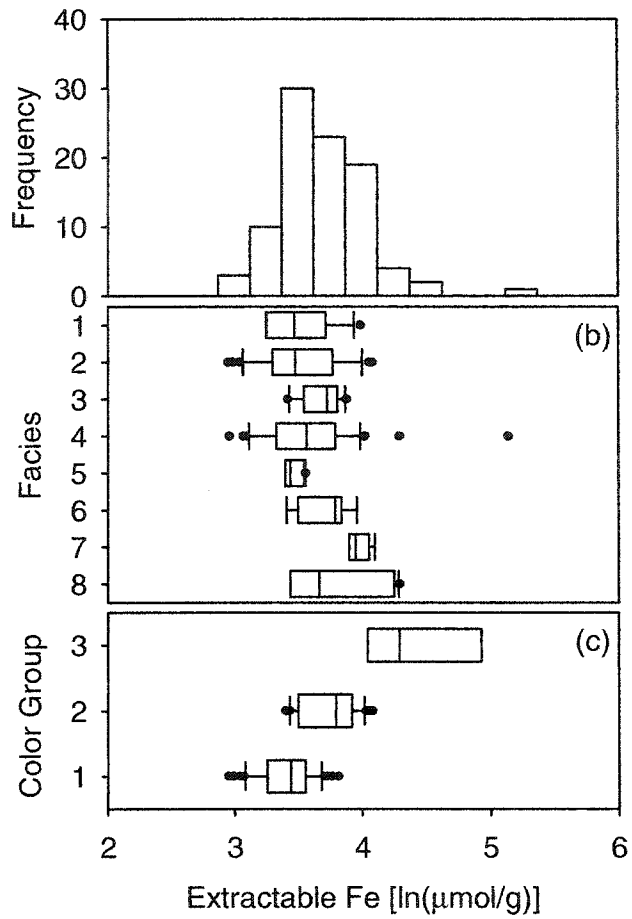


**Figure 3.8** Dithionite-citrate extractable iron: (a) histogram; (b) facies relationships; (c) color relationships. Color group 1 contains light gray, light brown gray, pale yellow, olive yellow, and yellow. Color group 2 contains very pale brown, pale brown, light olive brown, light yellow brown, grayish brown, and brownish yellow. Color group 3 contains yellow brown. Note the greater mean separation when samples are grouped by color rather than by facies.

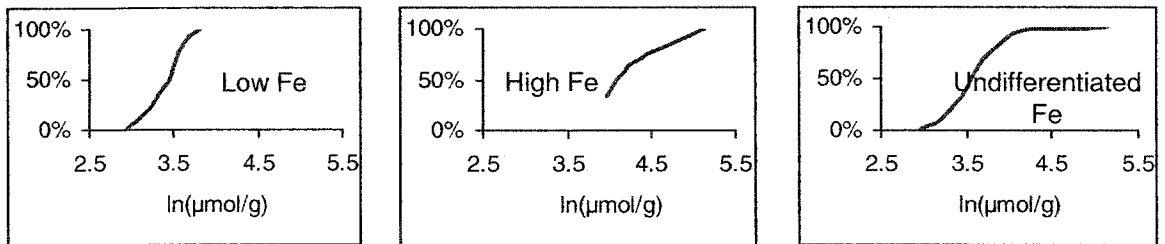
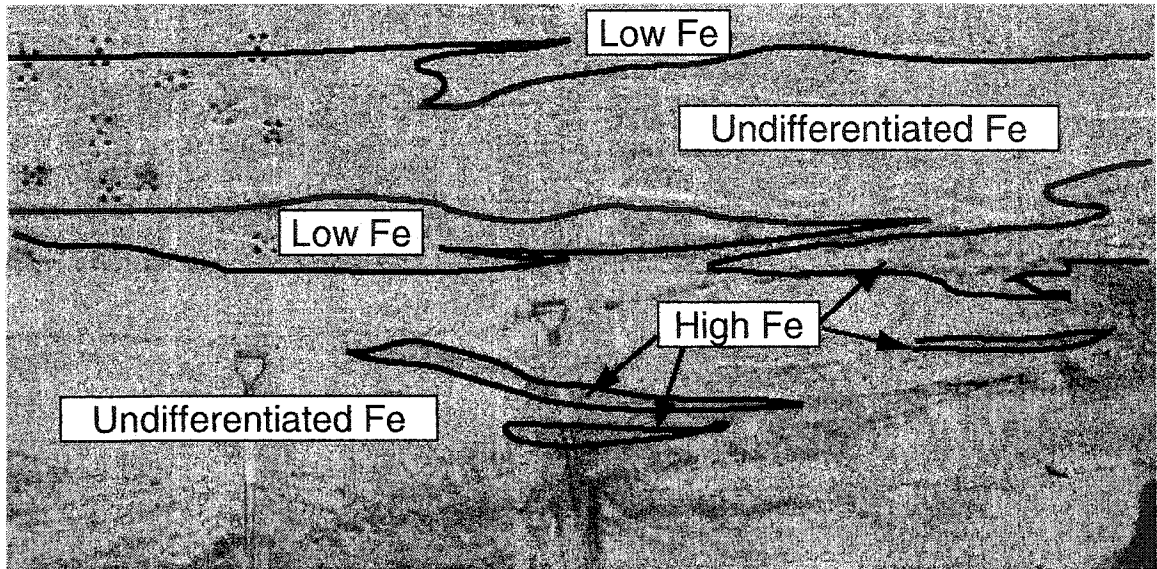


**Figure 3.9** Zone map and cumulative frequency plots for dithionite-citrate extractable iron. A comparison between this figure and Figure 3.7 shows that the high extractable iron zones are more slender and less continuous than the high extractable manganese zone.

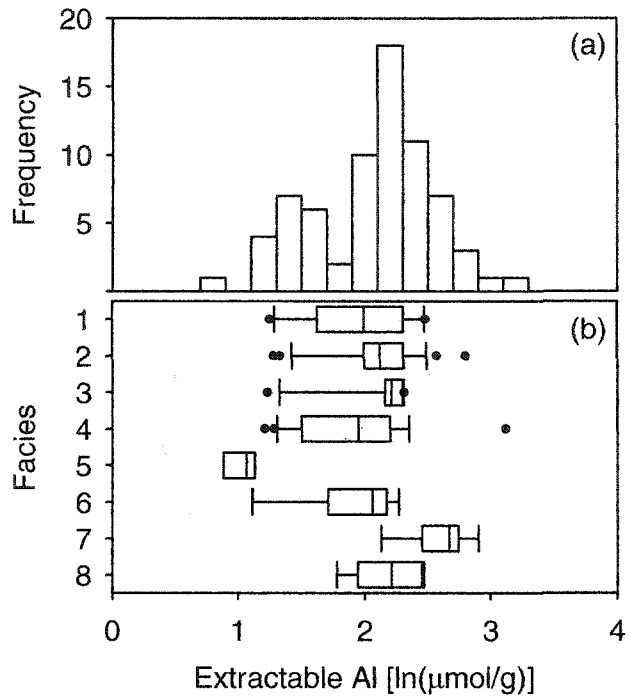


**Figure 3.10** Dithionite-citrate extractable aluminum: (a) histogram; (b) facies relationships. The box plots show that the multimodal nature of the extractable aluminum distribution is not controlled by facies differences.



## CHAPTER 4

### IMPACT OF CHEMICAL HETEROGENEITY ON REACTIVE TRANSPORT

#### Abstract

A numerical modeling approach was taken to evaluate the effects of the spatial pattern of aquifer reactivity on cobalt ( $\text{Co}^{2+}$ ) transport. Transport was simulated through a hypothetical sandy aquifer, consisting of inert quartz grains that were variably coated by reactive goethite. Three patterns of goethite distribution were examined: uniform, banded, and random. In each case the physically homogeneous modeling domain contained the same total number of reactive sites in order to isolate the effects of the spatial pattern of reactivity on solute migration. Model simulations in this system indicate that the pattern of reactivity affects  $\text{Co}^{2+}$  migration when the spatial scale of the heterogeneity is similar to the scale of the problem. Specifically, chemical heterogeneity increases plume mobility and dispersion, and the extent of dispersion increases with increasing goethite. The simulation results also suggest that: 1) physically homogeneous and chemically heterogeneous systems may be conceptualized and modeled as bundles of independent stream tubes, and 2) representing clusters of iron bands with cells containing a uniform distribution of goethite may underestimate  $\text{Co}^{2+}$  transport.

## Introduction

### Background

The influence of chemical heterogeneity on reactive transport is poorly understood. Numerical modeling studies by Bosma et al. (1993) and Burr et al. (1994) demonstrate that chemical heterogeneities enhance the longitudinal dispersion of a reactive solute plume when chemical and physical heterogeneities are negatively correlated. Tompson et al. (1996) conducted a series of numerical simulations in order to track the behavior of a co-contaminant mixture as it flowed through a hypothetical, heterogeneous sandy aquifer. They concluded that the correlation between chemical and physical heterogeneity was not as important as the abundance and spatial distribution of the reactive solid phase. Since Tompson's flow system was physically heterogeneous and the abundance of the reactive phase varied between simulations, it did not isolate the effects of the pattern of chemical heterogeneity on transport. The purpose of this project was to conduct a series of numerical simulations that investigate the impact of the spatial pattern of reactivity on solute transport. The modeling code OS3D (Steeffel and Yabusaki 1996) was selected for this purpose.

OS3D (Operator Splitting 3-Dimensional Reactive Transport) is a numerical software package for simulating multidimensional, multicomponent reactive transport in porous media. OS3D was chosen because it uses a surface complexation approach to model adsorption. The code explicitly models the chemical reactions that take place within the ground water and between the ground water and the aquifer's solid surfaces as the ground water flows through the system. It solves the nonlinear set of partial differential equations describing coupled reaction and transport using finite difference techniques. The finite difference approach enables the user to model advective, dispersive, and diffusive transport or any combination of these.

The simulations presented in this chapter examine the impact of chemical heterogeneities on cobalt ( $\text{Co}^{2+}$ ) transport. Although  $\text{Co}^{2+}$  is not an ideal surrogate for lead ( $\text{Pb}^{2+}$ ), the OS3D database lacks the thermodynamic data needed to model the adsorption and desorption of other divalent heavy metals.

### **Conceptual Model**

The flow system was conceptualized as a four by eight meter, two-dimensional vertical slice through a saturated body of quartz sand that was partially coated with goethite ( $\alpha\text{-FeOOH}$ ). Goethite is a common analog for (hydr)oxide grain coatings in reactive transport models (Davis and Kent 1990, Tompson et al. 1996), and it is the only (hydr)oxide in the OS3D database. The flow system was assumed to be physically homogeneous, and fluid movement was one-dimensional, steady state, and unaffected by the chemical composition of the pore water.

Parameterization of the flow system was based on available data from the Deerfield site and similar glacial deposits. OS3D default values were applied when field data were lacking. Mean porosities of the sand at the Cape Cod site, the Chalk River Nuclear Laboratories site, and the Deerfield site are 0.39, 0.38, and 0.42, respectively (Jackson and Inch 1989, Davis et al. 1993, Table 2.1), so the flow system was modeled with a porosity of 0.4. Darcy velocity was fixed at  $32.8 \text{ m yr}^{-1}$ , based on the average ground water velocity of  $82 \text{ m yr}^{-1}$  used by Tompson et al. (1996). Longitudinal dispersivity was set at 0.4 m in accordance with field studies conducted at the same 8 m scale of observation (Gelhar 1986). Transverse dispersivity was chosen to be one-tenth the longitudinal dispersivity (Gelhar et al. 1992), and the OS3D default value of  $1 \times 10^{-9} \text{ m}^2 \text{ s}^{-1}$  was selected for the diffusion coefficient. Values for molecular diffusion do not

vary much; they range from  $1 \times 10^{-9}$  to  $2 \times 10^{-9} \text{ m}^2 \text{ s}^{-1}$  at 25 °C, and are only 50 percent less at 5 °C (Fetter 1999).

The geochemical system consisted of two solid phases: inert quartz and reactive goethite. Local equilibrium was assumed, and the initial pH, temperature, and composition of the ground water were based on published values for a well in a stratified drift aquifer in south central New Hampshire (Table 4.1). This particular ground water was chosen because its pH mimicked sediment pH at the Cape Cod and Deerfield sites. Nevertheless, sodium and chloride concentrations ( $75$  and  $120 \text{ mg kg}^{-1}$ , respectively) indicate the well water was contaminated by road salt, so mean sodium and chloride concentrations for stratified drift aquifers in New Hampshire [ $6.4$  and  $9.9 \text{ mg kg}^{-1}$ , respectively (Ayotte and Toppin 1995)] were used in the simulations. The equilibrium speciation model SOLMINEQ.88 (DeBraal and Kharaka 1989) was used to determine the bicarbonate and ferric iron contents of the sodium- and chloride-adjusted well water as well as the important secondary species in the geochemical system.

The reactive site density on goethite ( $3.84 \times 10^{-6}$  moles of sites  $\text{m}^{-2}$ ) was taken from Davis and Kent (1990). This particular value was chosen because it is consistent with goethite site densities determined by Parfitt et al. (1977), Balistrieri and Murray (1981), Hayes (1987), and Lutzenkirchen et al. (2002). Moreover, it closely approximates the site densities found by adsorption on other (hydr)oxide minerals including ferrihydrite (Dzombak and Morel 1990), manganese oxides (Zasoski and Burau 1988), and gibbsite (Sposito 1984, Davis and Hem 1989).

The surface area of goethite in units of  $\text{m}^2 \text{ g}^{-1}$  of solution was calculated from the assumed porosity and measures of BET surface area for fully-coated Deerfield sand grains (see Appendix A):

$$\text{BET surface area} = 2.2 \text{ m}^2 \text{ g}^{-1} \text{ solid, and}$$

$$\text{Porosity} = \frac{V_{\text{Void}}}{V_{\text{Total}}} = \frac{0.4}{1.0}; \text{ therefore,}$$

$$V_{\text{Solid}} = 1 - 0.4 = 0.6, \text{ and}$$

$$\frac{2.2 \text{ m}^2}{\text{g solid}} \times \frac{2.65 \text{ g solid}}{\text{cm}^3 \text{ solid}} \times \frac{0.6 \text{ cm}^3 \text{ solid}}{0.4 \text{ cm}^3 \text{ solution}} \times \frac{\text{cm}^3 \text{ solution}}{\text{g solution}} = 8.75 \frac{\text{m}^2}{\text{g solution}}$$

Similarly, the initial reactive surface area of goethite ( $\text{m}^2$  goethite  $\text{m}^{-3}$  porous media) was derived from the BET surface area of fully-coated Deerfield sand grains and the mean bulk density of the Deerfield sediments:

$$\frac{2.2 \text{ m}^2}{\text{g rock}} \times \frac{1.5 \text{ g rock}}{\text{cm}^3} \times \frac{10^6 \text{ cm}^3}{\text{m}^3} = 3.3 \times 10^6 \text{ m}^{-1}$$

### **Methods**

The model grid for the 4 x 8 m flow system was discretized into 8 rows and 16 columns of equidimensional cells. Eight additional columns were added to the downstream end of the model domain for a total of 24 columns in order to prevent the downstream boundary from affecting the simulation results. Three sets of simulations were carried out using the same physical and chemical parameters, including the same total number of reactive sites. Only the spatial distribution of the reactive sites varied between simulation sets. The first set of model runs considered a homogeneous distribution of reactive sites (Figure 4.1a). In this case, the 128 cells in the first 16 columns had 10 percent of their mineral surfaces coated with goethite. The second set of simulations had a banded pattern of goethite coatings (Figure 4.1b). In this case, 32 cells in the first 16 columns had 40 percent of their solid surfaces coated with goethite, while the remaining cells contained only quartz. Notice in Figure 4.1b that each of the 4 band zones is 0.5 m wide. Individual iron bands are rarely 0.5 m wide in glacial aquifer

sediments – more often they are only a few millimeters or centimeters in width (see Figure 2.1). Explicitly accounting for such thin bands would require an unwieldy number of grid cells. Consequently, a simplifying assumption was made in which the 0.5 m wide band zones were conceptualized as containing alternating thin bands of goethite-coated and goethite-free quartz grains, but they were modeled as having 40 percent of their solid surfaces uniformly coated with goethite. The validity of this simplifying assumption will be explored in these modeling exercises.

The third set of simulations considered a random pattern of 32 goethite-containing cells, each having 40 percent of its solid surfaces coated with goethite (Figure 4.1c). The random pattern was selected to represent the irregularly distributed patches of goethite coatings present in some sandy aquifers. Again, the validity of representing irregularly-distributed coatings in a cell with a uniform 40 percent distribution of coatings will be evaluated in this study.

For all three sets of simulations a continuous source of  $\text{Co}^{2+}$  ( $1 \times 10^{-6}$  mol  $\text{kg}^{-1}$  or  $59 \mu\text{g kg}^{-1}$ ) and nonreactive tracer ( $1 \times 10^{-6}$  mol  $\text{kg}^{-1}$ ) was injected along the upstream (left hand) boundary of the model domain. Each simulation was run for one year. Breakthrough curves were plotted for  $x = 7.75$  m, and concentration versus distance plots were generated for the 0.2 yr and 1.0 yr time intervals.

## **Results**

OS3D initializes the concentrations of primary and secondary species in each cell prior to stepping through time. The initialization results confirmed that prior to  $\text{Co}^{2+}$  and tracer injection, the ground water's total charge was balanced, the pH was 5.4, and the goethite-containing cells in the two heterogeneous cases had four times as many reactive sites as the cells in the homogeneous case.

Output from the transient calculations demonstrated that there was no goethite precipitation in any cell after initialization. Volume.out files showed that goethite volumes were 0.0E+00 in the goethite-free cells for all times and distances, and the volumes never changed in the goethite-containing cells. Furthermore, rate.out files indicated that the rate of goethite precipitation was 0.0E+00 in the goethite-free cells, and it was  $10^{-13}$  to  $10^{-20}$  moles  $m^{-2} s^{-1}$  in the goethite-containing cells. Therefore, the spatial patterns of goethite distribution remained unchanged, and all three patterns had the same total number of reactive sites throughout the simulations.

### **Uniform Pattern of Goethite Grain Coatings**

Breakthrough curves for the uniform case presented in Figure 4.2a show that the nonreactive tracer arrived at the downstream observation point ( $x = 7.75$  m,  $y = 1.75$  m) at approximately the same time as the ground water. With an average ground water velocity of  $82$  m  $yr^{-1}$ , the water should take slightly less than 0.1 yr to flow 7.75 m:

$$t = \frac{7.75 \text{ m}}{82 \text{ m yr}^{-1}} = 0.095 \text{ yr}$$

This was also the time at which 50 percent of the maximum concentration of tracer was realized at the observation point. The breakthrough curves also show that  $Co^{2+}$  was not predicted to arrive at the observation point until 0.2 yr – its late arrival being due to sorption-related retardation.

The solute concentration vs. distance plot (Figure 4.2b) confirms that  $Co^{2+}$  concentrations were barely detectable at 7.75 m after 0.2 yr. It also indicates that tracer concentrations had reached their maximum level throughout the domain by 0.2 yr, while  $Co^{2+}$  concentrations gradually decreased with distance from the source.

### **Banded Pattern of Goethite Grain Coatings**

The tracer behaved the same in the banded case (Figure 4.3a) as in the homogenous case (Figure 4.2a) because it is unaffected by the presence of goethite. On the other hand,  $\text{Co}^{2+}$  behaved differently in the presence of goethite bands. Initial arrival of  $\text{Co}^{2+}$  occurred at 0.1 yr instead of 0.2 yr. The earlier arrival can be attributed to the enhanced mobility of  $\text{Co}^{2+}$  in the interband zones.

The concentration vs. distance plot (Figure 4.3b) illustrates the effect of the banded pattern on  $\text{Co}^{2+}$  migration.  $\text{Co}^{2+}$  concentrations drop dramatically at the four distances where the bands are located due to sorption to goethite. Concentrations remain essentially unchanged between the bands, and the lack of sorption in these regions allows the solute to travel at roughly the same velocity as the ground water.

### **Random Pattern of Goethite Grain Coatings**

Figure 4.4a is a set of breakthrough curves for the same observation point as in the homogeneous and banded cases ( $x = 7.75$  m,  $y = 1.75$  m). Note in this case that  $\text{Co}^{2+}$  is predicted to arrive *before* 0.1 yr. By contrast, Figure 4.4b for row 6 ( $x = 7.75$  m and  $y = 2.75$  m) shows the initial arrival of  $\text{Co}^{2+}$  *after* 0.1 yr, and it indicates that  $\text{Co}^{2+}$  concentrations are less than the banded case at all times.

These differences arise from disparities in the number of goethite-containing cells in the row containing the observation point. In the banded pattern there are four goethite cells in every row (Figure 4.1b). In the fourth row ( $y = 1.75$  m) of the random pattern there are only two goethite cells (Figure 4.1c), so there is less sorption and earlier arrival. There are seven goethite cells in the sixth row ( $y = 2.75$  m) of the random pattern (Figure 4.1c) – more than in the fourth row of the random pattern or in any row



of banded pattern. As a result, sorption is greatest, initial arrival is latest, and  $\text{Co}^{2+}$  concentrations are lower at all times.

The breakthrough results for rows four and six suggest there is little lateral mixing between cells, so each row of cells could be conceptualized as an isolated stream tube. The concentration vs. distance plots for the random case support this conceptualization.

The concentration vs. distance plot for row eight (Figure 4.5a) shows the impact of the three goethite-containing cells in row eight. The plot for the adjacent row (Figure 4.5b) also changes abruptly in three places, but these locations correspond to the three goethite-containing cells in row seven, not row eight. A comparison of plots for rows two and three (Figure 4.6) reveals the same trend. In row two, concentrations change abruptly at two locations corresponding to the two groups of goethite-containing cells in this row, while in row three, concentrations change abruptly at three different locations corresponding to the three clusters of goethite cells in this row.

### **Discussion**

The spatial pattern of chemical heterogeneity influenced  $\text{Co}^{2+}$  migration in these simulations. At early travel times, transport was retarded most in the chemically homogeneous case and least in the random case. For example, the first appearance of  $1.7 \times 10^{-8} \text{ mol kg}^{-1}$ , or 1 part per billion  $\text{Co}^{2+}$  at column 16 ( $x = 7.75 \text{ m}$ ) occurred after 0.21 yr in the homogeneous case, 0.12 yr in the banded case, and an average of 0.11 yr in the random case. Similarly, 50 percent of the injected  $\text{Co}^{2+}$  concentration ( $C_{50}$ ) arrived at column 16 after 0.45 yr in the homogeneous case, 0.42 yr in the banded case, and an average of 0.41 yr in the random case. The slightly earlier arrival times in the

random case vs. the banded case may be due to a small amount of lateral mixing as well as enhanced mobility in rows containing few goethite cells.

This overall trend was reversed at late travel times. The arrival of 90 percent of the injected  $\text{Co}^{2+}$  concentration ( $C_{90}$ ) at column 16 ( $x = 7.75$  m) was delayed the most in the random domain (0.84 yr) and the least in the homogeneous domain (0.72 yr). The early arrival and late time tailing of  $\text{Co}^{2+}$  in the banded and random domains are manifested in relatively shallow-sloping breakthrough curves (compare Figures 4.3a and 4.4 with Figure 4.2a). Physical heterogeneities cause this same process of dispersion in solute plumes. Previous studies have shown that chemical heterogeneities amplify plume spreading when permeability and sorption coefficients are negatively correlated (Bosma et al. 1993, Burr et al. 1994). The results presented in Figures 4.2 through 4.4 suggest that chemical heterogeneities also enhance dispersion in the absence of significant physical heterogeneity.

Changes in the percentage of goethite coatings change the speed with which  $\text{Co}^{2+}$  moves through the hypothetical aquifer. When the volume fraction of goethite is decreased, a smaller portion of the  $\text{Co}^{2+}$  mass sorbs to the goethite and the plume migrates more quickly. Furthermore, arrival time differences between the homogeneous and heterogeneous cases decrease when the goethite fraction is decreased (Table 4.2). These observations suggest that with reduced sorption, there is less enhanced dispersion.

### **Conclusions**

1. Heterogeneities in the spatial pattern of goethite grain coatings impact  $\text{Co}^{2+}$  transport by increasing plume dispersion and accelerating the arrival of the

plume's center of mass. The extent of dispersion enhancement is directly proportional to the volume fraction of goethite.

2. Breakthrough curves and concentration vs. distance plots suggest that physically homogeneous and chemically heterogeneous systems can be conceptualized and modeled as a collection of independent stream tubes. However, this conceptualization may not be appropriate for similar systems having larger transverse dispersivities, because even in this system there appears to have been a small amount of lateral mixing.
3. The results indicate that individual (hydr)oxide bands or patches should be modeled explicitly, whenever possible. In this study, retardation in the geochemically uniform domain was greater than that in the banded or random domains. Therefore, modeling groups of small-scale bands or irregular patches with cells containing uniform distributions of coatings may overestimate retardation and underestimate solute arrival times.

**Table 4.1**  
**Ground Water from a Glacial Aquifer in**  
**South-Central New Hampshire<sup>a</sup>**

| Chemical Constituent               | Well<br>WGW-19 <sup>b</sup> |
|------------------------------------|-----------------------------|
| pH                                 | 5.4                         |
| Temperature                        | 9.8                         |
| Alkalinity (as CaCO <sub>3</sub> ) | 10                          |
| Hardness (as CaCO <sub>3</sub> )   | 16                          |
| Total Dissolved Solids (TDS)       | 216                         |
| Calcium (Ca)                       | 5.1                         |
| Magnesium (Mg)                     | 0.87                        |
| Chloride (Cl)                      | 120                         |
| Sodium (Na)                        | 75                          |
| Potassium (K)                      | 1.8                         |
| Sulfate (SO <sub>4</sub> )         | 8                           |
| Silica (SiO <sub>2</sub> )         | 9.4                         |
| Aluminum (Al)                      | 0.090                       |
| Iron (Fe)                          | 0.350                       |
| Manganese (Mn)                     | 0.310                       |

<sup>a</sup> Source: Ayotte and Toppin, 1995.

<sup>b</sup> Concentrations in mg kg<sup>-1</sup>.

**Table 4.2**  
**Cobalt Arrival Times for Various Percentages of Goethite**

| Goethite <sup>2</sup> | Early Arrival <sup>1</sup> |        |                     |                         | C <sub>50</sub> Arrival <sup>5</sup> |        |        |            |
|-----------------------|----------------------------|--------|---------------------|-------------------------|--------------------------------------|--------|--------|------------|
|                       | Uniform                    | Banded | Random <sup>3</sup> | Difference <sup>4</sup> | Uniform                              | Banded | Random | Difference |
| 15, 60                | 0.29                       | 0.15   | 0.13                | 0.55                    | 0.63                                 | 0.58   | 0.56   | 0.11       |
| 10, 40                | 0.21                       | 0.12   | 0.11                | 0.48                    | 0.45                                 | 0.42   | 0.41   | 0.09       |
| 5, 20                 | 0.13                       | 0.10   | 0.09                | 0.31                    | 0.27                                 | 0.26   | 0.25   | 0.07       |

<sup>1</sup> Time (year) at which  $1.7 \times 10^{-8}$  mol kg<sup>-1</sup> (1 part per billion) Co<sup>2+</sup> arrived at x = 7.75 m.

<sup>2</sup> Percent goethite grain coatings in cells that contain grain coatings. First number is for the 128 goethite cells in the uniform case; second number is for the 32 goethite cells in the banded and random cases.

<sup>3</sup> Mean arrival time obtained by averaging arrival time results for rows one through eight in the random case.

<sup>4</sup> Difference between random and uniform case arrival times, where Difference = (uniform-random)/uniform.

<sup>5</sup> Time (year) at which  $5 \times 10^{-7}$  mol kg<sup>-1</sup> (50 percent of the maximum Co<sup>2+</sup> concentration) arrived at x = 7.75 m.

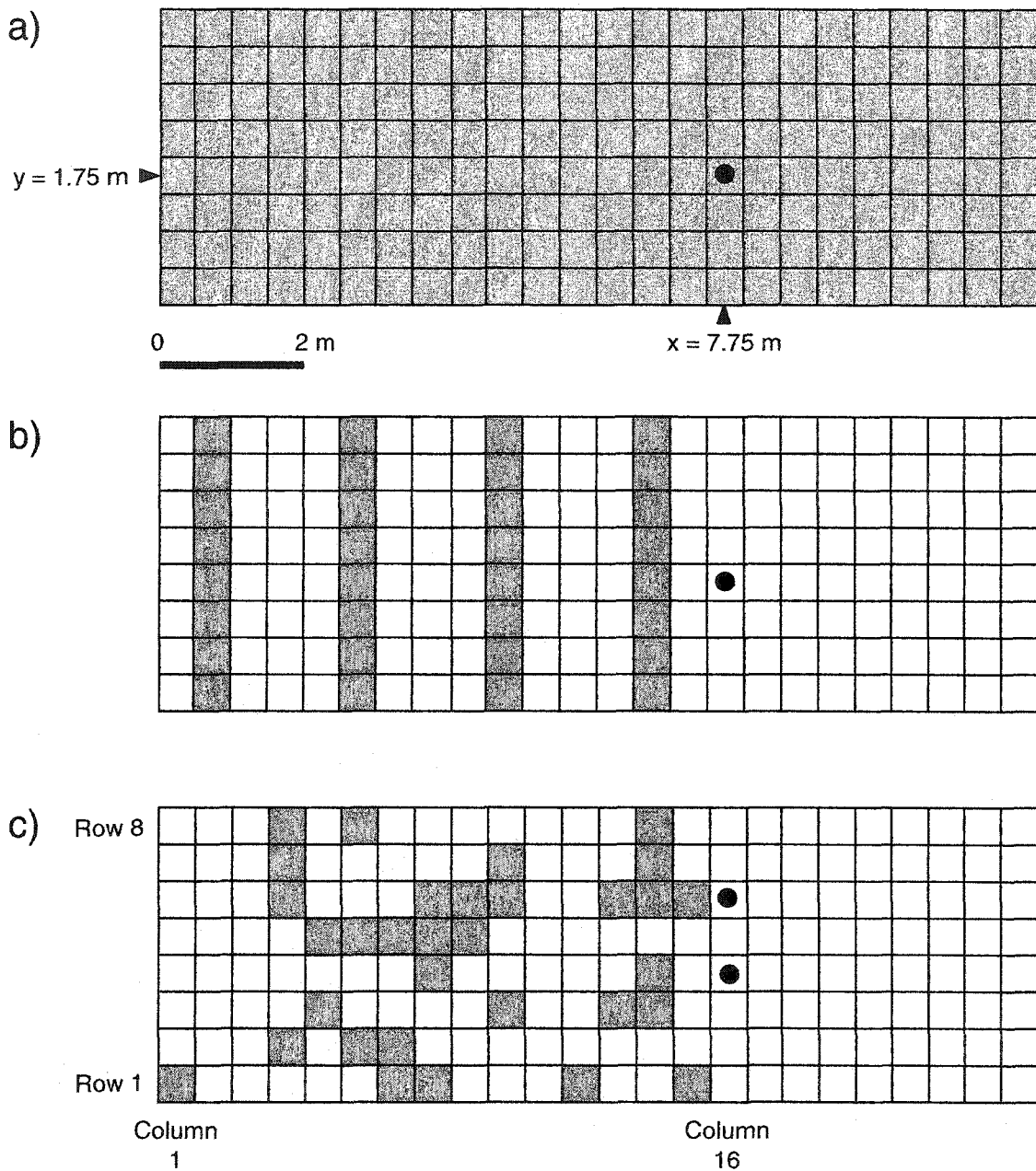


**Figure 4.1** Simulation domains for: (a) uniform distribution of goethite-coated grains, (b) banded pattern of goethite-coated grains, and (c) random pattern of goethite-coated grains. Black dots mark the observation points for the breakthrough curves presented in Figures 5.2 through 5.4. Note that the 4 x 8 m domain of interest (i.e. the first 16 columns from the left-hand boundary) is contained within a larger, 4 x 12 m model domain to prevent the downstream (right-hand) boundary from affecting the simulation results.

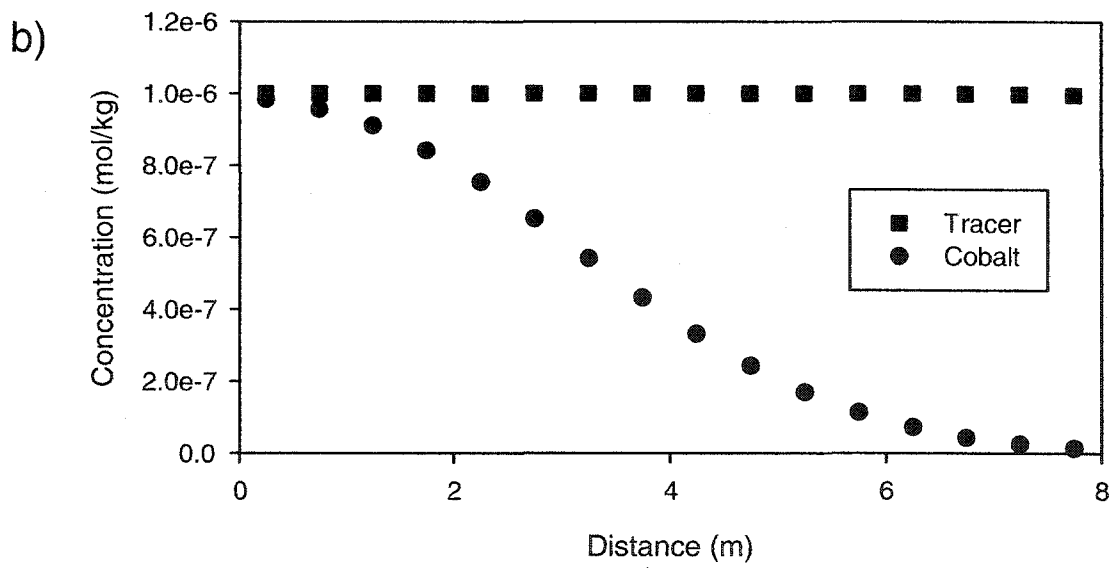
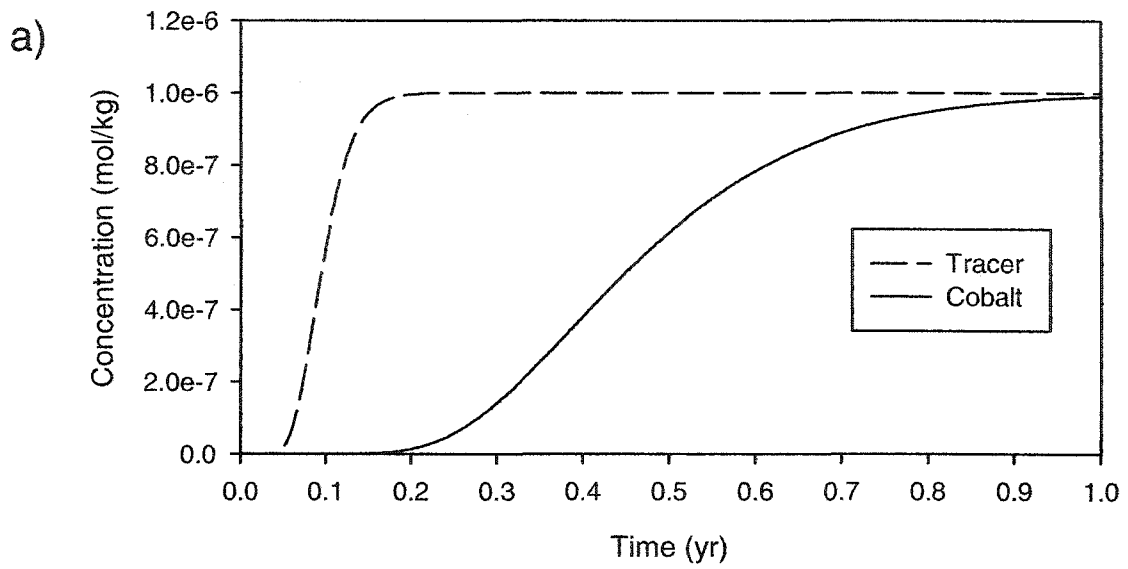


**Figure 4.2** (a) Breakthrough curves for uniform pattern of goethite coatings at  $x = 7.75$  m,  $y = 1.75$  m. (b) Solute concentrations for cobalt and tracer after 0.2 yr.

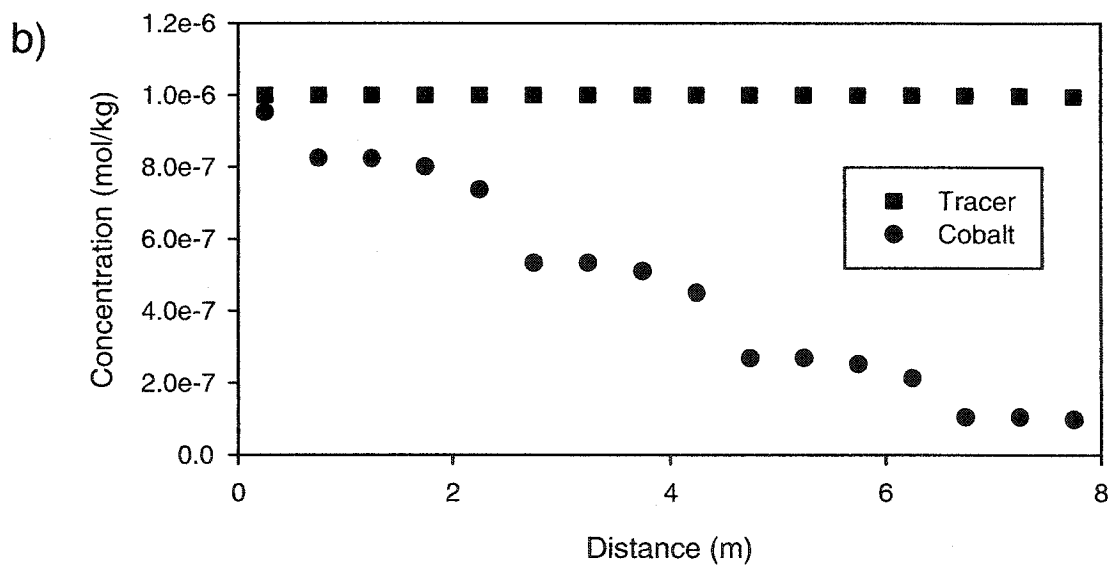
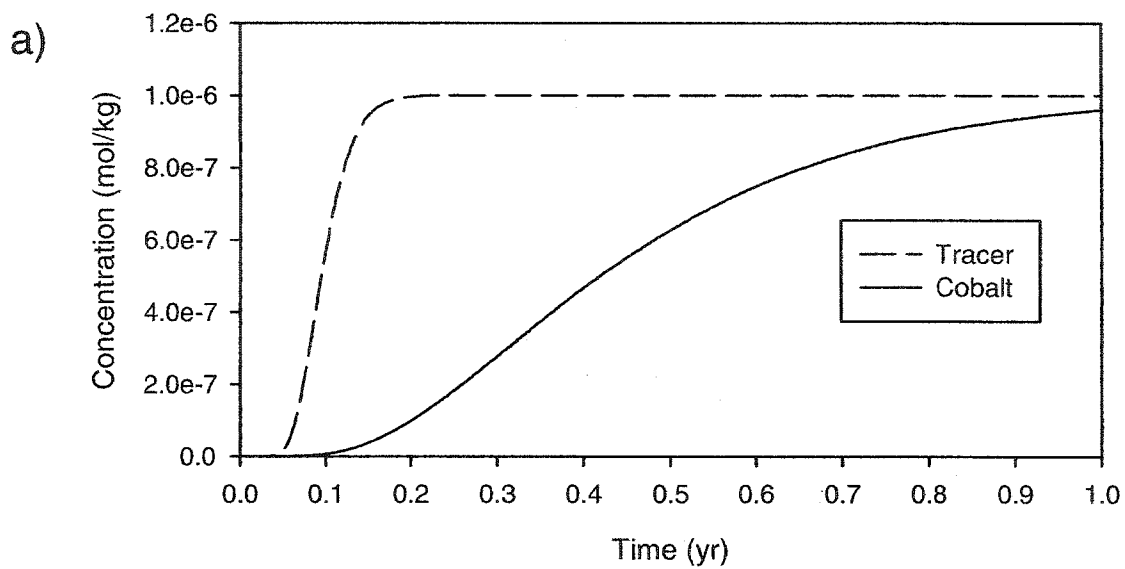


**Figure 4.3** (a) Breakthrough curves for banded pattern of goethite coatings at  $x = 7.75$  m,  $y = 1.75$  m. (b) Solute concentrations for cobalt and tracer after 0.2 yr.



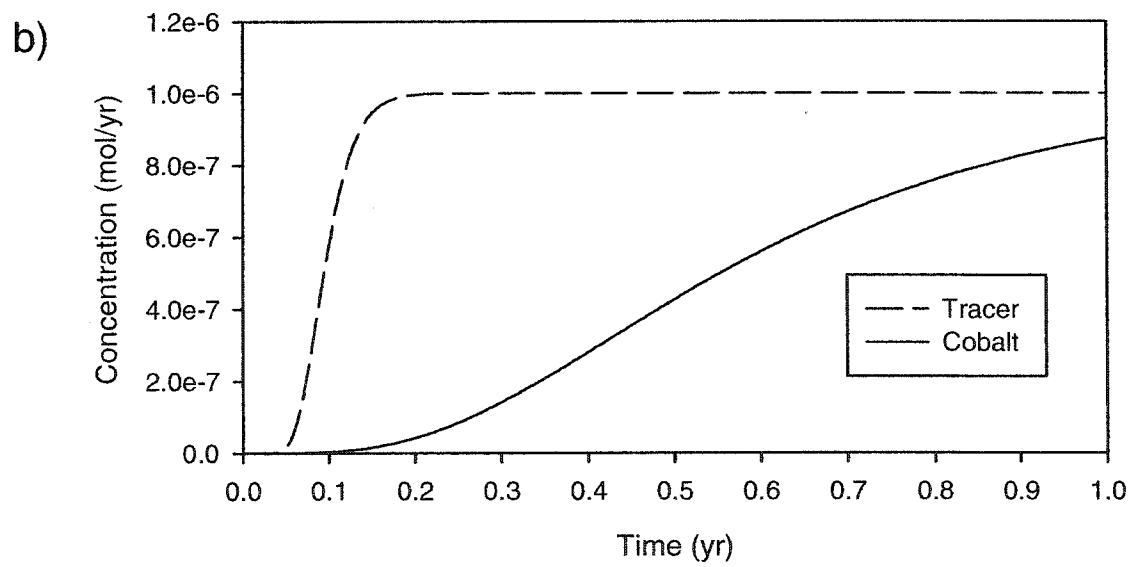
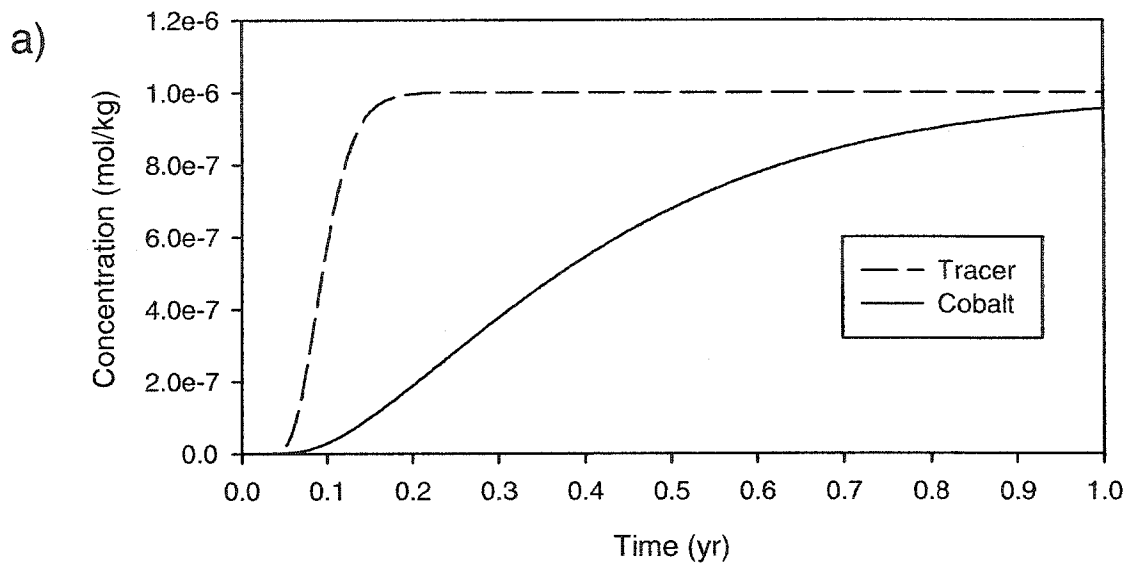


**Figure 4.4** Breakthrough curves for the random pattern of goethite coatings at: (a)  $x = 7.75$  m,  $y = 1.75$  m, and (b)  $x = 7.75$  m,  $y = 2.75$  m.

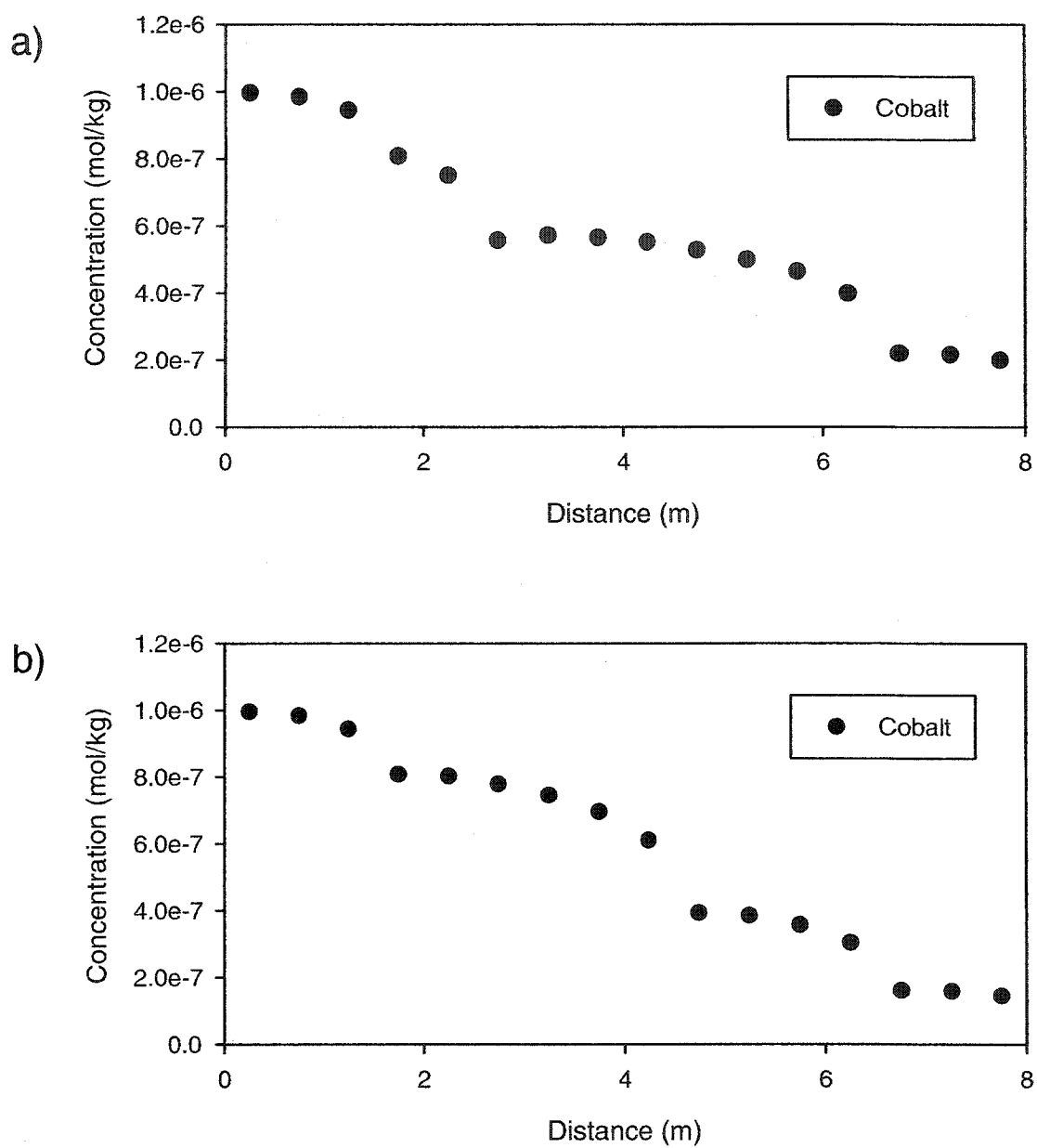


**Figure 4.5** (a) Cobalt concentrations across row 8 [y = 3.75 m] after 0.2 yr. (b) Cobalt concentrations across row 7 [y = 3.25 m] after 0.2 yr.

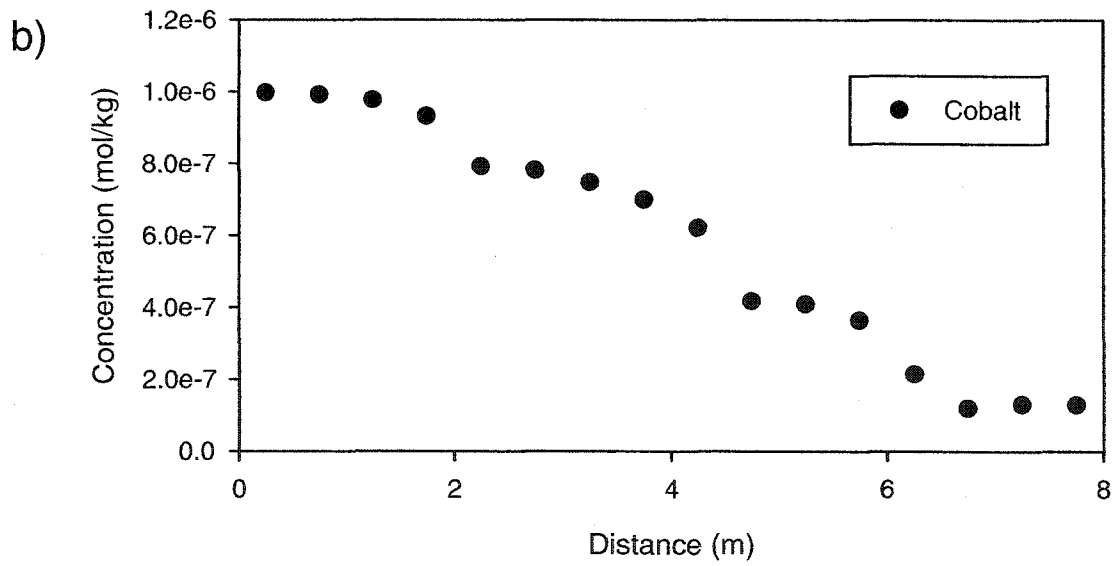
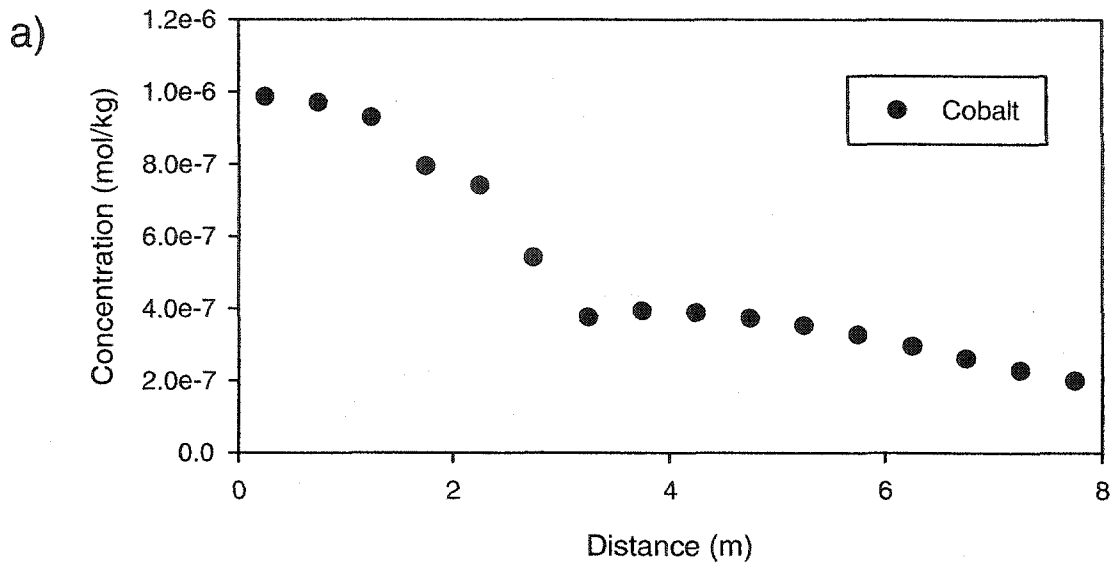


**Figure 4.6** (a) Cobalt concentrations across row 2 [ $y = 0.75$  m] after 0.2 yr. (b) Cobalt concentrations across row 3 [ $y = 1.25$  m] after 0.2 yr.

## CHAPTER 5

### SUMMARY

#### Project Conclusions

As stated in the project abstract, the first objective of this research was to identify the sediment properties controlling reactivity at the Deerfield site. The literature review presented in Chapter 1 reveals that aquifer reactivity is extremely complex. Several solid phases can be highly reactive, including: organic carbon compounds, carbonates, (hydr)oxides, phyllosilicate clay minerals, and weathered micas and magnetic minerals. More than one reactive solid is usually present in a system, and individual sites on each solid may have differing degrees of reactivity arising from variations in surface composition, roughness, and structure. To further complicate matters, reactivity is also affected by solution-related variables including: pH, temperature, ionic strength, redox state, adsorbate character and concentration, competitive ion effects, and the nature and abundance of soluble organic carbon compounds.

Despite the enormous complexity of the problem, the findings reported in Chapter 2 show that the majority of lead ( $\text{Pb}^{2+}$ ) sorption variation at the Deerfield site can be explained by a linear combination of four sediment properties: permeability, and dithionite citrate (DC)-extractable iron (Fe), manganese (Mn), and aluminum (Al). Consequently, it appears that: 1) reactivity is controlled by Fe-, Mn-, and Al-bearing (hydr)oxide grain coatings, and 2) estimates of  $\text{Pb}^{2+}$  sorption coefficients can be acquired from relatively simple and inexpensive measures of permeability and DC-

extractable metals. The preponderance of extractable Fe in every sample, the positive relationship between the extractable Fe/Al ratio and  $Pb^{2+}$  sorption, the yellow brown color of the iron-rich sediments, and the inability to see the coatings in thin sections under cross-polarized light suggest that the grain coatings consist primarily of poorly crystalline goethite with varying amounts of Al and Mn substitution for Fe.

Chapter 2 presents two alternative, or perhaps complementary, hypotheses to explain the quadratic relationship between  $Pb^{2+}$  sorption and permeability. The first hypothesis suggests that  $Pb^{2+}$  sorption is controlled by two reactive phases: clay minerals in the finest sediments and goethite grain coatings in the coarser sediments. This hypothesis is supported by: 1) observations of strong sorption in low permeability samples with high clay and/or silt contents, and 2) positive relationships between the extractable Fe/Al ratio and permeability and  $Pb^{2+}$  sorption. The second hypothesis explains the quadratic relationship between  $Pb^{2+}$  sorption and permeability in terms of differences in (hydr)oxide coating morphology and abundance. According to this hypothesis, sorption is strong in the finest sediments because they have high reactive surface areas by virtue of high (hydr)oxide concentrations and either thin continuous coatings or patchy coatings that cover a large number of sediment grains. Sorption is strong in the coarsest sediments, even though they contain low (hydr)oxide concentrations, because they have very thin, continuous coatings with much higher (hydr)oxide surface area to mass ratios compared to samples in which the (hydr)oxides are concentrated in patches. Estimates of reactive surface area, based on sample grain size, (hydr)oxide mass, and coating morphology and abundance, explain 65 percent of the variation in  $Pb^{2+}$  sorption.

Chapters 2 and 3 show that the sediment's reactive properties are only weakly to moderately correlated with its physical properties. Therefore, simple, economical,

physical property measurements cannot serve as surrogates for chemical property measurements at the Deerfield site. In addition, the physical and chemical properties at the Deerfield site exhibit very different spatial structures. Permeability and porosity variation increase rapidly with separation distance, directions of maximum and minimum continuity are  $15^\circ$  (subhorizontal) and  $105^\circ$  (subvertical), respectively, and correlation lengths in these directions are approximately 0.45 m and 0.1 m, respectively. By contrast, adjacent measures of extractable Mn are very similar, directions of maximum and minimum continuity are  $0^\circ$  and  $90^\circ$ , respectively, and correlation lengths are more than twice as large as those for permeability and porosity. Extractable Fe and extractable Al are uncorrelated at the scales studied.

The second objective of the research program was to evaluate the extent to which geologic information could be used to characterize chemical heterogeneity. Chapter 3 describes how lithologic facies explain the majority of variation in permeability and extractable Mn. Facies do not separate regions of significantly different extractable Fe; instead, 49 percent of its variation is explained by sediment color. Color also accounts for 60 percent of the variation in extractable Mn. Strong relationships with sediment facies and/or color enable detailed mapping of permeability, extractable Fe, and extractable Mn. Maps of extractable Fe and extractable Mn for the Deerfield site show that Fe-rich coatings are concentrated in narrow, isolated zones, while Mn-rich zones are more broad and diffuse. Differences in the geometries of Fe and Mn enrichment, petrographic observations, and SEM-EDS analyses indicate the grain coatings originated primarily from the post-depositional weathering of biotite and garnet coupled with local, redox-driven mobilization of the liberated Fe and Mn. The results suggest that information pertaining to sediment facies and color can help produce more

efficient and geologically realistic descriptions of heterogeneity in carbon-poor glaciofluvial sediments.

The final project objective was to assess the impact of chemical heterogeneity on reactive transport. A numerical modeling study presented in Chapter 4 examined the influence of the spatial pattern of (hydr)oxide grain coatings on cobalt ( $\text{Co}^{2+}$ ) transport through a hypothetical sandy aquifer. Results of the simulations suggest that chemical heterogeneity increases plume migration and dispersion. Consequently, models that fail to account for spatial variations in reactivity may underestimate solute transport and dispersion through chemically heterogeneous systems.

### **Suggestions for Future Research**

As with most research projects, this study generated more questions than it answered, thus highlighting the need for additional work. For example, more laboratory research is needed to account for the unexplained variation in the multiple regression models of  $\text{Pb}^{2+}$  sorption presented in Chapter 2. The unexplained variation may be due to the presence of additional reactive phases such as phyllosilicate clay minerals, or it may be due to limitations associated with the dithionite-citrate extractions. Selective extractions are not perfectly selective. They may not completely remove the target phase, they may dissolve nontarget phases, and/or they may redistribute trace elements among other mineral phases during the extraction process (Gruebel et al., 1988).

The Deerfield study focused on just a few chemical property analyses. Ideally, attempts to identify reactive phases should involve a broader suite of analyses. Supporting methods could include: 1) additional batch adsorption studies with different heavy metals, 2) additional selective extractions using alternative extracting solutions such as hydroxylamine hydrochloride, 3) evaluations of clay content and mineralogy,

and 4) adsorption studies using microprobe technology with trace metal isotopes to confirm that the adsorbate is associated with the suspect phase.

There is also a need to test and refine methods for characterizing grain coating morphology and numerical abundance. The relevant conclusions in Chapter 2 were based on visual observations of only ten thin sections made from samples collected from a single outcrop. Moreover, it was difficult to assign accurate values for the proportion of coated grains by visual inspection of thin sections. Image editing software (e.g. Adobe® Photoshop) that can take a digital image of a thin section, isolate the grain coatings based on color, and then calculate the number of locations with that color may provide a more accurate and unbiased estimate. Related areas of research would be to investigate the hydrobiogeochemical reasons for the differences in grain coating morphology, and to characterize the variation in BET surface area for fully coated sediment grains of different grain sizes and coating morphologies. The latter area of research is needed to convert the geometric surface areas of grain coatings to BET surface areas for surface complexation modeling.

Additional work on grain coating origins is needed to determine whether the grain coating heterogeneities are simply the product of in-situ oxidation of Fe- and Mn-bearing minerals in the vadose zone, coupled with infiltration-driven redistribution of the released Fe and Mn, or whether these vadose zone processes are overprinting the results of earlier dissolution, transport, and precipitation in the hyporheic zone (Harvey and Fuller 1998). The study could include simulating a depositional sequence from the field using stratigraphic modeling software, attempting to model the grain coating patterns observed in the field, and then critically evaluating the environmental conditions required to reproduce the patterns. The modeling effort would require coupling codes that



account for saturated and unsaturated flow, mineral weathering, chelation reactions and transport, and spatially and temporally variable redox conditions and microbial activity.

More research is also needed to improve physical and chemical heterogeneity characterization methods. An additional outcrop study with more exhaustive sampling and higher resolution (i.e. smaller) sediment samples may show significantly stronger correlations between sediment properties. The impacts of primary mineral color, soil moisture, and grain size on the extractable metal-color relationships identified in Chapter 3 should be assessed. The influence of individual bedding planes on physical and chemical heterogeneity should be evaluated to determine if, and to what extent, they account for the unexplained variation in the facies-based models described in Chapter 3. This type of analysis is particularly important for extractable Fe, since Fe-rich grain coatings appear to be associated with heavy mineral-rich laminae. A larger-scale (tens of meters) outcrop study could assess the applicability of the 8 m<sup>2</sup> outcrop results to scales needed for subsurface facies mapping. This larger-scale study could also search for links between stochastic descriptions of heterogeneity and facies-based models to see, for example, if spatial correlation structures are controlled by facies dimensions (Davis et al. 1997).

Several follow-up activities could further define the impact of grain coating heterogeneities on simulations of heavy metal transport. A rigorous sensitivity analysis, especially on the goethite-related parameters and the transverse dispersivity, could bolster the modeling conclusions discussed in Chapter 4. Additional model runs could investigate the scale-dependency of the findings. If differences in the spatial patterns of (hydr)oxide grain coatings yield negligible differences in reactive transport when the scale of observation is large and the frequency of the (hydr)oxide bands or patches is high, the modeling may be able to establish the relative scales of observation and

heterogeneity at which the differences become inconsequential under a given set of geochemical conditions.

Obviously, there is a need to test the portability of the outcrop study findings. Sediment cores from the saturated zone of the Rollins pit could be collected and analyzed, and perhaps a dewatered trench could be studied, to evaluate the extent to which the outcrop relations apply below the water table. The outcrop and subsurface studies could be repeated at similar sites to see if the results hold in other carbon-poor glaciofluvial deposits.

Finally, basin scale field and modeling studies in the Deerfield valley-fill aquifer are needed to document how chemical heterogeneity changes as the scale of observation increases, and to understand how these changes affect solute transport predictions. Basin-scale trends could be investigated in three sand and gravel pits: the Rollins pit where the current outcrop study was conducted (Figure 1.2); the State pit, situated 2.5 km down gradient (southeast) from the Rollins pit in relatively iron-rich deltaic deposits (Moore 1990); and a small borrow pit located approximately 1 km up gradient (northwest) of the Rollins pit in relatively homogeneous, iron-poor, meltwater stream deposits. Information from the three pits could advance our understanding of the geologic controls on heterogeneity over a wide range of spatial scales.

## REFERENCES

- Ainsworth, C. C., J. L. Pilon, P. L. Gassman, and W. G. Van Der Sluys. 1994. Cobalt, cadmium, and lead sorption to hydrous iron oxide: Residence time effect. *Soil Science Society of America Journal* 58: 1615-1623.
- Allen-King, R. M., R. M. Halket, D. R. Gaylord, and M. J. L. Robin. 1998. Characterizing the heterogeneity and correlation of perchloroethene sorption and hydraulic conductivity using a facies-based approach. *Water Resources Research* 34: 385-396.
- Anderson, B. J., E. A. Jenne, and T. T. Chao. 1973. The sorption of silver by poorly crystallized manganese oxides. *Geochimica et Cosmochimica Acta* 37: 611-622.
- Anderson, M. P. 1989. Hydrogeologic facies models to delineate large-scale spatial trends in glacial and glaciofluvial sediments. *Geological Society of America Bulletin* 101: 501-511.
- Ayotte, J. D. and K. W. Toppin. 1995. Geohydrology and water quality of stratified-drift aquifers in the Middle Merrimack River Basin, south-central New Hampshire. USGS Water-Resources Investigations Report 92-4192.
- Bajracharya, K. and D. A. Barry. 1997. Nonequilibrium solute transport parameters and their physical significance: numerical and experimental results. *Journal of Contaminant Hydrology* 24: 185-204.
- Balistrieri, L. S., and J. W. Murray. 1981. The surface chemistry of goethite in major ion seawater. *American Journal of Science* 281: 788-806.
- Ball, W. P., C. H. Buchler, T. C. Harmon, D. M. Mackay, and P. V. Roberts. 1990. Characterization of a sandy aquifer material at the grain scale. *Journal of Contaminant Hydrology* 5: 253-295.
- Ball, W. P. and P. V. Roberts. 1991. Long-term sorption of halogenated organic chemicals by aquifer material: 1. Equilibrium. *Environmental Science & Technology* 25: 1223-1236.
- Bancroft, G. M. and M. M. Hyland. 1990. Spectroscopic studies of adsorption/reduction reactions of aqueous metal complexes on sulphide surfaces. In *Mineral-Water Interface Geochemistry*. REVIEWS in MINERALOGY 23, ed. M. F. Hochella and A. F. White, 511-558. Washington, DC: Mineralogical Society of America.
- Barber, L. B. II, E. M. Thurman, and D. R. Runnells. 1992. Geochemical heterogeneity in a sand and gravel aquifer: Effect of sediment mineralogy and particle size on the sorption of chlorobenzenes. *Journal of Contaminant Hydrology* 9: 35-54.

- Bargar, J. R., G. E. Brown, and G. A. Parks. 1997a. Surface complexation of Pb(II) at oxide-water interfaces: XAFS and bond-valence determination of mononuclear and polynuclear Pb(II) sorption products on aluminum oxides. *Geochimica et Cosmochimica Acta* 61: 2617-2637.
- Bargar, J. R., G. E. Brown, and G. A. Parks. 1997b. Surface complexation of Pb(II) at oxide-water interfaces: XAFS and bond-valence determination of mononuclear Pb(II) sorption products and surface functional groups on iron oxides. *Geochimica et Cosmochimica Acta* 61: 2639-2652.
- Barnett, M. O., P. M. Jardine, and S. C. Brooks. 2002. U(VI) adsorption to heterogeneous subsurface media: Application of a surface complexation model. *Environmental Science & Technology* 36: 9370-942.
- Bear, J. 1972. *Dynamics of Fluids in Porous Media*. New York: Dover Publications.
- Benson, M. A. 1965. Spurious correlation in hydraulics and hydrology. *Journal of the Hydraulics Division, Proceedings of the American Society of Civil Engineers* 90, no. HY4: 35-42.
- Bethke, C. and P. V. Brady. 2000. How the  $K_d$  approach undermines ground water cleanup. *Ground Water* 38: 435-443.
- Bohn, H. L., B. L. McNeal, and G. A. O'Connor. 1985. *Soil Chemistry*, 2nd ed. New York: John Wiley & Sons.
- Bosma, W. J. P., A. Bellin, S. E. A. T. M. van der Zee, and A. Rinaldo. 1993. Linear equilibrium adsorbing solute transport in physically and chemically heterogeneous porous formations: 2. Numerical results. *Water Resources Research* 29: 4031-4043.
- Brady, P. V. and C. Bethke. 2000. Beyond the  $K_d$  approach. *Ground Water* 38: 321-322.
- Brown, G. E. 1990. Spectroscopic studies of chemisorption reaction mechanisms at oxide-water interfaces. In *Mineral-Water Interface Geochemistry*. REVIEWS in MINERALOGY 23, ed. M. F. Hochella and A. F. White, 309-364. Washington, DC: Mineralogical Society of America.
- Brunauer, S., P. H. Emmett, and E. Teller. 1938. Adsorption of gases in multimolecular layers. *Journal of the American Chemical Society* 60: 309-319.
- Burns, R. G. 1976. The uptake of cobalt into ferromanganese nodules, soils, and synthetic manganese (IV) oxides. *Geochimica et Cosmochimica Acta* 40: 95-102.
- Burr, D. T., E. A. Sudicky, and R. L. Naff. 1994. Non-reactive and reactive solute transport in three-dimensional heterogeneous porous media: mean displacement, plume spreading, and uncertainty. *Water Resources Research* 30: 791-815.

- Carle S. F., E. M. LaBolle, G. S. Weissmann, D. van Brocklin, and G. E. Fogg. 1998. Conditional simulation of hydrofacies architecture: A transition probability/Markov approach. In *Hydrogeologic Models of Sedimentary Aquifers*, ed. G. S. Fraser and J. M. Davis, 147-170. Tulsa, Oklahoma: SEPM (Society for Sedimentary Geology).
- Chao, T. T. 1972. Selective dissolution of manganese oxides from soils and sediments with acidified hydroxylamine hydrochloride. *Soil Science Society of America Proceedings* 26: 764-768.
- Chayes, F. 1949. On ratio correlation in petrography. *Journal of Geology* 57: 239-254.
- Chayes, F. 1971. *Ratio Correlation*. Chicago, Illinois: University of Chicago Press.
- Christensen, T. H., N. Lehmann, T. Jackson, and P. E. Holm. 1996. Cadmium and nickel distribution coefficients for sandy aquifer materials. *Journal of Contaminant Hydrology* 24: 75-84.
- Christmann, K. and G. Ertl. 1976. Interaction of hydrogen with Pt(111): The role of atomic steps. *Surface Science* 60: 365-384.
- Coats, K. H. and B. D. Smith. 1964. Dead-end pore volume and dispersion in porous media. *Society of Petroleum Engineering Journal* 4: 73-84.
- Coston, J. A., C. C. Fuller, and J. A. Davis. 1995. Pb<sup>2+</sup> and Zn<sup>2+</sup> adsorption by a natural Al- and Fe- bearing surface coating on an aquifer sand. *Geochimica et Cosmochimica Acta* 59: 3535-3547.
- Culley, J. L. B. 1993. Density and compressibility. In *Soil Sampling and Methods of Analysis*, ed. M. R. Carter, 529-540. Boca Raton, Florida: Lewis Publishers.
- Dagan, G. 1988. Time-dependent macrodispersion for solute transport in anisotropic heterogeneous aquifers. *Water Resources Research* 24: 1491-1500.
- Datta-Gupta, A., L. W. Lake, and G. A. Pope. 1995. Characterizing Heterogeneous Permeable Media with Spatial Statistics and Tracer Data Using Sequential Simulated Annealing. *Mathematical Geology* 27: 763-787.
- Davis, J. A. and D. B. Kent. 1990. Surface complexation modeling in aqueous geochemistry. In *Mineral-Water Interface Geochemistry*. REVIEWS in MINERALOGY 23, ed. M. F. Hochella, Jr. and A. F. White, 177-260. Washington, DC: Mineralogical Society of America.
- Davis, J. A. and J. D. Hem. 1989. The surface chemistry of aluminum oxides and hydroxides. In *The Environmental Chemistry of Aluminum*, ed. G. A. Sposito, 185-219. Boca Raton, Florida: CRC Press.

- Davis, J. A. and J. O. Leckie. 1978. Surface ionization and complexation at the oxide-water interface: II. Surface properties of amorphous iron oxyhydroxides and adsorption of metal ions. *Journal of Colloid Interface Science* 67: 90-107.
- Davis, J. A., C. C. Fuller, and A. D. Cook. 1987. A model for trace metal sorption processes at the calcite surface: Adsorption of  $\text{Cd}^{2+}$  and subsequent solid solution formation. *Geochimica et Cosmochimica Acta* 51: 1477-1490.
- Davis, J. A., C. C. Fuller, J. A. Coston, and E. Dixon. 1993. *Spatial heterogeneity of geochemical and hydrologic parameters affecting metal transport in groundwater*. U.S. Environmental Protection Agency, Environmental Research Brief, EPA/600/S-93/006. Ada, Oklahoma: Robert S. Kerr Environmental Research Laboratory.
- Davis, J. A., J. A. Coston, D. B. Kent, and C. C. Fuller. 1998. Application of the surface complexation concept to complex mineral assemblages. *Environmental Science & Technology* 32: 2820-2828.
- Davis, J. M., J. L. Wilson, F. M. Phillips, and M. B. Gotkowitz. 1997. Relationship between fluvial bounding surfaces and the permeability correlation structure. *Water Resources Research* 33: 1843-1854.
- DeBraal, J. D. and Y. K. Kharaka. 1989. SOLINPUT: A computer code to create and modify input files for the geochemical program SOLMINEQ.88. USGS Open-File Report 89-616.
- Deutsch, C. V. and A. G. Journel. 1998. *GSLIB Geostatistical Software Library and User's Guide*, 2nd ed. New York: Oxford University Press.
- Dixon, J. B., and H. C. W. Skinner. 1992. Manganese minerals in surface environments. In *Bio-mineralization processes of iron and manganese: modern and ancient environments*. CATENA SUPPLEMENT 21, ed. H. C. W. Skinner and R. W. Fitzpatrick, 31-50. Cremlingen-Destedt, Germany: CATENA VERLAG.
- Dzombak, D. A. and F. M. M. Morel. 1990. *Surface Complexation Modeling: Hydrous Ferric Oxide*. New York: John Wiley & Sons.
- Ernsberger, F. M. 1960. Structural effects in the chemical reactivity of silica and silicates. *Journal of Physics and Chemistry of Solids*. 13: 347-351.
- Fetter, C. W. 1999. *Contaminant Hydrogeology*, 2nd ed. New York: Macmillan Publishing.
- Freeze, R. A. 1975. A stochastic-conceptual analysis of one-dimensional groundwater flow in non uniform homogeneous media. *Water Resources Research* 11: 725-741.
- Freeze, R. A. and J. A. Cherry. 1979. *Ground Water*. Englewood Cliffs, New Jersey: Prentice-Hall.

- Freeze, R. A., J. Massmann, L. Smith, T. Sperling, and B. James. 1990. Hydrogeological decision analysis: 1. A framework. *Ground Water* 28: 738-766.
- Friedly, J. C., J. A. Davis, and D. B. Kent. 1995. Modeling hexavalent chromium reduction in groundwater in field-scale transport and laboratory batch experiments. *Water Resources Research* 31: 2783-2794.
- Fuller, C. C. and J. A. Davis. 1987. Processes and kinetics of Cd<sup>2+</sup> sorption by a calcareous aquifer sand. *Geochimica et Cosmochimica Acta* 51: 1491-1502.
- Fuller, C. C., J. A. Davis, and G. A. Waychunas. 1993. Surface-chemistry of ferrihydrite: 2. Kinetics of arsenate adsorption and coprecipitation. *Geochimica et Cosmochimica Acta* 57: 2271-2282.
- Fuller, C. C., J. A. Davis, J. A. Coston, and E. Dixon. 1996. Characterization of metal adsorption variability in a sand and gravel aquifer, Cape Cod, Massachusetts, U.S.A. *Journal of Contaminant Hydrology* 22: 165-187.
- Gelhar, L. W. 1986. Stochastic subsurface hydrology from theory to applications. *Water Resources Research* 22: 135S-145S.
- Gelhar, L. W. and C. L. Axness. 1983. Three-dimensional stochastic analysis of macrodispersion in aquifers. *Water Resources Research* 19: 161-180.
- Gelhar, L. W., C. Welty, and K. R. Rehfeldt. 1992. A critical review of data on field-scale dispersion in aquifers. *Water Resources Research* 28: 1955-1974.
- Gephart, G.D. 1985. *Surficial geologic map of the Candia Quadrangle, Rockingham County, New Hampshire*. Concord: State of New Hampshire Department of Resources and Economic Development.
- Grahame, D. C. 1947. The electrical double layer and the theory of electrocapillarity. *Chem. Rev.* 41: 441-501.
- Gruebel, K. A., J. A. Davis, and J. O. Leckie. 1998. The feasibility of using sequential extraction techniques for arsenic and selenium in soils and sediments. *Soil Science Society of America Journal* 52: 390-397.
- Harter, R. D. 1984. Curve-fit errors in Langmuir adsorption maxima. *Soil Science Society of America Journal* 48: 749-752.
- Harvey, J. W. and C. C. Fuller. 1998. Effect of enhanced manganese oxidation in the hyporheic zone on basin-scale geochemical mass balance. *Water Resources Research* 34: 623-636.
- Hayes, K. F. 1987. Equilibrium, spectroscopic, and kinetic studies of ion adsorption at the oxide/aqueous interface. Ph.D. diss., Stanford University.

- Hayes, K. F., A. L. Roe, G. E. Brown, K. O. Hodgson, J. O. Leckie, and G. A. Parks. 1987. In-situ X-ray absorption study of surface complexes: Selenium oxyanions on  $\alpha$ -FeOOH. *Science* 238: 783-786.
- Hess, H. H. 1959. Notes on operation of Frantz Isodynamic Magnetic Separator. Trenton, New Jersey: S. G. Frantz Company.
- Hochella, M. F. 1990. Atomic structure, microtopography, composition, and reactivity of mineral surfaces. In *Mineral-Water Interface Geochemistry*. REVIEWS in MINERALOGY 23, ed. M. F. Hochella and A. F. White, 87-132. Washington, DC: Mineralogical Society of America.
- Hochella, M. F. and A. F. White. 1990. Mineral-water interface geochemistry: An overview. In *Mineral-Water Interface Geochemistry*. REVIEWS in MINERALOGY 23, ed. M. F. Hochella and A. F. White, 1-16. Washington, DC: Mineralogical Society of America.
- Hohl, H. and W. Stumm. 1976. Interaction of  $Pb^{2+}$  with hydrous  $\alpha$ - $Al_2O_3$ . *Journal of Colloid Interface Science* 55: 281-288.
- Inch, K. J. and R. W. D. Killey. 1987. Surface area and radionuclide adsorption in contaminated aquifers. *Water Pollution Research Journal of Canada* 22: 85-98.
- Isaaks, E. H., and R. M. Srivastava. 1989. *An Introduction to Applied Geostatistics*. New York: Oxford University Press.
- Jackson, R. E., and K. J. Inch. 1989. The in-situ adsorption of  $^{90}Sr$  in a sand aquifer at the Chalk River Nuclear laboratories. *Journal of Contaminant Hydrology* 4: 27-50.
- James, R. O. and G. A. Parks. 1982. Characterization of aqueous colloids by their electrical double-layer and intrinsic surface chemical properties. *Surface and Colloid Science*. 12: 119-214.
- James, R. O. and T. W. Healy. 1972. Adsorption of hydrolysable metal ions at the oxide-water interface: II. Charge reversal of  $SiO_2$  and  $TiO_2$  colloids by adsorbed Co(II), La(III), and Th(IV) as model systems. *Journal of Colloid Interface Science* 40: 53-64.
- Jenne, E. A. 1968. Controls on Mn, Fe, Co, Ni, Cu, and Zn concentrations in soils and water: the significant role of hydrous Mn and Fe oxides. In *Trace Inorganics in Water*. ACS Symposium Series 73, ed. R. A. Baker, 337-387. Washington, DC: American Chemical Society.
- Kaplan, D. I., I. V. Kutnyakov, A. P. Gamerdinger, R. J. Serne, and K. E. Parker. 2000. Gravel-corrected  $K_d$  values. *Ground Water* 38: 851-857.
- Kapoor, V., and L. W. Gelhar. 1994a. Transport in three-dimensionally heterogeneous aquifers 1. Dynamics of concentration fluctuations. *Water Resources Research* 30: 1775-1788.



- Kapoor, V., and L. W. Gelhar. 1994b. Transport in three-dimensionally heterogeneous aquifers 2. Predictions and observations of concentration fluctuations. *Water Resources Research* 30: 1789-1801.
- Karickhoff, S. W., D. S. Brown, and T. A. Scott. 1979. Sorption of hydrophobic pollutants on natural sediments. *Water Research* 13: 241-248.
- Katz, D. L., and R. L. Lee. 1990. *Natural Gas Engineering: Production and Storage*. New York: McGraw-Hill.
- Kerwin, C. M., S. T. Allard, J. Laird, and W. Bothner. 2004. The rocks speak and the Proterozoic shrinks: Results from mapping and REE chemistry of the Massabesic Gneiss Complex. *New England Intercollegiate Geological Conference Guide Book* 96: 77-87.
- Kent, D. B., R. H. Abrams, J. A. Davis, J. A. Coston, and D. R. LeBlanc. 2000. Modeling the influence of variable pH on the transport of zinc in a contaminated aquifer using semiempirical surface complexation models. *Water Resources Research* 36: 3411-3425.
- Koltermann, C. E. and S. M. Gorelick. 1996. Heterogeneity in sedimentary deposits: A review of structure-imitating, process-imitating, and descriptive approaches. *Water Resources Research* 32: 2617-2658.
- Kou, S. 1986. Concurrent sorption of phosphate and zinc, cadmium, or calcium by a hydrous ferric oxide. *Soil Science Society of America Journal* 50: 1412-1419.
- Lee, C. M. and D. L. Macalady. 1989. Towards a standard method for the measurement of organic carbon in sediments. *International Journal of Environmental Analytical Chemistry* 35: 219-225.
- Lee, S. Y. and M. L. Jackson. 1977. Surface charge density determination of micaceous minerals by  $^{235}\text{U}$  fission particle track method. *Clays and Clay Minerals* 25: 295-301.
- Lehmann, R. G. and R. D. Harter. 1984. Assessment of copper-soil bond strength by desorption kinetics. *Soil Science Society of America Journal* 48: 769-772.
- Lion, L. W., R. S. Altmann, and J. O. Leckie. 1982. Trace metal adsorption characteristics of estuarine particulate matter: evaluation of contribution of Fe/Mn oxide and organic surface coatings. *Environmental Science & Technology* 16: 660-666.
- Lorens, R. B. 1981. Sr, Cd, Mn and Co distribution coefficients in calcite as a function of calcite precipitation rate. *Geochimica et Cosmochimica Acta* 45: 553-561.
- Lutzenkirchen, J., J. F. Boily, L. Lovgren, S. Sjöberg. 2002. Limitations of the potentiometric titration technique in determining the proton active site density of goethite surfaces. *Geochimica et Cosmochimica Acta* 66: 3389-3396.

- Mackay, D. M., W. P. Ball, and M. G. Durant. 1986. Variability of aquifer sorption properties in a field experiment on groundwater transport of organic solutes: Methods and preliminary results. *Journal of Contaminant Hydrology* 1: 119-132.
- McBride, M. B. 1979. Chemisorption and precipitation of  $Mn^{2+}$  at  $CaCO_3$  surfaces. *Soil Science Society of America Journal* 43: 693-698.
- McCarthy, J. F. and J. M. Zachara. 1989. Subsurface transport of contaminants. *Environmental Science & Technology* 23: 496-502.
- McKenzie, R. M. 1972. The sorption of some heavy metals by the lower oxides of manganese. *Geoderma* 8: 29-35.
- Moore, R. B. 1990. *Geohydrology and water quality of stratified-drift aquifers in the Exeter, Lamprey, and Oyster River basins, southeastern New Hampshire*. USGS Water Resources Investigations Report 88-4128.
- Munsell Color Company. 1975. Munsell soil color charts. Baltimore, Maryland: Munsell Color Company.
- Nielsen, D. R., M. Th. van Genuchten, and J. W. Biggar. 1986. Water flow and solute transport in the unsaturated zone. *Water Resources Research* 22: 89S-108S.
- Pannatier, Y. 1996. *VARIOWIN: Software for spatial data analysis in 2D*. New York: Springer-Verlag.
- Papelis, C. 1995. X-ray photoelectron spectroscopic studies of cadmium and selenite adsorption on aluminum oxides. *Environmental Science & Technology* 29: 1526-1533.
- Papelis, C., P. V. Roberts, and J. O. Leckie. 1995. Modeling the rate of cadmium and selenite adsorption on micro- and mesoporous transition aluminas. *Environmental Science & Technology* 29: 1099-1108.
- Papini, M. P., Y. D. Kahie, B. Troia, and M. Majone. 1999. Adsorption of lead at variable pH onto a natural porous medium: modeling of batch and column experiments. *Environmental Science & Technology* 33: 4457-4464.
- Parfitt, R. L., V. C. Farmer, and J. D. Russell. 1977. Adsorption on hydrous oxides: 1. Oxalate and benzoate on goethite. *Journal of Soil Science* 28: 29-39.
- Parks, G. A. 1990. Surface energy and adsorption at mineral/water interfaces: An introduction. In *Mineral-Water Interface Geochemistry*. REVIEWS in MINERALOGY 23, ed. M. F. Hochella and A. F. White, 133-176. Washington, DC: Mineralogical Society of America.
- Pearson, K. 1896-1897. On a form of spurious correlation which may arise when indices are used in the measurement of organs. *Royal Society of London Proceedings* 60: 489-502.

- Perdereau, J. and G. Rhead 1971. LEED studies of adsorption on vicinal copper surfaces. *Surface Science* 24: 555-571.
- Pickens, J. F. and G. E. Grisak. 1981. Scale-dependent dispersion in a stratified granular aquifer. *Water Resources Research* 17: 1191-1211.
- Poeter, E. P. and M. C. Hill. 1997. Inverse models: A necessary next step in ground-water modeling. *Ground Water* 35: 250-260.
- Post, D. F., S. J. Levine, R. B. Bryant, M. D. Mays, A. K. Batchily, R. Escadafal, and A. R. Huete. 1993. Correlations between field and laboratory measurements of soil color. In *Soil Color*. SSSA Special Publication Number 31, ed. J. M. Bigham and E. J. Ciolkosz, 35-50. Madison, Wisconsin: Soil Science Society of America.
- Postma, D., and C. A. J. Appello. 2000. Reduction of Mn-oxides by ferrous iron in a flow system: Column experiment and reactive transport modeling. *Geochimica et Cosmochimica Acta* 64: 1237-1247.
- Rautman, C. A. and J. D. Istok. 1996. Probabilistic assessment of ground-water contamination: 1. Geostatistical framework. *Ground Water* 34: 899-909.
- Robin, J. J. L., E. A. Sudicky, R. W. Gillham, and R. G. Kachanoski. 1991. Spatial variability of strontium distribution coefficients and their correlation with hydraulic conductivity in the Canadian Forces Base Borden Aquifer. *Water Resources Research* 27: 2619-2632.
- Ross, G. J. and C. Wang. 1993. Extractable Al, Fe, Mn, and Si. In *Soil Sampling and Methods of Analysis*, ed. M. R. Carter, 239-246. Boca Raton, Florida: Lewis Publishers.
- Sall, J., and A. Lehman. 1996. *JMP Start Statistics: A Guide to Statistical and Data Analysis Using JMP® and JMP IN® Software*. Belmont, California: Duxbury Press.
- Scheibe T. D. and C. J. Murray. 1998. Simulation of geologic patterns: A comparison of stochastic simulation techniques for groundwater transport modeling. In *Hydrogeologic Models of Sedimentary Aquifers*, ed. G. S. Fraser and J. M. Davis, 107-118. Tulsa, Oklahoma: SEPM (Society for Sedimentary Geology).
- Scheinost, A. C., S. Abend, K. I. Pandya, and D. L. Sparks. 2001. Kinetic controls on Cu and Pb sorption by ferrihydrite. *Environmental Science & Technology* 35: 1090-1096.
- Schindler, P. W. 1990. Co-adsorption of metal ions and organic ligands: formation of ternary surface complexes. In *Mineral-Water Interface Geochemistry*. REVIEWS in MINERALOGY 23, ed. M. F. Hochella and A. F. White, 281-308. Washington, DC: Mineralogical Society of America.

- Schwarzenbach, R. P. and J. Westall. 1981. Transport of nonpolar organic compounds from surface water to groundwater: Laboratory sorption studies. *Environmental Science & Technology* 15: 1360-1367.
- Schwertmann, U. 1993. Relations between iron oxides, soil color, and soil formation. In *Soil Color*. SSSA Special Publication Number 31, ed. J. M. Bigham and E. J. Ciolkosz, 51-70. Madison, Wisconsin: Soil Science Society of America.
- Schwertmann U., and R. W. Fitzpatrick. 1992. Iron minerals in surface environments. In *Biomineralization processes of iron and manganese: modern and ancient environments*. CATENA SUPPLEMENT 21, ed. H. C. W. Skinner and R. W. Fitzpatrick, 7-30. Cremlingen-Destedt, Germany: CATENA VERLAG.
- Skinner, H. C. W., and R. W. Fitzpatrick. 1992. Iron and manganese biomineralization. In *Biomineralization processes of iron and manganese: modern and ancient environments*. CATENA SUPPLEMENT 21, ed. H. C. W. Skinner and R. W. Fitzpatrick, 1-6. Cremlingen-Destedt, Germany: CATENA VERLAG.
- Smith J. L. 1980. Spatial variability of flow parameters in a stratified sand. *Mathematical Geology* 13: 1-21.
- Sposito, G. 1990. Molecular models of ion adsorption on mineral surfaces. In *Mineral-Water Interface Geochemistry*. REVIEWS in MINERALOGY 23, ed. M. F. Hochella and A. F. White, 261-280. Washington, DC: Mineralogical Society of America.
- Sposito, G. A. 1984. *The Surface Chemistry of Soils*. New York: Oxford University Press.
- Sposito, G. A. 1989. *The Chemistry of Soils*. New York: Oxford University Press.
- Steeffel, C. I. and S. B. Yabusaki. 1996. *OS3D/GIMRT, Software for Multicomponent-Multidimensional Reactive Transport, User Manual and Programmer's Guide*. PNL-11166. Richland, Washington: Pacific Northwest National Laboratory.
- Stollenwerk, K. G. 1998. Molybdate transport in a chemically complex aquifer; Field measurements compared with solute-transport model predictions. *Water Resources Research* 34: 2727-2740.
- Strawn, D. G., A. M. Scheidegger, and D. L. Sparks. 1998. Kinetics and mechanisms of Pb(II) sorption and desorption at the aluminum oxide-water interface. *Environmental Science & Technology* 32: 2596-2601.
- Stumm, W. and J. J. Morgan. 1996. *Aquatic Chemistry*, 3rd ed. New York: John Wiley & Sons.
- Szecsody, J. E., A. Chilakapati, J. M. Zachara, and A. L. Garvin. 1998. Influence of iron oxide inclusion shape on Co<sup>III</sup>EDTA reactive transport through spatially heterogeneous sediment. *Water Resources Research* 34: 2501-2514.

- Tessier, A., F. Rapin, and R. Carignan. 1985. Trace metals in oxic lake sediments: possible adsorption onto iron oxyhydroxides. *Geochimica et Cosmochimica Acta* 49: 183-194.
- Tompson, F. B., A. L. Schafer, and R. W. Smith. 1996. Impacts of physical and chemical heterogeneity on cocontaminant transport in a sandy porous medium. *Water Resources Research* 32: 801-818.
- Tonkin, J. W., L. S. Balistrieri, and J. W. Murray. 2002. Modeling metal removal onto natural particles formed during mixing of acid rock drainage with ambient surface water. *Environmental Science & Technology* 36: 484-492.
- Torrent, J., and V. Barron. 1993. Laboratory measurement of soil color: Theory and practice. In *Soil Color*. SSSA Special Publication Number 31, ed. J. M. Bigham and E. J. Ciolkosz, 21-33. Madison, Wisconsin: Soil Science Society of America.
- Travis, C. C. and E. L. Etnier. 1981. A survey of sorption relationships for reactive solutes in soil. *Journal of Environmental Quality* 10: 8-17.
- van Genuchten, M. Th. and P. J. Wierenga. 1976. Mass-transfer studies in sorbing porous media, 1. Analytical solutions. *Soil Science Society of America Journal* 40: 473-480.
- van Genuchten, M. Th., J. M. Davidson, and P. J. Wierenga. 1974. An evaluation of kinetic and equilibrium equations for the prediction of pesticide movement through porous media. *Soil Science Society of America Proceedings* 38: 29-35.
- Wang, F., J. Chen, and W. Forsling. 1997. Modeling sorption of trace metals on natural sediments by surface complexation models. *Environmental Science & Technology* 31: 448-453.
- Webb E. K. and M. P. Anderson. 1996. Simulation of preferential flow in three-dimensional, heterogeneous conductivity fields with realistic internal architecture. *Water Resources Research* 32: 533-545.
- Wen, X., Q. Du, and H. Tang. 1998. Surface complexation model for the heavy metal adsorption on natural sediment. *Environmental Science & Technology* 32: 870-875.
- Wood, W. W. 1996. Diffusion: The source of confusion? *Ground Water* 34: 193.
- Wood, W. W., T. F. Kraemer, and P.P. Hearn, Jr. 1990. Intragranular diffusion: An important mechanism influencing solute transport in clastic aquifers? *Science* 247: 1569-1572.
- Woodbury A. D. and E. A. Sudicky. 1991. The geostatistical characteristics of the Borden aquifer. *Water Resources Research* 27: 533-546.

- Xu, N., M. F. Hochella, G. E. Brown, and G. A. Parks. 1996. Co(II) sorption at the calcite-water interface: 1. X-ray photoelectron spectroscopic study. *Geochimica et Cosmochimica Acta* 60: 2801-2815.
- Yang, J., R. Zhang, J. Wu, and M. B. Allen. 1997. Stochastic Analysis of adsorbing solute transport in three-dimensional, heterogeneous, unsaturated soils. *Water Resources Research* 33: 1947-1956.
- Zachara J. M., P. L. Glassman, S. C. Smith, and D. Taylor. 1995. Oxidation and adsorption of Co(II)EDTA<sup>2-</sup> complexes in subsurface materials with iron and manganese oxide grain coatings. *Geochimica et Cosmochimica Acta* 59: 4449-4463.
- Zasoski, R. J. and R. G. Burau. 1988. Sorption and sorptive interaction of cadmium and zinc on hydrous manganese oxide. *Soil Science Society of America Journal* 52: 81-87.
- Zheng, C. 1990. *MT3D, A modular three-dimensional transport model for simulation of advection, dispersion, and chemical reactions of contaminants in groundwater systems*. Report to the Kerr Environmental Research Laboratory. Ada, Oklahoma: U.S. Environmental Protection Agency.

## **APPENDIX A**

### **SUPPLEMENTAL INFORMATION ON MATERIALS AND METHODS**

### Scale of Observation

The decision to study physical and chemical heterogeneities at the scale of a few centimeters to a few meters was based in part on the work of Kapoor and Gelhar (1994b). They demonstrated the necessity to characterize permeability heterogeneities at a scale larger than the local dispersivity scale (i.e. larger than the millimeter scale) and much smaller than the contaminant plume scale in order to evaluate solute concentrations in aquifers.

Kapoor and Gelhar (1994a) derived a conservation equation for concentration variance in order to quantify the variability around a mean solute concentration predicted by the advection dispersion equation (ADE). Solutions to the coupled ADE and concentration variance equations show that variability in concentrations around the mean decreases with time. The rate of decrease is determined by the interaction between local dispersion and permeability heterogeneities that occur at scales between that of local dispersion and that of the plume. Local dispersivities dissipate concentration variance quickly if the permeability scale is relatively small. Conversely, the variance decreases slowly if the permeability scale is relatively large (Kapoor and Gelhar, 1994b).

Kapoor and Gelhar (1994b) also analyzed bromide concentration fluctuations in tracer test data from the USGS Cape Cod site near Falmouth, Massachusetts and found that concentration fluctuations dissipated with time. "[Their] observations at the Cape along with the theoretical results show that it is critically important to include the dissipation action of local dispersion in any realistic assessment of concentration fluctuations". The nature of the fluctuation dissipation mechanism creates the need for intensive characterization of permeability at scales ranging from centimeters to



hundreds of meters. The upper limit of this range is site-specific and depends on the spatial extent of the contaminant plume.

Heterogeneities were investigated at the low end of this scale in order to capture as much variability in the reactive properties of the media as was practical. Reactivity was studied in terms of the sediments' ability to adsorb lead ( $\text{Pb}^{2+}$ ), and (hydr)oxide grain coatings were assumed to be the dominant reactive phase. This assumption is supported by results from previous studies of cation adsorption in unconsolidated, carbon-poor sediments (Jenne, 1968; Lion et al., 1982; Tessier et al., 1985; Jackson and Inch, 1989; Fuller et al., 1996). Reconnaissance at the Deerfield site indicated the (hydr)oxide grain coatings were generally distributed in millimeter- to centimeter-wide bands. Sampling at the centimeter scale provided sufficient sediment to characterize several physical and geochemical properties, and it preserved important features of the reactive heterogeneities at the site.

### **Sampling Strategy**

The sampling program was designed to provide sufficient information to characterize the spatial variation of sediment properties at the centimeter- to meter-scale. The sampling protocol divided the total sample space into eight, one square meter units. Each 1 m<sup>2</sup> unit was further divided into 25, 20 cm x 20 cm subunits. Twelve subunits were randomly selected from each of the 8 units for a total of 96 subunits. Five points were sampled from each of the 96 subunits to yield 480 samples (Figure 3.1).

The selection of subunits, the location of the lower left sample point in each subunit, and the combination of x and y distances between the corner points in each subunit were randomly selected (Chapter 3). However, an iterative process was used to

find optimal values for: (a) the total number of sample points, (b) the total number of sampled subunits, (c) the number of sample points in each subunit, (d) the separation distances between corner points in each subunit, and (e) the threshold value for assigning separation distances. Values for (a), (b), (c), (d), and (e) were varied in the variogram program **gamv2** (Deutsch and Journel, 1998) until an optimum combination was identified. The combination of 480, 96, 5, 4 cm and 9 cm, and 0.7, for (a) through (e) respectively, was deemed best because it minimized the number of samples needed to produce variograms with at least 100 pairs of points per lag for all lags between 3 cm and 100 cm in the 0°, 30°, 60°, and 90° directions when the lag increment was no more than 10 cm.

### **Grain Coatings**

The 24 hour dithionite-citrate (DC) extraction method was selected for several reasons. First, DC extraction is common in studies of oxide grain coatings, so our values could be readily compared to those from other field sites. Second, DC dissolves hematite, goethite, ferrihydrite, lepidocrosite, and noncrystalline hydrous iron oxides as well as organically-complexed iron, and it does not attack magnetite or crystalline silicates (Ross and Wang, 1993). Consequently, it provides a reasonable estimate of the nonsilicate, nonmagnetite iron content of a sample. By contrast, sodium pyrophosphate extraction only removes organically-complexed iron, and ammonium oxalate only dissolves noncrystalline secondary iron oxides and organically-bound iron. Furthermore, ammonium oxalate dissolves considerable amounts of magnetite and finely-divided, easily weathered iron-bearing silicates. Third, DC also attacks oxides and hydroxides of manganese and aluminum. Although hydroxylamine hydrochloride (HA) is the method of choice for dissolving manganese (Chao, 1972), the method requires a

shaking, temperature-controlled water bath (which was not available), and there is no consensus in the literature regarding the proper extraction time and temperature for the dissolution of both crystalline and amorphous iron and manganese (hydr)oxides using HA.

Quality assurance/quality control practices were incorporated into the analytical program for sample extracts. Multiple method blanks and blind duplicates were included in every sample run to determine the accuracy and precision of the analyses.

### Reactivity

Preliminary batch experiments with a wide variety of sediments from the Deerfield site indicated that adsorption isotherms were linear for  $\text{Pb}^{2+}$  concentrations below 48  $\mu\text{M}$ . Therefore, one point linear isotherms were developed for 72 samples by: 1) calculating the amount of  $\text{Pb}^{2+}$  sorbed from a 10  $\mu\text{M}$   $\text{Pb}^{2+}$  solution, and 2) assuming the sample isotherms passed through the origins of the sorbed vs. equilibrium solution concentration plots. The slope of the linear isotherm for each sample was the partition coefficient, or  $K_d$  for that sample.

There is no consensus in the literature regarding the appropriate equilibration time for divalent heavy metal adsorption experiments. Coston (1995) investigated the time dependence of  $\text{Pb}^{2+}$  and  $\text{Zn}^{2+}$  adsorption onto similar sediments from the Cape Cod site and found that adsorption appeared to reach equilibrium in 48 hours. Ainsworth et al. (1994) studied the adsorption of  $\text{Co}^{2+}$ ,  $\text{Cd}^{2+}$ , and  $\text{Pb}^{2+}$  onto synthetic iron oxides by conducting batch experiments with equilibration times ranging from 16 to 96 hours, and Zachara et. al. (1995) used a 16-hour equilibration time for  $\text{Co}^{2+}$  adsorption onto naturally-occurring oxide-coated sediments. Our 24-hour equilibration time was a compromise agreed upon by myself and the members of my doctoral committee.

### **Magnetic Susceptibility**

The concentrations of ferromagnesian minerals in 71 sorption samples were estimated by magnetic susceptibility using a Frantz<sup>®</sup> Electromagnetic Separator (Hess 1959). Magnetic susceptibility was evaluated on the less than one millimeter size fraction, because the magnetic separator could not accommodate sediment grains larger than one millimeter in diameter.

Optimum separation was achieved with a 25° forward slope, a 10° side slope, and a 0.4 amp magnetic field. The relatively low, 0.4 amp setting was needed to separate muscovite from the paramagnetic fraction. However, careful inspection of the paramagnetic fraction for each of the 71 samples revealed that many contained not only primary iron-bearing minerals, but also quartz, feldspar, and muscovite grains with thick iron coatings. Since the electromagnetic separator could not isolate primary iron-bearing minerals from thickly-coated felsic minerals, the magnetic fraction was excluded from statistical analyses.

### **Surface Area**

Total sample surface area was measured using the BET method with nitrogen gas as the adsorptive (Brunauer et al., 1938). In the BET method, the adsorption of nitrogen gas at increasing partial pressures is plotted against the partial pressure of the gas to create an adsorption isotherm. Total sample surface area is derived from the isotherm parameters.

The surface areas of 43 samples were initially computed from three-point nitrogen gas adsorption isotherms. However, the quality of this data was suspect because of poor agreement between sample duplicates. Since the adsorption

isotherms often behaved poorly between the second and third data points, sample surface areas were recalculated using only the first two isotherm points. This method improved agreement between duplicate pairs (replicate measures now differed by 23 to 40 percent instead of 220 to 360 percent); nevertheless, intrasample variability was still unacceptably large.

The quality of the surface area data may have been compromised by the 0.2 to 0.4 g sample mass. Mackay et al. (1986) found that ten grams of Borden sand were required to yield accurate and precise measurements with nitrogen gas. Unfortunately, the available BET measurement apparatus could not accommodate samples larger than 0.4 g, nor could it use krypton gas which has been shown to be accurate and precise with sample masses of approximately 0.5 g (Mackay et al. 1986). Because of low measurement precision, the BET surface areas were replaced by permeability-based estimates in Chapter 2. In Chapter 4, the BET surface area of sample 5041 was used to calculate goethite surface areas for reactive transport modeling. Estimates of BET surface area for sample 5041 were identical when calculated from three point or two point isotherms.

### **Sediment Color**

Some of the unexplained variation in the extractable metal-color relationships was likely due to the influence of primary mineral color. For example, the low values and chromas in some of the low extractable Mn samples may have been caused by the presence of dark, uncoated minerals such as biotite. Additional noise may have been due to slight variations in illumination conditions. Visual estimates of soil color can be reasonably accurate and precise when the spectral quality, intensity, and angular size of the light source, the background, and the incident and viewing angles are carefully

controlled (Torrent and Barron, 1993). All of the 91 samples were viewed between 10 a.m. and 5 p.m. in the same room, at the same table, on the same background, under the same artificial lighting. Nonetheless, the light entering the room from the outside varied with the time of day and presence/absence of clouds. The extent to which these subtle variations in lighting affected color judgments is not known.

Another limitation of the color analysis is measurement precision. The Munsell Soil Color charts contain only two sheets of color chips that bracket the range of colors found in our samples (hues 10YR and 2.5Y). Moreover, these sheets only have values in integer increments. Sometimes samples with perceptibly different colors had to be assigned the same color, simply because there was an inadequate number of color chips from which to choose.

Commercially available diffuse reflectance spectrophotometers can give more accurate and precise color measurements than visual matching, provided the standards and sediment samples are carefully prepared (Torrent and Barron, 1993). However, there is no standard method for sample preparation, and the manner of preparation markedly affects sample color. For instance, grinding causes a dramatic increase in sample hue, value, and chroma, and grinding is necessary to obtain reproducible reflectance readings (Torrent and Barron, 1993). Unfortunately, grinding also reduces the influence of grain coatings on sample color, so the method may be inappropriate for studies of sediment color-grain coating relationships.

Munsell colors were also converted to the red, green, and blue (RGB) color classification system used in digital imaging in order to look for relationships between sample "redness" and DC-extractable Fe content. Software available on the Munsell web site converted the Munsell colors to RGB colors, and indicated that many 2.5Y colors have more RGB "red" in them than 10YR colors. Indeed, our two reddest looking

colors (10YR 5/6 and 10YR 5/8) contained less RGB "red" than almost every other color we assigned to our samples. Use of the RGB color system may be appropriate for hematite-dominated sediments, but the approach appears to be inappropriate when the iron-rich sediments are yellow brown.

## **APPENDIX B**

### **MAPPING AQUIFER HETEROGENEITY**



## Introduction

Numerical models of groundwater flow and solute transport require maps of the media's physical and reactive properties. These images are used as input to the mathematical models governing flow and transport. Since the exact locations of geologic boundaries, the values of hydrogeologic parameters, and the patterns of heterogeneities in natural systems are complex and ultimately unknowable, maps of these features are plagued by uncertainties. Freeze et al. (1990) categorized the uncertainties as geologic uncertainties and parameter uncertainties. Geologic uncertainties are those related to the locations of geologic boundaries such as aquifer boundaries and boundaries between stratigraphic units. Parameter uncertainties refer to uncertainties in the values of hydrogeologic parameters such as permeability and reactivity.

Both sources of uncertainty can be reduced by collecting site-specific data. Uncertainty in the values of hydrogeologic parameters can be reduced by taking direct measurements of the hydrogeologic properties themselves, or by taking measurements of geologic properties that serve as surrogates. Uncertainty in the locations of geologic boundaries can be reduced by mapping outcrop boundaries and collecting geophysical data.

Koltermann and Gorelick (1996) group the methods for creating heterogeneity maps into three categories: structure-imitating, process-imitating, and descriptive. This overview, which is based on the Kolterman and Gorelick paper, emphasizes geostatistical-based structure-imitating approaches and descriptive approaches, because at present, they are best suited to generating maps of both physical and chemical heterogeneities.

### Structure-Imitating Approach

Structure-imitating methods represent spatial patterns in subsurface hydrogeologic properties independent of the geologic processes responsible for the patterns. There are two broad categories of structure-imitating methods: those based on geostatistics, and those based on conceptual depositional models. Geostatistical methods take a probabilistic view of the system; consequently, hydrogeologic properties at every location in the modeling domain are represented by random variables. The spatial set of random variables for a given property constitutes a random field for that property. The spatial relationships between the random variables in a random field are most often described by a variogram function model (Isaaks and Srivastava 1989). The variogram function quantifies the phenomenon that data points close to one another tend to have values that are more similar than points that are further apart.

Geostatistical kriging algorithms use the sample data and the variogram model of spatial correlation to return the conditional expected value and variance of a random variable's distribution at each location in the random field (Figure B.1). Kriging methods produce a single image that is best in terms of local (point) accuracy, but they do not consider the statistical properties of the ensemble of point estimates. By contrast, geostatistical simulation algorithms return a randomly selected value from the conditional distribution function at each location, and create multiple, equally probable images of the distribution of a property (Figure B.2). Every map is identical to each other and to the original data with respect to its univariate (histogram) and bivariate (variogram) character. Since each simulated map is consistent with the known data, the model of spatial correlation estimated from the data, *and* the statistical character of the sample histogram, simulation methods provide a better representation of reality in a

holistic sense and are preferable when spatial structure is of greater importance than local accuracy.

Some kriging and simulation algorithms assume the random variables are Gaussian, while others do not have this restricting assumption. Gaussian algorithms are popular because they are relatively simple, and because log-transformed permeability and hydraulic conductivity data sets often fit a normal distribution (Freeze 1975, Smith 1980, Woodbury and Sudicky 1991). However, Gaussian algorithms are limited to a single isotropic or anisotropic variogram model. The single model of spatial continuity and the imposed Gaussian distribution shape create two limitations in Gaussian-based geostatistical methods: they only consider a single scale of heterogeneity or a self-similar (fractal) scaling of heterogeneity, and they assume a continuous spatial variation in sediment properties. As a result, they cannot preserve abrupt changes in hydrogeologic properties across geologic boundaries, and they tend to underrepresent the abundance and connectedness of extreme values in heterogeneous systems (Davis et al. 1997). Gaussian imaging methods are most appropriate for sedimentary deposits that lack discrete structures having strongly contrasting characteristics.

Non-Gaussian geostatistical methods are more flexible. They are not restricted to Gaussian distributions, they can be used with continuous or categorical variables, they provide more ways to include geologic and geophysical data, and they can accommodate multiple models of spatial continuity. Indicator kriging and simulation methods are common non-Gaussian approaches to modeling heterogeneity. The first step in an indicator approach is to subdivide the sample data into categories – for example, high, medium, and low permeability – by choosing meaningful cutoff values. Then, the sample data are transformed to indicators with respect to each cutoff by

assigning the value of one to every sample whose permeability is less than or equal to the particular cutoff value, and assigning zeros to the remaining samples. A map of the indicators and a variogram model of their spatial correlation are produced for each cutoff. And finally, the transformed sample data, indicator variograms, and nonparametric cumulative distributions are used by the kriging and simulation algorithms to construct heterogeneity maps.

Indicator methods are not restricted to hard data. They can be used with any soft information, such as rock type or sediment color, that can be subdivided into categories. Furthermore, the ability to specify nonparametric distribution functions at each unsampled location in a random field, and the ability to model the spatial continuity of each indicator category with its own variogram, enables the modeler to account for the existence and connectedness of regions having extreme values, such as high or low permeability regions that serve as preferential flow paths or barriers.

Other non-Gaussian geostatistical approaches to modeling heterogeneity include Boolean, simulated annealing, and Markov chain methods. Boolean algorithms simulate the spatial distribution of geometric objects such as clay lenses. Geologic information pertaining to the spatial arrangement of the objects – representative lens lengths, width/thickness and width/length ratios, etc. – are used to constrain the geometry of the objects and develop probabilistic rules that control their spatial distribution (Deutsch and Journel 1998). Two drawbacks of Boolean methods are: 1) the simulations are unconditional, which means they do not reproduce data values at their respective locations; and 2) they can only simulate simple shapes and hence cannot accurately reproduce facies geometries.

Simulated annealing algorithms were originally created to model magma crystallization, but more recently have been used to delineate aquifer heterogeneity

(Datta-Gupta et al. 1995). Simulated annealing uses an objective function to minimize the differences between the properties of a simulated image and the desired spatial structure. The first step in a simulated annealing approach is to generate an initial map. Hard data are assigned to their respective grid node locations, and values are assigned to the remaining nodes by sampling from the data histogram. Next, an iterative process either swaps node values that are not associated with the hard data (Deutsch and Journel 1998), or replaces these node values with other values drawn at random from the data histogram (Datta-Gupta et al. 1995). The iterative process continues until the objective function is reduced to a minimum state and the image has the desired spatial structure. The method is very flexible – flow and transport data as well as many types of geologic information can be incorporated into the objective function in order to constrain the simulations.

Markov chain simulation is similar to variogram-based Gaussian and indicator simulation; however, it incorporates statistics involving  $m$  by  $n$  points rather than pairs of points. The multivariate nature of the Markov chain approach enables it to characterize more complex geometries than can be characterized by standard bivariate Gaussian and indicator methods (Carle et al. 1998, Scheibe and Murray 1998).

One of the greatest strengths of geostatistical methods is their ability to quantify uncertainty in the value and distribution of hydrogeologic properties. One of their greatest weaknesses is their inability to model the processes of deposition, diagenesis, and structural deformation that are responsible for heterogeneity in sedimentary deposits. This weakness may manifest itself in the generation of geologically unfeasible images of heterogeneity.

Geostatistical methods comprise one of the two major groups of structure-imitating methods. The other group consists of sedimentation pattern-imitating

methods. These methods attempt to reproduce the spatial patterns and lithologies of sedimentary deposits observed in the field using rules – about sediment supplies, facies relations, subsidence rates, etc. – from conceptual depositional models. Once the arrangement and character of the sedimentary units has been simulated, hydrogeologic properties are assigned to the units. For example, permeability may be estimated for each unit from empirical equations that relate permeability to the unit's simulated grain size distribution (Webb and Anderson 1996).

An advantage of sedimentation pattern-imitating methods is they describe the subsurface distribution of hydrogeologic properties in terms of discrete geologic units based on conceptual models of depositional environments. Unfortunately, sedimentation pattern-imitating methods suffer the same limitation as geostatistical methods – i.e. they do not explicitly represent geologic processes. In addition, model inputs and hydrogeologic parameters can be difficult to estimate, and the methods cannot be conditioned to hard data (Koltermann and Gorelick 1996). Still, results can be calibrated to a field area by selecting those images from multiple model runs that best match the arrangement, geometry, and lithology of the sedimentary units at a site.

### **Process-Imitating Approach**

Unlike structure-imitating approaches, process-imitating methods generate images using mathematical models that explicitly account for the physical and chemical processes governing: fluid flow and solute transport, or sediment erosion, transport, and deposition. Methods based on the calibration of groundwater flow and solute transport models use hydraulic head, solute concentration, and solute arrival time data in conjunction with hydrogeologic property data to generate heterogeneity maps. Geologic information is incorporated in the aquifer conceptual model, and the governing

equations for flow and transport are solved to produce a close fit to observed head and concentration data. Automated calibration methods that use nonlinear least-squares regression create best fit maps of parameter values and quantify confidence limits on parameter estimates (Poeter and Hill 1996). The greatest limitation of the model calibration approach is that it generally cannot resolve small-scale heterogeneities, since head and concentration data are normally obtained from widely-spaced wells.

Geologic process models are similar to sedimentation pattern-imitating models, because they also simulate the evolution of sedimentary units. However, these models rely on mathematical relationships that describe the processes of erosion, transport, and deposition caused by wind, water, and mass movements. Some models also include equations that govern horizontal and vertical land surface motion, sea level change, and climate change. Process models are the most conceptually pleasing because they explicitly relate heterogeneity to the processes that create it. Unfortunately, they are limited by our ability to mathematically represent geologic processes, and they cannot condition simulations to measured hydrogeologic parameters.

### **Descriptive Approach**

Descriptive methods generate a single deterministic image of heterogeneity from site specific data and conceptual depositional models. Koltermann and Gorelick (1996) list four steps in the development of a descriptive heterogeneity map. First, a lithofacies map of the interpreted geology is constructed from geologic and geophysical data. Second, hydrostratigraphic units – distinct, mappable units with internally consistent hydrogeologic properties – are defined. The hydrogeologic properties within each unit may be estimated by direct methods, such as air-permeameter measurements (Davis et al. 1997), or by indirect methods such as empirical grain size-permeability relationships.

Third, a zone map of the flow domain is created by associating the facies defined in step one with the hydrostratigraphic units defined in step two. Finally, a digital map is produced by superimposing a grid on the zone map.

Descriptive methods identify the actual locations of high and low permeability or reactivity zones in contrast to probabilistic methods which simply indicate the likelihood of such features occurring at a given location in the flow system. The problem with purely descriptive approaches is the enormous amount of time and effort required to adequately characterize a site.

Every heterogeneity imaging method has limitations. Therefore, the best approaches to mapping heterogeneity are probably hybrid methods, because they can utilize a greater range of hard and soft information, and they can overcome limitations associated with individual methods.



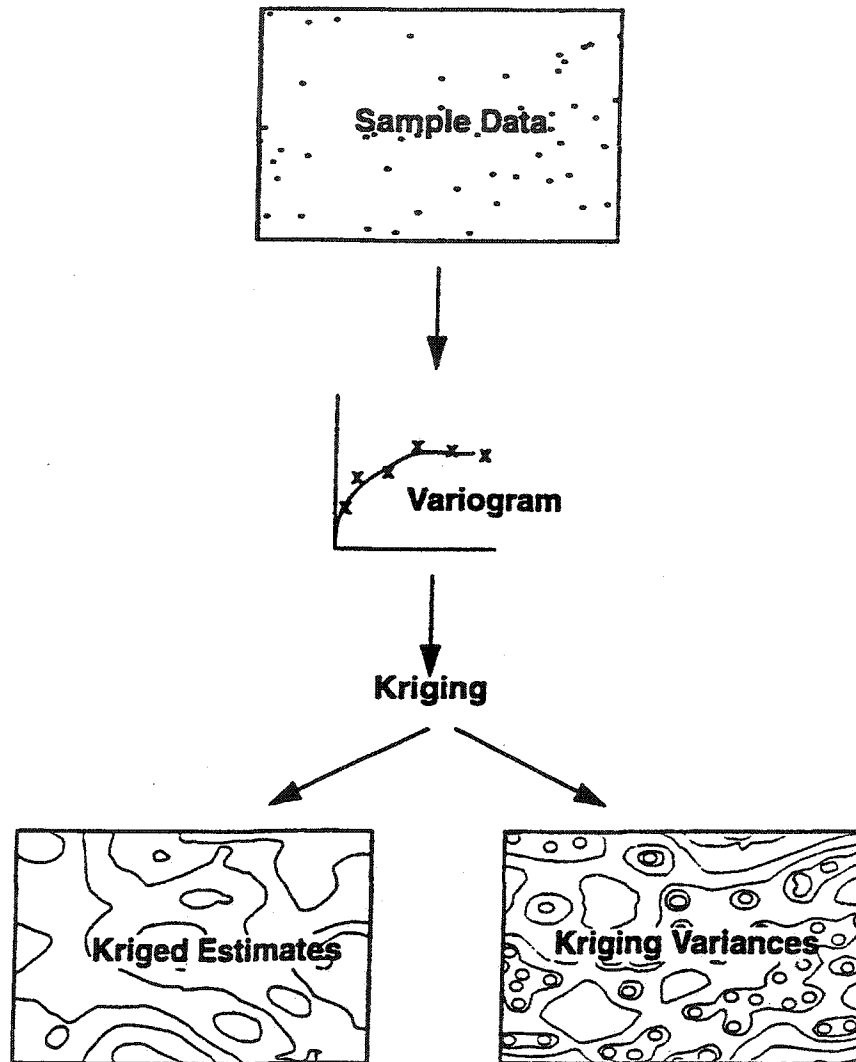


**Figure B.1** Schematic representation of the kriging approach to estimating the spatial distribution of hydrogeologic properties. *Source:* Rautmann and Istok (1996).

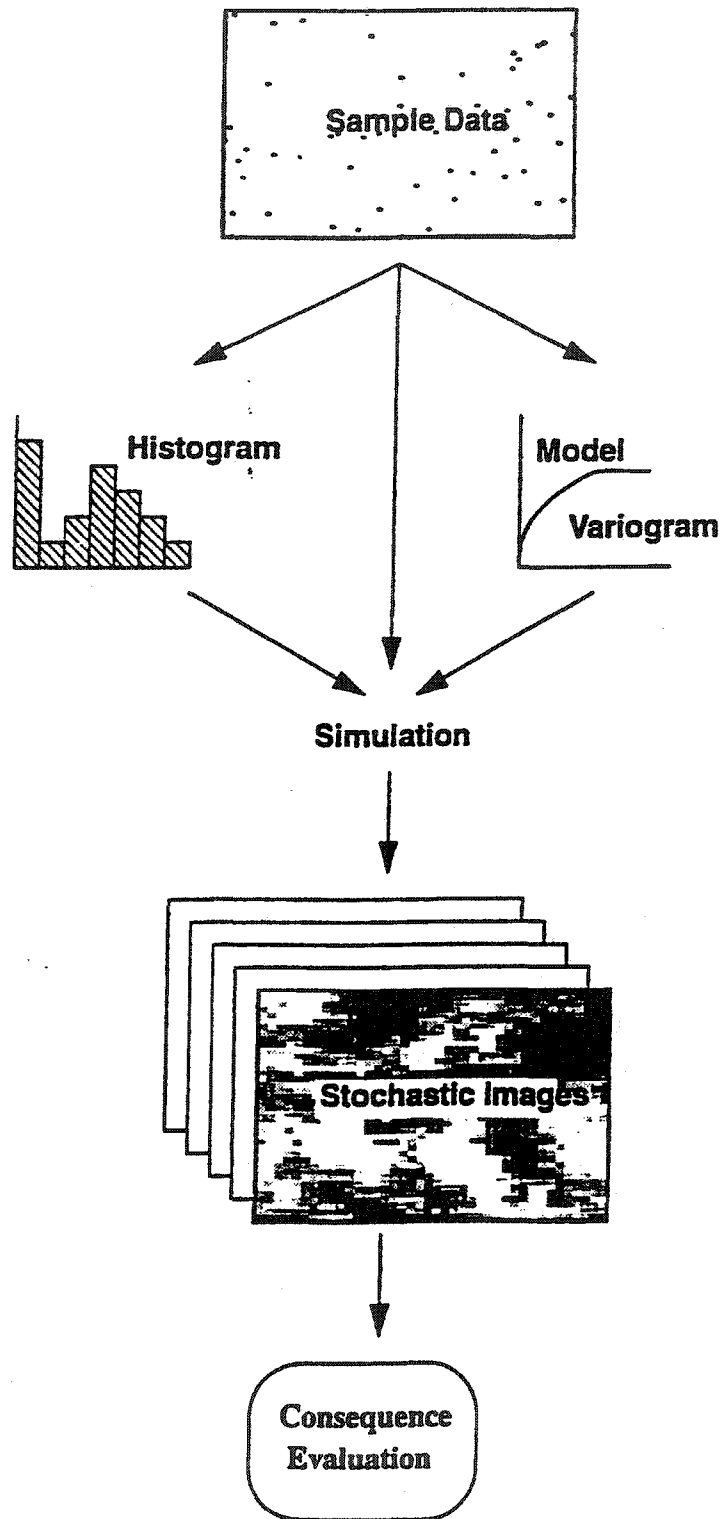


**Figure B.2** Schematic representation of the simulation approach to estimating the spatial distribution of hydrogeologic properties. *Source:* Rautmann and Istok (1996).

## **APPENDIX C**

### **SCANNING ELECTRON MICROSCOPE (SEM-EDS) RESULTS**

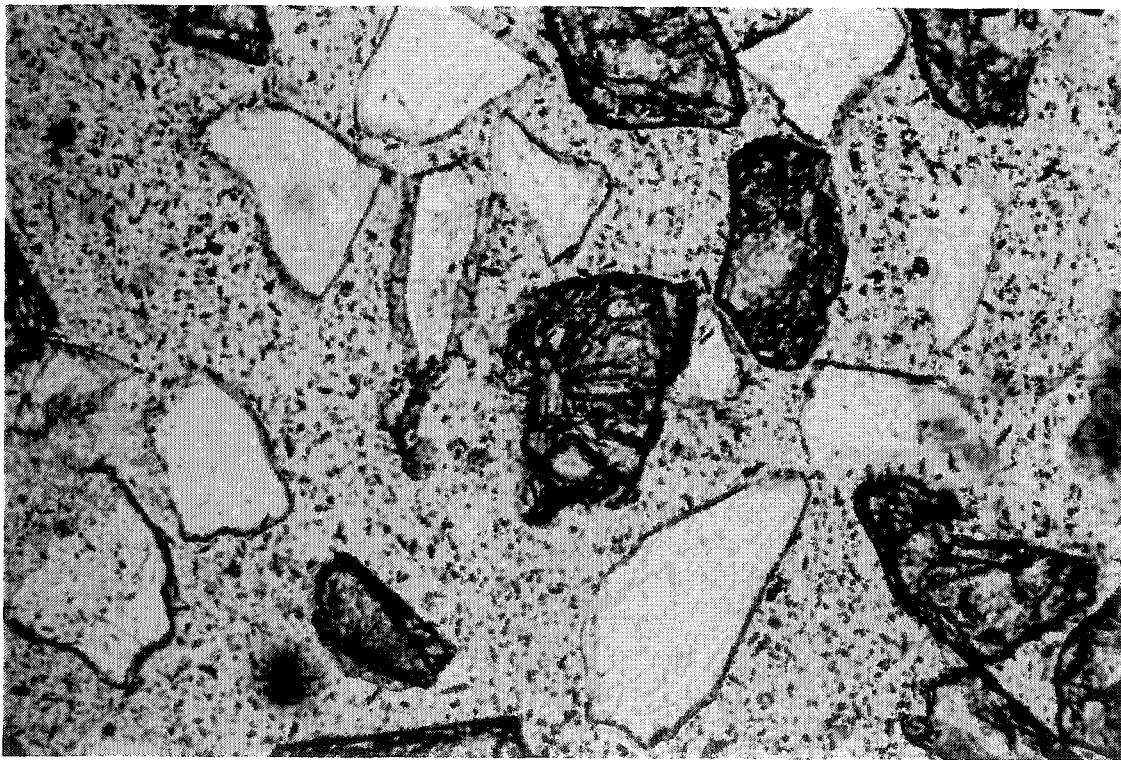
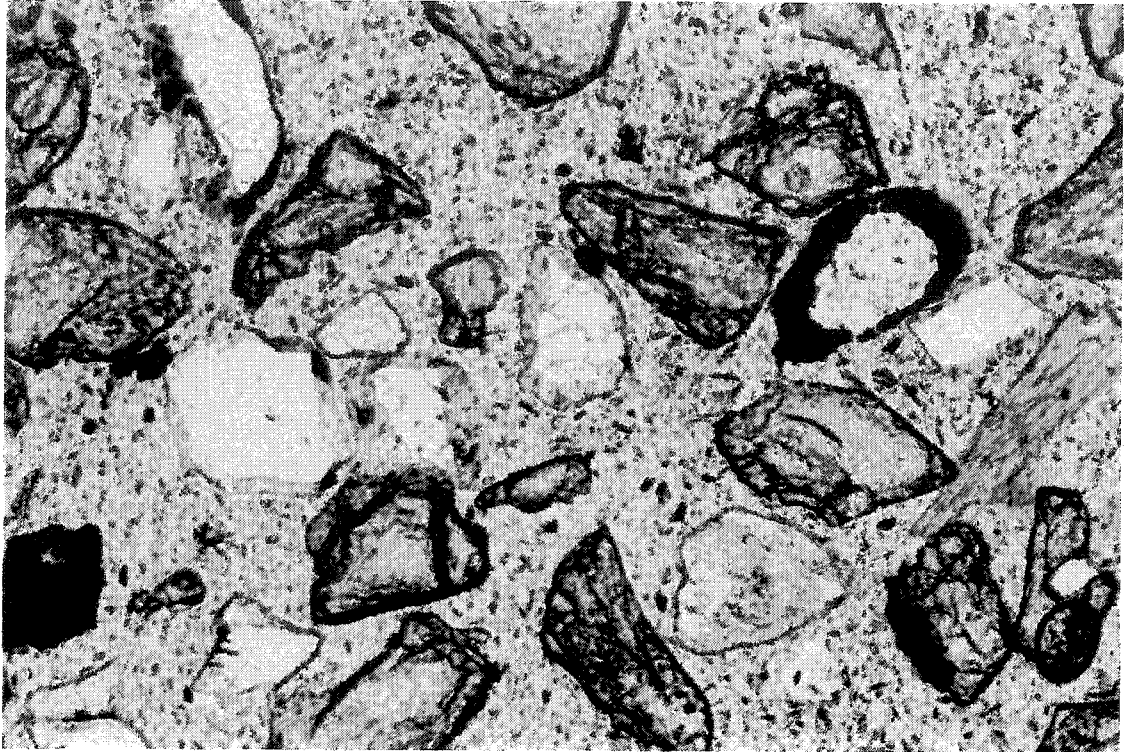


**Figure C.1** Photomicrographs of sample 4H. Note the thick, patchy (hydr)oxide coatings and the abundance of garnets (the high relief mineral). Scale: 1 in = 0.1 mm.

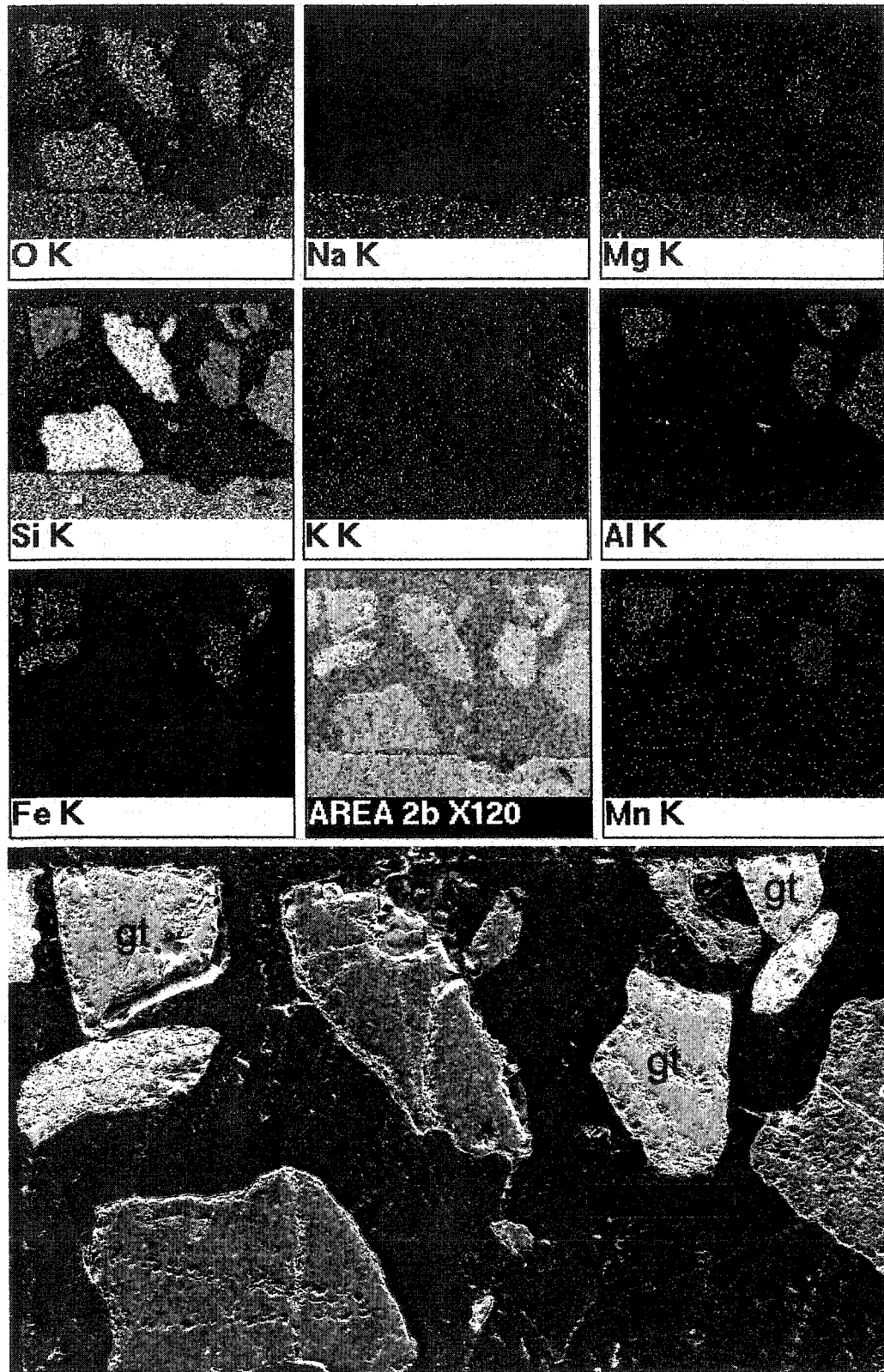


**Figure C.2** SEM images and SEM-EDS elemental analysis maps for area 2 of sample 4H. Area 2 contains three Fe- and Mn-rich garnets.

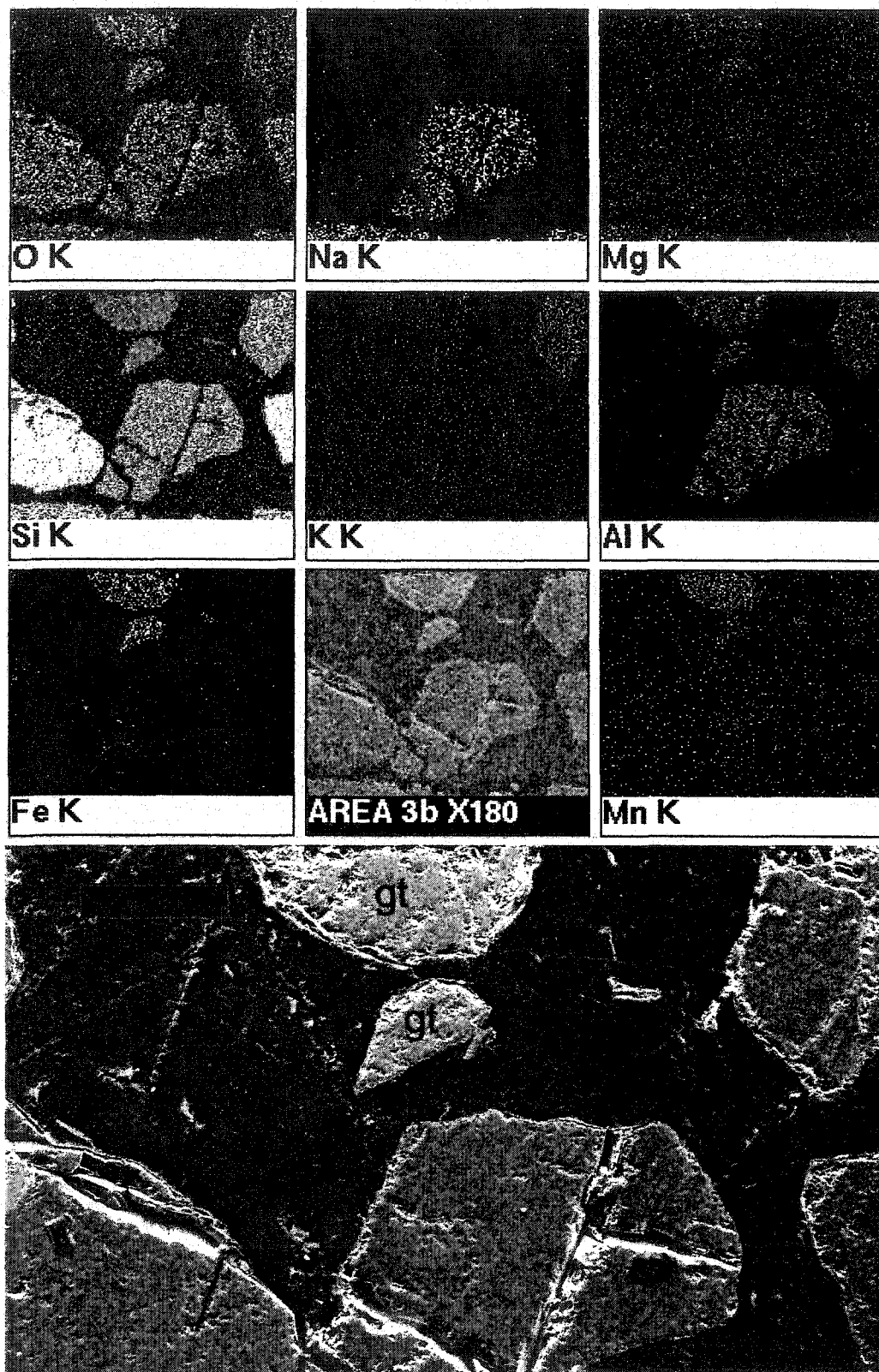


**Figure C.3** SEM images and SEM-EDS elemental analysis maps for area 3 of sample 4H. Area 3 contains two Fe- and Mn-rich garnets.

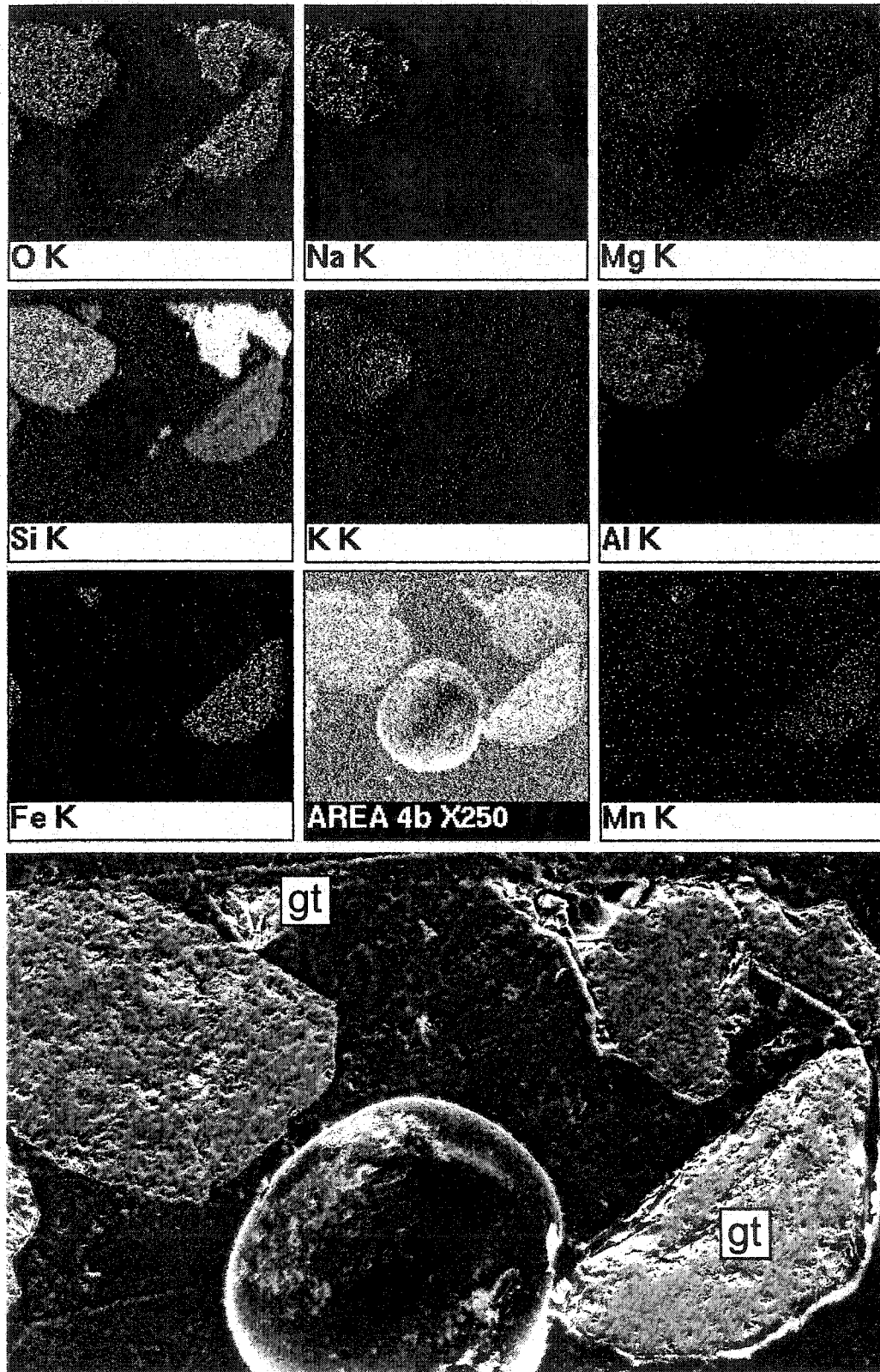


**Figure C.4** SEM images and SEM-EDS elemental analysis maps for area 4 of sample 4H. Area 4 contains two Fe- and Mn-rich garnets.



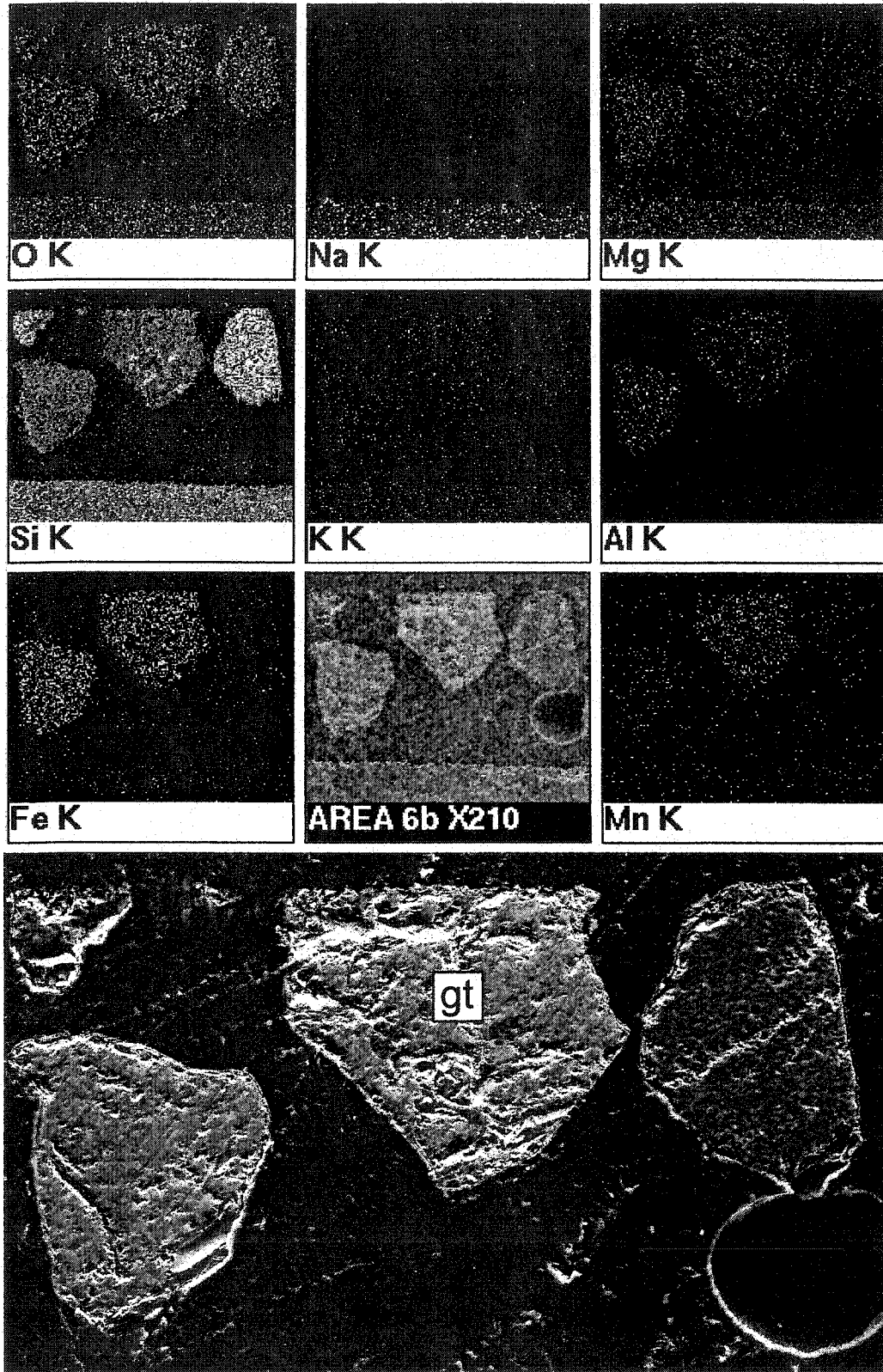


**Figure C.5** SEM images and SEM-EDS elemental analysis maps for area 6 of sample 4H. Area 6 contains one Fe- and Mn-rich garnet.



**APPENDIX D**

**DATA SUMMARY OF MEASURED SEDIMENT PROPERTIES**



**Table D.1  
Analytical Results for Measured Sediment Properties**

| Sample | X-Coordinate<br>(cm) * | Y-Coordinate<br>(cm) * | Facies | Permeability<br>(cm <sup>2</sup> ) | Porosity | Bulk Density<br>(g/cm <sup>3</sup> ) | BET Surface Area<br>(m <sup>2</sup> /g) | Magnetic Fraction<br>(wt. %) | Organic Carbon<br>(wt. %) | Inorganic Carbon<br>(wt. %) | DC-Extractable Fe<br>(µmol/g) | DC-Extractable Mn<br>(µmol/g) | DC-Extractable Al<br>(µmol/g) | K <sub>d</sub><br>(ml/g) | Hue  | Value | Chroma |
|--------|------------------------|------------------------|--------|------------------------------------|----------|--------------------------------------|---|------------------------------|---------------------------|-----------------------------|-------------------------------|-------------------------------|-------------------------------|--------------------------|------|-------|--------|
| 1053   | 310                    | 147                    | 2      | 5.26E-07                           | 0.426    | 1.52                                 | —                                       | —                            | —                         | —                           | —                             | —                             | —                             | —                        | —    | —     | —      |
| 1054   | 306                    | 152                    | 2      | 5.49E-07                           | 0.430    | 1.51                                 | —                                       | —                            | —                         | —                           | —                             | —                             | —                             | —                        | —    | —     | —      |
| 1055   | 315                    | 152                    | 2      | 5.56E-07                           | 0.437    | 1.49                                 | —                                       | —                            | —                         | —                           | —                             | —                             | —                             | —                        | —    | —     | —      |
| 1061   | 305                    | 188                    | 1      | 7.14E-07                           | 0.388    | 1.62                                 | 1.073                                   | 2.06                         | —                         | —                           | 25.79                         | 0.42                          | 3.51                          | 11.14                    | 2.5Y | 7     | 3      |
| 1062   | 309                    | 188                    | 1      | 7.18E-07                           | 0.399    | 1.59                                 | —                                       | —                            | —                         | —                           | —                             | —                             | —                             | —                        | —    | —     | —      |
| 1063   | 307                    | 192                    | 1      | 7.57E-07                           | 0.419    | 1.54                                 | —                                       | —                            | —                         | —                           | —                             | —                             | —                             | —                        | —    | —     | —      |
| 1064   | 305                    | 197                    | 1      | 3.67E-07                           | 0.417    | 1.55                                 | —                                       | —                            | —                         | —                           | —                             | —                             | —                             | —                        | —    | —     | —      |
| 1065   | 309                    | 197                    | 1      | 4.67E-07                           | 0.424    | 1.53                                 | —                                       | —                            | —                         | —                           | —                             | —                             | —                             | —                        | —    | —     | —      |
| 1071   | 362                    | 189                    | 1      | 1.04E-06                           | 0.402    | 1.58                                 | 0.599                                   | 2.40                         | —                         | —                           | 25.88                         | 0.14                          | 3.94                          | 17.12                    | 2.5Y | 7     | 3      |
| 1072   | 366                    | 189                    | 1      | 1.01E-06                           | 0.398    | 1.60                                 | —                                       | —                            | —                         | —                           | —                             | —                             | —                             | —                        | —    | —     | —      |
| 1073   | 364                    | 191                    | 1      | 7.85E-07                           | 0.411    | 1.56                                 | —                                       | —                            | —                         | —                           | —                             | —                             | —                             | —                        | —    | —     | —      |
| 1074   | 362                    | 193                    | 1      | 7.85E-07                           | 0.393    | 1.61                                 | —                                       | —                            | —                         | —                           | —                             | —                             | —                             | —                        | —    | —     | —      |
| 1075   | 366                    | 193                    | 1      | 6.95E-07                           | 0.413    | 1.56                                 | —                                       | —                            | —                         | —                           | —                             | —                             | —                             | —                        | —    | —     | —      |
| 1081   | 363                    | 108                    | 4      | 7.93E-07                           | 0.421    | 1.53                                 | —                                       | 1.94                         | —                         | —                           | 49.89                         | 0.34                          | 6.12                          | 23.19                    | 10YR | 6     | 6      |
| 1082   | 367                    | 108                    | 4      | 1.10E-06                           | 0.432    | 1.50                                 | —                                       | —                            | —                         | —                           | —                             | —                             | —                             | —                        | —    | —     | —      |
| 1083   | 365                    | 112                    | 3      | 2.48E-07                           | 0.366    | 1.68                                 | —                                       | —                            | —                         | —                           | —                             | —                             | —                             | —                        | —    | —     | —      |
| 1084   | 363                    | 117                    | 3      | 4.08E-07                           | 0.423    | 1.53                                 | —                                       | —                            | —                         | —                           | —                             | —                             | —                             | —                        | —    | —     | —      |
| 1085   | 367                    | 117                    | 3      | 3.75E-07                           | 0.431    | 1.51                                 | —                                       | —                            | —                         | —                           | —                             | —                             | —                             | —                        | —    | —     | —      |
| 1091   | 367                    | 123                    | 2      | 6.16E-07                           | 0.309    | 1.83                                 | 1.093                                   | 7.24                         | —                         | —                           | 52.57                         | 0.88                          | 8.97                          | 13.57                    | 10YR | 5     | 6      |
| 1092   | 371                    | 123                    | 2      | 6.91E-07                           | 0.325    | 1.79                                 | —                                       | —                            | —                         | —                           | —                             | —                             | —                             | —                        | —    | —     | —      |
| 1093   | 369                    | 125                    | 2      | 6.82E-07                           | 0.439    | 1.49                                 | —                                       | —                            | —                         | —                           | —                             | —                             | —                             | —                        | —    | —     | —      |
| 1094   | 367                    | 127                    | 2      | 5.51E-07                           | 0.445    | 1.47                                 | —                                       | —                            | —                         | —                           | —                             | —                             | —                             | —                        | —    | —     | —      |

**Table D.1  
Analytical Results for Measured Sediment Properties**

| Sample | X-Coordinate (cm) * | Y-Coordinate (cm) * | Facies | Permeability (cm <sup>3</sup> ) | Porosity | Bulk Density (g/cm <sup>3</sup> ) | BET Surface Area (m <sup>2</sup> /g) | Magnetic Fraction (wt. %) | Organic Carbon (wt. %) | Inorganic Carbon (wt. %) | DC-Extractable Fe (µmol/g) | DC-Extractable Mn (µmol/g) | DC-Extractable Al (µmol/g) | K <sub>d</sub> (ml/g) | Hue  | Value | Chroma |
|--------|---------------------|---------------------|--------|---------------------------------|----------|-----------------------------------|--------------------------------------|---------------------------|------------------------|--------------------------|----------------------------|----------------------------|----------------------------|-----------------------|------|-------|--------|
| 1095   | 371                 | 127                 | 2      | 5.53E-07                        | 0.444    | 1.47                              | —                                    | —                         | —                      | —                        | —                          | —                          | —                          | —                     | —    | —     | —      |
| 1101   | 365                 | 164                 | 2      | 2.20E-07                        | 0.427    | 1.52                              | 0.651                                | 2.30                      | 0.052                  | 0.0000                   | 56.51                      | 0.04                       | 6.88                       | 57.50                 | 10YR | 6     | 6      |
| 1102   | 369                 | 164                 | 2      | 2.96E-07                        | 0.414    | 1.55                              | —                                    | —                         | —                      | —                        | —                          | —                          | —                          | —                     | —    | —     | —      |
| 1103   | 367                 | 166                 | 2      | 4.60E-07                        | 0.415    | 1.55                              | —                                    | —                         | —                      | —                        | —                          | —                          | —                          | —                     | —    | —     | —      |
| 1104   | 365                 | 168                 | 2      | 3.68E-07                        | 0.415    | 1.55                              | —                                    | —                         | —                      | —                        | —                          | —                          | —                          | —                     | —    | —     | —      |
| 1105   | 369                 | 168                 | 2      | 4.61E-07                        | 0.417    | 1.55                              | —                                    | —                         | —                      | —                        | —                          | —                          | —                          | —                     | —    | —     | —      |
| 1111   | 390                 | 180                 | 1      | 1.42E-07                        | 0.445    | 1.47                              | —                                    | 3.60                      | 0.032                  | 0.0003                   | 45.66                      | 0.35                       | 6.93                       | 113.55                | 10YR | 6     | 6      |
| 1112   | 394                 | 180                 | 1      | 1.67E-07                        | 0.438    | 1.49                              | —                                    | —                         | —                      | —                        | —                          | —                          | —                          | —                     | —    | —     | —      |
| 1113   | 392                 | 185                 | 1      | 8.52E-07                        | 0.426    | 1.52                              | —                                    | —                         | —                      | —                        | —                          | —                          | —                          | —                     | —    | —     | —      |
| 1114   | 390                 | 189                 | 2      | 8.87E-07                        | 0.410    | 1.56                              | —                                    | —                         | —                      | —                        | —                          | —                          | —                          | —                     | —    | —     | —      |
| 1115   | 394                 | 189                 | 2      | 8.90E-07                        | 0.417    | 1.54                              | —                                    | —                         | —                      | —                        | —                          | —                          | —                          | —                     | —    | —     | —      |
| 1121   | 389                 | 104                 | 3      | 2.22E-06                        | 0.408    | 1.57                              | 0.481                                | 3.59                      | —                      | —                        | 30.49                      | 0.21                       | 3.42                       | 30.63                 | 2.5Y | 7     | 4      |
| 1122   | 393                 | 104                 | 3      | 1.75E-06                        | 0.388    | 1.62                              | —                                    | —                         | —                      | —                        | —                          | —                          | —                          | —                     | —    | —     | —      |
| 1123   | 391                 | 109                 | 4      | 2.01E-06                        | 0.390    | 1.62                              | —                                    | —                         | —                      | —                        | —                          | —                          | —                          | —                     | —    | —     | —      |
| 1124   | 389                 | 113                 | 4      | 3.91E-07                        | 0.425    | 1.52                              | —                                    | —                         | —                      | —                        | —                          | —                          | —                          | —                     | —    | —     | —      |
| 1125   | 393                 | 113                 | 4      | 4.49E-07                        | 0.436    | 1.49                              | —                                    | —                         | —                      | —                        | —                          | —                          | —                          | —                     | —    | —     | —      |
| 2011   | 268                 | 142                 | 2      | 6.29E-07                        | 0.433    | 1.50                              | 0.420                                | —                         | —                      | —                        | 33.15                      | 0.18                       | —                          | —                     | 2.5Y | 7     | 3      |
| 2012   | 272                 | 142                 | 2      | 7.97E-07                        | 0.439    | 1.49                              | —                                    | —                         | —                      | —                        | —                          | —                          | —                          | —                     | —    | —     | —      |
| 2013   | 270                 | 147                 | 2      | 7.72E-07                        | 0.432    | 1.51                              | —                                    | —                         | —                      | —                        | —                          | —                          | —                          | —                     | —    | —     | —      |
| 2014   | 268                 | 151                 | 2      | 1.34E-06                        | 0.454    | 1.45                              | —                                    | —                         | —                      | —                        | —                          | —                          | —                          | —                     | —    | —     | —      |
| 2015   | 272                 | 151                 | 2      | 1.10E-06                        | 0.439    | 1.49                              | —                                    | —                         | —                      | —                        | —                          | —                          | —                          | —                     | —    | —     | —      |
| 2021   | 229                 | 125                 | 2      | 1.70E-06                        | 0.427    | 1.52                              | —                                    | 3.14                      | —                      | —                        | 26.40                      | 0.84                       | 3.78                       | 8.26                  | 2.5Y | 6     | 2      |

**Table D.1  
Analytical Results for Measured Sediment Properties**

| Sample | X-Coordinate (cm) * | Y-Coordinate (cm) * | Facies | Permeability (cm <sup>2</sup> ) | Porosity | Bulk Density (g/cm <sup>3</sup> ) | BET Surface Area (m <sup>2</sup> /g) | Magnetic Fraction (wt. %) | Organic Carbon (wt. %) | Inorganic Carbon (wt. %) | DC-Extractable Fe (µmol/g) | DC-Extractable Mn (µmol/g) | DC-Extractable Al (µmol/g) | K <sub>d</sub> (ml/g) | Hue  | Value | Chroma |
|--------|---------------------|---------------------|--------|---------------------------------|----------|-----------------------------------|--------------------------------------|---------------------------|------------------------|--------------------------|----------------------------|----------------------------|----------------------------|-----------------------|------|-------|--------|
| 2022   | 233                 | 125                 | 2      | 1.65E-06                        | 0.433    | 1.50                              |                                      |                           |                        |                          |                            |                            |                            |                       |      |       |        |
| 2023   | 231                 | 127                 | 2      | 1.42E-06                        | 0.440    | 1.48                              |                                      |                           |                        |                          |                            |                            |                            |                       |      |       |        |
| 2024   | 229                 | 129                 | 2      | 1.13E-06                        | 0.425    | 1.52                              |                                      |                           |                        |                          |                            |                            |                            |                       |      |       |        |
| 2025   | 233                 | 129                 | 2      | 1.19E-06                        | 0.426    | 1.52                              |                                      |                           |                        |                          |                            |                            |                            |                       |      |       |        |
| 2031   | 285                 | 141                 | 2      | 6.44E-07                        | 0.412    | 1.56                              | 0.392                                | 3.28                      |                        |                          | 27.16                      | 0.33                       | 7.20                       | 4.90                  | 2.5Y | 7     | 3      |
| 2032   | 294                 | 141                 | 2      | 7.17E-07                        | 0.434    | 1.50                              |                                      |                           |                        |                          |                            |                            |                            |                       |      |       |        |
| 2033   | 290                 | 143                 | 2      | 8.29E-07                        | 0.435    | 1.50                              |                                      |                           |                        |                          |                            |                            |                            |                       |      |       |        |
| 2034   | 285                 | 145                 | 2      | 9.39E-07                        | 0.449    | 1.46                              |                                      |                           |                        |                          |                            |                            |                            |                       |      |       |        |
| 2035   | 294                 | 145                 | 2      | 7.92E-07                        | 0.429    | 1.51                              |                                      |                           |                        |                          |                            |                            |                            |                       |      |       |        |
| 2041   | 220                 | 187                 | 2      | 2.39E-07                        | 0.440    | 1.48                              | 0.666                                | 2.34                      |                        |                          | 38.60                      | 0.12                       | 8.98                       | 5.06                  | 2.5Y | 7     | 6      |
| 2042   | 224                 | 187                 | 2      | 2.60E-07                        | 0.436    | 1.49                              |                                      |                           |                        |                          |                            |                            |                            |                       |      |       |        |
| 2043   | 222                 | 189                 | **     | 3.26E-07                        | 0.411    | 1.56                              |                                      |                           |                        |                          |                            |                            |                            |                       |      |       |        |
| 2044   | 220                 | 191                 | 1      | 6.63E-07                        | 0.435    | 1.50                              |                                      |                           |                        |                          |                            |                            |                            |                       |      |       |        |
| 2045   | 224                 | 191                 | 1      | 5.77E-07                        | 0.434    | 1.50                              |                                      |                           |                        |                          |                            |                            |                            |                       |      |       |        |
| 2051   | 264                 | 183                 | 2      | 3.48E-07                        | 0.433    | 1.50                              |                                      | 3.33                      |                        |                          | 32.32                      | 0.16                       | 7.53                       | 4.05                  | 2.5Y | 6     | 6      |
| 2052   | 268                 | 183                 | 2      | 3.30E-07                        | 0.424    | 1.53                              |                                      |                           |                        |                          |                            |                            |                            |                       |      |       |        |
| 2053   | 266                 | 185                 | 2      | 2.28E-07                        | 0.433    | 1.50                              |                                      |                           |                        |                          |                            |                            |                            |                       |      |       |        |
| 2054   | 264                 | 187                 | 2      | 2.07E-07                        | 0.437    | 1.49                              |                                      |                           |                        |                          |                            |                            |                            |                       |      |       |        |
| 2055   | 268                 | 187                 | 2      | 2.39E-07                        | 0.482    | 1.37                              |                                      |                           |                        |                          |                            |                            |                            |                       |      |       |        |
| 2061   | 243                 | 181                 | 2      | 3.00E-07                        | 0.419    | 1.54                              |                                      | 3.04                      |                        |                          | 31.57                      | 0.18                       | 8.58                       | 4.69                  | 2.5Y | 7     | 6      |
| 2062   | 252                 | 181                 | 2      | 3.73E-07                        | 0.414    | 1.55                              |                                      |                           |                        |                          |                            |                            |                            |                       |      |       |        |
| 2063   | 247                 | 183                 | 2      | 3.38E-07                        | 0.425    | 1.52                              |                                      |                           |                        |                          |                            |                            |                            |                       |      |       |        |

**Table D.1  
Analytical Results for Measured Sediment Properties**

| Sample | X-Coordinate (cm) * | Y-Coordinate (cm) * | Facies | Permeability (cm <sup>2</sup> ) | Porosity | Bulk Density (g/cm <sup>3</sup> ) | BET Surface Area (m <sup>2</sup> /g) | Magnetic Fraction (wt. %) | Organic Carbon (wt. %) | Inorganic Carbon (wt. %) | DC-Extractable Fe (µmol/g) | DC-Extractable Mn (µmol/g) | DC-Extractable Al (µmol/g) | K <sub>d</sub> (ml/g) | Hue  | Value | Chroma |
|--------|---------------------|---------------------|--------|---------------------------------|----------|-----------------------------------|--------------------------------------|---------------------------|------------------------|--------------------------|----------------------------|----------------------------|----------------------------|-----------------------|------|-------|--------|
| 2064   | 243                 | 185                 | 1      | 4.83E-07                        | 0.436    | 1.49                              |                                      |                           |                        |                          |                            |                            |                            |                       |      |       |        |
| 2065   | 252                 | 185                 | 2      | 3.43E-07                        | 0.439    | 1.49                              |                                      |                           |                        |                          |                            |                            |                            |                       |      |       |        |
| 2071   | 247                 | 144                 | 2      | 1.13E-06                        | 0.444    | 1.47                              |                                      | 2.74                      |                        |                          | 22.40                      | 0.34                       | 4.56                       | 3.46                  | 2.5Y | 7     | 3      |
| 2072   | 251                 | 144                 | 2      | 1.14E-06                        | 0.447    | 1.47                              |                                      |                           |                        |                          |                            |                            |                            |                       |      |       |        |
| 2073   | 249                 | 146                 | 2      | 8.10E-07                        | 0.438    | 1.49                              |                                      |                           |                        |                          |                            |                            |                            |                       |      |       |        |
| 2074   | 247                 | 148                 | 2      | 5.83E-07                        | 0.443    | 1.48                              |                                      |                           |                        |                          |                            |                            |                            |                       |      |       |        |
| 2075   | 251                 | 148                 | 2      | 5.65E-07                        | 0.443    | 1.48                              |                                      |                           |                        |                          |                            |                            |                            |                       |      |       |        |
| 2081   | 227                 | 142                 | 2      | 4.71E-07                        | 0.432    | 1.50                              |                                      |                           |                        |                          | 39.47                      | 0.50                       |                            |                       | 2.5Y | 7     | 4      |
| 2082   | 231                 | 142                 | 2      | 4.76E-07                        | 0.418    | 1.54                              |                                      |                           |                        |                          |                            |                            |                            |                       |      |       |        |
| 2083   | 229                 | 144                 | 2      | 7.42E-07                        | 0.440    | 1.48                              |                                      |                           |                        |                          |                            |                            |                            |                       |      |       |        |
| 2084   | 227                 | 146                 | 2      | 7.97E-07                        | 0.447    | 1.47                              |                                      |                           |                        |                          |                            |                            |                            |                       |      |       |        |
| 2085   | 231                 | 146                 | 2      | 7.10E-07                        | 0.439    | 1.49                              |                                      |                           |                        |                          |                            |                            |                            |                       |      |       |        |
| 2091   | 265                 | 164                 | 2      | 6.55E-07                        | 0.436    | 1.50                              |                                      |                           |                        |                          | 19.86                      | 0.06                       |                            |                       | 2.5Y | 7     | 4      |
| 2092   | 269                 | 164                 | 2      | 6.37E-07                        | 0.436    | 1.49                              |                                      |                           |                        |                          |                            |                            |                            |                       |      |       |        |
| 2093   | 267                 | 166                 | 2      | 4.67E-07                        | 0.427    | 1.52                              |                                      |                           |                        |                          |                            |                            |                            |                       |      |       |        |
| 2094   | 265                 | 168                 | 2      | 3.07E-07                        | 0.443    | 1.48                              |                                      |                           |                        |                          |                            |                            |                            |                       |      |       |        |
| 2095   | 269                 | 168                 | 2      | 3.88E-07                        | 0.450    | 1.46                              |                                      |                           |                        |                          |                            |                            |                            |                       |      |       |        |
| 2101   | 204                 | 142                 | 2      | 4.53E-07                        | 0.440    | 1.48                              | 0.639                                | 3.79                      |                        |                          | 31.90                      | 0.16                       | 8.12                       | 7.09                  | 2.5Y | 6     | 6      |
| 2102   | 208                 | 142                 | 2      | 4.10E-07                        | 0.433    | 1.50                              |                                      |                           |                        |                          |                            |                            |                            |                       |      |       |        |
| 2103   | 206                 | 144                 | 2      | 4.25E-07                        | 0.447    | 1.47                              |                                      |                           |                        |                          |                            |                            |                            |                       |      |       |        |
| 2104   | 204                 | 146                 | 2      | 7.60E-07                        | 0.439    | 1.49                              |                                      |                           |                        |                          |                            |                            |                            |                       |      |       |        |
| 2105   | 208                 | 146                 | 2      | 7.48E-07                        | 0.441    | 1.48                              |                                      |                           |                        |                          |                            |                            |                            |                       |      |       |        |

**Table D.1  
Analytical Results for Measured Sediment Properties**

| Sample | X-Coordinate (cm) * | Y-Coordinate (cm) * | Facies | Permeability (cm <sup>3</sup> ) | Porosity | Bulk Density (g/cm <sup>3</sup> ) | BET Surface Area (m <sup>2</sup> /g) | Magnetic Fraction (wt. %) | Organic Carbon (wt. %) | Inorganic Carbon (wt. %) | DC-Extractable Fe (µmol/g) | DC-Extractable Mn (µmol/g) | DC-Extractable Al (µmol/g) | K <sub>d</sub> (ml/g) | Hue  | Value | Chroma |
|--------|---------------------|---------------------|--------|---------------------------------|----------|-----------------------------------|--------------------------------------|---------------------------|------------------------|--------------------------|----------------------------|----------------------------|----------------------------|-----------------------|------|-------|--------|
| 2111   | 210                 | 102                 | 4      | 6.51E-07                        | 0.445    | 1.47                              | —                                    | 2.04                      | —                      | —                        | 28.23                      | 0.88                       | 4.11                       | 14.93                 | 2.5Y | 7     | 3      |
| 2112   | 219                 | 102                 | 4      | 5.13E-07                        | 0.441    | 1.48                              | —                                    | —                         | —                      | —                        | —                          | —                          | —                          | —                     | —    | —     | —      |
| 2113   | 214                 | 104                 | 4      | 5.56E-07                        | 0.371    | 1.67                              | —                                    | —                         | —                      | —                        | —                          | —                          | —                          | —                     | —    | —     | —      |
| 2114   | 210                 | 106                 | 3      | 4.93E-07                        | 0.365    | 1.68                              | —                                    | —                         | —                      | —                        | —                          | —                          | —                          | —                     | —    | —     | —      |
| 2115   | 219                 | 106                 | 3      | 2.17E-07                        | 0.326    | 1.79                              | —                                    | —                         | —                      | —                        | —                          | —                          | —                          | —                     | —    | —     | —      |
| 2121   | 203                 | 160                 | 2      | 8.12E-07                        | 0.451    | 1.46                              | 0.494                                | 2.37                      | —                      | —                        | 28.13                      | 0.10                       | 7.65                       | 6.22                  | 2.5Y | 6     | 6      |
| 2122   | 207                 | 160                 | 2      | 7.06E-07                        | 0.441    | 1.48                              | —                                    | —                         | —                      | —                        | —                          | —                          | —                          | —                     | —    | —     | —      |
| 2123   | 205                 | 162                 | 2      | 6.69E-07                        | 0.436    | 1.49                              | —                                    | —                         | —                      | —                        | —                          | —                          | —                          | —                     | —    | —     | —      |
| 2124   | 203                 | 164                 | 2      | 9.19E-07                        | 0.439    | 1.49                              | —                                    | —                         | —                      | —                        | —                          | —                          | —                          | —                     | —    | —     | —      |
| 2125   | 207                 | 164                 | 2      | 9.85E-07                        | 0.445    | 1.47                              | —                                    | —                         | —                      | —                        | —                          | —                          | —                          | —                     | —    | —     | —      |
| 3011   | 168                 | 143                 | 2      | 3.35E-07                        | 0.417    | 1.54                              | 0.570                                | 3.36                      | —                      | —                        | 46.28                      | 0.41                       | 10.78                      | 6.63                  | 10YR | 6     | 8      |
| 3012   | 172                 | 143                 | 2      | 4.62E-07                        | 0.433    | 1.50                              | —                                    | —                         | —                      | —                        | —                          | —                          | —                          | —                     | —    | —     | —      |
| 3013   | 170                 | 148                 | 2      | 8.22E-07                        | 0.434    | 1.50                              | —                                    | —                         | —                      | —                        | —                          | —                          | —                          | —                     | —    | —     | —      |
| 3014   | 168                 | 152                 | 2      | 4.18E-07                        | 0.423    | 1.53                              | —                                    | —                         | —                      | —                        | —                          | —                          | —                          | —                     | —    | —     | —      |
| 3015   | 172                 | 152                 | 2      | 4.03E-07                        | 0.426    | 1.52                              | —                                    | —                         | —                      | —                        | —                          | —                          | —                          | —                     | —    | —     | —      |
| 3021   | 109                 | 108                 | 3      | 2.75E-07                        | 0.445    | 1.47                              | —                                    | 2.99                      | —                      | —                        | 34.87                      | 0.16                       | 8.63                       | 6.18                  | 2.5Y | 7     | 6      |
| 3022   | 118                 | 108                 | 3      | 2.50E-07                        | 0.446    | 1.47                              | —                                    | —                         | —                      | —                        | —                          | —                          | —                          | —                     | —    | —     | —      |
| 3023   | 114                 | 113                 | 3      | 2.23E-07                        | 0.422    | 1.53                              | —                                    | —                         | —                      | —                        | —                          | —                          | —                          | —                     | —    | —     | —      |
| 3024   | 109                 | 117                 | 3      | 3.53E-07                        | 0.379    | 1.64                              | —                                    | —                         | —                      | —                        | —                          | —                          | —                          | —                     | —    | —     | —      |
| 3025   | 118                 | 117                 | 3      | 3.70E-07                        | 0.406    | 1.57                              | —                                    | —                         | —                      | —                        | —                          | —                          | —                          | —                     | —    | —     | —      |
| 3031   | 121                 | 120                 | 2      | 4.26E-07                        | 0.447    | 1.47                              | 1.201                                | 3.36                      | —                      | —                        | 43.14                      | 0.38                       | 13.10                      | 5.68                  | 2.5Y | 7     | 4      |
| 3032   | 125                 | 120                 | 2      | 4.56E-07                        | 0.446    | 1.47                              | —                                    | —                         | —                      | —                        | —                          | —                          | —                          | —                     | —    | —     | —      |

**Table D.1  
Analytical Results for Measured Sediment Properties**

| Sample | X-Coordinate<br>(cm) * | Y-Coordinate<br>(cm) * | Facies | Permeability<br>(cm <sup>2</sup> ) | Porosity | Bulk Density<br>(g/cm <sup>3</sup> ) | BET Surface Area<br>(m <sup>2</sup> /g) | Magnetic Fraction<br>(wt. %) | Organic Carbon<br>(wt. %) | Inorganic Carbon<br>(wt. %) | DC-Extractable Fe<br>(µmol/g) | DC-Extractable Mn<br>(µmol/g) | DC-Extractable Al<br>(µmol/g) | K <sub>d</sub><br>(ml/g) | Hue  | Value | Chroma |
|--------|------------------------|------------------------|--------|------------------------------------|----------|--------------------------------------|---|------------------------------|---------------------------|-----------------------------|-------------------------------|-------------------------------|-------------------------------|--------------------------|------|-------|--------|
| 3033   | 123                    | 122                    | 2      | 8.26E-07                           | 0.427    | 1.52                                 |   |                              |                           |                             |                               |                               |                               |                          |      |       |        |
| 3034   | 121                    | 124                    | 2      | 1.04E-06                           | 0.440    | 1.48                                 |   |                              |                           |                             |                               |                               |                               |                          |      |       |        |
| 3035   | 125                    | 124                    | 2      | 8.18E-07                           | 0.407    | 1.57                                 |   |                              |                           |                             |                               |                               |                               |                          |      |       |        |
| 3041   | 141                    | 150                    | 2      | 8.56E-07                           | 0.430    | 1.51                                 |   | 2.60                         |                           |                             | 57.78                         | 0.19                          | 11.10                         | 6.12                     | 10YR | 6     | 8      |
| 3042   | 145                    | 150                    | 2      | 7.18E-07                           | 0.433    | 1.50                                 |   |                              |                           |                             |                               |                               |                               |                          |      |       |        |
| 3043   | 143                    | 152                    | 2      | 4.80E-07                           | 0.437    | 1.49                                 |   |                              |                           |                             |                               |                               |                               |                          |      |       |        |
| 3044   | 141                    | 154                    | 2      | 4.42E-07                           | 0.417    | 1.54                                 |   |                              |                           |                             |                               |                               |                               |                          |      |       |        |
| 3045   | 145                    | 154                    | 2      | 4.39E-07                           | 0.437    | 1.49                                 |   |                              |                           |                             |                               |                               |                               |                          |      |       |        |
| 3051   | 143                    | 103                    | 3      | 2.87E-07                           | 0.410    | 1.56                                 |   |                              |                           |                             |                               |                               |                               |                          |      |       |        |
| 3052   | 147                    | 103                    | 3      | 3.01E-07                           | 0.428    | 1.52                                 |   |                              |                           |                             |                               |                               |                               |                          |      |       |        |
| 3053   | 145                    | 105                    | 3      | 2.52E-07                           | 0.403    | 1.58                                 |   |                              |                           |                             |                               |                               |                               |                          |      |       |        |
| 3054   | 143                    | 107                    | 3      | 4.01E-07                           | 0.393    | 1.61                                 |   |                              |                           |                             |                               |                               |                               |                          |      |       |        |
| 3055   | 147                    | 107                    | 3      | 2.68E-07                           | 0.366    | 1.68                                 |   |                              |                           |                             |                               |                               |                               |                          |      |       |        |
| 3061   | 148                    | 165                    | 2      | 7.07E-07                           | 0.435    | 1.50                                 |   |                              |                           |                             | 19.19                         | 0.06                          |                               |                          | 2.5Y | 7     | 4      |
| 3062   | 152                    | 165                    | 2      | 7.41E-07                           | 0.444    | 1.47                                 |   |                              |                           |                             |                               |                               |                               |                          |      |       |        |
| 3063   | 150                    | 167                    | 2      | 4.99E-07                           | 0.429    | 1.51                                 |   |                              |                           |                             |                               |                               |                               |                          |      |       |        |
| 3064   | 148                    | 169                    | 2      | 2.44E-07                           | 0.448    | 1.46                                 |   |                              |                           |                             |                               |                               |                               |                          |      |       |        |
| 3065   | 152                    | 169                    | 2      | 3.70E-07                           | 0.434    | 1.50                                 |   |                              |                           |                             |                               |                               |                               |                          |      |       |        |
| 3071   | 184                    | 188                    | 1      | 5.65E-07                           | 0.435    | 1.50                                 |   | 2.34                         |                           |                             | 26.09                         | 0.06                          | 6.53                          | 3.87                     | 2.5Y | 7     | 4      |
| 3072   | 188                    | 188                    | 1      | 5.10E-07                           | 0.421    | 1.53                                 |   |                              |                           |                             |                               |                               |                               |                          |      |       |        |
| 3073   | 186                    | 190                    | 1      | 6.23E-07                           | 0.422    | 1.53                                 |   |                              |                           |                             |                               |                               |                               |                          |      |       |        |
| 3074   | 184                    | 192                    | 1      | 5.22E-07                           | 0.419    | 1.54                                 |   |                              |                           |                             |                               |                               |                               |                          |      |       |        |



**Table D.1  
Analytical Results for Measured Sediment Properties**

| Sample | X-Coordinate (cm) * | Y-Coordinate (cm) * | Facies | Permeability (cm <sup>2</sup> ) | Porosity | Bulk Density (g/cm <sup>3</sup> ) | BET Surface Area (m <sup>2</sup> /g) | Magnetic Fraction (wt. %) | Organic Carbon (wt. %) | Inorganic Carbon (wt. %) | DC-Extractable Fe (µmol/g) | DC-Extractable Mn (µmol/g) | DC-Extractable Al (µmol/g) | K <sub>d</sub> (ml/g) | Hue  | Value | Chroma |
|--------|---------------------|---------------------|--------|---------------------------------|----------|-----------------------------------|--------------------------------------|---------------------------|------------------------|--------------------------|----------------------------|----------------------------|----------------------------|-----------------------|------|-------|--------|
| 3075   | 188                 | 192                 | 1      | 5.31E-07                        | 0.424    | 1.53                              | —                                    | —                         | —                      | —                        | —                          | —                          | —                          | —                     | —    | —     | —      |
| 3081   | 184                 | 141                 | 2      | 5.44E-07                        | 0.444    | 1.47                              | 0.653                                | 4.65                      | —                      | —                        | 33.19                      | 0.15                       | 8.09                       | 4.76                  | 2.5Y | 6     | 6      |
| 3082   | 193                 | 141                 | 2      | 5.32E-07                        | 0.437    | 1.49                              | —                                    | —                         | —                      | —                        | —                          | —                          | —                          | —                     | —    | —     | —      |
| 3083   | 188                 | 143                 | 2      | 4.84E-07                        | 0.453    | 1.45                              | —                                    | —                         | —                      | —                        | —                          | —                          | —                          | —                     | —    | —     | —      |
| 3084   | 184                 | 145                 | 2      | 8.52E-07                        | 0.450    | 1.46                              | —                                    | —                         | —                      | —                        | —                          | —                          | —                          | —                     | —    | —     | —      |
| 3085   | 193                 | 145                 | 2      | 9.15E-07                        | 0.443    | 1.48                              | —                                    | —                         | —                      | —                        | —                          | —                          | —                          | —                     | —    | —     | —      |
| 3091   | 126                 | 149                 | 2      | 7.62E-07                        | 0.430    | 1.51                              | 0.319                                | 2.41                      | —                      | —                        | 26.69                      | 0.12                       | 7.86                       | 5.97                  | 2.5Y | 7     | 3      |
| 3092   | 130                 | 149                 | 2      | 6.05E-07                        | 0.432    | 1.51                              | —                                    | —                         | —                      | —                        | —                          | —                          | —                          | —                     | —    | —     | —      |
| 3093   | 128                 | 151                 | 2      | 6.45E-07                        | 0.450    | 1.46                              | —                                    | —                         | —                      | —                        | —                          | —                          | —                          | —                     | —    | —     | —      |
| 3094   | 126                 | 153                 | 2      | 5.11E-07                        | 0.431    | 1.51                              | —                                    | —                         | —                      | —                        | —                          | —                          | —                          | —                     | —    | —     | —      |
| 3095   | 130                 | 153                 | 2      | 5.10E-07                        | 0.431    | 1.51                              | —                                    | —                         | —                      | —                        | —                          | —                          | —                          | —                     | —    | —     | —      |
| 3101   | 105                 | 125                 | 2      | 4.22E-07                        | 0.446    | 1.47                              | —                                    | 3.99                      | —                      | —                        | 36.12                      | 0.31                       | 8.86                       | 4.77                  | 2.5Y | 7     | 4      |
| 3102   | 109                 | 125                 | 2      | 4.89E-07                        | 0.422    | 1.53                              | —                                    | —                         | —                      | —                        | —                          | —                          | —                          | —                     | —    | —     | —      |
| 3103   | 107                 | 127                 | 2      | 1.22E-06                        | 0.438    | 1.49                              | —                                    | —                         | —                      | —                        | —                          | —                          | —                          | —                     | —    | —     | —      |
| 3104   | 105                 | 129                 | 2      | 6.43E-07                        | 0.434    | 1.50                              | —                                    | —                         | —                      | —                        | —                          | —                          | —                          | —                     | —    | —     | —      |
| 3105   | 109                 | 129                 | 2      | 7.11E-07                        | 0.427    | 1.52                              | —                                    | —                         | —                      | —                        | —                          | —                          | —                          | —                     | —    | —     | —      |
| 3111   | 167                 | 110                 | 3      | 3.39E-07                        | 0.402    | 1.58                              | 0.667                                | 3.63                      | —                      | —                        | 41.17                      | 0.31                       | 9.18                       | 7.37                  | 2.5Y | 7     | 4      |
| 3112   | 171                 | 110                 | 3      | 3.56E-07                        | 0.411    | 1.56                              | —                                    | —                         | —                      | —                        | —                          | —                          | —                          | —                     | —    | —     | —      |
| 3113   | 169                 | 112                 | 3      | 3.38E-07                        | 0.413    | 1.55                              | —                                    | —                         | —                      | —                        | —                          | —                          | —                          | —                     | —    | —     | —      |
| 3114   | 167                 | 114                 | 3      | 2.41E-07                        | 0.409    | 1.57                              | —                                    | —                         | —                      | —                        | —                          | —                          | —                          | —                     | —    | —     | —      |
| 3115   | 171                 | 114                 | 3      | 2.20E-07                        | 0.429    | 1.51                              | —                                    | —                         | —                      | —                        | —                          | —                          | —                          | —                     | —    | —     | —      |
| 3121   | 161                 | 127                 | 2      | 1.05E-06                        | 0.432    | 1.51                              | 0.550                                | —                         | —                      | —                        | 26.99                      | 0.49                       | —                          | —                     | 2.5Y | 6     | 2      |

**Table D.1  
Analytical Results for Measured Sediment Properties**

| Sample | X-Coordinate<br>(cm) * | Y-Coordinate<br>(cm) * | Facies | Permeability<br>(cm <sup>2</sup> ) | Porosity | Bulk Density<br>(g/cm <sup>3</sup> ) | BET Surface Area<br>(m <sup>2</sup> /g) | Magnetic Fraction<br>(wt. %) | Organic Carbon<br>(wt. %) | Inorganic Carbon<br>(wt. %) | DC-Extractable Fe<br>(µmol/g) | DC-Extractable Mn<br>(µmol/g) | DC-Extractable Al<br>(µmol/g) | K <sub>d</sub><br>(ml/g) | Hue  | Value | Chroma |
|--------|------------------------|------------------------|--------|------------------------------------|----------|--------------------------------------|---|------------------------------|---------------------------|-----------------------------|-------------------------------|-------------------------------|-------------------------------|--------------------------|------|-------|--------|
| 3122   | 165                    | 127                    | 2      | 1.11E-06                           | 0.433    | 1.50                                 | —                                       | —                            | —                         | —                           | —                             | —                             | —                             | —                        | —    | —     | —      |
| 3123   | 163                    | 132                    | 2      | 8.41E-07                           | 0.434    | 1.50                                 | —                                       | —                            | —                         | —                           | —                             | —                             | —                             | —                        | —    | —     | —      |
| 3124   | 161                    | 136                    | 2      | 7.58E-07                           | 0.431    | 1.51                                 | —                                       | —                            | —                         | —                           | —                             | —                             | —                             | —                        | —    | —     | —      |
| 3125   | 165                    | 136                    | 2      | 8.52E-07                           | 0.450    | 1.46                                 | —                                       | —                            | —                         | —                           | —                             | —                             | —                             | —                        | —    | —     | —      |
| 4011   | 50                     | 110                    | 3      | 2.54E-07                           | 0.424    | 1.53                                 | —                                       | 4.52                         | 0.041                     | 0.0001                      | 48.58                         | 0.36                          | 10.02                         | 5.64                     | 10YR | 6     | 8      |
| 4012   | 54                     | 110                    | 3      | 3.76E-07                           | 0.446    | 1.47                                 | —                                       | —                            | —                         | —                           | —                             | —                             | —                             | —                        | —    | —     | —      |
| 4013   | 52                     | 112                    | 3      | 2.67E-07                           | 0.434    | 1.50                                 | —                                       | —                            | —                         | —                           | —                             | —                             | —                             | —                        | —    | —     | —      |
| 4014   | 50                     | 114                    | 3      | 3.96E-07                           | 0.435    | 1.50                                 | —                                       | —                            | —                         | —                           | —                             | —                             | —                             | —                        | —    | —     | —      |
| 4015   | 54                     | 114                    | 3      | 4.36E-07                           | 0.429    | 1.51                                 | —                                       | —                            | —                         | —                           | —                             | —                             | —                             | —                        | —    | —     | —      |
| 4021   | 4                      | 147                    | 2      | 5.24E-07                           | 0.444    | 1.47                                 | —                                       | —                            | —                         | —                           | 45.47                         | 0.18                          | —                             | —                        | 10YR | 6     | 6      |
| 4022   | 8                      | 147                    | 2      | 4.85E-07                           | 0.433    | 1.50                                 | —                                       | —                            | —                         | —                           | —                             | —                             | —                             | —                        | —    | —     | —      |
| 4023   | 6                      | 149                    | 2      | 2.62E-07                           | 0.444    | 1.47                                 | —                                       | —                            | —                         | —                           | —                             | —                             | —                             | —                        | —    | —     | —      |
| 4024   | 4                      | 151                    | 2      | 1.44E-07                           | 0.526    | 1.26                                 | —                                       | —                            | —                         | —                           | —                             | —                             | —                             | —                        | —    | —     | —      |
| 4025   | 8                      | 151                    | 2      | 1.61E-07                           | 0.497    | 1.33                                 | —                                       | —                            | —                         | —                           | —                             | —                             | —                             | —                        | —    | —     | —      |
| 4031   | 80                     | 122                    | 2      | 3.58E-07                           | 0.442    | 1.48                                 | —                                       | —                            | —                         | —                           | —                             | —                             | —                             | —                        | —    | —     | —      |
| 4032   | 84                     | 122                    | 2      | 3.68E-07                           | 0.443    | 1.48                                 | —                                       | —                            | —                         | —                           | —                             | —                             | —                             | —                        | —    | —     | —      |
| 4033   | 82                     | 124                    | 2      | 3.94E-07                           | 0.452    | 1.45                                 | —                                       | —                            | —                         | —                           | —                             | —                             | —                             | —                        | —    | —     | —      |
| 4034   | 80                     | 126                    | 2      | 7.26E-07                           | 0.438    | 1.49                                 | —                                       | —                            | —                         | —                           | —                             | —                             | —                             | —                        | —    | —     | —      |
| 4035   | 84                     | 126                    | 2      | 8.97E-07                           | 0.442    | 1.48                                 | —                                       | —                            | —                         | —                           | —                             | —                             | —                             | —                        | —    | —     | —      |
| 4041   | 80                     | 190                    | 1      | 2.48E-07                           | 0.450    | 1.46                                 | 0.669                                   | 4.35                         | —                         | —                           | 34.76                         | 0.10                          | 7.76                          | 6.26                     | 2.5Y | 6     | 6      |
| 4042   | 84                     | 190                    | 1      | 2.56E-07                           | 0.444    | 1.47                                 | —                                       | —                            | —                         | —                           | —                             | —                             | —                             | —                        | —    | —     | —      |
| 4043   | 82                     | 194                    | 1      | 3.14E-07                           | 0.452    | 1.45                                 | —                                       | —                            | —                         | —                           | —                             | —                             | —                             | —                        | —    | —     | —      |

**Table D.1  
Analytical Results for Measured Sediment Properties**

| Sample | X-Coordinate (cm) * | Y-Coordinate (cm) * | Facies | Permeability (cm <sup>2</sup> ) | Porosity | Bulk Density (g/cm <sup>3</sup> ) | BET Surface Area (m <sup>2</sup> /g) | Magnetic Fraction (wt. %) | Organic Carbon (wt. %) | Inorganic Carbon (wt. %) | DC-Extractable Fe (µmol/g) | DC-Extractable Mn (µmol/g) | DC-Extractable Al (µmol/g) | K <sub>d</sub> (ml/g) | Hue  | Value | Chroma |
|--------|---------------------|---------------------|--------|---------------------------------|----------|-----------------------------------|--------------------------------------|---------------------------|------------------------|--------------------------|----------------------------|----------------------------|----------------------------|-----------------------|------|-------|--------|
| 4044   | 80                  | 199                 | 1      | 2.83E-07                        | 0.445    | 1.47                              |                                      |                           |                        |                          |                            |                            |                            |                       |      |       |        |
| 4045   | 84                  | 199                 | 1      | 3.40E-07                        | 0.460    | 1.43                              |                                      |                           |                        |                          |                            |                            |                            |                       |      |       |        |
| 4051   | 1                   | 182                 | 1      | 2.73E-07                        | 0.435    | 1.50                              |                                      | 6.99                      |                        |                          | 54.01                      | 0.22                       | 11.95                      | 5.85                  | 10YR | 6     | 6      |
| 4052   | 5                   | 182                 | 1      | 2.51E-07                        | 0.439    | 1.49                              |                                      |                           |                        |                          |                            |                            |                            |                       |      |       |        |
| 4053   | 3                   | 186                 | 1      | 3.18E-07                        | 0.456    | 1.44                              |                                      |                           |                        |                          |                            |                            |                            |                       |      |       |        |
| 4054   | 1                   | 191                 | 1      | 3.26E-07                        | 0.458    | 1.44                              |                                      |                           |                        |                          |                            |                            |                            |                       |      |       |        |
| 4055   | 5                   | 191                 | 1      | 3.22E-07                        | 0.464    | 1.42                              |                                      |                           |                        |                          |                            |                            |                            |                       |      |       |        |
| 4061   | 67                  | 169                 | 2      | 3.90E-07                        | 0.460    | 1.43                              | 0.536                                |                           |                        |                          | 34.98                      | 0.08                       |                            |                       | 2.5Y | 7     | 6      |
| 4062   | 71                  | 169                 | 2      | 2.01E-07                        | 0.452    | 1.45                              |                                      |                           |                        |                          |                            |                            |                            |                       |      |       |        |
| 4063   | 69                  | 171                 | 2      | 3.22E-07                        | 0.443    | 1.48                              |                                      |                           |                        |                          |                            |                            |                            |                       |      |       |        |
| 4064   | 67                  | 173                 | 2      | 3.14E-07                        | 0.433    | 1.50                              |                                      |                           |                        |                          |                            |                            |                            |                       |      |       |        |
| 4065   | 71                  | 173                 | 2      | 3.26E-07                        | 0.431    | 1.51                              |                                      |                           |                        |                          |                            |                            |                            |                       |      |       |        |
| 4071   | 26                  | 161                 | 2      | 2.63E-07                        | 0.472    | 1.40                              |                                      |                           |                        |                          | 32.25                      | 0.07                       |                            |                       | 2.5Y | 7     | 6      |
| 4072   | 30                  | 161                 | 2      | 2.03E-07                        | 0.467    | 1.41                              |                                      |                           |                        |                          |                            |                            |                            |                       |      |       |        |
| 4073   | 28                  | 166                 | 2      | 4.84E-07                        | 0.464    | 1.42                              |                                      |                           |                        |                          |                            |                            |                            |                       |      |       |        |
| 4074   | 26                  | 170                 | 2      | 1.89E-07                        | 0.465    | 1.42                              |                                      |                           |                        |                          |                            |                            |                            |                       |      |       |        |
| 4075   | 30                  | 170                 | 2      | 2.05E-07                        | 0.470    | 1.40                              |                                      |                           |                        |                          |                            |                            |                            |                       |      |       |        |
| 4081   | 84                  | 163                 | 2      | 4.07E-07                        | 0.456    | 1.44                              |                                      |                           |                        |                          | 30.77                      | 0.07                       |                            |                       | 2.5Y | 6     | 6      |
| 4082   | 88                  | 163                 | 2      | 6.99E-07                        | 0.455    | 1.44                              |                                      |                           |                        |                          |                            |                            |                            |                       |      |       |        |
| 4083   | 86                  | 165                 | 2      | 1.69E-07                        | 0.469    | 1.41                              |                                      |                           |                        |                          |                            |                            |                            |                       |      |       |        |
| 4084   | 84                  | 167                 | 2      | 1.60E-07                        | 0.472    | 1.40                              |                                      |                           |                        |                          |                            |                            |                            |                       |      |       |        |
| 4085   | 88                  | 167                 | 2      | 1.45E-07                        | 0.474    | 1.39                              |                                      |                           |                        |                          |                            |                            |                            |                       |      |       |        |

**Table D.1  
Analytical Results for Measured Sediment Properties**

| Sample | X-Coordinate<br>(cm) * | Y-Coordinate<br>(cm) * | Facies | Permeability<br>(cm <sup>3</sup> ) | Porosity | Bulk Density<br>(g/cm <sup>3</sup> ) | BET Surface Area<br>(m <sup>2</sup> /g) | Magnetic Fraction<br>(wt. %) | Organic Carbon<br>(wt. %) | Inorganic Carbon<br>(wt. %) | DC-Extractable Fe<br>(µmol/g) | DC-Extractable Mn<br>(µmol/g) | DC-Extractable Al<br>(µmol/g) | K <sub>d</sub><br>(ml/g) | Hue  | Value | Chroma |
|--------|------------------------|------------------------|--------|------------------------------------|----------|--------------------------------------|---|------------------------------|---------------------------|-----------------------------|-------------------------------|-------------------------------|-------------------------------|--------------------------|------|-------|--------|
| 4091   | 29                     | 142                    | 2      | 1.51E-07                           | 0.474    | 1.39                                 | 0.816                                   | 3.20                         | —                         | —                           | 32.52                         | 0.13                          | 9.73                          | 8.52                     | 2.5Y | 7     | 4      |
| 4092   | 33                     | 142                    | 2      | 1.97E-07                           | 0.481    | 1.38                                 | —                                       | —                            | —                         | —                           | —                             | —                             | —                             | —                        | —    | —     | —      |
| 4093   | 31                     | 144                    | 2      | 3.74E-07                           | 0.411    | 1.56                                 | —                                       | —                            | —                         | —                           | —                             | —                             | —                             | —                        | —    | —     | —      |
| 4094   | 29                     | 146                    | 2      | 4.09E-07                           | 0.434    | 1.50                                 | —                                       | —                            | —                         | —                           | —                             | —                             | —                             | —                        | —    | —     | —      |
| 4095   | 33                     | 146                    | 2      | 3.89E-07                           | 0.449    | 1.46                                 | —                                       | —                            | —                         | —                           | —                             | —                             | —                             | —                        | —    | —     | —      |
| 4101   | 47                     | 181                    | 1      | 2.69E-07                           | 0.430    | 1.51                                 | 0.857                                   | 2.61                         | —                         | —                           | 30.07                         | 0.13                          | 8.61                          | 6.94                     | 2.5Y | 7     | 6      |
| 4102   | 56                     | 181                    | 1      | 3.87E-07                           | 0.441    | 1.48                                 | —                                       | —                            | —                         | —                           | —                             | —                             | —                             | —                        | —    | —     | —      |
| 4103   | 51                     | 183                    | 1      | 2.39E-07                           | 0.426    | 1.52                                 | —                                       | —                            | —                         | —                           | —                             | —                             | —                             | —                        | —    | —     | —      |
| 4104   | 47                     | 185                    | 1      | 2.71E-07                           | 0.442    | 1.48                                 | —                                       | —                            | —                         | —                           | —                             | —                             | —                             | —                        | —    | —     | —      |
| 4105   | 56                     | 185                    | 1      | 2.57E-07                           | 0.434    | 1.50                                 | —                                       | —                            | —                         | —                           | —                             | —                             | —                             | —                        | —    | —     | —      |
| 4111   | 26                     | 189                    | 1      | 2.64E-07                           | 0.456    | 1.44                                 | 0.735                                   | 3.67                         | —                         | —                           | 37.38                         | 0.17                          | 11.73                         | 6.36                     | 2.5Y | 6     | 6      |
| 4112   | 30                     | 189                    | 1      | 2.87E-07                           | 0.452    | 1.45                                 | —                                       | —                            | —                         | —                           | —                             | —                             | —                             | —                        | —    | —     | —      |
| 4113   | 28                     | 193                    | 1      | 2.91E-07                           | 0.440    | 1.48                                 | —                                       | —                            | —                         | —                           | —                             | —                             | —                             | —                        | —    | —     | —      |
| 4114   | 26                     | 198                    | 1      | 4.12E-07                           | 0.476    | 1.39                                 | —                                       | —                            | —                         | —                           | —                             | —                             | —                             | —                        | —    | —     | —      |
| 4115   | 30                     | 198                    | 1      | 3.47E-07                           | 0.461    | 1.43                                 | —                                       | —                            | —                         | —                           | —                             | —                             | —                             | —                        | —    | —     | —      |
| 4121   | 41                     | 145                    | 2      | 4.98E-07                           | 0.437    | 1.49                                 | 2.210                                   | 3.28                         | —                         | —                           | 45.14                         | 0.25                          | 10.25                         | 10.06                    | 2.5Y | 6     | 6      |
| 4122   | 45                     | 145                    | 2      | 4.62E-07                           | 0.433    | 1.50                                 | —                                       | —                            | —                         | —                           | —                             | —                             | —                             | —                        | —    | —     | —      |
| 4123   | 43                     | 147                    | 2      | 3.77E-07                           | 0.447    | 1.47                                 | —                                       | —                            | —                         | —                           | —                             | —                             | —                             | —                        | —    | —     | —      |
| 4124   | 41                     | 149                    | 2      | 5.08E-07                           | 0.430    | 1.51                                 | —                                       | —                            | —                         | —                           | —                             | —                             | —                             | —                        | —    | —     | —      |
| 4125   | 45                     | 149                    | 2      | 4.61E-07                           | 0.418    | 1.54                                 | —                                       | —                            | —                         | —                           | —                             | —                             | —                             | —                        | —    | —     | —      |
| 5011   | 108                    | 60                     | 4      | 6.59E-07                           | 0.432    | 1.51                                 | 0.798                                   | —                            | —                         | —                           | 22.60                         | 0.19                          | —                             | —                        | 2.5Y | 7     | 3      |
| 5012   | 112                    | 60                     | 4      | 6.72E-07                           | 0.441    | 1.48                                 | —                                       | —                            | —                         | —                           | —                             | —                             | —                             | —                        | —    | —     | —      |

**Table D.1  
Analytical Results for Measured Sediment Properties**

| Sample | X-Coordinate (cm) * | Y-Coordinate (cm) * | Facies | Permeability (cm <sup>2</sup> ) | Porosity | Bulk Density (g/cm <sup>3</sup> ) | BET Surface Area (m <sup>2</sup> /g) | Magnetic Fraction (wt. %) | Organic Carbon (wt. %) | Inorganic Carbon (wt. %) | DC-Extractable Fe (µmol/g) | DC-Extractable Mn (µmol/g) | DC-Extractable Al (µmol/g) | K <sub>d</sub> (ml/g) | Hue  | Value | Chroma |
|--------|---------------------|---------------------|--------|---------------------------------|----------|-----------------------------------|--------------------------------------|---------------------------|------------------------|--------------------------|----------------------------|----------------------------|----------------------------|-----------------------|------|-------|--------|
| 5013   | 110                 | 62                  | 4      | 6.88E-07                        | 0.430    | 1.51                              | —                                    | —                         | —                      | —                        | —                          | —                          | —                          | —                     | —    | —     | —      |
| 5014   | 108                 | 64                  | 4      | 7.53E-07                        | 0.438    | 1.49                              | —                                    | —                         | —                      | —                        | —                          | —                          | —                          | —                     | —    | —     | —      |
| 5015   | 112                 | 64                  | 4      | 8.90E-07                        | 0.448    | 1.46                              | —                                    | —                         | —                      | —                        | —                          | —                          | —                          | —                     | —    | —     | —      |
| 5021   | 107                 | 85                  | 3      | 4.04E-07                        | 0.414    | 1.55                              | —                                    | 4.20                      | —                      | —                        | 42.23                      | 0.36                       | 10.08                      | 7.32                  | 10YR | 6     | 6      |
| 5022   | 111                 | 85                  | 3      | 2.93E-07                        | 0.406    | 1.57                              | —                                    | —                         | —                      | —                        | —                          | —                          | —                          | —                     | —    | —     | —      |
| 5023   | 109                 | 87                  | 3      | 3.45E-07                        | 0.398    | 1.60                              | —                                    | —                         | —                      | —                        | —                          | —                          | —                          | —                     | —    | —     | —      |
| 5024   | 107                 | 89                  | 3      | 3.20E-07                        | 0.438    | 1.49                              | —                                    | —                         | —                      | —                        | —                          | —                          | —                          | —                     | —    | —     | —      |
| 5025   | 111                 | 89                  | 3      | 2.99E-07                        | 0.423    | 1.53                              | —                                    | —                         | —                      | —                        | —                          | —                          | —                          | —                     | —    | —     | —      |
| 5031   | 189                 | 60                  | 4      | 7.36E-07                        | 0.444    | 1.47                              | —                                    | 2.10                      | —                      | —                        | 28.51                      | 0.10                       | 7.00                       | 4.82                  | 2.5Y | 7     | 4      |
| 5032   | 198                 | 60                  | 4      | 8.17E-07                        | 0.430    | 1.51                              | —                                    | —                         | —                      | —                        | —                          | —                          | —                          | —                     | —    | —     | —      |
| 5033   | 194                 | 65                  | 4      | 6.88E-07                        | 0.426    | 1.52                              | —                                    | —                         | —                      | —                        | —                          | —                          | —                          | —                     | —    | —     | —      |
| 5034   | 189                 | 69                  | 4      | 5.35E-07                        | 0.416    | 1.55                              | —                                    | —                         | —                      | —                        | —                          | —                          | —                          | —                     | —    | —     | —      |
| 5035   | 198                 | 69                  | 4      | 6.56E-07                        | 0.447    | 1.47                              | —                                    | —                         | —                      | —                        | —                          | —                          | —                          | —                     | —    | —     | —      |
| 5041   | 120                 | 81                  | 4      | 4.71E-07                        | 0.376    | 1.65                              | 2.249                                | 34.04                     | —                      | —                        | 170.2                      | 2.88                       | 22.62                      | 11.89                 | 10YR | 5     | 6      |
| 5042   | 124                 | 81                  | 4      | 4.94E-07                        | 0.402    | 1.59                              | —                                    | —                         | —                      | —                        | —                          | —                          | —                          | —                     | —    | —     | —      |
| 5043   | 122                 | 83                  | 3      | 3.16E-07                        | 0.432    | 1.51                              | —                                    | —                         | —                      | —                        | —                          | —                          | —                          | —                     | —    | —     | —      |
| 5044   | 120                 | 85                  | 3      | 3.39E-07                        | 0.365    | 1.68                              | —                                    | —                         | —                      | —                        | —                          | —                          | —                          | —                     | —    | —     | —      |
| 5045   | 124                 | 85                  | 3      | 3.50E-07                        | 0.321    | 1.80                              | —                                    | —                         | —                      | —                        | —                          | —                          | —                          | —                     | —    | —     | —      |
| 5051   | 167                 | 85                  | 4      | 4.99E-07                        | 0.415    | 1.55                              | —                                    | 6.20                      | —                      | —                        | 42.74                      | 0.63                       | 10.44                      | 13.72                 | 10YR | 6     | 4      |
| 5052   | 171                 | 85                  | 4      | 5.84E-07                        | 0.486    | 1.36                              | —                                    | —                         | —                      | —                        | —                          | —                          | —                          | —                     | —    | —     | —      |
| 5053   | 169                 | 87                  | 4      | 9.96E-07                        | 0.471    | 1.40                              | —                                    | —                         | —                      | —                        | —                          | —                          | —                          | —                     | —    | —     | —      |
| 5054   | 167                 | 89                  | 4      | 9.86E-07                        | 0.444    | 1.47                              | —                                    | —                         | —                      | —                        | —                          | —                          | —                          | —                     | —    | —     | —      |

**Table D.1  
Analytical Results for Measured Sediment Properties**

| Sample | X-Coordinate (cm) * | Y-Coordinate (cm) * | Facies | Permeability (cm <sup>2</sup> ) | Porosity | Bulk Density (g/cm <sup>3</sup> ) | BET Surface Area (m <sup>2</sup> /g) | Magnetic Fraction (wt. %) | Organic Carbon (wt. %) | Inorganic Carbon (wt. %) | DC-Extractable Fe (µmol/g) | DC-Extractable Mn (µmol/g) | DC-Extractable Al (µmol/g) | K <sub>d</sub> (ml/g) | Hue  | Value | Chroma |
|--------|---------------------|---------------------|--------|---------------------------------|----------|-----------------------------------|--------------------------------------|---------------------------|------------------------|--------------------------|----------------------------|----------------------------|----------------------------|-----------------------|------|-------|--------|
| 5055   | 171                 | 89                  | 4      | 1.10E-06                        | 0.464    | 1.42                              | —                                    | —                         | —                      | —                        | —                          | —                          | —                          | —                     | —    | —     | —      |
| 5061   | 104                 | 41                  | 4      | 2.27E-06                        | 0.446    | 1.47                              | 0.740                                | —                         | —                      | —                        | 38.75                      | 2.46                       | —                          | —                     | 2.5Y | 6     | 3      |
| 5062   | 108                 | 41                  | 4      | 2.44E-06                        | 0.421    | 1.53                              | —                                    | —                         | —                      | —                        | —                          | —                          | —                          | —                     | —    | —     | —      |
| 5063   | 106                 | 43                  | 4      | 1.53E-06                        | 0.440    | 1.48                              | —                                    | —                         | —                      | —                        | —                          | —                          | —                          | —                     | —    | —     | —      |
| 5064   | 104                 | 45                  | 4      | 1.67E-06                        | 0.441    | 1.48                              | —                                    | —                         | —                      | —                        | —                          | —                          | —                          | —                     | —    | —     | —      |
| 5065   | 108                 | 45                  | 4      | 1.55E-06                        | 0.436    | 1.49                              | —                                    | —                         | —                      | —                        | —                          | —                          | —                          | —                     | —    | —     | —      |
| 5071   | 182                 | 90                  | 4      | 6.52E-07                        | 0.452    | 1.45                              | —                                    | 2.52                      | —                      | —                        | 40.51                      | 0.67                       | 9.28                       | 3.01                  | 2.5Y | 7     | 3      |
| 5072   | 186                 | 90                  | 4      | 5.98E-07                        | 0.446    | 1.47                              | —                                    | —                         | —                      | —                        | —                          | —                          | —                          | —                     | —    | —     | —      |
| 5073   | 184                 | 94                  | 3      | 3.70E-07                        | 0.385    | 1.63                              | —                                    | —                         | —                      | —                        | —                          | —                          | —                          | —                     | —    | —     | —      |
| 5074   | 182                 | 99                  | 3      | 2.50E-07                        | 0.402    | 1.58                              | —                                    | —                         | —                      | —                        | —                          | —                          | —                          | —                     | —    | —     | —      |
| 5075   | 186                 | 99                  | 3      | 2.85E-07                        | 0.394    | 1.61                              | —                                    | —                         | —                      | —                        | —                          | —                          | —                          | —                     | —    | —     | —      |
| 5081   | 164                 | 69                  | 4      | 5.76E-07                        | 0.433    | 1.50                              | —                                    | 2.60                      | —                      | —                        | 50.53                      | 0.21                       | 7.76                       | 13.08                 | 10YR | 6     | 8      |
| 5082   | 168                 | 69                  | 4      | 5.50E-07                        | 0.415    | 1.55                              | —                                    | —                         | —                      | —                        | —                          | —                          | —                          | —                     | —    | —     | —      |
| 5083   | 166                 | 74                  | 4      | 4.99E-07                        | 0.413    | 1.55                              | —                                    | —                         | —                      | —                        | —                          | —                          | —                          | —                     | —    | —     | —      |
| 5084   | 164                 | 78                  | 4      | 7.12E-07                        | 0.446    | 1.47                              | —                                    | —                         | —                      | —                        | —                          | —                          | —                          | —                     | —    | —     | —      |
| 5085   | 168                 | 78                  | 4      | 6.43E-07                        | 0.437    | 1.49                              | —                                    | —                         | —                      | —                        | —                          | —                          | —                          | —                     | —    | —     | —      |
| 5091   | 161                 | 48                  | 4      | 9.20E-07                        | 0.408    | 1.57                              | —                                    | 3.66                      | —                      | —                        | 34.36                      | 0.24                       | 7.39                       | 3.18                  | 2.5Y | 6     | 6      |
| 5092   | 165                 | 48                  | 4      | 9.95E-07                        | 0.416    | 1.55                              | —                                    | —                         | —                      | —                        | —                          | —                          | —                          | —                     | —    | —     | —      |
| 5093   | 163                 | 50                  | 4      | 6.14E-07                        | 0.416    | 1.55                              | —                                    | —                         | —                      | —                        | —                          | —                          | —                          | —                     | —    | —     | —      |
| 5094   | 161                 | 52                  | 4      | 1.06E-06                        | 0.419    | 1.54                              | —                                    | —                         | —                      | —                        | —                          | —                          | —                          | —                     | —    | —     | —      |
| 5095   | 165                 | 52                  | 4      | 1.05E-06                        | 0.422    | 1.53                              | —                                    | —                         | —                      | —                        | —                          | —                          | —                          | —                     | —    | —     | —      |
| 5101   | 147                 | 83                  | 4      | 7.51E-07                        | 0.460    | 1.43                              | —                                    | 2.94                      | —                      | —                        | 38.58                      | 0.32                       | 10.47                      | 3.88                  | 2.5Y | 7     | 4      |

**Table D.1  
Analytical Results for Measured Sediment Properties**

| Sample | X-Coordinate (cm) * | Y-Coordinate (cm) * | Facies | Permeability (cm <sup>2</sup> ) | Porosity | Bulk Density (g/cm <sup>3</sup> ) | BET Surface Area (m <sup>2</sup> /g) | Magnetic Fraction (wt.%) | Organic Carbon (wt.%) | Inorganic Carbon (wt.%) | DC-Extractable Fe (µmol/g) | DC-Extractable Mn (µmol/g) | DC-Extractable Al (µmol/g) | K <sub>d</sub> (ml/g) | Hue  | Value | Chroma |
|--------|---------------------|---------------------|--------|---------------------------------|----------|-----------------------------------|--------------------------------------|--------------------------|-----------------------|-------------------------|----------------------------|----------------------------|----------------------------|-----------------------|------|-------|--------|
| 5102   | 151                 | 83                  | 4      | 7.47E-07                        | 0.456    | 1.44                              | —                                    | —                        | —                     | —                       | —                          | —                          | —                          | —                     | —    | —     | —      |
| 5103   | 149                 | 85                  | **     | 4.04E-07                        | 0.340    | 1.75                              | —                                    | —                        | —                     | —                       | —                          | —                          | —                          | —                     | —    | —     | —      |
| 5104   | 147                 | 87                  | 3      | 2.28E-07                        | 0.397    | 1.60                              | —                                    | —                        | —                     | —                       | —                          | —                          | —                          | —                     | —    | —     | —      |
| 5105   | 151                 | 87                  | 3      | 2.43E-07                        | 0.401    | 1.59                              | —                                    | —                        | —                     | —                       | —                          | —                          | —                          | —                     | —    | —     | —      |
| 5111   | 140                 | 69                  | 4      | 7.72E-07                        | 0.459    | 1.43                              | 0.267                                | 2.80                     | —                     | —                       | 31.53                      | 0.21                       | 7.32                       | 4.89                  | 2.5Y | 7     | 4      |
| 5112   | 144                 | 69                  | 4      | 8.91E-07                        | 0.448    | 1.46                              | —                                    | —                        | —                     | —                       | —                          | —                          | —                          | —                     | —    | —     | —      |
| 5113   | 142                 | 71                  | 4      | 7.24E-07                        | 0.440    | 1.48                              | —                                    | —                        | —                     | —                       | —                          | —                          | —                          | —                     | —    | —     | —      |
| 5114   | 140                 | 73                  | 4      | 6.70E-07                        | 0.436    | 1.49                              | —                                    | —                        | —                     | —                       | —                          | —                          | —                          | —                     | —    | —     | —      |
| 5115   | 144                 | 73                  | 4      | 6.80E-07                        | 0.434    | 1.50                              | —                                    | —                        | —                     | —                       | —                          | —                          | —                          | —                     | —    | —     | —      |
| 5121   | 125                 | 67                  | 4      | 9.66E-07                        | 0.441    | 1.48                              | 0.511                                | 0.83                     | —                     | —                       | 19.29                      | 0.46                       | 4.38                       | 3.46                  | 2.5Y | 7     | 3      |
| 5122   | 129                 | 67                  | 4      | 7.67E-07                        | 0.441    | 1.48                              | —                                    | —                        | —                     | —                       | —                          | —                          | —                          | —                     | —    | —     | —      |
| 5123   | 127                 | 69                  | 4      | 7.32E-07                        | 0.449    | 1.46                              | —                                    | —                        | —                     | —                       | —                          | —                          | —                          | —                     | —    | —     | —      |
| 5124   | 125                 | 71                  | 4      | 5.41E-07                        | 0.449    | 1.46                              | —                                    | —                        | —                     | —                       | —                          | —                          | —                          | —                     | —    | —     | —      |
| 5125   | 129                 | 71                  | 4      | 5.37E-07                        | 0.459    | 1.43                              | —                                    | —                        | —                     | —                       | —                          | —                          | —                          | —                     | —    | —     | —      |
| 6011   | 307                 | 82                  | 4      | 6.47E-07                        | 0.386    | 1.63                              | —                                    | —                        | —                     | —                       | 50.6                       | 0.56                       | —                          | —                     | 10YR | 6     | 4      |
| 6012   | 316                 | 82                  | 4      | 1.37E-06                        | 0.412    | 1.56                              | —                                    | —                        | —                     | —                       | —                          | —                          | —                          | —                     | —    | —     | —      |
| 6013   | 311                 | 84                  | 4      | 8.30E-07                        | 0.463    | 1.42                              | —                                    | —                        | —                     | —                       | —                          | —                          | —                          | —                     | —    | —     | —      |
| 6014   | 307                 | 86                  | 4      | 8.38E-07                        | 0.463    | 1.42                              | —                                    | —                        | —                     | —                       | —                          | —                          | —                          | —                     | —    | —     | —      |
| 6015   | 316                 | 86                  | 4      | 7.81E-07                        | 0.450    | 1.46                              | —                                    | —                        | —                     | —                       | —                          | —                          | —                          | —                     | —    | —     | —      |
| 6021   | 349                 | 43                  | 5      | 3.55E-06                        | 0.402    | 1.58                              | 0.506                                | —                        | —                     | —                       | 34.87                      | 1.01                       | —                          | —                     | 2.5Y | 5     | 3      |
| 6022   | 353                 | 43                  | 5      | 3.55E-06                        | 0.392    | 1.61                              | —                                    | 3.25                     | —                     | —                       | 30.03                      | 1.12                       | 2.13                       | 62.09                 | —    | —     | —      |
| 6023   | 351                 | 47                  | 5      | 3.55E-06                        | 0.386    | 1.63                              | —                                    | —                        | —                     | —                       | —                          | —                          | —                          | —                     | —    | —     | —      |

**Table D.1  
Analytical Results for Measured Sediment Properties**

| Sample | X-Coordinate (cm) * | Y-Coordinate (cm) * | Facies | Permeability (cm <sup>2</sup> ) | Porosity | Bulk Density (g/cm <sup>3</sup> ) | BET Surface Area (m <sup>2</sup> /g) | Magnetic Fraction (wt. %) | Organic Carbon (wt. %) | Inorganic Carbon (wt. %) | DC-Extractable Fe (µmol/g) | DC-Extractable Mn (µmol/g) | DC-Extractable Al (µmol/g) | K <sub>d</sub> (ml/g) | Hue  | Value | Chroma |
|--------|---------------------|---------------------|--------|---------------------------------|----------|-----------------------------------|--------------------------------------|---------------------------|------------------------|--------------------------|----------------------------|----------------------------|----------------------------|-----------------------|------|-------|--------|
| 6024   | 349                 | 52                  | 5      | 3.55E-06                        | 0.406    | 1.57                              |                                      |                           |                        |                          |                            |                            |                            |                       |      |       |        |
| 6025   | 353                 | 52                  | 5      | 3.55E-06                        | 0.423    | 1.53                              |                                      |                           |                        |                          |                            |                            |                            |                       |      |       |        |
| 6031   | 305                 | 1                   | 6      | 2.45E-06                        | 0.413    | 1.56                              |                                      | 2.50                      |                        |                          | 52.35                      | 0.82                       | 9.70                       | 27.30                 | 2.5Y | 5     | 3      |
| 6032   | 309                 | 1                   | 6      | 2.43E-06                        | 0.426    | 1.52                              |                                      |                           |                        |                          |                            |                            |                            |                       |      |       |        |
| 6033   | 307                 | 5                   | 6      | 1.86E-06                        | 0.437    | 1.49                              |                                      |                           |                        |                          |                            |                            |                            |                       |      |       |        |
| 6034   | 305                 | 10                  | 6      | 1.35E-06                        | 0.431    | 1.51                              |                                      |                           |                        |                          |                            |                            |                            |                       |      |       |        |
| 6035   | 309                 | 10                  | 6      | 1.58E-06                        | 0.429    | 1.51                              |                                      |                           |                        |                          |                            |                            |                            |                       |      |       |        |
| 6041   | 365                 | 61                  | 5      | 3.47E-06                        | 0.402    | 1.58                              |                                      | 3.85                      |                        |                          | 35.03                      | 1.94                       |                            | 42.54                 | 2.5Y | 6     | 2      |
| 6042   | 374                 | 61                  | 5      | 3.55E-06                        | 0.403    | 1.58                              |                                      |                           |                        |                          |                            |                            |                            |                       |      |       |        |
| 6043   | 369                 | 63                  | 5      | 1.65E-06                        | 0.381    | 1.64                              |                                      |                           |                        |                          |                            |                            |                            |                       |      |       |        |
| 6044   | 365                 | 65                  | 4      | 3.55E-06                        | 0.351    | 1.72                              |                                      |                           |                        |                          |                            |                            |                            |                       |      |       |        |
| 6045   | 374                 | 65                  | 4      | 1.52E-06                        | 0.404    | 1.58                              |                                      |                           |                        |                          |                            |                            |                            |                       |      |       |        |
| 6051   | 348                 | 25                  | **     | 4.54E-07                        | 0.406    | 1.57                              |                                      | 2.96                      |                        |                          | 29.32                      | 0.72                       | 4.76                       | 34.62                 | 2.5Y | 7     | 3      |
| 6052   | 352                 | 25                  | 7      | 5.73E-08                        | 0.441    | 1.48                              |                                      | 2.80                      | 0.067                  | 0.0005                   | 49.5                       | 0.58                       | 8.43                       | 37.81                 |      |       |        |
| 6053   | 350                 | 27                  | 7      | 1.41E-07                        | 0.422    | 1.53                              |                                      |                           |                        |                          |                            |                            |                            |                       |      |       |        |
| 6054   | 348                 | 29                  | **     | 3.95E-07                        | 0.452    | 1.45                              |                                      |                           |                        |                          |                            |                            |                            |                       |      |       |        |
| 6055   | 352                 | 29                  | 5      | 3.55E-06                        | 0.418    | 1.54                              |                                      |                           |                        |                          |                            |                            |                            |                       |      |       |        |
| 6061   | 301                 | 46                  | 4      | 3.55E-06                        | 0.370    | 1.67                              |                                      |                           |                        |                          |                            |                            |                            |                       |      |       |        |
| 6062   | 305                 | 46                  | 4      | 3.55E-06                        | 0.416    | 1.55                              | 0.473                                |                           |                        |                          | 36.58                      | 1.61                       |                            |                       | 2.5Y | 6     | 3      |
| 6063   | 303                 | 48                  | 4      | 2.06E-06                        | 0.377    | 1.65                              |                                      |                           |                        |                          |                            |                            |                            |                       |      |       |        |
| 6064   | 301                 | 50                  | 4      | 2.27E-06                        | 0.406    | 1.57                              |                                      |                           |                        |                          |                            |                            |                            |                       |      |       |        |
| 6065   | 305                 | 50                  | 4      | 2.39E-06                        | 0.340    | 1.75                              |                                      |                           |                        |                          |                            |                            |                            |                       |      |       |        |



**Table D.1**  
**Analytical Results for Measured Sediment Properties**

| Sample | X-Coordinate (cm) * | Y-Coordinate (cm) * | Facies | Permeability (cm <sup>2</sup> ) | Porosity | Bulk Density (g/cm <sup>3</sup> ) | BET Surface Area (m <sup>2</sup> /g) | Magnetic Fraction (wt. %) | Organic Carbon (wt. %) | Inorganic Carbon (wt. %) | DC-Extractable Fe (μmol/g) | DC-Extractable Mn (μmol/g) | DC-Extractable Al (μmol/g) | K <sub>d</sub> (ml/g) | Hue  | Value | Chroma |
|--------|---------------------|---------------------|--------|---------------------------------|----------|-----------------------------------|--------------------------------------|---------------------------|------------------------|--------------------------|----------------------------|----------------------------|----------------------------|-----------------------|------|-------|--------|
| 6071   | 362                 | 47                  | 5      | 3.55E-06                        | 0.402    | 1.58                              | 0.912                                | 4.44                      | —                      | —                        | 30.28                      | 1.04                       | 2.77                       | 48.86                 | 2.5Y | 5     | 2      |
| 6072   | 371                 | 47                  | 5      | 3.55E-06                        | 0.410    | 1.56                              | —                                    | —                         | —                      | —                        | —                          | —                          | —                          | —                     | —    | —     | —      |
| 6073   | 367                 | 49                  | 5      | 3.55E-06                        | 0.432    | 1.51                              | —                                    | —                         | —                      | —                        | —                          | —                          | —                          | —                     | —    | —     | —      |
| 6074   | 362                 | 51                  | 5      | 3.55E-06                        | 0.411    | 1.56                              | —                                    | —                         | —                      | —                        | —                          | —                          | —                          | —                     | —    | —     | —      |
| 6075   | 371                 | 51                  | 5      | 3.55E-06                        | 0.398    | 1.60                              | —                                    | —                         | —                      | —                        | —                          | —                          | —                          | —                     | —    | —     | —      |
| 6081   | 390                 | 63                  | 5      | 3.55E-06                        | 0.410    | 1.56                              | —                                    | 2.40                      | 0.036                  | 0.0013                   | 30.10                      | 0.84                       | 3.05                       | 51.70                 | 2.5Y | 5     | 3      |
| 6082   | 394                 | 63                  | 5      | 3.55E-06                        | 0.433    | 1.50                              | —                                    | —                         | —                      | —                        | —                          | —                          | —                          | —                     | —    | —     | —      |
| 6083   | 392                 | 67                  | 5      | 1.86E-06                        | 0.415    | 1.55                              | —                                    | —                         | —                      | —                        | —                          | —                          | —                          | —                     | —    | —     | —      |
| 6084   |                     |                     |        |                                 |          |                                   |                                      |                           |                        |                          |                            |                            |                            |                       |      |       |        |
|        |                     |                     |        |                                 |          |                                   |                                      |                           |                        |                          |                            |                            |                            |                       |      |       |        |
| 6085   |                     |                     |        |                                 |          |                                   |                                      |                           |                        |                          |                            |                            |                            |                       |      |       |        |
|        |                     |                     |        |                                 |          |                                   |                                      |                           |                        |                          |                            |                            |                            |                       |      |       |        |
| 6091   | 330                 | 43                  | 5      | 3.55E-06                        | 0.401    | 1.59                              | —                                    | 2.80                      | —                      | —                        | 32.01                      | 0.85                       | 3.17                       | 70.63                 | 2.5Y | 5     | 2      |
| 6092   | 334                 | 43                  | 5      | 3.51E-06                        | 0.409    | 1.56                              | —                                    | —                         | —                      | —                        | —                          | —                          | —                          | —                     | —    | —     | —      |
| 6093   | 332                 | 45                  | 5      | 3.55E-06                        | 0.424    | 1.53                              | —                                    | —                         | —                      | —                        | —                          | —                          | —                          | —                     | —    | —     | —      |
| 6094   | 330                 | 47                  | 5      | 3.55E-06                        | 0.420    | 1.54                              | —                                    | —                         | —                      | —                        | —                          | —                          | —                          | —                     | —    | —     | —      |
| 6095   | 334                 | 47                  | 5      | 3.55E-06                        | 0.424    | 1.53                              | —                                    | —                         | —                      | —                        | —                          | —                          | —                          | —                     | —    | —     | —      |
| 6101   | 381                 | 29                  | 6      | 1.82E-06                        | 0.390    | 1.62                              | —                                    | 3.37                      | —                      | —                        | 44.46                      | 1.40                       | 8.49                       | 24.97                 | 10YR | 6     | 3      |
| 6102   | 390                 | 29                  | 6      | 1.36E-06                        | 0.386    | 1.63                              | —                                    | —                         | —                      | —                        | —                          | —                          | —                          | —                     | —    | —     | —      |
| 6103   | 386                 | 31                  | 7      | 8.93E-08                        | 0.460    | 1.43                              | —                                    | 3.49                      | —                      | —                        | 57.04                      | 0.52                       | 18.11                      | 42.86                 | —    | —     | —      |
| 6104   | 381                 | 33                  | 7      | 3.11E-07                        | 0.424    | 1.53                              | —                                    | —                         | —                      | —                        | —                          | —                          | —                          | —                     | —    | —     | —      |
| 6105   | 390                 | 33                  | 7      | 4.21E-07                        | 0.411    | 1.56                              | —                                    | —                         | —                      | —                        | —                          | —                          | —                          | —                     | —    | —     | —      |
| 6111   | 382                 | 84                  | 4      | 1.21E-06                        | 0.400    | 1.59                              | —                                    | —                         | —                      | —                        | 48.97                      | 0.29                       | —                          | —                     | 10YR | 6     | 6      |
| 6112   | 386                 | 84                  | 4      | 1.30E-06                        | 0.366    | 1.68                              | —                                    | —                         | —                      | —                        | —                          | —                          | —                          | —                     | —    | —     | —      |

Table D.1  
Analytical Results for Measured Sediment Properties

| Sample | X-Coordinate (cm) * | Y-Coordinate (cm) * | Facies | Permeability (cm <sup>2</sup> ) | Porosity | Bulk Density (g/cm <sup>3</sup> ) | BET Surface Area (m <sup>2</sup> /g) | Magnetic Fraction (wt. %) | Organic Carbon (wt. %) | Inorganic Carbon (wt. %) | DC-Extractable Fe (µmol/g) | DC-Extractable Mn (µmol/g) | DC-Extractable Al (µmol/g) | K <sub>d</sub> (ml/g) | Hue  | Value | Chroma |
|--------|---------------------|---------------------|--------|---------------------------------|----------|-----------------------------------|--------------------------------------|---------------------------|------------------------|--------------------------|----------------------------|----------------------------|----------------------------|-----------------------|------|-------|--------|
| 6113   | 384                 | 88                  | 4      | 1.59E-06                        | 0.393    | 1.61                              |                                      |                           |                        |                          |                            |                            |                            |                       |      |       |        |
| 6114   | 382                 | 93                  | 4      | 2.03E-06                        | 0.373    | 1.66                              |                                      |                           |                        |                          |                            |                            |                            |                       |      |       |        |
| 6115   | 386                 | 93                  | 4      | 1.75E-06                        | 0.395    | 1.60                              |                                      |                           |                        |                          |                            |                            |                            |                       |      |       |        |
| 6121   | 363                 | 29                  | 7      | 1.17E-07                        | 0.442    | 1.48                              | 1.262                                | 3.62                      |                        |                          | 52.18                      | 0.59                       | 12.97                      | 68.54                 | 10YR | 7     | 4      |
| 6122   | 367                 | 29                  | 7      | 7.72E-08                        | 0.373    | 1.66                              |                                      | 3.32                      |                        |                          | 49.59                      | 0.61                       | 14.77                      | 24.45                 |      |       |        |
| 6123   | 365                 | 31                  | 7      | 1.81E-07                        | 0.439    | 1.49                              |                                      |                           |                        |                          |                            |                            |                            |                       |      |       |        |
| 6124   | 363                 | 33                  | **     | 5.09E-07                        | 0.434    | 1.50                              |                                      |                           |                        |                          |                            |                            |                            |                       |      |       |        |
| 6125   | 367                 | 33                  | **     | 4.57E-07                        | 0.449    | 1.46                              |                                      |                           |                        |                          |                            |                            |                            |                       |      |       |        |
| 7011   | 25                  | 43                  | 4      | 9.96E-07                        | 0.433    | 1.50                              |                                      |                           |                        |                          | 22.07                      | 0.44                       |                            |                       | 2.5Y | 7     | 3      |
| 7012   | 29                  | 43                  | 4      | 9.96E-07                        | 0.425    | 1.53                              |                                      |                           |                        |                          |                            |                            |                            |                       |      |       |        |
| 7013   | 27                  | 48                  | 4      | 7.26E-07                        | 0.423    | 1.53                              |                                      |                           |                        |                          |                            |                            |                            |                       |      |       |        |
| 7014   | 25                  | 52                  | 4      | 1.09E-06                        | 0.451    | 1.46                              |                                      |                           |                        |                          |                            |                            |                            |                       |      |       |        |
| 7015   | 29                  | 52                  | 4      | 9.82E-07                        | 0.449    | 1.46                              |                                      |                           |                        |                          |                            |                            |                            |                       |      |       |        |
| 7021   | 8                   | 5                   | 8      | 1.66E-06                        | 0.357    | 1.70                              |                                      | 2.41                      |                        |                          | 31.22                      | 1.00                       | 5.96                       | 6.32                  | 2.5Y | 6     | 3      |
| 7022   | 12                  | 5                   | 8      | 9.47E-07                        | 0.356    | 1.71                              |                                      |                           |                        |                          |                            |                            |                            |                       |      |       |        |
| 7023   | 10                  | 7                   | 8      | 1.39E-06                        | 0.368    | 1.67                              |                                      |                           |                        |                          |                            |                            |                            |                       |      |       |        |
| 7024   | 8                   | 9                   | 8      | 9.27E-07                        | 0.290    | 1.88                              |                                      |                           |                        |                          |                            |                            |                            |                       |      |       |        |
| 7025   | 12                  | 9                   | 8      | 8.07E-07                        | 0.341    | 1.75                              |                                      |                           |                        |                          |                            |                            |                            |                       |      |       |        |
| 7031   | 6                   | 43                  | 4      | 1.12E-06                        | 0.416    | 1.55                              | 0.527                                |                           |                        |                          | 39.66                      | 0.76                       |                            |                       | 2.5Y | 6     | 2      |
| 7032   | 10                  | 43                  | 4      | 1.30E-06                        | 0.421    | 1.53                              |                                      |                           |                        |                          |                            |                            |                            |                       |      |       |        |
| 7033   | 8                   | 47                  | 4      | 8.73E-07                        | 0.434    | 1.50                              |                                      |                           |                        |                          |                            |                            |                            |                       |      |       |        |
| 7034   | 6                   | 52                  | 4      | 7.58E-07                        | 0.422    | 1.53                              |                                      |                           |                        |                          |                            |                            |                            |                       |      |       |        |

**Table D.1  
Analytical Results for Measured Sediment Properties**

| Sample | X-Coordinate<br>(cm) * | Y-Coordinate<br>(cm) * | Facies | Permeability<br>(cm <sup>2</sup> ) | Porosity | Bulk Density<br>(g/cm <sup>3</sup> ) | BET Surface Area<br>(m <sup>2</sup> /g) | Magnetic Fraction<br>(wt. %) | Organic Carbon<br>(wt. %) | Inorganic Carbon<br>(wt. %) | DC-Extractable Fe<br>(µmol/g) | DC-Extractable Mn<br>(µmol/g) | DC-Extractable Al<br>(µmol/g) | K <sub>d</sub><br>(ml/g) | Hue  | Value | Chroma |
|--------|------------------------|------------------------|--------|------------------------------------|----------|--------------------------------------|---|------------------------------|---------------------------|-----------------------------|-------------------------------|-------------------------------|-------------------------------|--------------------------|------|-------|--------|
| 7035   | 10                     | 52                     | 4      | 7.19E-07                           | 0.433    | 1.50                                 | —                                       | —                            | —                         | —                           | —                             | —                             | —                             | —                        | —    | —     | —      |
| 7041   | 20                     | 24                     | 8      | 1.22E-06                           | 0.387    | 1.62                                 | —                                       | 2.11                         | 0.037                     | 0.0005                      | 33.58                         | 1.09                          | 11.83                         | 3.27                     | 2.5Y | 6     | 2      |
| 7042   | 24                     | 24                     | 8      | 1.26E-06                           | 0.359    | 1.70                                 | —                                       | —                            | —                         | —                           | —                             | —                             | —                             | —                        | —    | —     | —      |
| 7043   | 22                     | 28                     | 8      | 1.12E-06                           | 0.384    | 1.63                                 | —                                       | —                            | —                         | —                           | —                             | —                             | —                             | —                        | —    | —     | —      |
| 7044   | 20                     | 33                     | 8      | 1.51E-06                           | 0.371    | 1.67                                 | —                                       | —                            | —                         | —                           | —                             | —                             | —                             | —                        | —    | —     | —      |
| 7045   | 24                     | 33                     | **     | 1.05E-06                           | 0.336    | 1.76                                 | —                                       | —                            | —                         | —                           | —                             | —                             | —                             | —                        | —    | —     | —      |
| 7051   | 42                     | 49                     | 4      | 9.39E-07                           | 0.442    | 1.48                                 | 0.474                                   | —                            | —                         | —                           | 32.74                         | 0.84                          | —                             | —                        | 2.5Y | 6     | 4      |
| 7052   | 46                     | 49                     | 4      | 1.07E-06                           | 0.438    | 1.49                                 | —                                       | —                            | —                         | —                           | —                             | —                             | —                             | —                        | —    | —     | —      |
| 7053   | 44                     | 54                     | 4      | 9.32E-07                           | 0.443    | 1.48                                 | —                                       | —                            | —                         | —                           | —                             | —                             | —                             | —                        | —    | —     | —      |
| 7054   | 42                     | 58                     | 4      | 7.67E-07                           | 0.444    | 1.47                                 | —                                       | —                            | —                         | —                           | —                             | —                             | —                             | —                        | —    | —     | —      |
| 7055   | 46                     | 58                     | 4      | 7.17E-07                           | 0.438    | 1.49                                 | —                                       | —                            | —                         | —                           | —                             | —                             | —                             | —                        | —    | —     | —      |
| 7061   | 70                     | 68                     | 4      | 7.32E-07                           | 0.435    | 1.50                                 | —                                       | —                            | —                         | —                           | —                             | —                             | —                             | —                        | —    | —     | —      |
| 7062   | 74                     | 68                     | 4      | 7.26E-07                           | 0.441    | 1.48                                 | —                                       | —                            | —                         | —                           | —                             | —                             | —                             | —                        | —    | —     | —      |
| 7063   | 72                     | 70                     | 4      | 8.70E-07                           | 0.447    | 1.47                                 | —                                       | —                            | —                         | —                           | —                             | —                             | —                             | —                        | —    | —     | —      |
| 7064   | 70                     | 72                     | 4      | 7.81E-07                           | 0.456    | 1.44                                 | —                                       | —                            | —                         | —                           | —                             | —                             | —                             | —                        | —    | —     | —      |
| 7065   | 74                     | 72                     | 4      | 8.21E-07                           | 0.454    | 1.45                                 | —                                       | —                            | —                         | —                           | —                             | —                             | —                             | —                        | —    | —     | —      |
| 7071   | 25                     | 6                      | 8      | 8.81E-07                           | 0.305    | 1.84                                 | 0.412                                   | —                            | —                         | —                           | 72.87                         | 2.25                          | —                             | —                        | —    | —     | —      |
| 7072   | 34                     | 6                      | 8      | 7.34E-07                           | 0.385    | 1.63                                 | —                                       | 8.86                         | —                         | —                           | 69.77                         | 1.68                          | 11.54                         | 6.11                     | —    | —     | —      |
| 7073   | 30                     | 8                      | 8      | 7.70E-07                           | 0.321    | 1.80                                 | —                                       | —                            | —                         | —                           | —                             | —                             | —                             | —                        | —    | —     | —      |
| 7074   | 25                     | 10                     | 8      | 1.33E-06                           | 0.373    | 1.66                                 | —                                       | —                            | —                         | —                           | —                             | —                             | —                             | —                        | —    | —     | —      |
| 7075   | 34                     | 10                     | 8      | 1.31E-06                           | 0.324    | 1.79                                 | —                                       | —                            | —                         | —                           | —                             | —                             | —                             | —                        | —    | —     | —      |
| 7081   | 69                     | 45                     | 4      | 1.44E-06                           | 0.450    | 1.46                                 | —                                       | —                            | —                         | —                           | 22.70                         | 1.21                          | —                             | —                        | 2.5Y | 6     | 2      |

**Table D.1  
Analytical Results for Measured Sediment Properties**

| Sample | X-Coordinate<br>(cm) * | Y-Coordinate<br>(cm) * | Facies | Permeability<br>(cm <sup>2</sup> ) | Porosity | Bulk Density<br>(g/cm <sup>3</sup> ) | BET Surface Area<br>(m <sup>2</sup> /g) | Magnetic Fraction<br>(wt.%) | Organic Carbon<br>(wt.%) | Inorganic Carbon<br>(wt.%) | DC-Extractable Fe<br>(µmol/g) | DC-Extractable Mn<br>(µmol/g) | DC-Extractable Al<br>(µmol/g) | K <sub>d</sub><br>(ml/g) | Hue  | Value | Chroma |
|--------|------------------------|------------------------|--------|------------------------------------|----------|--------------------------------------|---|-----------------------------|--------------------------|----------------------------|-------------------------------|-------------------------------|-------------------------------|--------------------------|------|-------|--------|
| 7082   | 73                     | 45                     | 4      | 1.30E-06                           | 0.448    | 1.46                                 |   |                             |                          |                            |                               |                               |                               |                          |      |       |        |
| 7083   | 71                     | 47                     | 4      | 9.44E-07                           | 0.447    | 1.46                                 |   |                             |                          |                            |                               |                               |                               |                          |      |       |        |
| 7084   | 69                     | 49                     | 4      | 7.84E-07                           | 0.437    | 1.49                                 |   |                             |                          |                            |                               |                               |                               |                          |      |       |        |
| 7085   | 73                     | 49                     | 4      | 1.04E-06                           | 0.458    | 1.43                                 |   |                             |                          |                            |                               |                               |                               |                          |      |       |        |
| 7091   | 83                     | 45                     | 4      | 1.35E-06                           | 0.441    | 1.48                                 |   | 1.55                        |                          |                            | 27.19                         | 0.85                          | 4.96                          | 5.25                     | 2.5Y | 6     | 2      |
| 7092   | 87                     | 45                     | 4      | 1.19E-06                           | 0.448    | 1.46                                 |   |                             |                          |                            |                               |                               |                               |                          |      |       |        |
| 7093   | 85                     | 47                     | 4      | 1.00E-06                           | 0.440    | 1.48                                 |   |                             |                          |                            |                               |                               |                               |                          |      |       |        |
| 7094   | 83                     | 49                     | 4      | 9.83E-07                           | 0.446    | 1.47                                 |   |                             |                          |                            |                               |                               |                               |                          |      |       |        |
| 7095   | 87                     | 49                     | 4      | 1.05E-06                           | 0.442    | 1.48                                 |   |                             |                          |                            |                               |                               |                               |                          |      |       |        |
| 7101   | 61                     | 29                     | 4      | 1.85E-06                           | 0.381    | 1.64                                 |   | 2.33                        |                          |                            | 33.54                         | 1.18                          |                               |                          | 2.5Y | 6     | 3      |
| 7102   | 65                     | 29                     | 4      | 1.52E-06                           | 0.333    | 1.77                                 |   |                             |                          |                            |                               |                               |                               |                          |      |       |        |
| 7103   | 63                     | 31                     | 4      | 1.31E-06                           | 0.371    | 1.67                                 |   |                             |                          |                            |                               |                               |                               |                          |      |       |        |
| 7104   | 61                     | 33                     | 4      | 1.61E-06                           | 0.383    | 1.64                                 |   |                             |                          |                            |                               |                               |                               |                          |      |       |        |
| 7105   | 65                     | 33                     | 4      | 1.89E-06                           | 0.389    | 1.62                                 |   |                             |                          |                            |                               |                               |                               |                          |      |       |        |
| 7111   | 69                     | 87                     | 3      | 4.39E-07                           | 0.405    | 1.58                                 |   | 3.01                        |                          |                            | 45.11                         | 0.28                          | 9.01                          | 4.47                     | 10YR | 6     | 6      |
| 7112   | 73                     | 87                     | 3      | 3.38E-07                           | 0.409    | 1.57                                 |   |                             |                          |                            |                               |                               |                               |                          |      |       |        |
| 7113   | 71                     | 89                     | 3      | 2.43E-07                           | 0.419    | 1.54                                 |   |                             |                          |                            |                               |                               |                               |                          |      |       |        |
| 7114   | 69                     | 91                     | 3      | 2.67E-07                           | 0.430    | 1.51                                 |   |                             |                          |                            |                               |                               |                               |                          |      |       |        |
| 7115   | 73                     | 91                     | 3      | 2.62E-07                           | 0.442    | 1.48                                 |   |                             |                          |                            |                               |                               |                               |                          |      |       |        |
| 7121   | 40                     | 61                     | 4      | 6.21E-07                           | 0.436    | 1.49                                 |   |                             |                          |                            | 21.63                         | 0.54                          | 4.52                          | 5.31                     | 2.5Y | 7     | 3      |
| 7122   | 44                     | 61                     | 4      | 6.30E-07                           | 0.443    | 1.48                                 |   |                             |                          |                            |                               |                               |                               |                          |      |       |        |
| 7123   | 42                     | 66                     | 4      | 6.24E-07                           | 0.449    | 1.46                                 |   |                             |                          |                            |                               |                               |                               |                          |      |       |        |

**Table D.1  
Analytical Results for Measured Sediment Properties**

| Sample | X-Coordinate (cm) * | Y-Coordinate (cm) * | Facies | Permeability (cm <sup>2</sup> ) | Porosity | Bulk Density (g/cm <sup>3</sup> ) | BET Surface Area (m <sup>2</sup> /g) | Magnetic Fraction (wt. %) | Organic Carbon (wt. %) | Inorganic Carbon (wt. %) | DC-Extractable Fe (µmol/g) | DC-Extractable Mn (µmol/g) | DC-Extractable Al (µmol/g) | K <sub>d</sub> (m/g) | Hue  | Value | Chroma |
|--------|---------------------|---------------------|--------|---------------------------------|----------|-----------------------------------|--------------------------------------|---------------------------|------------------------|--------------------------|----------------------------|----------------------------|----------------------------|----------------------|------|-------|--------|
| 7124   | 40                  | 70                  | 4      | 5.86E-07                        | 0.436    | 1.49                              |                                      |                           |                        |                          |                            |                            |                            |                      |      |       |        |
| 7125   | 44                  | 70                  | 4      | 6.29E-07                        | 0.446    | 1.47                              |                                      |                           |                        |                          |                            |                            |                            |                      |      |       |        |
| 8011   | 229                 | 84                  | 4      | 8.70E-07                        | 0.455    | 1.44                              |                                      |                           |                        |                          | 32.10                      | 1.02                       |                            |                      | 2.5Y | 6     | 3      |
| 8012   | 238                 | 84                  | 4      | 6.59E-07                        | 0.448    | 1.46                              |                                      |                           |                        |                          |                            |                            |                            |                      |      |       |        |
| 8013   | 234                 | 86                  | 4      | 6.28E-07                        | 0.445    | 1.47                              |                                      |                           |                        |                          |                            |                            |                            |                      |      |       |        |
| 8014   | 229                 | 88                  | 4      | 5.95E-07                        | 0.438    | 1.49                              |                                      |                           |                        |                          |                            |                            |                            |                      |      |       |        |
| 8015   | 238                 | 88                  | 4      | 9.73E-07                        | 0.458    | 1.43                              |                                      |                           |                        |                          |                            |                            |                            |                      |      |       |        |
| 8021   | 207                 | 89                  | 4      | 6.59E-07                        | 0.444    | 1.47                              |                                      |                           |                        |                          | 35.6                       | 0.97                       |                            |                      | 2.5Y | 7     | 3      |
| 8022   | 211                 | 89                  | 4      | 7.54E-07                        | 0.451    | 1.45                              |                                      |                           |                        |                          |                            |                            |                            |                      |      |       |        |
| 8023   | 209                 | 93                  | 4      | 4.81E-07                        | 0.435    | 1.50                              |                                      |                           |                        |                          |                            |                            |                            |                      |      |       |        |
| 8024   | 207                 | 98                  | 4      | 6.09E-07                        | 0.426    | 1.52                              |                                      |                           |                        |                          |                            |                            |                            |                      |      |       |        |
| 8025   | 211                 | 98                  | 4      | 7.14E-07                        | 0.434    | 1.50                              |                                      |                           |                        |                          |                            |                            |                            |                      |      |       |        |
| 8031   | 287                 | 6                   | 6      | 1.77E-06                        | 0.421    | 1.53                              | 0.420                                | 3.02                      |                        |                          | 30.38                      | 1.46                       | 3.05                       | 34.09                | 2.5Y | 6     | 3      |
| 8032   | 291                 | 6                   | 6      | 1.70E-06                        | 0.422    | 1.53                              |                                      |                           |                        |                          |                            |                            |                            |                      |      |       |        |
| 8033   | 289                 | 10                  | 6      | 1.99E-06                        | 0.425    | 1.52                              |                                      |                           |                        |                          |                            |                            |                            |                      |      |       |        |
| 8034   | 287                 | 15                  | 6      | 7.80E-07                        | 0.398    | 1.59                              |                                      |                           |                        |                          |                            |                            |                            |                      |      |       |        |
| 8035   | 291                 | 15                  | 6      | 1.56E-06                        | 0.402    | 1.58                              |                                      |                           |                        |                          |                            |                            |                            |                      |      |       |        |
| 8041   | 246                 | 10                  | 6      | 8.05E-07                        | 0.429    | 1.51                              | 0.723                                | 3.09                      |                        |                          | 34.01                      | 1.42                       | 7.83                       | 23.48                | 10YR | 6     | 4      |
| 8042   | 250                 | 10                  | 6      | 8.23E-07                        | 0.427    | 1.52                              |                                      |                           |                        |                          |                            |                            |                            |                      |      |       |        |
| 8043   | 248                 | 12                  | 8      | 3.55E-06                        | 0.403    | 1.58                              |                                      |                           |                        |                          |                            |                            |                            |                      |      |       |        |
| 8044   | 246                 | 14                  | 8      | 3.55E-06                        | 0.394    | 1.61                              |                                      |                           |                        |                          |                            |                            |                            |                      |      |       |        |
| 8045   | 250                 | 14                  | 8      | 3.36E-06                        | 0.359    | 1.70                              |                                      |                           |                        |                          |                            |                            |                            |                      |      |       |        |

**Table D.1  
Analytical Results for Measured Sediment Properties**

| Sample | X-Coordinate (cm) * | Y-Coordinate (cm) * | Facies | Permeability (cm <sup>2</sup> ) | Porosity | Bulk Density (g/cm <sup>3</sup> ) | BET Surface Area (m <sup>2</sup> /g) | Magnetic Fraction (wt. %) | Organic Carbon (wt. %) | Inorganic Carbon (wt. %) | DC-Extractable Fe (µmol/g) | DC-Extractable Mn (µmol/g) | DC-Extractable Al (µmol/g) | K <sub>d</sub> (ml/g) | Hue  | Value | Chroma |
|--------|---------------------|---------------------|--------|---------------------------------|----------|-----------------------------------|--------------------------------------|---------------------------|------------------------|--------------------------|----------------------------|----------------------------|----------------------------|-----------------------|------|-------|--------|
| 8051   | 287                 | 84                  | 4      | 8.34E-07                        | 0.449    | 1.46                              | —                                    | —                         | —                      | —                        | 24.89                      | 0.78                       | —                          | —                     | 2.5Y | 6     | 2      |
| 8052   | 291                 | 84                  | 4      | 8.49E-07                        | 0.462    | 1.43                              | —                                    | —                         | —                      | —                        | —                          | —                          | —                          | —                     | —    | —     | —      |
| 8053   | 289                 | 86                  | 4      | 8.58E-07                        | 0.456    | 1.44                              | —                                    | —                         | —                      | —                        | —                          | —                          | —                          | —                     | —    | —     | —      |
| 8054   | 287                 | 88                  | 4      | 6.46E-07                        | 0.443    | 1.48                              | —                                    | —                         | —                      | —                        | —                          | —                          | —                          | —                     | —    | —     | —      |
| 8055   | 291                 | 88                  | 4      | 7.21E-07                        | 0.447    | 1.47                              | —                                    | —                         | —                      | —                        | 42.35                      | 0.51                       | —                          | —                     | 10YR | 6     | 6      |
| 8061   | 268                 | 62                  | 4      | 1.19E-06                        | 0.360    | 1.70                              | 0.476                                | —                         | —                      | —                        | —                          | —                          | —                          | —                     | —    | —     | —      |
| 8062   | 272                 | 62                  | 4      | 8.28E-07                        | 0.415    | 1.55                              | —                                    | —                         | —                      | —                        | —                          | —                          | —                          | —                     | —    | —     | —      |
| 8063   | 270                 | 64                  | 4      | 1.20E-06                        | 0.387    | 1.62                              | —                                    | —                         | —                      | —                        | —                          | —                          | —                          | —                     | —    | —     | —      |
| 8064   | 268                 | 66                  | 4      | 7.76E-07                        | 0.386    | 1.63                              | —                                    | —                         | —                      | —                        | —                          | —                          | —                          | —                     | —    | —     | —      |
| 8065   | 272                 | 66                  | 4      | 1.17E-06                        | 0.375    | 1.66                              | —                                    | —                         | —                      | —                        | —                          | —                          | —                          | —                     | —    | —     | —      |
| 8071   | 281                 | 69                  | 4      | 2.46E-06                        | 0.368    | 1.67                              | —                                    | —                         | —                      | —                        | 30.90                      | 1.08                       | —                          | —                     | 2.5Y | 6     | 3      |
| 8072   | 285                 | 69                  | 4      | 6.28E-07                        | 0.338    | 1.75                              | —                                    | —                         | —                      | —                        | —                          | —                          | —                          | —                     | —    | —     | —      |
| 8073   | 283                 | 71                  | 4      | 2.37E-06                        | 0.404    | 1.58                              | —                                    | —                         | —                      | —                        | —                          | —                          | —                          | —                     | —    | —     | —      |
| 8074   | 281                 | 73                  | 4      | 1.81E-06                        | 0.403    | 1.58                              | —                                    | —                         | —                      | —                        | —                          | —                          | —                          | —                     | —    | —     | —      |
| 8075   | 285                 | 73                  | 4      | 1.60E-06                        | 0.382    | 1.64                              | —                                    | —                         | —                      | —                        | —                          | —                          | —                          | —                     | —    | —     | —      |
| 8081   | 264                 | 86                  | 4      | 1.34E-06                        | 0.472    | 1.40                              | 1.418                                | 3.32                      | 0.035                  | 0.0004                   | 55.60                      | 1.06                       | 5.23                       | 76.69                 | 2.5Y | 6     | 3      |
| 8082   | 273                 | 86                  | 4      | 1.37E-06                        | 0.473    | 1.40                              | —                                    | —                         | —                      | —                        | —                          | —                          | —                          | —                     | —    | —     | —      |
| 8083   | 269                 | 88                  | 4      | 9.66E-07                        | 0.453    | 1.45                              | —                                    | —                         | —                      | —                        | —                          | —                          | —                          | —                     | —    | —     | —      |
| 8084   | 264                 | 90                  | 4      | 9.44E-07                        | 0.453    | 1.45                              | —                                    | —                         | —                      | —                        | —                          | —                          | —                          | —                     | —    | —     | —      |
| 8085   | 273                 | 90                  | 4      | 9.94E-07                        | 0.466    | 1.42                              | —                                    | —                         | —                      | —                        | —                          | —                          | —                          | —                     | —    | —     | —      |
| 8091   | 242                 | 87                  | 4      | 1.04E-06                        | 0.459    | 1.43                              | 0.476                                | 2.78                      | —                      | —                        | 35.56                      | 0.76                       | 3.58                       | 54.05                 | 2.5Y | 6     | 2      |
| 8092   | 246                 | 87                  | 4      | 9.19E-07                        | 0.448    | 1.46                              | —                                    | —                         | —                      | —                        | —                          | —                          | —                          | —                     | —    | —     | —      |

**Table D.1**  
**Analytical Results for Measured Sediment Properties**

| Sample | X-Coordinate (cm) * | Y-Coordinate (cm) * | Facies | Permeability (cm <sup>2</sup> ) | Porosity | Bulk Density (g/cm <sup>3</sup> ) | BET Surface Area (m <sup>2</sup> /g) | Magnetic Fraction (wt. %) | Organic Carbon (wt. %) | Inorganic Carbon (wt. %) | DC-Extractable Fe (μmol/g) | DC-Extractable Mn (μmol/g) | DC-Extractable Al (μmol/g) | K <sub>d</sub> (ml/g) | Hue  | Value | Chroma |
|--------|---------------------|---------------------|--------|---------------------------------|----------|-----------------------------------|--------------------------------------|---------------------------|------------------------|--------------------------|----------------------------|----------------------------|----------------------------|-----------------------|------|-------|--------|
| 8093   | 244                 | 89                  | 4      | 9.24E-07                        | 0.446    | 1.47                              | —                                    | —                         | —                      | —                        | —                          | —                          | —                          | —                     | —    | —     | —      |
| 8094   | 242                 | 91                  | 4      | 8.93E-07                        | 0.449    | 1.46                              | —                                    | —                         | —                      | —                        | —                          | —                          | —                          | —                     | —    | —     | —      |
| 8095   | 246                 | 91                  | 4      | 9.41E-07                        | 0.444    | 1.47                              | —                                    | —                         | —                      | —                        | —                          | —                          | —                          | —                     | —    | —     | —      |
| 8101   | 208                 | 10                  | 8      | 1.67E-06                        | 0.344    | 1.74                              | 0.524                                | 3.19                      | —                      | —                        | 31.33                      | 1.73                       | 7.39                       | 9.82                  | 2.5Y | 6     | 3      |
| 8102   | 217                 | 10                  | 8      | 3.55E-06                        | 0.383    | 1.64                              | —                                    | —                         | —                      | —                        | —                          | —                          | —                          | —                     | —    | —     | —      |
| 8103   | 213                 | 12                  | 8      | 2.22E-06                        | 0.385    | 1.63                              | —                                    | —                         | —                      | —                        | —                          | —                          | —                          | —                     | —    | —     | —      |
| 8104   | 208                 | 14                  | 8      | 1.60E-06                        | 0.396    | 1.60                              | —                                    | —                         | —                      | —                        | —                          | —                          | —                          | —                     | —    | —     | —      |
| 8105   | 217                 | 14                  | 8      | 9.21E-07                        | 0.368    | 1.67                              | —                                    | 4.45                      | —                      | —                        | 45.72                      | 1.11                       | 9.09                       | 16.99                 | —    | —     | —      |
| 8111   | 208                 | 26                  | 4      | 4.70E-07                        | 0.349    | 1.73                              | —                                    | —                         | —                      | —                        | 53.74                      | 1.84                       | —                          | —                     | 2.5Y | 6     | 3      |
| 8112   | 217                 | 26                  | 7      | 1.10E-07                        | 0.437    | 1.49                              | —                                    | 3.84                      | —                      | —                        | 60.31                      | 1.75                       | 14.45                      | 140.46                | —    | —     | —      |
| 8113   | 212                 | 28                  | 4      | 3.55E-06                        | 0.378    | 1.65                              | —                                    | —                         | —                      | —                        | —                          | —                          | —                          | —                     | —    | —     | —      |
| 8114   | 208                 | 30                  | 4      | 2.37E-06                        | 0.394    | 1.61                              | —                                    | —                         | —                      | —                        | —                          | —                          | —                          | —                     | —    | —     | —      |
| 8115   | 217                 | 30                  | 4      | 3.50E-06                        | 0.410    | 1.56                              | —                                    | —                         | —                      | —                        | —                          | —                          | —                          | —                     | —    | —     | —      |
| 8121   | 260                 | 3                   | 6      | 2.13E-06                        | 0.418    | 1.54                              | 0.426                                | 3.17                      | —                      | —                        | 44.61                      | 0.85                       | 6.76                       | 15.66                 | 2.5Y | 6     | 4      |
| 8122   | 264                 | 3                   | 6      | 1.86E-06                        | 0.410    | 1.56                              | —                                    | —                         | —                      | —                        | —                          | —                          | —                          | —                     | —    | —     | —      |
| 8123   | 262                 | 5                   | 6      | 1.62E-06                        | 0.417    | 1.54                              | —                                    | —                         | —                      | —                        | —                          | —                          | —                          | —                     | —    | —     | —      |
| 8124   | 260                 | 7                   | 6      | 1.32E-06                        | 0.431    | 1.51                              | —                                    | —                         | —                      | —                        | —                          | —                          | —                          | —                     | —    | —     | —      |
| 8125   | 264                 | 7                   | 6      | 1.81E-06                        | 0.425    | 1.52                              | —                                    | —                         | —                      | —                        | —                          | —                          | —                          | —                     | —    | —     | —      |

\* Origin for spatial coordinate is lower left-hand corner of 8 m<sup>2</sup> sampling domain (see Figure 4.1).

\*\* Sample location straddles the boundary between two facies.

Sample Number 1062  
 Sample mass (g): 26.582

| Sieve diameter (mm) | Fraction (g) | Fraction % | % Coarser | % Finer |
|---------------------|--------------|------------|-----------|---------|
| 2                   | 0.057        | 0.214      | 0.214     | 99.786  |
| 1                   | 1.446        | 5.440      | 5.654     | 94.346  |
| 0.5                 | 5.993        | 22.545     | 28.200    | 71.800  |
| 0.25                | 15.605       | 58.705     | 86.905    | 13.095  |
| 0.125               | 2.666        | 10.029     | 96.934    | 3.066   |
| 0.063               | 0.742        | 2.791      | 99.725    | 0.275   |
| < 0.063             | 0.073        | 0.275      | 100.000   | 0.000   |
| % Recovery:         | 100.0        |            |           |         |

$d_{60}$  0.45       $d_{50}$  0.41       $d_{10}$  0.22       $d_{60}/d_{10}$  2.05

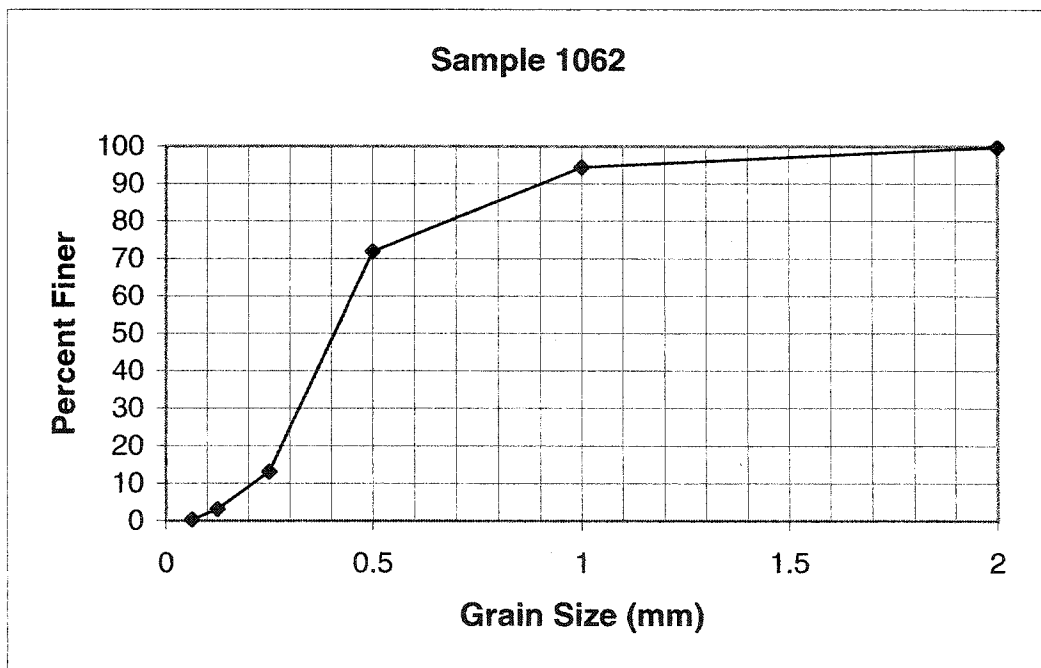


**Figure D.1** Grain size distribution curve for sample 1062. 1062 is texturally and mineralogically equivalent to thin section sample 1061.



Sample Number 1112  
 Sample mass (g): 22.085

| Sieve diameter (mm) | Fraction (g) | Fraction % | % Coarser | % Finer |
|---------------------|--------------|------------|-----------|---------|
| 2                   | 0.000        | 0.000      | 0.000     | 99.864  |
| 1                   | 0.104        | 0.471      | 0.471     | 99.393  |
| 0.5                 | 0.320        | 1.449      | 1.920     | 97.944  |
| 0.25                | 4.201        | 19.022     | 20.942    | 78.922  |
| 0.125               | 9.766        | 44.220     | 65.162    | 34.702  |
| 0.063               | 5.586        | 25.293     | 90.455    | 9.409   |
| < 0.063             | 2.078        | 9.409      | 99.864    | 0.000   |
| % Recovery          | 99.9         |            |           |         |

$d_{60}$  0.19       $d_{50}$  0.17       $d_{10}$  0.07       $d_{60}/d_{10}$  2.71

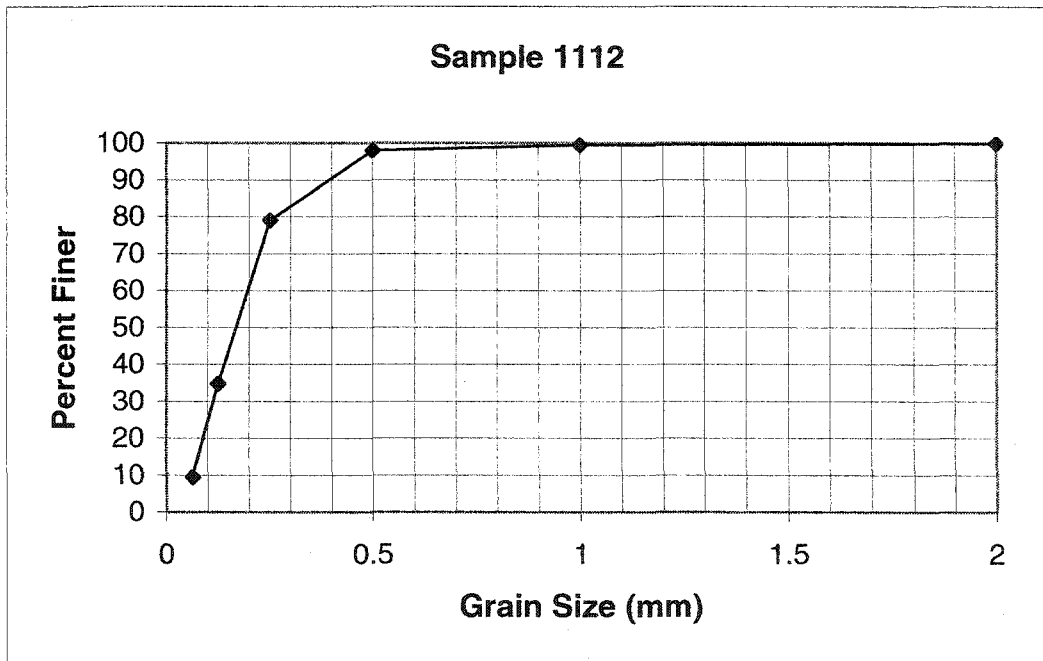
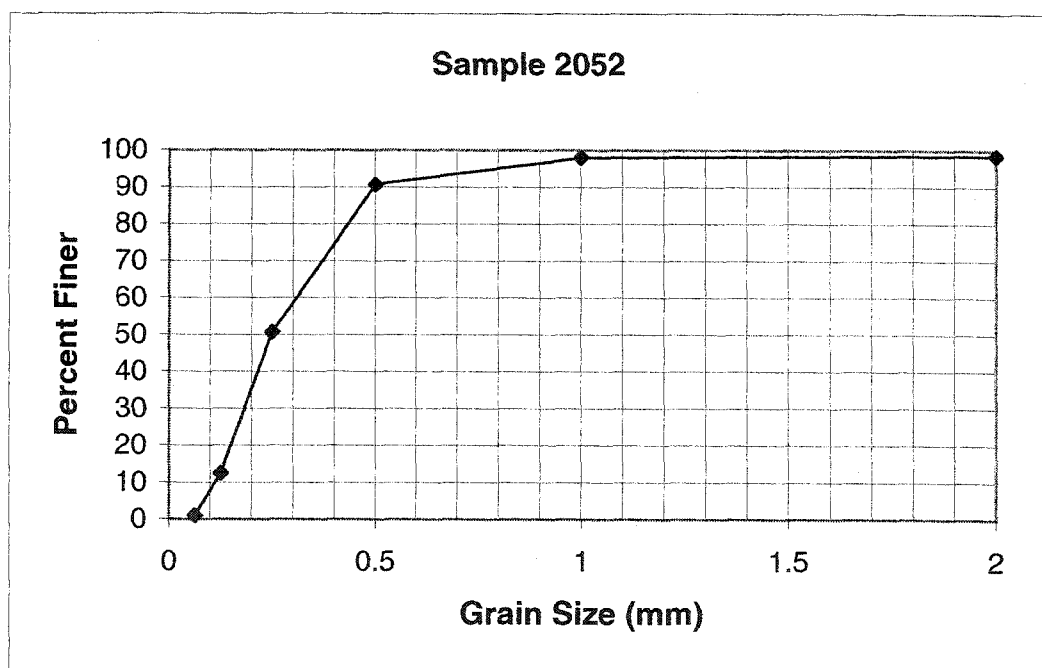


Figure D.2 Grain size distribution curve for sample 1112. 1112 is texturally and mineralogically equivalent to thin section sample 1111.

Sample Number 2052  
 Sample mass (g): 26.800

| Sieve diameter (mm) | Fraction (g) | Fraction % | % Coarser | % Finer |
|---------------------|--------------|------------|-----------|---------|
| 2                   | 0.371        | 1.384      | 1.384     | 98.567  |
| 1                   | 0.177        | 0.660      | 2.045     | 97.907  |
| 0.5                 | 1.946        | 7.261      | 9.306     | 90.646  |
| 0.25                | 10.732       | 40.045     | 49.351    | 50.601  |
| 0.125               | 10.233       | 38.183     | 87.534    | 12.418  |
| 0.063               | 3.077        | 11.481     | 99.015    | 0.937   |
| < 0.063             | 0.251        | 0.937      | 99.951    | 0.000   |
| % Recovery:         |              | 100.0      |           |         |

$d_{60}$  0.31       $d_{50}$  0.25       $d_{10}$  0.12       $d_{60}/d_{10}$  2.58



**Figure D.3** Grain size distribution curve for sample 2052. 2052 is texturally and mineralogically equivalent to thin section sample 2051.

Sample Number 2072  
 Sample mass (g): 25.984

| Sieve diameter (mm) | Fraction (g) | Fraction % | % Coarser | % Finer |
|---------------------|--------------|------------|-----------|---------|
| 2                   | 0.000        | 0.000      | 0.000     | 99.931  |
| 1                   | 0.324        | 1.247      | 1.247     | 98.684  |
| 0.5                 | 10.796       | 41.549     | 42.796    | 57.135  |
| 0.25                | 12.630       | 48.607     | 91.402    | 8.528   |
| 0.125               | 1.687        | 6.492      | 97.895    | 2.036   |
| 0.063               | 0.461        | 1.774      | 99.669    | 0.262   |
| < 0.063             | 0.068        | 0.262      | 99.931    | 0.000   |
| % Recovery:         | 99.9         |            |           |         |

$d_{60}$  0.53       $d_{50}$  0.46       $d_{10}$  0.26       $d_{60}/d_{10}$  2.04

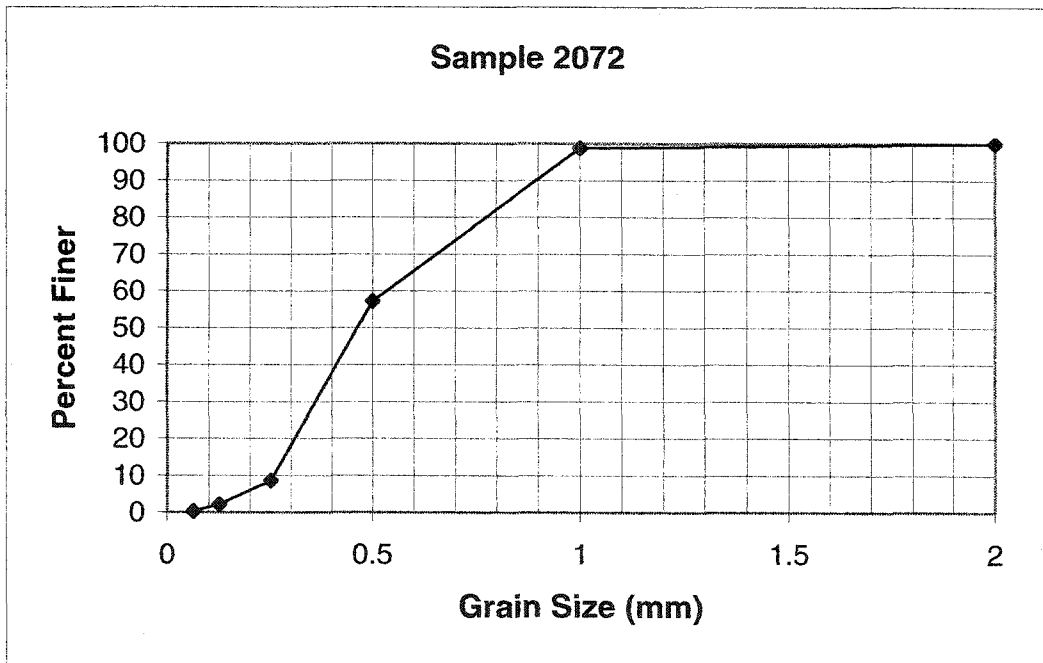


**Figure D.4** Grain size distribution curve for sample 2072. 2072 is texturally and mineralogically equivalent to thin section sample 2071.

Sample Number 5052  
 Sample mass (g): 22.420

| Sieve diameter (mm) | Fraction (g) | Fraction % | % Coarser | % Finer |
|---------------------|--------------|------------|-----------|---------|
| 2                   | 0.007        | 0.031      | 0.031     | 98.470  |
| 1                   | 1.485        | 6.624      | 6.655     | 91.847  |
| 0.5                 | 6.560        | 29.260     | 35.914    | 62.587  |
| 0.25                | 7.490        | 33.408     | 69.322    | 29.179  |
| 0.125               | 5.524        | 24.639     | 93.961    | 4.541   |
| 0.063               | 0.832        | 3.711      | 97.672    | 0.830   |
| < 0.063             | 0.186        | 0.830      | 98.501    | 0.000   |
| % Recovery:         |              | 98.5       |           |         |

$d_{60}$  0.48       $d_{50}$  0.4       $d_{10}$  0.15       $d_{60}/d_{10}$  3.20

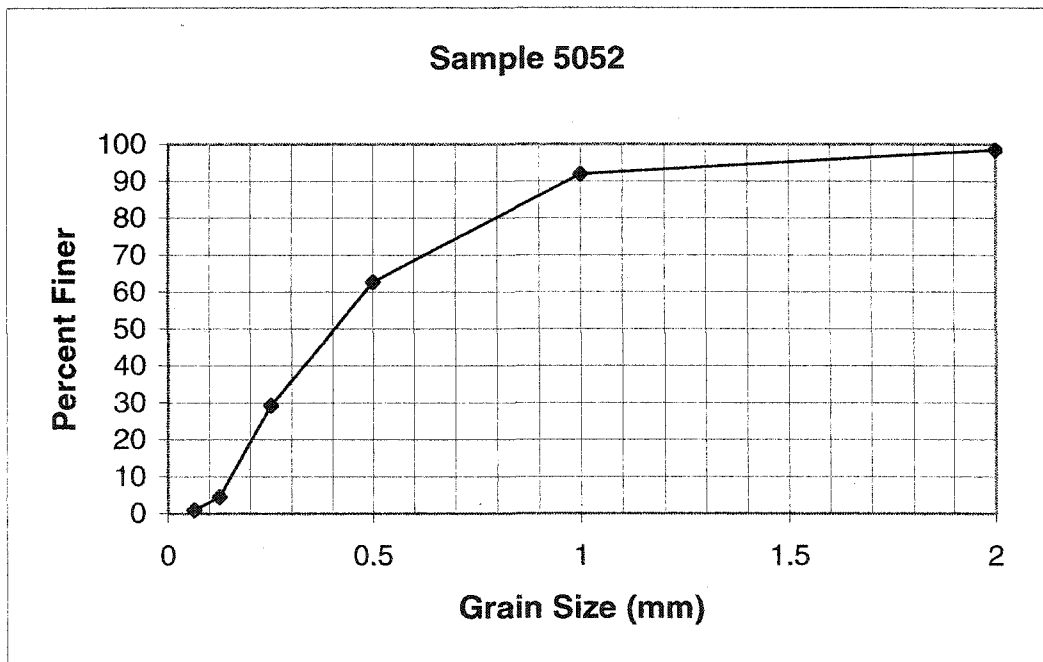


**Figure D.5** Grain size distribution curve for sample 5052. 5052 is texturally and mineralogically equivalent to thin section sample 5051.

Sample Number 6025  
 Sample mass (g): 25.011

| Sieve diameter (mm) | Fraction (g) | Fraction % | % Coarser | % Finer |
|---------------------|--------------|------------|-----------|---------|
| 2                   | 7.306        | 29.211     | 29.211    | 70.749  |
| 1                   | 10.753       | 42.993     | 72.204    | 27.756  |
| 0.5                 | 6.305        | 25.209     | 97.413    | 2.547   |
| 0.25                | 0.543        | 2.171      | 99.584    | 0.376   |
| 0.125               | 0.066        | 0.264      | 99.848    | 0.112   |
| 0.063               | 0.028        | 0.112      | 99.960    | 0.000   |
| < 0.063             | 0.000        | 0.000      | 99.960    | 0.000   |
| % Recovery:         | 100.0        |            |           |         |

$d_{60}$  1.75       $d_{50}$  1.52       $d_{10}$  0.65       $d_{60}/d_{10}$  2.69

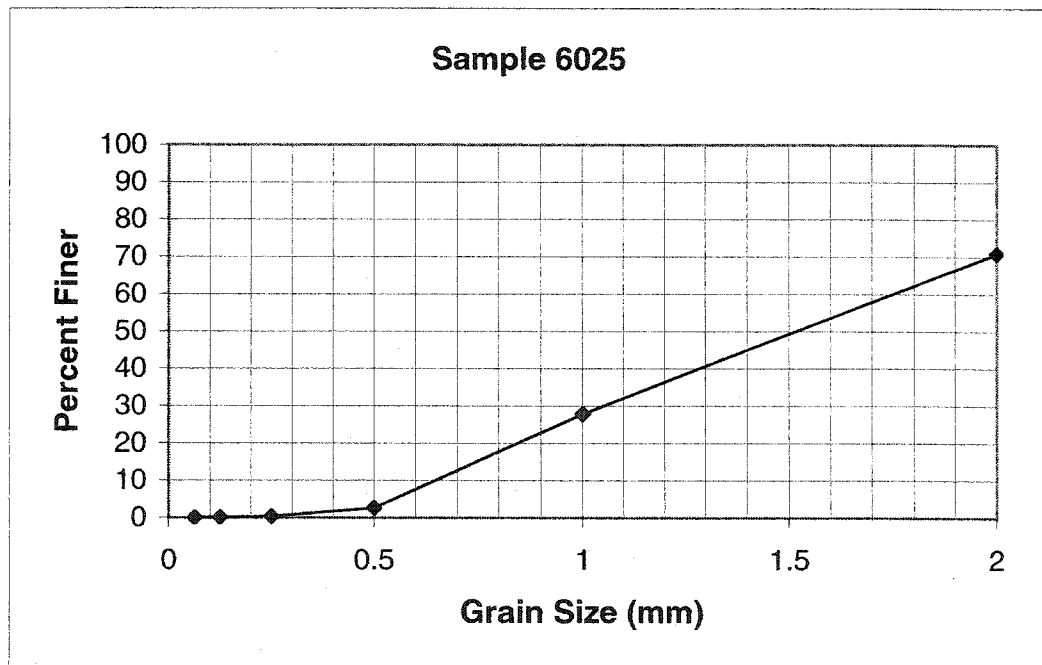


**Figure D.6** Grain size distribution curve for sample 6025. 6025 is texturally and mineralogically equivalent to thin section sample 6022.

Sample Number 6032  
 Sample mass (g): 25.634

| Sieve diameter (mm) | Fraction (g) | Fraction % | % Coarser | % Finer |
|---------------------|--------------|------------|-----------|---------|
| 2                   | 0.120        | 0.468      | 0.468     | 99.672  |
| 1                   | 4.674        | 18.234     | 18.702    | 81.439  |
| 0.5                 | 15.837       | 61.781     | 80.483    | 19.657  |
| 0.25                | 4.371        | 17.052     | 97.535    | 2.606   |
| 0.125               | 0.610        | 2.380      | 99.914    | 0.226   |
| 0.063               | 0.058        | 0.226      | 100.140   | 0.000   |
| < 0.063             | 0.000        | 0.000      | 100.140   | 0.000   |
| % Recovery          | 100.1        |            |           |         |

$d_{60}$  0.83       $d_{50}$  0.75       $d_{10}$  0.36       $d_{60}/d_{10}$  2.31

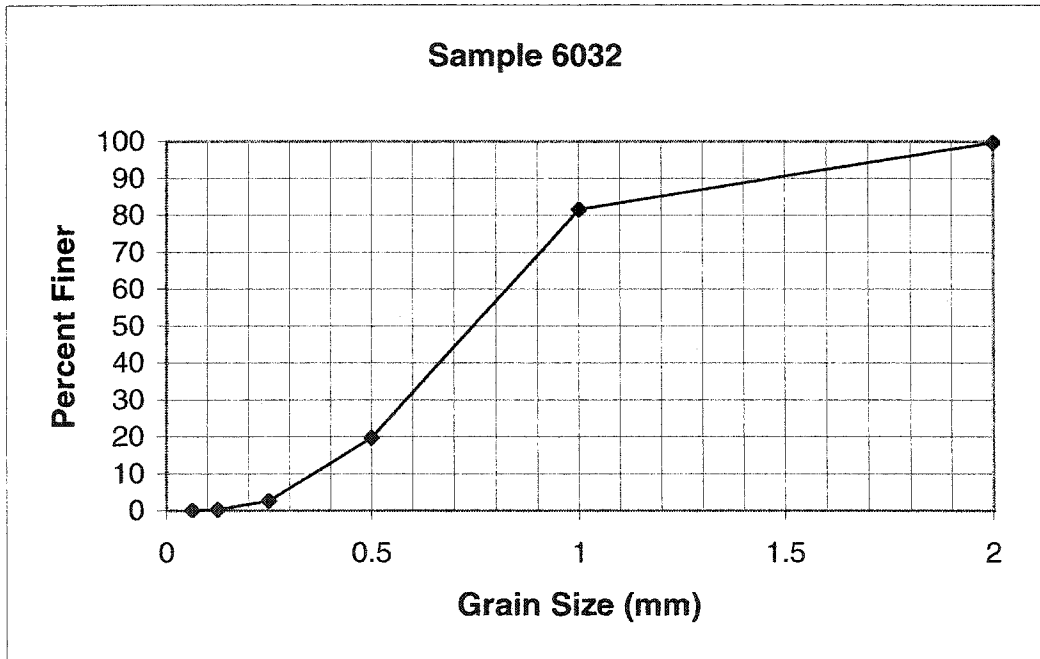


Figure D.7 Grain size distribution curve for sample 6032. 6032 is texturally and mineralogically equivalent to thin section sample 6031.

Sample Number 7073  
 Sample mass (g): 24.935

| Sieve diameter (mm) | Fraction (g) | Fraction % | % Coarser | % Finer |
|---------------------|--------------|------------|-----------|---------|
| 2                   | 11.800       | 47.323     | 47.323    | 52.440  |
| 1                   | 2.477        | 9.934      | 57.257    | 42.507  |
| 0.5                 | 3.374        | 13.531     | 70.788    | 28.975  |
| 0.25                | 4.651        | 18.652     | 89.441    | 10.323  |
| 0.125               | 2.041        | 8.185      | 97.626    | 2.138   |
| 0.063               | 0.386        | 1.548      | 99.174    | 0.590   |
| < 0.063             | 0.147        | 0.590      | 99.763    | 0.000   |
| % Recovery          | 99.8         |            |           |         |

$d_{60}$  2       $d_{50}$  1.73       $d_{10}$  0.25       $d_{60}/d_{10}$  8.00

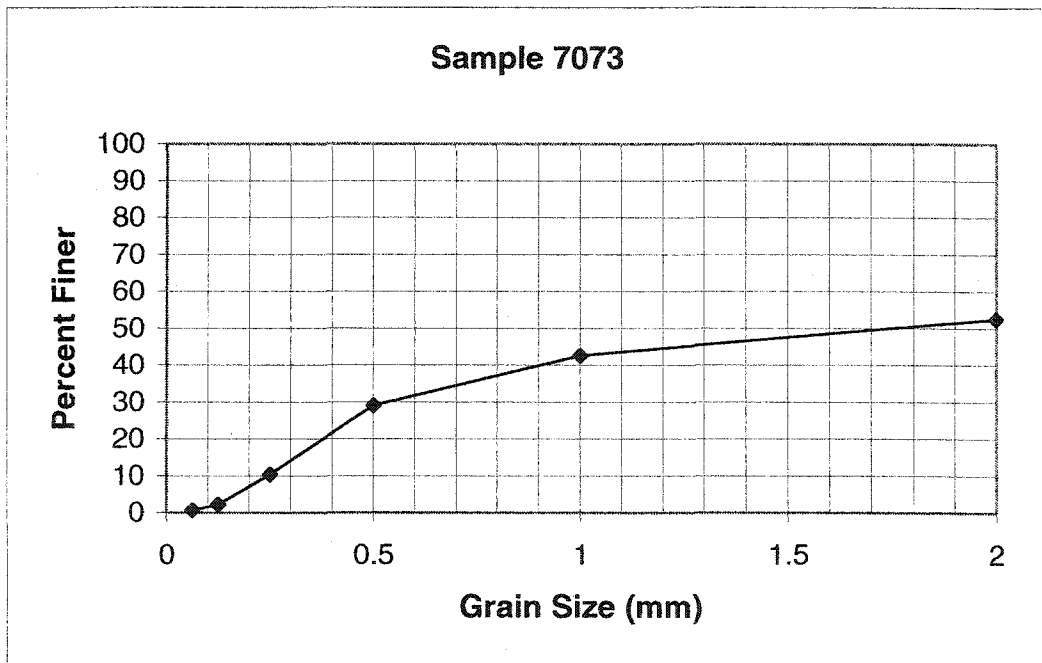
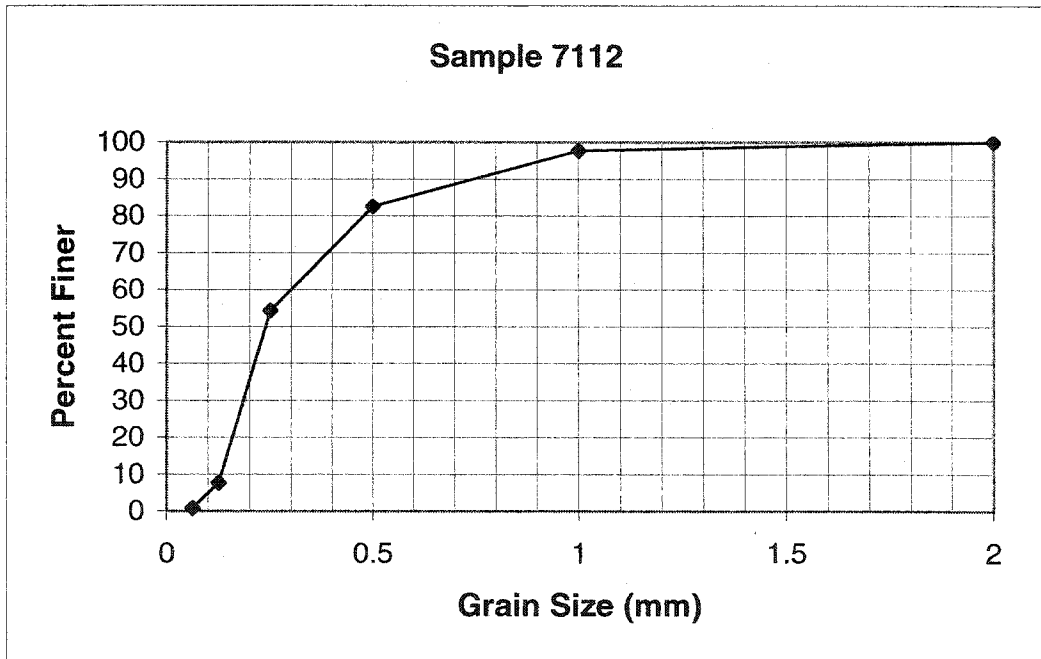


Figure D.8 Grain size distribution curve for sample 7073. 7073 is texturally and mineralogically equivalent to thin section sample 7072.

Sample Number 7112  
 Sample mass (g): 25.216

| Sieve diameter (mm) | Fraction (g) | Fraction % | % Coarser | % Finer |
|---------------------|--------------|------------|-----------|---------|
| 2                   | 0.011        | 0.044      | 0.044     | 99.996  |
| 1                   | 0.598        | 2.372      | 2.415     | 97.625  |
| 0.5                 | 3.816        | 15.133     | 17.548    | 82.491  |
| 0.25                | 7.115        | 28.216     | 45.765    | 54.275  |
| 0.125               | 11.756       | 46.621     | 92.386    | 7.654   |
| 0.063               | 1.724        | 6.837      | 99.223    | 0.817   |
| < 0.063             | 0.206        | 0.817      | 100.040   | 0.000   |
| % Recovery          | 100.0        |            |           |         |

$d_{60}$  0.3       $d_{50}$  0.24       $d_{10}$  0.13       $d_{60}/d_{10}$  2.31



**Figure D.9** Grain size distribution curve for sample 7112. 7112 is texturally and mineralogically equivalent to thin section sample 7111.



Sample Number 8112  
 Sample mass (g): 15.286

| Sieve diameter (mm) | Fraction (g) | Fraction % | % Coarser | % Finer |
|---------------------|--------------|------------|-----------|---------|
| 2                   | 0.016        | 0.105      | 0.105     | 98.142  |
| 1                   | 0.363        | 2.375      | 2.479     | 95.767  |
| 0.5                 | 0.679        | 4.442      | 6.921     | 91.325  |
| 0.25                | 2.031        | 13.287     | 20.208    | 78.039  |
| 0.125               | 5.941        | 38.866     | 59.074    | 39.173  |
| 0.063               | 4.079        | 26.685     | 85.758    | 12.489  |
| < 0.063             | 1.909        | 12.489     | 98.247    | 0.000   |
| % Recovery          | 98.2         |            |           |         |

$d_{60}$  0.19       $d_{50}$  0.16       $d_{10}$  0.06       $d_{60}/d_{10}$  3.17

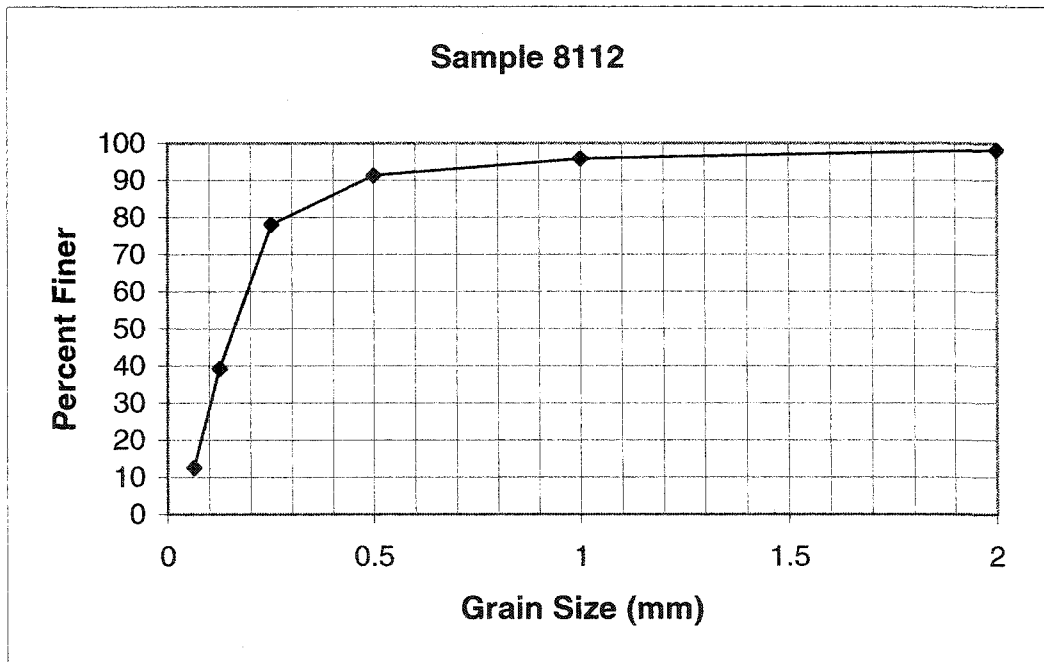


**Figure D.10** Grain size distribution curve for sample 8112. 8112 is texturally and mineralogically equivalent to thin section sample 6103.